



MATHMODEL'18

II INTERNATIONAL SCIENTIFIC CONFERENCE
12 - 15 DECEMBER, 2018, BOROVETS, BULGARIA

**MATHEMATICAL
MODELING**

PROCEEDINGS

YEAR II ISSUE 1(2)/2018

ISSN (Print) 2535-0978

ISSN (Online) 2603-3003

Published by
SCIENTIFIC-TECHNICAL UNION of MECHANICAL ENGINEERING - INDUSTRY 4.0
Sofia, BULGARIA

II INTERNATIONAL SCIENTIFIC CONFERENCE

MATHEMATICAL MODELING

Year II

Volume 1/2

DECEMBER 2018

ISSN 2535-0978 (Print)
ISSN 2603-3003 (Online)

PROCEEDINGS

THEMATIC FIELDS

1. THEORETICAL FOUNDATIONS AND SPECIFICITY OF MATHEMATICAL MODELLING
3. MATHEMATICAL MODELLING OF SOCIO-ECONOMIC PROCESSES AND SYSTEMS
2. MATHEMATICAL MODELLING OF TECHNOLOGICAL PROCESSES AND SYSTEMS
4. MATHEMATICAL MODELLING OF MEDICAL-BIOLOGICAL PROCESSES AND SYSTEMS

**12 – 15 DECEMBER, 2018,
BOROVETS, BULGARIA**

PUBLISHER:

**SCIENTIFIC TECHNICAL UNION OF MECHANICAL
ENGINEERING “INDUSTRY-4.0”**

108, Rakovski Str., 1000 Sofia, Bulgaria

tel. (+359 2) 987 72 90,

tel./fax (+359 2) 986 22 40,

office@mathmodel.eu

www.mathmodel.eu

INTERNATIONAL EDITORIAL BOARD

Chairman:		
Prof. ANDREY FIRSOV Peter the Great St.Petersburg Polytechnic University		RU
Members:		
Abilmazhin Adamov, Prof.	L.N.Gumilyov Eurasian National University	KZ
Alexander Guts, Prof.	Omsk State University	RU
Alexei Zhabko, Prof.	Saint Petersburg State University	RU
Andrey Markov, Prof.	Baltic State Technical University	RU
Andrii Matviichuk, Prof.	Kyiv National Economics University	UA
Andrzej Nowakowski, Prof.	University of Lodz	PL
Anton Makarov, Dr.	Saint Petersburg State University	RU
Armands Gricans, Assoc. Prof.	Daugavpils University	LV
Artūras Dubickas, Prof.	Vilnius University	LT
Avinir Makarov, Prof.	Saint Petersburg State University of Industrial Technologies and Design	RU
Christo Boyadjiev, Prof.	Institute of Chemical Engineering, BAS	BG
Daniela Marinova, Dssoc. Prof.	Technical University of Sofia	BG
Dimitrios Poulakis, Prof.	Aristotle University of Thessaloniki	GR
Evgeniy Smirnov, Assoc. Prof.	Volgograd State Technical University	RU
Galia Angelova, Prof. DSc	Institute of Information and Communication Technologies, BAS	BG
Giovanni Borgioli, Assoc. Prof.	University of Florence	IT
Haskiz Coskun, Prof.	Karadeniz Technical University of Trabzon	TR
Idilia Bachkova, Prof.	University of Chemical Technology and Metallurgy	BG
Irena Stojkovska, Prof.	Ss. Cyril and Methodius University in Skopje	MK
Ivana Štajner-Papuga, Prof.	University of Novi Sad	RS
Kanagat Aldazharov, Assoc. Prof.	Kazakh Economics University	KZ
Karl Kunisch, Prof.	University of Graz	AT
Mahomed Agamirza ogly Dunyamalyev, Prof.	Azerbaijan Technical University	AZ
Marius Giuclea, Prof.	The Bucharest University of Economics Studies	RO
Mihail Okrepilov, Prof.	D.I. Mendeleyev Institute for Metrology (VNIIM)	RU
Milena Racheva, Assoc. Prof.	Technical University of Gabrovo	BG
Mohamed Kara, Dr.	Ferhat Abbas Sétif 1 University	DZ
Mohamed Taher El-mayah, Prof	MTI University	EG
Neli Dimitrova, Prof.	Institute of Mathematics and Informatics, BAS	BG
Nina Bijedic, Prof.	Dzemal Bijedic University of Mostar	BA
Oleg Obradović, Prof.	University of Montenegro	ME
Olga Pritomanova, Assoc. Prof.	Oles Honchar Dnipropetrovsk National University	UA
Özkan Öcalan, Prof.	Akdeniz University of Antalya	TR
Pașe Găvrută, Prof.	Politehnic University of Timisoara	RO
Pavel Satrapa, Assoc. Prof.	Technical University of Liberec	CZ
Pavel Tvrdík, Prof.	Czech Technical University in Prague	CZ
Pavlina Yordanova, Assoc. Prof.	Shumen University	BG
Petr Trusov, Prof.	Perm State Technical University	RU
Rannveig Björnsdóttir, Prof.	University of Akureyri	IS
Roumen Anguelov, Prof.	University of Pretoria	ZA
Sándor Szabó, Dr. Prof.	University of Pécs	HU
Sashko Martinovski, Assoc. Prof.	St. Kliment Ohridski University of Bitola	MK
Sergey Bosnyakov, Prof.	Moscow Institute of Physics and Technology	RU
Sergey Kshevetskii, Prof.	Immanuel Kant Baltic Federal University	RU
Snejana Hristova, Prof.	University of Plovdiv	BG
Svetlana Lebed, Assoc. Prof.	Brest State Technical University	BY
Tomasz Szarek, Prof.	University of Gdansk	PL
Valeriy Serov, Prof.	University of Oulu	FI
Vasily Maximov, Prof.	Saint Petersburg State University of Industrial Technologies and Design	RU
Ventsi Rumchev, Prof.	Curtin University, Perth	AU
Veronika Stoffová, Prof.	University of Trnava	SK
Veselka Pavlova, Prof.	University of National and World Economy	BG
Viorica Sudacevschi, Assoc. Prof.	Technical University of Moldova	MD
Vladimir Janković, Prof.	University of Belgrade	RS
Vladislav Holodnov, Prof.	Saint Petersburg State Institute of Technology	RU
Vyacheslav Demidov, Prof.	Saint Petersburg State University of Industrial Technologies and Design	RU
Yordan Yordanov, Assoc. Prof.	University of Sofia	BG
Yuriy Kuznetsov, Prof.	Nizhny Novgorod State University	RU
Zdenka Kolar - Begović, Prof.	University of Osijek	HR

CONTENTS

THEORETICAL FOUNDATIONS AND SPECIFICITY OF MATHEMATICAL MODELLING

SUBSTANTIATION OF J.-G. SUN'S HYPOTHESIS, WHICH LIES IN THE BASIS OF THE THEORY OF ANALYTICAL DEPENDENCE OF EIGENVALUES OF MATRIX FROM "DISTURBING" PARAMETERS UNDER MULTI-PARAMETRIC PERTURBATION OF THE MATRIX ELEMENTS Prof. Dr.Tech.Sci. Andrei N. Firsov, Master's student Le Van Khanh	5
THE COMPUTATION OF ROTOR'S MOTION IN CYLINDRICAL CHAMBER FILLED WITH VISCOUS GAS Prof., Dr. Dementev O.	8
MIXED VARIATIONAL PROPERTIES FOR SOME FOURTH-ORDER BEAM PROBLEMS Prof. Andreev A. Dsc., Assoc. Prof Racheva M. Dsc.	11
MODELING OF THE 3D UNSTEADY MULTISCALE MULTIPHASE FLUID FLOW WITH SHOCKS: NUMERICAL METHODS AND IMPLEMENTATION ALGORITHMS Korneev B., Levchenko V. PhD.	15
IMPLICIT EULER TIME DISCRETIZATION AND FDM WITH NEWTON METHOD IN NONLINEAR HEAT TRANSFER MODELING Ph.D. Filipov S., Prof. D.Sc. Faragó I.	19
APPLICATION OF LAPLACE TRANSFORM IN FINANCE Daci A. PhD, Tola S. PhD.	24
INVESTIGATION OF CONVERGENCE OF ξ APPROXIMATIONS ON COMPLEX NUMBER PLANE Assist Prof. PhD. Işım Genç Demiriz	28
A FUZZY APPROACH TO THE EMISSION ESTIMATION Assoc. Prof. Ph.D. Filiz Kanbay	30
OPTIMAL ERROR INDICATORS FOR CONVECTION DOMINATED PROBLEMS Petr Lukáš	33

MATHEMATICAL MODELLING OF TECHNOLOGICAL PROCESSES AND SYSTEMS

AIR SPACE ROUTING AND FLIGHTS PLANNING: A PROBLEM STATEMENT AND DISCUSSION OF APPROACHES TO SOLUTION Assoc. Prof. PhD. Aliksieiev V.	34
MODELING OF MAGNETIC HYSTERESIS UNDER WEAK MAGNETIC FIELDS AND TRIAXIAL STRESS STATE Mushnikov A.N., Kryucheva K. D.	38
MATHEMATICAL MODELS OF CALCULATIONS OF PARAMETERS OF CRYSTALLIZATION OF BINARY ALLOYS BY MEANS OF COMPUTER THERMAL ANALYSIS Ass. Prof., Dr. Eng. Donii O., Ass. Prof., Dr. Eng. Khristenko V., Omelko L., Ass. Kotliar S.	41
APPLYING QUEUE THEORY AT STUDY OF REFUSALS OF REQUESTS RECEIVED IN UNIVERSAL AUTOMOTIVE SERVICE Assist. Prof. Grozev D. PhD., M.Sc. Georgiev I. PhD., , Assist. Prof. Milchev M. PhD.	44
COMPUTER MODELLING OF RADIAL-SHEAR ROLLING OF AUSTENITIC STAINLESS STEEL AISI-321 D.t.s., prof. Naizabekov A.B., c.t.s. ass. prof. Lezhnev S.N., PhD Arbuz A.S., PhD Panin E.A., d.t.s. Koinov T.A.	48
EVALUATION OF ROBUSTNESS IN ASR FOR DIFFERENT 'FRONT-END' METHODS Tola S. PhD., Daci A. PhD	52
OPTIMAL HYDRO-THERMAL COORDINATION WITH A MAXIMUM RES POWER UTILIZATION STRATEGY CONSTRAINTS MODEL M.Sc. Trashlieva V. PhD., M.Sc. Radeva T. PhD	54
OPTIMAL HYDRO-THERMAL COORDINATION WITH A MAXIMUM RES POWER UTILIZATION STRATEGY CONSTRAINTS: RESULTS AND ANALISYS M.Sc. Trashlieva V. PhD., M.Sc. Radeva T. PhD.	58
ON A MATHEMATICAL MODEL OF LAND-USE CHANGE Assoc. Prof. M.Sc. Kolev M. PhD., M.Sc. Urumova A., Assoc. Prof. M.Sc. Kolev B. PhD.	62

RESEARCHING THE CAPABILITIES OF INFORMATION TECHNOLOGIES FOR EDJUCATION IN DESIGN, 3D MODELING AND VISUALIZATION OF THE WORKING OF COMPLEX MECHANISMS S. Il. Antonov	65
MATHEMATICAL MODELLING OF PIEZOELECTRIC DISK TRANSFORMER WITH RING ELECTRODES IN PRIMARY ELECTRICAL CIRCUIT Dr. Bazilo C., PhD.	69
ИЗСЛЕДВАНЕ НА КРЕНА НА АВТОМОБИЛ ПОСРЕДСТВОМ МОДЕЛ НА ПРУЖИННО ОБЪРНАТО МАХАЛО гл. ас. д-р инж. Павлов Н. Л.	72
ИЗСЛЕДВАНЕ НА ДИФЕРЕНТА НА АВТОМОБИЛ ПОСРЕДСТВОМ МОДЕЛ НА ПРУЖИННО ОБЪРНАТО МАХАЛО гл. ас. д-р инж. Павлов Н. Л.	75

MATHEMATICAL MODELLING OF SOCIO-ECONOMIC PROCESSES AND SYSTEMS

COMPLEX SPATIAL MODELLING POSSIBILITIES OF THE SOCIO-ECONOMIC CHANGES OF HUNGARY - POTENTIAL APPROACHES AND METHODS PhD Lennert J.	78
COMPARISON OF APPROACHES TO ESTIMATION OF TRANSITION MATRIX FOR THE TERRORIST THREAT MARKOV MODEL Ing. Martin Tejkal, Doc. RNDr. Jaroslav Michálek, CSc.	81
USE OF ICT RESOURCES IN THE HUMANITARIAN SUBJECTS IN BULGARIAN SCHOOLS M.Sc. Boneva Y., Assist. Prof. PhD. Paunova-Hubenova E., Assist. Prof. Terzieva V., PhD. Dimitrov S.	85

4. MATHEMATICAL MODELLING OF MEDICAL-BIOLOGICAL PROCESSES AND SYSTEMS

AUTOMATIC GENERATION OF A NATIONAL DIABETES REGISTER FROM OUTPATIENT RECORDS Dimitar Tcharaktchiev, Zhivko Angelov, Svetla Boytcheva, Galia Angelova	89
A MODEL OF BINDING OF DOXORUBICIN WITH HEPARIN AND ENOXAPARIN Eng. Matuszak M. L., Msc. Eng. Dalek P., Prof. Langner M., PhD Przybyło M.	93
DETERMINATION OF SURFACTANT EFFECTIVE DIFFUSION COEFFICIENT USING INVERSE PROBLEM FOR WARD-TORDAI EQUATION M.Sc. Eng. Stasiak M., M.Sc. Eng. Andrzejewski A., Prof. Prochaska K.	96
CLASSIFICATION OF PROTEIN STRUCTURES BY USING FUZZY KNN CLASSIFIER AND PROTEIN VOXEL-BASED DESCRIPTOR Prof. Dr. Mirceva G., Prof. Dr. Naumoski A., Prof. Dr. Kulakov A.	99
MODELLING THE RELATIONSHIP BETWEEN SATURATED OXYGEN AND DISTOMS' ABUNDANCE USING WEIGTHED PATTERN TREES WITH ALGEBRAIC OPERATORS Prof. Dr. Naumoski A., Prof. Dr. Mirceva G., Prof. Dr. Mitreski K.	102

SUBSTANTIATION OF J.-G. SUN'S HYPOTHESIS, WHICH LIES IN THE BASIS OF THE THEORY OF ANALYTICAL DEPENDENCE OF EIGENVALUES OF MATRIX FROM "DISTURBING" PARAMETERS UNDER MULTI-PARAMETRIC PERTURBATION OF THE MATRIX ELEMENTS

ОБОСНОВАНИЕ ГИПОТЕЗЫ J.-G. SUN'А, ЛЕЖАЩЕЙ В ОСНОВЕ ТЕОРИИ АНАЛИТИЧЕСКОЙ ЗАВИСИМОСТИ СОБСТВЕННЫХ ЗНАЧЕНИЙ МАТРИЦЫ ОТ "ВОЗМУЩАЮЩИХ" ПАРАМЕТРОВ ПРИ МНОГОПАРАМЕТРИЧЕСКОМ ВОЗМУЩЕНИИ МАТРИЧНЫХ ЭЛЕМЕНТОВ

Prof. Dr.Tech.Sci. Andrei N. Firsov¹, Master's student Le Van Khanh²
Institute of Computer Science and Technology – Peter the Great Saint-Petersburg Polytechnic University, Russia
E-mail: ¹anfirs@yandex.ru, ²levankhanhth@gmail.com

Abstract: The paper gives a rigorous justification of Ji-Guang Sun's hypothesis about the properties of the eigenvalues of the matrix of a linear dynamical system under multiparametric perturbation of its elements.

KEYWORDS: DYNAMICAL SYSTEMS WITH SMALL PERTURBATIONS, INVERSE STABILITY PROBLEM.

1. Introduction

The concept of stability of dynamic systems characterizes the property of a system to operate stably in modes where there are uncertainties in the values of certain system elements. Due to the complexity, and sometimes the practical impossibility to indicate the necessary and sufficient allowable ranges of variation of the corresponding parameters, at least sufficient estimates may be of great interest. On the other hand, practice shows that the desire for universality of theoretical results, as a rule, leads to great difficulties in the application of such results for solving specific problems. We believe that the consideration of such considerations should underlie the construction of theoretical structures aimed at solving specific applied problems. In this paper, we propose a solution to the problem of conditions sufficient to preserve the stability property of a linear dynamical system under small perturbations of its matrix. In this case, an estimate of the smallness of the perturbation parameters is given.

2. Formulation of the problem

Let's consider a dynamic system:

$$\frac{dX(t)}{dt} = AX(t) \quad (2.1)$$

$$A = (a_{ij})_{i,j=1}^n, X(t) = (x_1(t), x_2(t), \dots, x_n(t))^T.$$

Here A denotes an "unperturbed" matrix. Suppose the matrix A has simple different eigenvalues $\lambda_j, j = 1, 2, \dots, n$ and

$\operatorname{Re}(\lambda_j) < 0, j = 1, 2, \dots, n$, that is, the system (2.1) is supposed to be sustainable.

Let further

$$\vec{\varepsilon} = (\varepsilon_{11}, \dots, \varepsilon_{1n}, \varepsilon_{21}, \dots, \varepsilon_{2n}, \dots, \varepsilon_{nn})^T \in \mathbb{R}^{n^2},$$

where ε_{ij} – unknown "perturbations" of the elements of the original matrix. Let's consider perturbation parameters ε_{ij} will be small enough in the sense that the quantity ε_{ij}^2 can be neglected in comparison with ε_{ij} : $\varepsilon_{ij}^2 \ll |\varepsilon_{ij}|$. The ultimate goal is a "sufficient" estimate of the magnitude of the elements ε_{ij} of a "perturbed" system

$$\frac{dX(t)}{dt} = A(\vec{\varepsilon})X(t), \quad (2.2)$$

under which the stability property of its solutions is preserved.

Further we will consider that

$$A(\varepsilon_{11}, \varepsilon_{12}, \dots, \varepsilon_{1n}, \varepsilon_{21}, \dots, \varepsilon_{2n}, \dots, \varepsilon_{nn}) = A + \sum_{i,j=1}^n \varepsilon_{ij} A_{ij}, \quad (2.3)$$

where A_{ij} – are known matrices. Ji-Guang Sun has proved [1], that in the case of the validity of "Sun's hypothesis" (see (3.1), (3.2) below), eigenvalues $\lambda_j(\vec{\varepsilon}), j = 1, 2, \dots, n$ of a perturbed matrix $A(\vec{\varepsilon})$ are fairly smooth functions of parameters $\varepsilon_{ij}, i, j = 1, 2, \dots, n$ in the neighborhood of zero. This allows, if we assume the validity of the Sun's hypothesis, to answer the question raised above about the stability conditions of a perturbed system (2.2) (see [2]). In this paper we will show that the "hypothesis" (3.1), (3.2) is in fact a theorem.

Under the norms of matrices and vectors, we will further understand the corresponding Euclidean norms.

3. Proof of Sun's hypothesis

The main results on the dependence of eigenvalues on perturbing parameters were obtained by T. Kato [3] (for one parameter) and by J.-G. Sun [1] (for several parameters). However, when formulating the results, J.-G. Sun expressed a hypothesis about the nature of the dependence of the eigenvalues on the perturbation parameters, which he did not prove. In this paper, we justify this hypothesis.

In [1] J.-G. Sun stated the following hypothesis, on which the proof of the main theorem in the paper [1] was based:

Sun's hypothesis. Let λ_s – non-multiple eigenvalue,

generally speaking, asymmetric matrix $A \in \mathbb{R}^{n \times n}$, \vec{x}_s and \vec{y}_s – corresponding right and left eigenvectors, at the same time we

accept, that $\|\vec{x}_s\| = 1$ (where $\|\vec{x}_s\| = \sqrt{\sum_{i=1}^n (x_{si})^2}$, $x_{si}, i = 1, \dots, n$

are coordinates of the vector \vec{x}_s) and $\vec{y}_s^T \cdot \vec{x}_s = 1$. Then for any λ_s

there exist such $\tilde{X}, \tilde{Y} \in \mathbb{R}^{n \times (n-1)}$, that for matrices $X = (\vec{x}_s, \tilde{X})$

and $Y = (\vec{y}_s, \tilde{Y})$, the following relations hold:

$$Y^T X = I_n, \quad (3.1)$$

$$Y^T A X = \begin{pmatrix} \lambda_s & 0_{1 \times (n-1)} \\ 0_{(n-1) \times 1} & \tilde{A} \end{pmatrix}, \lambda_s \notin \lambda(\tilde{A}). \quad (3.2)$$

where $\lambda_s, s = \overline{1, n}$ – are non-multiple matrix eigenvalues A .

Here we give a detailed *proof* of this result. Let us consider the matrix

$$Z' = \begin{pmatrix} 1 & 0 & \dots & 0 \\ 0 & 1 & \dots & 0 \\ \vdots & \vdots & \ddots & \vdots \\ 0 & 0 & \dots & 1 \\ 0 & 0 & \dots & 0 \end{pmatrix}_{n \times n} = \begin{pmatrix} x_{s1} & 1 & 0 & \dots & 0 \\ x_{s2} & 0 & 1 & \dots & 0 \\ \vdots & \vdots & \vdots & \ddots & \vdots \\ x_{s(n-1)} & 0 & 0 & \dots & 1 \\ x_{sn} & 0 & 0 & \dots & 0 \end{pmatrix}_{n \times n}.$$

Applying the Gram-Schmidt orthogonalization (see, for example [4, 5]) to the matrix Z' , we obtain the matrix $Z = (\tilde{x}_s, \tilde{Y})$ - orthonormal in the columns, i.e.

$$\tilde{Y}^T \tilde{x}_s = 0_{(n-1) \times 1}. \quad (3.3)$$

It is also easy to check that $\det Y = (y_s, \tilde{Y}) \neq 0$.

Let $H = \{h_{i,j}\}_{i=1, j=1}^n \equiv Y^{-1} = (y_s, \tilde{Y})^{-1}$, and consider the matrix $X = (\tilde{x}_s, \tilde{X})$, where

$$\tilde{X}_{(n-1)} = \left[\{h_{i,j}\}_{i=2, j=1}^n \right]^T = \left[(h_2)^T \quad (h_3)^T \quad \dots \quad (h_n)^T \right],$$

where $h_i, i = 2, \dots, n$ - are rows of the matrix H , i.e.

$$\tilde{y}_s^T \tilde{X} = 0_{1 \times (n-1)} \text{ and } \tilde{Y}^T \tilde{X} = I_{(n-1)}. \quad (3.4)$$

From (3.3) and (3.4) we have:

$$\begin{aligned} Y^T X &= (\tilde{y}_s, \tilde{Y})^T (\tilde{x}_s, \tilde{X}) = \begin{pmatrix} \tilde{y}_s^T \tilde{x}_s & \tilde{y}_s^T \tilde{X} \\ \tilde{Y}^T \tilde{x}_s & \tilde{Y}^T \tilde{X} \end{pmatrix} \\ &= \begin{pmatrix} 1 & 0_{1 \times (n-1)} \\ 0_{(n-1) \times 1} & I_{n-1} \end{pmatrix} = I_n, \end{aligned}$$

therefore, we have a relationship (3.1).

Consider further:

$$\begin{aligned} Y^T A &= (\tilde{y}_s, Y_2, Y_3, \dots, Y_n)^T (\tilde{a}_1, \tilde{a}_2, \dots, \tilde{a}_n) = \\ &= \begin{pmatrix} \tilde{y}_s^T \tilde{a}_1 & \tilde{y}_s^T \tilde{a}_2 & \dots & \tilde{y}_s^T \tilde{a}_n \\ A^* \end{pmatrix} = \begin{pmatrix} \tilde{y}_s^T A \\ A^* \end{pmatrix} = \begin{pmatrix} \lambda_s \tilde{y}_s^T \\ A^* \end{pmatrix}, \end{aligned} \quad (3.5)$$

where $\tilde{a}_j, j = 1, 2, \dots, n$ are matrix columns of the matrix A , and matrix $A^* \in \mathbb{R}^{(n-1) \times n}$. $Y_j, j = 2, 3, \dots, n$ - are matrix columns of Y .

Next, multiply the expression (3.5) by the matrix X on the right:

$$\begin{aligned} Y^T A X &= \begin{pmatrix} \lambda_s \tilde{y}_s^T \\ A^* \end{pmatrix} (\tilde{x}_s, X_2, X_3, \dots, X_n) = \\ &= \begin{pmatrix} \lambda_s \tilde{y}_s^T \tilde{x}_s & \lambda_s \tilde{y}_s^T X_2 & \dots & \lambda_s \tilde{y}_s^T X_n \\ A^{**} \end{pmatrix} = \\ &= \begin{pmatrix} \lambda_s & 0_{1 \times (n-1)} \\ A^{**} \end{pmatrix}, \end{aligned} \quad (3.6)$$

where $X_j, j = 2, 3, \dots, n$ - are matrix columns of X , and matrix $A^{**} \in \mathbb{R}^{(n-1) \times n}$.

Next we have for AX :

$$AX = \begin{pmatrix} \tilde{a}^1 \\ \tilde{a}^2 \\ \vdots \\ \tilde{a}^n \end{pmatrix} \cdot (\tilde{x}_s, X_2, X_3, \dots, X_n) = (\lambda_s \tilde{x}_s, A'), \quad (3.7)$$

where \tilde{a}^i - are rows of matrix A ; $X_j, j = 2, 3, \dots, n$ - are columns of matrix X , and matrix $A' \in \mathbb{R}^{n \times (n-1)}$.

Next, multiply the expression (3.7) by Y^T on the left:

$$\begin{aligned} Y^T A X &= (\tilde{y}_s, Y_2, Y_3, \dots, Y_n)^T \cdot (\lambda_s \tilde{x}_s, A') \\ &= \begin{pmatrix} \lambda_s & A'' \\ 0_{(n-1) \times 1} \end{pmatrix}, \end{aligned} \quad (3.8)$$

where $Y_j, j = 2, 3, \dots, n$ - are the columns of matrix Y , and matrix $A'' \in \mathbb{R}^{n \times (n-1)}$.

From the property of matrix associativity, and taking into account expressions (3.6), (3.8), we are convinced of the validity of equality (3.2).

We now give an example of the application of the results.

Let the matrix A have three different negative eigenvalues

$$\lambda_1, \lambda_2, \lambda_3.$$

Let $\tilde{x}_1 = (x_{11} \ x_{12} \ x_{13})^T$ and $\tilde{y}_1 = (y_{11} \ y_{12} \ y_{13})^T$ - right and left eigenvectors corresponding to λ_1 . At the same time, the eigenvectors satisfy the following conditions:

$$\|\tilde{x}_1\| = 1 \text{ и } \tilde{y}_1^T \tilde{x}_1 = 1.$$

The case $x_{11} \neq \pm 1$.

Let construct matrices Y, X in this case (see above). Let

$$Z' = \begin{pmatrix} 1 & 0 \\ \tilde{x}_1 & 0 \\ 0 & 1 \\ 0 & 0 \end{pmatrix} \equiv \begin{pmatrix} x_{11} & 1 & 0 \\ x_{12} & 0 & 1 \\ x_{13} & 0 & 0 \end{pmatrix}, \quad \tilde{x}_1 = \begin{pmatrix} x_{11} \\ x_{12} \\ x_{13} \end{pmatrix}.$$

Applying Gram-Schmidt orthogonalization to the matrix Z' we obtain the matrix orthonormal in the columns

$$Z = (\tilde{x}_1, \tilde{Y}) = \begin{pmatrix} x_{11} & \frac{1-x_{11}^2}{\sqrt{1-x_{11}^2}} & 0 \\ x_{12} & \frac{-x_{11}x_{12}}{\sqrt{1-x_{11}^2}} & \frac{x_{13}}{\sqrt{1-x_{11}^2}} \\ x_{13} & \frac{-x_{11}x_{13}}{\sqrt{1-x_{11}^2}} & \frac{-x_{12}}{\sqrt{1-x_{11}^2}} \end{pmatrix},$$

with the condition

$$x_{11} \neq \pm 1. \quad (3.9)$$

Similarly, in accordance with the above, we obtain the matrix $Y = (\tilde{y}_1, \tilde{Y})$:

$$Y = \begin{pmatrix} y_{11} & \frac{1-y_{11}^2}{\sqrt{1-y_{11}^2}} & 0 \\ y_{12} & \frac{-y_{11}y_{12}}{\sqrt{1-y_{11}^2}} & \frac{y_{13}}{\sqrt{1-y_{11}^2}} \\ y_{13} & \frac{-y_{11}y_{13}}{\sqrt{1-y_{11}^2}} & \frac{-y_{12}}{\sqrt{1-y_{11}^2}} \end{pmatrix}. \quad (3.10)$$

Its determinant is equal to

$$\det(Y) = \frac{(1-y_{11}^2)(x_{11}y_{11} + x_{12}y_{12} + x_{13}y_{13})}{(1-x_{11}^2)} = 1,$$

whence it follows that there exists an inverse matrix for Y :

$$H = \begin{pmatrix} x_{11} & x_{12} & x_{13} \\ \frac{x_{12}y_{12} + x_{13}y_{13}}{\sqrt{1-x_{11}^2}} & \frac{-y_{11}x_{12}}{\sqrt{1-x_{11}^2}} & \frac{-x_{13}y_{11}}{\sqrt{1-x_{11}^2}} \\ \frac{x_{11}(x_{12}y_{13} - x_{13}y_{12})}{\sqrt{1-x_{11}^2}} & \frac{-x_{11}^2y_{13} - x_{11}y_{11}x_{13} - y_{13}}{\sqrt{1-x_{11}^2}} & \frac{x_{11}^2y_{12} - x_{11}y_{11}x_{12} - y_{12}}{\sqrt{1-x_{11}^2}} \end{pmatrix}$$

Next, we build the matrix $X = (\tilde{x}_1, (h_2)^T, (h_3)^T)^T$, where

h_2, h_3 – rows of matrix H , i.e.

$$X = (\tilde{x}_1, \tilde{X}) = \begin{pmatrix} x_{11} & \frac{x_{12}y_{12} + x_{13}y_{13}}{\sqrt{1-x_{11}^2}} & \frac{x_{11}(x_{12}y_{13} - x_{13}y_{12})}{\sqrt{1-x_{11}^2}} \\ x_{12} & \frac{-y_{11}x_{12}}{\sqrt{1-x_{11}^2}} & -\frac{x_{11}^2y_{13} - x_{11}y_{11}x_{13} - y_{13}}{\sqrt{1-x_{11}^2}} \\ x_{13} & \frac{-x_{13}y_{11}}{\sqrt{1-x_{11}^2}} & \frac{x_{11}y_{12} - x_{11}y_{11}x_{12} - y_{12}}{\sqrt{1-x_{11}^2}} \end{pmatrix}, \quad (3.11)$$

$$\det(X) = 1$$

It is not difficult to see that $X = (Y^{-1})^T$, so $Y^T X = I$, i.e. (3.1) is right.

From (3.10) and (3.11) we finally get:

$$Y^T AX = \begin{pmatrix} \lambda_1 \tilde{y}_1^T \tilde{x}_1 & 0 & 0 \\ 0 & \tilde{a}_{22} & \tilde{a}_{23} \\ 0 & \tilde{a}_{32} & \tilde{a}_{33} \end{pmatrix} \quad (3.12)$$

and $\tilde{A} = \begin{pmatrix} \tilde{a}_{22} & \tilde{a}_{23} \\ \tilde{a}_{32} & \tilde{a}_{33} \end{pmatrix}$,

as required.

The case of $x_{11} = \pm 1$ is considered by direct calculation.

4. Conclusions

The paper presents a proof of the hypothesis of J.-G. Sun, which is the basis of the theorem on the analytical properties of the eigenvalues of a matrix in the case of multiparameter perturbation of its elements.

5. Literature

1. Sun Ji-Guang. Eigenvalues and eigenvectors of a matrix dependent on several parameters. J. Comput. Math., 3, 351-364 (1985).
2. Bulkina E, Firsov A. Numerical-analytical method for solving the inverse problem of stability for technical systems with multiple uncertain parameters. "Machines. Technologies. Materials." International journal for science, technics and innovations for the industry (Bulgaria). Issue 11/2016, p. 12-14.
3. Kato T. A Short Introduction to Perturbation Theory for Linear Operators, N.-Y.: Springer-Verlag, 1982.
4. Beklemishev D.V. The course of analytical geometry and linear algebra, Moscow: FIZMATLIT, 2005 (in Russian).
5. Lancaster P., Tismenetsky M. The theory of matrices (2nd ed), N.-Y.: Academic Press, 1985.

THE COMPUTATION OF ROTOR'S MOTION IN CYLINDRICAL CHAMBER FILLED WITH VISCOUS GAS

РАСЧЕТ ДВИЖЕНИЯ РОТОРА В ЦИЛИНДРИЧЕСКОЙ КАМЕРЕ, ЗАПОЛНЕННОЙ ВЯЗКИМ ГАЗОМ

Prof., Dr. Dementev O.
Chelyabinsk State University, Chelyabinsk, Russia
e-mail: dement@csu.ru

Abstract: The problem rotor's movement in a stationary circular cylindrical chamber having finite length and filled with viscous gas is solved by the method of direct numerical integration of the set of equations describing pressure distribution in a thin layer of viscous gas and the motion of a rotating statically disbalanced cylinder. The rotor moving in the gravitational field is influenced by the impressed forces which vary periodically in time. Unsteady pressure equation is approximated by the symmetric stable finite-difference scheme of the second order accuracy. Stability criteria of a rotating rigid unstable cylinder (a rotor) motion subject to problem parameters are studied. The inner cylinder is influenced by outer forces which vary periodically in time. Trajectories of the rotor stationary motion for various velocities of rotation, disbalance values, amplitudes and frequencies of outer forces are calculated. Conditions of contact free motion of the cylinder, rotating in the chamber, are determined.

Keywords: Influence of form, stability, gas, rotation.

1. Let us consider two horizontal coaxial circular cylinders with length L and radius R_1 and R_2 . The space between the cylinders is filled with viscous gas. The center of mass of the inner rigid solid cylinder (rotor) situated outside its rotational axis (static instability). The rotor moves round its symmetry axis with constant angular speed ω . Outer cylinder (chamber) is immovable. A gap between the cylinders is significantly less than their radii that is why to determine pressure distribution in a thin layer of viscous gas one can use Reynolds equation. In cylindrical coordinate system (r, φ, z) , axis z of which is oriented along the axis of outer cylinder, the equation for pressure p is the following [1,2].

$$(1) \quad \frac{1}{12\mu} \frac{\partial}{\partial z} \left(h^3 \rho \frac{\partial p}{\partial z} \right) + \frac{1}{12\mu R_1^2} \left(h^3 \rho \frac{\partial p}{\partial \varphi} \right) = \frac{\partial}{\partial t} (\rho h) + \frac{\omega}{2} \frac{\partial}{\partial \varphi} (\rho h),$$

where ρ is gas density; $h = h(\varphi)$ – local thickness of a gap between cylindrical surfaces ($R_1 \leq r \leq R_1 + h$); μ – coefficient of dynamic viscosity of gas.

Boundary conditions:

$$(2) \quad \text{given } z = \pm L/2 \quad p = p_0$$

(p_0 – pressure in the medium around the layer). Having found the field of pressure in the gas layer from the problem (1), (2), let us find the force applied by the gas to the rotating cylinder of length L :

$$(3) \quad F_x = -2 \int_0^{L/2} \int_0^{2\pi} p R_1 \cos \varphi dz d\varphi, \\ F_y = -2 \int_0^{L/2} \int_0^{2\pi} p R_1 \sin \varphi dz d\varphi$$

While calculating reaction of a gas layer we took into account only pressure forces. They are much more than frictional forces [2] with the accuracy which was used while deriving the equation (1). Motion of a cylinder rotating in the gravitational field under the action of outer forces which periodically change in time is described by the equations (in the coordinate system, connected with the center of the immovable chamber).

$$(4) \quad m\ddot{x} = F_x + m\delta\omega^2 \cos \omega t + mg(1 + a_1 \cos \omega_1 t), \\ m\ddot{y} = F_y + m\delta\omega^2 \sin \omega t + mga_2 \sin \omega_1 t.$$

Here m – rotor mass; δ – value of shift of mass center from rotation axis; g – acceleration due to gravity; a_1, a_2 – amplitudes of outer

periodic effects (i.e., a case when metal cylinder moves in alternating electromagnetic field); ω_1 – frequency of outer effects. At the beginning rotation axis coincides with a chamber axis.

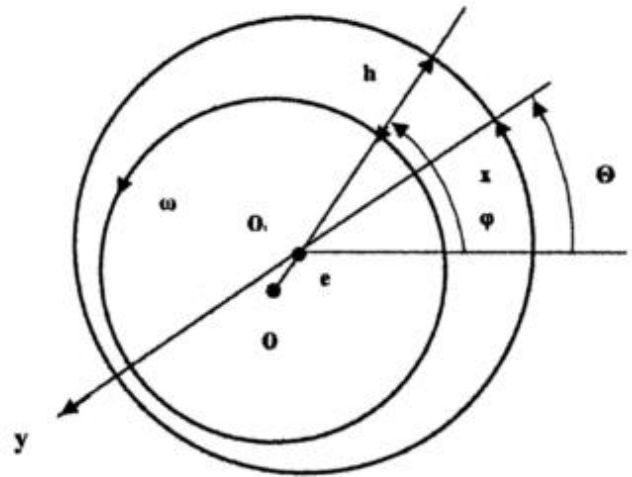


Fig. 1

2. Let us solve the problem of a rotor motion by the method of direct numerical integration of the set of equations describing a cylinder motion and pressure distribution in a gas layer [3, 4]. Let us rewrite the equation (1) in the form of the law of energy conservation of the volume $R_1 \Delta \varphi \Delta z h_j$; including the node i, j of the lattice in cylindrical coordinate system [5] ($\Delta \varphi$ – angular step dimension and Δz – is the step in a coordinate):

$$(5) \quad R_1 \Delta \varphi \Delta z \frac{\partial}{\partial t} (h_j \rho_{ij}) - \frac{h_j^3 \Delta \varphi R_1}{12\mu \Delta z} \left[\rho_{i+\frac{1}{2},j} (-p_{ij} + p_{i+1,j}) - \rho_{i-\frac{1}{2},j} (p_{ij} + p_{i-1,j}) \right] \left[\rho_{i,j+\frac{1}{2}} h_{j+\frac{1}{2}}^3 (p_{i,j+1} - p_{ij}) - \rho_{i,j-\frac{1}{2}} h_{j-\frac{1}{2}}^3 (p_{ij} - p_{i,j-1}) \right] + \frac{\omega R_1 \Delta z}{2} \left[\rho_{i,j+\frac{1}{2}} h_{j+\frac{1}{2}} - \rho_{i,j-\frac{1}{2}} h_{j-\frac{1}{2}} \right] = 0 \\ (i = 0, 1, 2, \dots, I-1, \quad j = 1, 2, \dots, J).$$

here

$$\Delta\varphi = \frac{2\pi}{J}; \Delta z = \frac{L}{2I}; \varphi_j = j\Delta\varphi; h_j = C - x\cos\varphi_j - y\sin\varphi_j;$$

C – mean value of radial gap; I, J – quantity lattice nodes in axial and peripheral direction. Relation between pressure and gas density is defined by ratio $\frac{p}{\rho} = \text{const}$.

Boundary condition (2) in the form of finite difference are the following:

$$(6) \quad p_{i,j} = p_0, p_{-1,j} = p_{1,j}, p_{i,0} = p_{0,j}, p_{i,j+1} = p_{i,1} \\ (i = 1, 2, \dots, I, j = 1, 2, \dots, J).$$

Here $\Delta\varphi = 2\pi/J$; $\Delta z = L/2I$; $\varphi_j = j\Delta\varphi$; I, J – quantity of lattice nodes in axial and peripheral direction. Relation between pressure and gas density is defined by the ratio $p/\rho = \text{const}$.

While writing ratios we used conditions of periodicity

$$p(z, \varphi) = p(z, \varphi + 2\pi)$$

and smoothness $\left(\frac{\partial p}{\partial z}\right)_{z=0} = 0$.

Let us consider equations (5) in dimensionless form, using the following units of measurements: a distance across the layer – C (mean value of radial gap), a distance along the layer – R_1 , time – $1/\omega$, pressure – p_0 :

$$(7) \quad 2\Delta\varphi\Delta z \frac{\partial}{\partial t}(h_j \rho_{i,j}) - \\ h_j^3 \frac{\Delta\varphi}{\Delta z} [\rho_{i+1/2,j}(p_{i-1,j} - p_{i,j}) - \rho_{i-1/2,j}(p_{i,j} - p_{i+1,j})] \\ = \frac{\Delta z}{\Delta\varphi} [\rho_{i,j+1/2} h_{j+1/2}^3 (p_{i,j+1} - p_{i,j}) - \\ - h_{j-1/2}^3 \rho_{i,j-1/2} (p_{i,j} - p_{i,j-1})] + \\ + \Delta\Delta z (\rho_{i,j+1/2} h_{j+1/2} - \rho_{i,j-1/2} h_{j-1/2}); \\ (h_j = 1 - x\cos\varphi_j - y\sin\varphi_j).$$

Using the method of varying direction [6] let us reduce the set problem of calculation of pressure field in a layer to a sequence of one-dimensional problems where we assign coefficients, non-linear terms and mass outlay of gas in axial direction to time moment $t_{k+1/2}$ (k – number of a time step) and other values – to t_k . Let us approximate the derivative $\partial p / \partial t$ by the difference formula of the second order centered with respect to $t_{k+1/4}$. We solve the derived nonlinear difference system of equations along the lattice lines considering index j as a parameter by the sweep method. Initial approach $p_{i,j}^0$ at every time step is defined with the help of linear extrapolation

$$(p_{i,j}^{k+1/2})^0 = 1, 5p_{i,j}^k - 0, 5p_{i,j}^{k-1} \quad k = 1, 2, \dots$$

where at the first time step $(p_{i,j}^{1/2})^0 = p_{i,j}^0$.

At the next stage of the method of varying directions in equations (7) let us refer linear components of mass outlays in peripheral directions to t_{k+1} and coefficients and other members of the equations to $t_{k+1/2}$, the derivative $\partial p / \partial t$ center with respect to

$t_{k+3/4}$. Then, following the method of the cyclic sweep method [7] find the pressure in all lattice nodes and the force effecting a rotor from a gas layer in the time moment t_{k+1} .

3. Let us consider the motion of a rotating unstable rotor in the field of gravity without periodic effects ($a_1 = a_2 = 0$). A rotor, being at the initial period of time in the center of a chamber, begins to move. Orbits of steady-state motion of the rotor are nearly circular ($\delta' = \delta/C = 0,3$; the velocity of rotation $n = 50 \text{ rev/s}$; $n = 350 \text{ rev/s}$).

Let us turn to studying motion of a rotor in the presence of set external periodic disturbances of the finite amplitude. Let us set disturbances only in vertical direction, i.e., we assume that $a_1 = 1$, $a_2 = 0$ and $\omega_1 = \omega$ (frequencies of the rotor motion and of external disturbances coincide). Calculations of trajectories of the rotor motion are carried out for the speed values of its rotation n in the interval from 50 to 3000 revolutions per second at the change of relative disbalance δ' from 0,1 to 1. Steady-state orbits of the rotor motion are close to vertical elliptic ones. It was found that at small ($n < n_1$) and big ($n > n_2$) velocities of rotation the motion of the cylinder was not stable: stationary closed trajectories of the axis of revolution were not formed and the rotor touched the chamber (Fig. 2). There is a limited zone of rotor velocities $[n_1, n_2]$ (Fig. 3) for a constant value of disbalance where it is possible for a rotor to move avoiding a contact with a chamber. Left boundary of a zone of steady-state orbits formation practically does not depend on relative disbalance and right boundary moves to the domain of big velocities of revolution with decreased disbalance. Small ellipticity of the chamber (the function of a gap in this case had the form of ([8]) $h_j = 1,066 - 0,133\cos^2\varphi_j - x\cos\varphi_j - y\sin\varphi_j$) caused extension of formation zone for steady-state elliptic trajectories by means of increasing of the biggest critical velocity of revolution n_2 . When velocity increases by the factor of 10 (from 50 to 1500 rev/s) the maximal amplitude of the orbit a increases by the factor of 33.

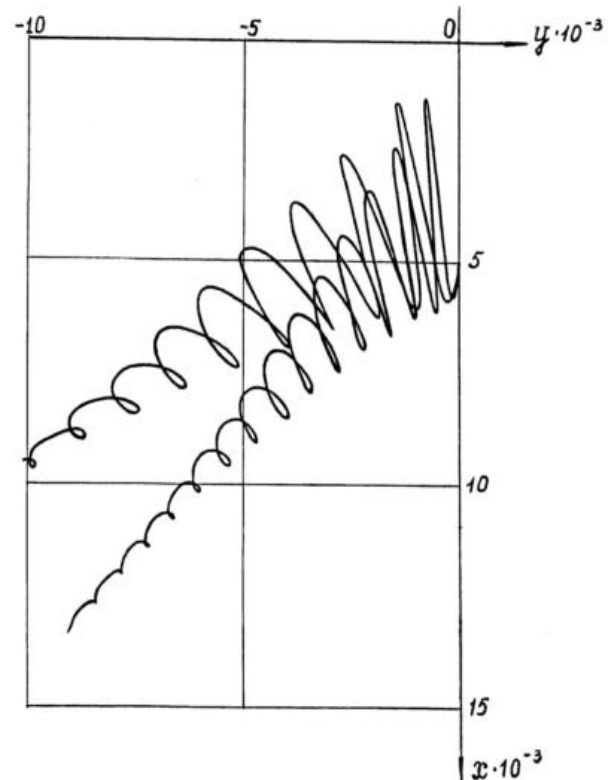


Fig. 2

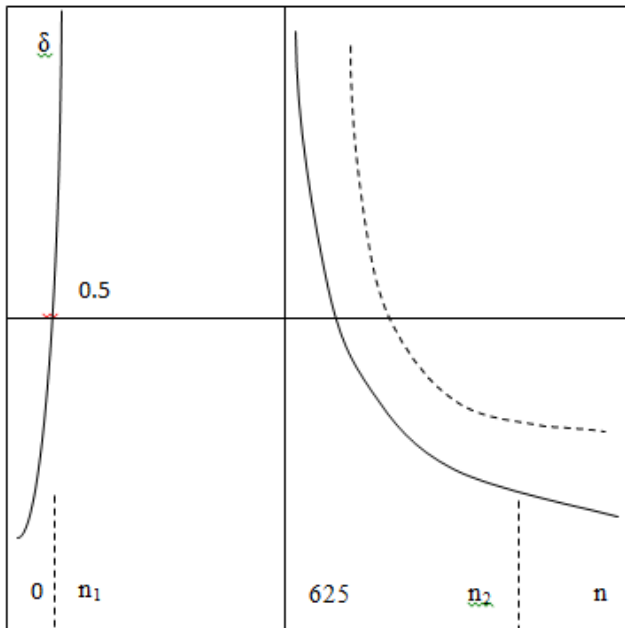


Fig.3

Increasing of the amplitude of horizontal disturbances a_2 up to 10 at low-frequency disturbances ($\omega_1 = 1s^{-1}$) actually does not distort steady-state circular trajectories of the rotor motion and does not cause their destruction. This conclusion confirms calculations carried out for velocities of cylinder rotation in the interval from 100 to 500 rev/s. At the amplitude of external effects equal to $a_2 = 100$

($a_1 = 0, \omega_1 = 1s^{-1}, n = 150$ rev/s) a cylinder gets in touch with a chamber very quickly ($\delta' = 0.3; a_1 = 0, a_2 = 1, \omega_1 = \omega = 2\pi 150 s^{-1}; a_1 = 0, a_2 = 0.1, \omega_1 = 1 s^{-1}, n = 150$ and 100 rev/s). Change of disbalance from 0,1 to 0,85 in the presence of vertical disturbances with the frequency equal a half of the rotor revolution frequency ($\omega = 200\pi s^{-1}, a_2 = 0, a_1 = 1$) does not influence significantly a formation and orientation of steady – state trajectories of the rotor. Influence of vertical disturbances of finite amplitude in comparison with the case of absence of disturbances causes increase of the amplitude of the steady-state trajectory by the factor of 8-10, shift of the orbit centre from the first quarter to the third quarter of the plane (x, y) and transformation of a circular orbit into an elliptic one.

$\omega = 200\pi s^{-1}, a_2 = 0, a_1 = 1$) does not influence significantly a formation and orientation of steady – state trajectories of the rotor. Influence of vertical disturbances of finite amplitude in comparison with the case of absence of disturbances causes increase of the amplitude of the steady-state trajectory by the factor of 8-10, shift of the orbit centre from the first quarter to the third quarter of the plane (x, y) and transformation of a circular orbit into an elliptic one.

REFERENCES

1. Kelzon A., Zimansky U., Yakovlev V. "The Dynamic of Rotor's in elastically Supports", Moscow, Nauka, 1982.
2. Konstantinesku V. "A Gaseous bearings" [russian translation]. Mashinostroenie, Moscow, "MIR" 1968.
3. Tondl A. "Some Problems of Rotor Dynamics", Publishing House of the Czechoslovak Academy of Sciences, Prague, London, 1965.
4. Loitzansky L. "Mechanics of fluid and gas", Moscow, Nauka,, 1978.
5. Agishev G. "Research method of dynamic rotor's rotating in radial gaseous Bearings". Mashinovedenie. 1984; No 2. P. 131-157.
6. Samarsky A. "Introduction in theory of differences schemes", Moscow, Nauka, 1984.
7. Samarsky A., Nikolaev E. "Methods of solution of grid equations", Moscow, Nauka, 1978.
8. Dementiev O.N., Makhova V.A. "The computation of rotor's motion in cylindrical chamber". J. Appl. Mech. and Tech. Phys. (PMTF), No. 5. 1991, P. 68-72.

MIXED VARIATIONAL PROPERTIES FOR SOME FOURTH-ORDER BEAM PROBLEMS

Prof. Andreev A. Dsc.^{1,2}, Assoc. Prof Racheva M. Dsc.¹,
 Technical University of Gabrovo, Bulgaria ¹
 Institute of Information and Communication Technologies – BAS, Bulgaria ²
 {andreev; milena}@tugab.bg

Abstract: In this paper we study eigenvalue problems for fourth-order ordinary differential equations. These boundary problems usually describe the bending vibrations of a homogeneous beam. Our aim here is to present mixed variational forms depending on a wide class of boundary conditions. In particular, we show when the symmetry in variational formulations is available. This property ensures real spectrum of the corresponding problem. The effect of the theoretical results is illustrated by some realistic examples.

Keywords: EIGENVALUE, FOURTH-ORDER PROBLEM, MIXED FORMULATION, BILINEAR FORM

2010 Mathematical Subject Classification: 65N25, 65N30

1. Introduction

We consider the eigenvalue problem

$$y^{IV}(x) - (q(x)y'(x))' = \lambda r(x)y(x), \quad 0 < x < l, \quad (1)$$

subject to some boundary conditions. Here, λ is a spectral parameter; $q(x)$ and $r(x)$ are real-valued positive and continuous functions.

Problem (1) arises in the dynamical boundary-value problem describing free bending vibrations of a homogeneous beam (see, e.g. [1]).

In order to apply the various Galerkin type numerical methods, we have to present the two-point problem (1) in a weak form, when taking into account the boundary conditions. The problems of the type under consideration are appropriate to be presented in a mixed form [2,3] for purpose to be solved numerically by means of mixed numerical methods. An advantage of the mixed variational method is that, along with the unknown function (the displacement), one find an approximation also of its second derivative [2].

Let $H^m(0, l)$ be the usual Sobolev space for a positive integer m .

Then for $z(x) \in H^2[0, l]$ from (1) we easily get the system:

$$\begin{cases} -y'' = z \\ -z'' - (qy')' = \lambda r y. \end{cases} \quad (2)$$

2. Main Result

The principal purpose is to find from (2) a mixed variational formulation according to the boundary conditions and similarly to prove under which type of boundary conditions the resulting mixed mathematical model is symmetric.

Let us introduce the test functions $y_I(x) \in H^1(0, l)$ and $z_I(x) \in H^1(0, l)$. Multiplying the first equation from (2) by z_I and the second by y_I and integrating on the interval $[0, l]$, we obtain:

$$\begin{cases} -\int_0^l y'' z_I dx = \int_0^l z z_I dx \\ -\int_0^l [z' - (qy')] y_I dx = \lambda \int_0^l r y y_I dx, \end{cases}$$

which yields

$$\begin{cases} -y' z_I|_0^l + \int_0^l y' z_I' dx = \int_0^l z z_I dx \\ -[z' - (qy')] y_I|_0^l + \int_0^l [z' y_I + qy' y_I] dx = \lambda \int_0^l r y y_I dx. \end{cases} \quad (3)$$

We denote by ξ any of the endpoints, i.e. $\xi = 0; l$. Taking into account the boundary conditions, the products $y' z_I$ and $[z' - (qy')] y_I$ should be presented at the endpoints as symmetric expressions with respect to the pairs of functions $z; y$ and $z_I; y_I$ and thus the problem under consideration would have symmetric mixed formulation.

(A) $y' z_I$ is a symmetric expression at the endpoint $\xi = 0; l$ when the boundary conditions at $\xi = 0; l$ are of the type:

- $(a_1) \quad y'(\xi) = 0;$
- $(a_2) \quad y''(\xi) = 0.$

As $-y'' = z$, the boundary condition of (2) is $z(\xi) = 0$. This would be an essential condition for the system (2), hence the function z_I would also satisfy this condition for (3);

- $(a_3) \quad k_I y''(\xi) + y'(\xi) = 0$, with $k_I \neq 0$.

This boundary condition is of type $y'(\xi) - k_I z(\xi) = 0$ for the system (2).

Thus at the point $\xi = 0; l$ we have either $y'(\xi) z_I(\xi) = 0$ or $y'(\xi) z_I(\xi) = k_I z(\xi) z_I(\xi)$, where $k_I \neq 0$. That means:

$$-y'z_I|_0^l = k_{I,0} z(0) z_I(0) - k_{I,l} z(l) z_I(l), \quad (4)$$

where the constants $k_{I,0}$ and $k_{I,l}$ could be equal to zero.

(B) $[z' - (qy')]y_I$ represents a symmetric expression at the endpoints, if the boundary conditions at $\xi = 0; l$ are of the type:

$$\bullet \quad (b_I) \quad y(\xi) = 0.$$

This is an essential boundary condition, consequently the function y_I would satisfy it;

$\bullet \quad (b_2) \quad y'''(\xi) - q(\xi)y'(\xi) = 0$, which for the problem (2) is transformed to:

$$z'(\xi) - q(\xi)y'(\xi) = 0;$$

$\bullet \quad (b_3) \quad y'''(\xi) - q(\xi)y'(\xi) = k_2 y(\xi) + \lambda k_3 y(\xi)$, with $(k_2, k_3) \neq (0, 0)$.

For the problem (2) this equality takes the form:

$$z'(\xi) - q(\xi)y'(\xi) = k_2 y(\xi) + \lambda k_3 y(\xi).$$

Hence, it is clear that if at the endpoint $\xi = 0; l$ there is a boundary condition of type $(b_I) - (b_3)$, then either

$$[z'(\xi) - q(\xi)y'(\xi)]y_I(\xi) = 0$$

or

$$[z'(\xi) - q(\xi)y'(\xi)]y_I(\xi) = -(k_2 + \lambda k_3)y(\xi)y_I(\xi),$$

where $(k_2, k_3) \neq (0, 0)$.

That means:

$$\begin{aligned} & -[z' - (qy')]y_I|_0^l \\ & = (k_{2,0} + \lambda k_{3,0})y(0)y_I(0) - (k_{2,l} + \lambda k_{3,l})y(l)y_I(l), \end{aligned} \quad (5)$$

and it is possible that $(k_{2,\xi}, k_{3,\xi}) = (0, 0)$ for $\xi = 0; l$.

From the variational presentation (3), as well as from (4) and (5), it follows the system:

$$\begin{aligned} & \int_0^l y' z_I dx - \int_0^l z z_I dx + k_{I,0} z(0) z_I(0) - k_{I,l} z(l) z_I(l) = 0 \\ & \int_0^l z' y_I dx + \int_0^l q y' y_I dx + k_{2,0} y(0) y_I(0) - k_{2,l} y(l) y_I(l) \\ & = \lambda \left[\int_0^l r y y_I dx - k_{3,0} y(0) y_I(0) + k_{3,l} y(l) y_I(l) \right]. \end{aligned} \quad (6)$$

The considerations above allow us to formulate the following theorem:

Theorem 1. The mixed problem (2) has symmetric variational formulation if at any endpoint the boundary conditions are of the type $(a_i), (b_j), i, j = 1, 2, 3$.

Let us introduce the following symmetrical bilinear forms:

$$a(u, v) = \int_0^l u' v' dx; \quad b(u, v) = \int_0^l r u v dx;$$

$$a_I(u, v) = \int_0^l q u' v' dx; \quad b_I(u, v) = \int_0^l u v dx;$$

$$c_I(u, v) = k_{I,0} u(0) v(0) - k_{I,l} u(l) v(l);$$

$$c_2(u, v) = k_{2,0} u(0) v(0) - k_{2,l} u(l) v(l);$$

$$c_3(u, v) = k_{3,0} u(0) v(0) - k_{3,l} u(l) v(l).$$

From (6), it is easy to present the variational formulation in symmetric equation

$$\begin{aligned} & a(y, z_I) + a(y_I, z) + a_I(y, y_I) - b_I(z, z_I) + c_I(z, z_I) + c_2(y, y_I) \\ & = \lambda [b(y, y_I) - c_3(y, y_I)] \end{aligned} \quad (7)$$

Obviously, the last presentation is symmetric with respect to the couples of functions (z, y) and (z_I, y_I) .

3 Application to Some Actual Problems

In this section we consider various tasks illustrating the result of Theorem 1. Some of them contain the spectral parameter in the boundary conditions (see, e.g. [4, 8-13]).

Problem 1. First we consider a mathematical model describing free bending vibrations of a homogeneous beam of constant rigidity. Both ends are fixed elastically and on these ends the servocontrol forces are in acting [6, 7, 8]:

$$y^{IV}(x) - (q(x)y'(x))' = \lambda r(x)y(x), \quad 0 < x < l,$$

$$y''(0) = y''(l) = 0,$$

$$y'''(0) - q(0)y'(0) - a\lambda y(0) = 0,$$

$$y'''(l) - q(l)y'(l) - c\lambda y(l) = 0.$$

Here $q(x)$ is a positive and absolutely continuous function on $[0, l]$, a and c are real constants such that $a > 0, c < 0$.

The first two boundary conditions are of type (a_2) .

Comparing with the adopted notations we have:

$$l = l; \quad r(x) = r; \quad k_{i,\xi} = 0, i = 1, 2, \xi = 0; l,$$

whereas

$$k_{3,0} = a, \quad k_{3,l} = c.$$

Also $c_1(u, v) = c_2(u, v) \equiv 0$ and on account of the sign of a and c the bilinear form $c_3(u, v) = au(0)v(0) - cu(1)v(1)$ is positive.

It should be noted that the last two boundary conditions, containing the spectral parameter λ , are related to the type (b_3) .

In this way, the Problem 1 assumes symmetric mixed variational formulation.

Problem 2. Let us consider the bending vibrations of a homogeneous rod, in cross-section of which the longitudinal force acts. The left end is fixed rigidly and the right one is fixed elastically and on the some endpoints the inertial mass is concentrated [6, 9]:

$$y^{IV}(x) - (q(x)y'(x))' = \lambda r(x)y(x), \quad 0 < x < l,$$

$$y(0) = y'(0) = 0,$$

$$y''(l) - b_1 y'(l) - a_1 \lambda y(l) = 0,$$

$$y'''(l) - q(l)y'(l) - a_2 \lambda y(l) = 0.$$

Here $q(x)$ is a positive and absolutely continuous function in $[0, l]$, a_1 , a_2 and b_1 are real constants.

For this problem we have: $l = l$; $r(x) = 1$.

The boundary conditions at the left endpoint are of type (b_1) and (a_1) , respectively and furthermore

$$k_{1,0} = k_{2,0} = k_{3,0} = 0.$$

The last boundary condition is of type (b_3) with

$$k_{2,l} = 0, \quad k_{3,l} = a_2.$$

Such being the case, Problem 2 would have symmetric mixed variational formulation if the third boundary condition is of type (a_i) , $i = 1, 2, 3$. This is fulfilled in case when $a_1 = 0$ only, at that the condition is of type (a_2) if $b_1 = 0$ and of type (a_3) otherwise.

Problem 3. Consider the spectral problem [10]:

$$y^{IV}(x) - (q(x)y'(x))' = \lambda y(x), \quad 0 < x < l,$$

$$y''(0) \sin \alpha - y'(0) \cos \alpha = 0,$$

$$(y'''(0) - q(0)y'(l)) \sin \beta + y(0) \cos \beta = 0,$$

$$y''(l) \sin \gamma + y'(l) \cos \gamma = 0,$$

$$(y'''(l) - q(l)y'(l))(c\lambda + d) - (a\lambda + b)y(l) = 0,$$

where $q(x)$ is a positive and absolutely continuous function on the interval $[0, l]$ and $\alpha, \beta, \gamma, a, b, c, d$ are real constants such that

$$\alpha, \beta, \gamma \in \left[0, \frac{\pi}{2}\right].$$

First, let us note that $r(x)$ is assumed to be constant (equal to 1).

Evidently the first boundary condition is of type:

(a_1) when $\alpha = 0$ and thus $k_{1,0} = 0$;

(a_2) when $\alpha = \frac{\pi}{2}$ and again $k_{1,0} = 0$;

(a_3) when $\alpha \in \left(0, \frac{\pi}{2}\right)$ and thus $k_{1,0} = \tan \alpha$.

Similarly, the third boundary condition is of type:

(a_1) when $\gamma = 0$ and thus $k_{1,l} = 0$;

(a_2) when $\gamma = \frac{\pi}{2}$ and again $k_{1,l} = 0$;

(a_3) when $\gamma \in \left(0, \frac{\pi}{2}\right)$ and thus $k_{1,l} = -\tan \gamma$.

For the second boundary condition we establish that it is of type:

(b_1) when $\beta = 0$, then $k_{2,0} = k_{3,0} = 0$;

(b_2) when $\beta = \frac{\pi}{2}$ and again $k_{2,0} = k_{3,0} = 0$;

(b_3) when $\beta \in \left(0, \frac{\pi}{2}\right)$, consequently $k_{2,0} = -\cot \beta$; $k_{3,0} = 0$.

According to Theorem 1, Problem 3 assumes symmetric mixed variational formulation if the last boundary condition is of type (b_j) , $j = 1, 2, 3$. The only way of this is $c = 0$, which yields that the last boundary condition is of type:

(b_3) when $a \neq 0, b \neq 0, d \neq 0$, at that $k_{2,l} = \frac{b}{d}$, $k_{3,l} = \frac{a}{d}$;

(b_2) when $a = b = 0, d \neq 0$, thus $k_{2,l} = k_{3,l} = 0$;

(b_1) when $(a, b) \neq (0, 0), d = 0$ and $k_{2,l} = k_{3,l} = 0$.

As a conclusion, Problem 3 has got a symmetric mixed variational representation in case when $c = 0$ only.

Problem 4. This problem is derived from a wave equation which describes the vibration of a nonhomogeneous rod or beam clamped at one end (e.g., [5, 7, 11]):

$$y^{IV}(x) - (q(x)y'(x))' = \lambda r(x)y(x), \quad 0 < x < l,$$

$$y(0) = y'(0) = 0,$$

$$y''(l) \sin \gamma + y'(l) \cos \gamma = 0,$$

$$(y'''(l) - q(l)y'(l)) \sin \delta - y(l) \cos \delta = 0,$$

where the coefficients $r(x)$ and $q(x)$ are assumed to be real-valued and continuous functions, $r(x) > 0$, $\gamma \in \left[0, \frac{\pi}{2}\right]$, $\delta \in [0, \pi]$.

The boundary conditions at the left endpoint are of type (b_1) and (a_1) , respectively, so that for Problem 4

$$k_{1,0} = k_{2,0} = k_{3,0} = 0.$$

Just like for Problem 3, the third boundary condition is of type:

(a_1) when $\gamma = 0$ and thus $k_{1,l} = 0$;

(a_2) when $\gamma = \frac{\pi}{2}$ and again $k_{1,l} = 0$;

(a_3) when $\gamma \in \left(0, \frac{\pi}{2}\right)$ and thus $k_{1,l} = -\tan \gamma$.

In much the same manner, the fourth boundary condition is of type:

(b_1) when $\delta = 0$ or $\delta = \pi$, then $k_{2,l} = k_{3,l} = 0$;

(b_2) when $\delta = \frac{\pi}{2}$ and again $k_{2,l} = k_{3,l} = 0$;

(b_3) when $\delta \in \left(0, \frac{\pi}{2}\right) \cup \left(\frac{\pi}{2}, \pi\right)$ and in this case $k_{2,l} = \cot \delta$; $k_{3,l} = 0$.

Ultimately, in any case Problem 4 have symmetric mixed variational formulation.

Problem 5. At last we consider one more problem for which the spectral parameter appears in the boundary conditions [12, 13]:

$$y^{IV}(x) - (q(x)y'(x))' = \lambda r(x)y(x), \quad 0 < x < \pi,$$

$$y(0) = y'(0) = y'(\pi) = 0,$$

$$y'''(\pi) - q(\pi)y'(\pi) + m\lambda y(\pi) = 0.$$

Here, $q(x)$ and $r(x)$ are real-valued functions from the space $C[0, \pi]$, $r(x) > 0$, and $m \in \mathbb{R}$ is a physical parameter [13] and $l = \pi$.

The first three boundary conditions are of type (b_1) , (a_1) and (a_2) , respectively, so that

$$k_{1,0} = k_{2,0} = k_{3,0} = 0 \text{ and } k_{1,\pi} = 0.$$

The last boundary condition is of type (b_3) , and $k_{2,\pi} = 0$, $k_{3,\pi} = -m$.

Therefore, $c_1(u, v) = 0$, $c_1(u, v) = 0$, $c_3(u, v) = m u(\pi) v(\pi)$ and in any case Problem 5 have symmetric mixed variational formulation.

3. Conclusions

The paper contains a useful result related to the mixed formulation of fourth-order eigenvalue problems. Namely, requirements on the boundary conditions providing symmetrical presentation of the problem are proved. This result is demonstrated for various beam problems.

Acknowledgements This work was partially supported by the Technical University of Gabrovo under grant D1804E/2018.

References

1. W. Weaver, S. P. Timoshenko, D. H. Young. Vibration problems in engineering. John Wiley & Sons, 1990.
2. I. Babuška, J. Osborn, Eigenvalue Problems, In Handbook of Numerical Analysis, Vol. II, (Eds. P. G. Lions and Ciarlet P.G.), Finite Element Methods (Part 1) North-Holland, Amsterdam, 641-787, 1991.
3. M. Racheva, Mixed variational formulation for some fourth order beam problems, Comp. rend. Acad. bulg. Sci. Tome 64, No 11, 2011, 1525-1532.
4. M. R. Racheva, A. B. Andreev, Variational aspects of one-dimensional fourth-order problems with eigenvalue parameter in the boundary conditions, Sib. JNM, No4(5), 373 – 380, 2002.
5. L. Collatz, Eigenwertprobleme und ihren numerische Behandlung, Chelsea, New York, 1948.
6. B. B. Bolotin. Vibrations in technique: Handbook in 6 volumes, The vibrations of linear systems, I, Engineering Industry, Moscow, 1978.
7. M. Roseau. Vibrations in Mechanical Systems. Springer-Verlag, Berlin, New York, 1987.
8. Z. S. Aliyev, F. M. Namazov, Spectral properties of a fourth-order eigenvalue problem with spectral parameter in the boundary conditions. Electronic Journal of Differential Equations, 2017(307), 1-11.
9. S. B. Guliyeva, Basis properties of the system of eigenfunctions of a fourth order eigenvalue problem with spectral parameter in the boundary conditions, Transactions of NAS of Azerbaijan, Issue Mathematics, 37 (4), 42–48 (2017).
10. N. B. Kerimov, Z. S. Aliev, On the basis property of the system of eigenfunctions of a spectral problem with spectral parameter in the boundary condition, Differential Equations 43.7, 905-915 (2007).
11. J. B. Amara, Sturm theory for the equation of vibrating beam. Journal of Mathematical Analysis and Applications, 349(1), 1-9 (2009).
12. J. B. Amara, Fourth order spectral problem with eigenvalue in the boundary conditions, North-Holland Mathematics Studies. Vol. 197, North-Holland, 49-58 (2004).
13. J. B. Amara, A. A. Vladimirov, On a fourth-order problem with spectral and physical parameters in the boundary condition, Izvestiya: Mathematics 68.4 (2004): 645. (in Russian)

MODELING OF THE 3D UNSTEADY MULTISCALE MULTIPHASE FLUID FLOW WITH SHOCKS: NUMERICAL METHODS AND IMPLEMENTATION ALGORITHMS

Korneev B., Levchenko V. PhD.

Keldysh Institute of Applied Mathematics RAS, Moscow, Russian Federation
boris.korneev@phystech.edu, lev@keldysh.ru

Abstract: Numerical simulation is widely applied in the fluid dynamic research. Unsteady multiphase flow with high Mach and Reynolds numbers has high physical and mathematical fidelity and a special approach of its correct modeling is required. In this paper the appropriate numerical methods and special algorithms of implementation are developed for high-performance numerical modeling using the modern computational systems. The results of validation tasks and problems of practical importance are presented.

Keywords: COMPUTATIONAL FLUID DYNAMICS, GPU COMPUTING, LRnLA ALGORITHMS, SHOCK WAVES, DROPLET BREAKUP

Introduction

Since the second half of the twentieth century, high-performance computer technologies have been widely used to solve problems in computational fluid dynamics [1]. At the moment, computational fluid dynamics (CFD) is one of the main methods for solving engineering problems of designing parts, devices and other objects with the required fluid dynamic properties.

For high-precision modeling “from the first principles,” meaning without specifying and narrowing the mathematical formulation of the problem, it may be necessary (but not sufficient) to use detailed grids and a large number of iterations in the calculation. Let some estimates be given. The numerical region is characterized by some size range, which is usually determined by the characteristic spatial scale for the simulated process. The number of discrete elements along one axis is usually has to be taken in the range of $10^2 - 10^3$ or more. Consequently, the number of cells used for a three-dimensional numerical experiment is estimated from 10^6 and can reach $10^9 - 10^{12}$ and more. The number of iterations in time is determined by the characteristic time scale for the considered process, taking into account the restrictions on the time step, for example, the Courant condition. The number of time steps can be up to 10^6 or more for actual tasks. Thus, the number of operations for calculating a single cell of a numerical scheme is $10^{12} - 10^{18}$ for one numerical experiment. The operation of calculating a single cell of a numerical scheme may require dozens of elementary operations of addition-multiplication for the simplest explicit schemes up to tens of thousands, depending on the complexity of the numerical scheme.

To solve problems of this scale [2], it is necessary to use modern computer hardware with a complex hierarchical structure of computing units and memory system. From set of modern computing systems the ones equipped with graphical accelerators are outstanding due to their high performance at a relatively low cost [3; 4]. For the effective use of such computing systems it is necessary to develop and use suitable calculation algorithms that take into account their features. So, effective implementation must be adapted to the hierarchical memory structure from the CPU memory to the registers CPU/GPU without creating bottlenecks that slow down the speed of calculation [5]. In addition, the problem of efficient parallelization of the algorithm, taking into account the massive parallelism of the GPU, remains relevant. A separate issue remains the requirement of saving memory when building an implementation algorithm, with the help of which it is possible to simulate a domain with as large as possible number of cells within the available memory of the given computer. Due to the fact that the video card's memory is less than the RAM of the CPU, the video card's memory is often not enough to store the entire computing area, which makes the problem to exchange between the GPU

memory and the CPU one. To build an effective implementation, it is advisable to take into account these issues.

The content of the paper is the following. In the next section the mathematical and numerical model is set. Then the proper implementation algorithm is described. Third section is devoted to the validation of the program based upon the algorithm and numerical scheme. In the following section the simulation results of some real tasks of practical importance is considered. In the conclusion we summarize the research.

1. Governing equations and numerical scheme

1.1 Equations of gas dynamics

The system of Navier-Stokes equations describing the dynamics of a viscous compressible fluid or gas in three-dimensional space [6], is represented as

$$\frac{\partial U}{\partial t} + \frac{\partial F_i}{\partial x_i} = 0,$$

where $U = (\rho, \rho u_i, E)$ are the gas variables, $[F(U)]_i = \left[\rho u_i, \rho u_i u_j + P_{ij}, u_i E + P_{ij} u^j - \kappa \frac{\partial T}{\partial x_i} \right]$ are fluxes, pressure tensor $P_{ij} = p\delta_{ij} - \mu \left(\frac{\partial u_i}{\partial x_j} + \frac{\partial u_j}{\partial x_i} \right) - \frac{\partial u_k}{\partial x_k} \left(\zeta - \frac{2}{3}\mu \right) \delta_{ij}$ taking the viscous forces into the account. The system is extended by the equation of state $p = p(\rho, \varepsilon)$. More complex equations of state are considered for the fluid mixtures [7].

We rewrite the fluxes to separate pure convective (Euler) and viscous (Navier-Stokes) parts as follows:

$$\frac{\partial U}{\partial t} + \frac{F_i^{Eu}}{\partial x_i} + \frac{F_i^{NS}}{\partial x_i} = 0,$$

where $F_i^{Eu} = [\rho u_i, \rho u_i u_j + p\delta_{ij}, u_i(E + p)]$ and

$$F_i^{NS} = [0, -\mu \left(\frac{\partial u_i}{\partial x_j} + \frac{\partial u_j}{\partial x_i} - \frac{\partial u_k}{\partial x_k} \left(\zeta - \frac{2}{3}\mu \right) \delta_{ij} \right), -\mu \left(\frac{\partial u_i}{\partial x_j} + \frac{\partial u_j}{\partial x_i} \right) u^j - \frac{\partial u_k}{\partial x_k} \left(\zeta - \frac{2}{3}\mu \right) u_i - \kappa \frac{\partial T}{\partial x_i}].$$

1.2 Runge-Kutta discontinuous Galerkin method

Suppose we construct a numerical solution of the fluid dynamics system in the domain $G \in \mathbb{R}^3$, $t > 0$ with boundary ∂G with some given initial conditions for $t = 0$ and boundary conditions. We introduce the discretization of the space G using a grid of finite volumes.

In each cell L , we introduce a set of basis functions $\{\varphi^n\}$, and the solution will be sought as an expansion in this basis for each

component of the desired vector $U = u_s(t)\varphi^s(x)$, while the basis coefficients are functions of time.

In this paper, we use a generalization of this method to approximate dissipative terms in the Navier-Stokes equation, known as the LDG method (local discontinuous Galerkin method [8]). We introduce a set of new variables for spatial derivatives in the flux F_i^{NS}

$$W = \frac{\partial u_i}{\partial x_j}, \quad S = \frac{\partial T}{\partial x^i};$$

and for them we apply the same expansion in the basis.

Obtained expressions are inserted into the main equations and the condition of the orthogonality of the residual to all basis functions is accepted to obtain the system of ODE on the basis coefficients:

$$\frac{du_m(t)}{dt} + \oint_{\partial L} (F_i^{Eu} + F_i^{NS}) \varphi_m n^i d\Sigma - \iiint_L F_i \frac{\partial \varphi_m}{\partial x_i} dV = 0;$$

$$w_m(t) = \oint_{\partial L} u_i n^j \varphi_m d\Sigma - \iiint_L u_i \frac{\partial \varphi_m}{\partial x_j} dV;$$

$$s_m(t) = \oint_{\partial L} T n^j \varphi_m d\Sigma - \iiint_L T \frac{\partial \varphi_m}{\partial x_j} dV;$$

Calculation of $\oint_{\partial L} F_i^{Eu} \varphi_m n^i d\Sigma$ is made using the specified Riemann solver [9].

Numerical solution of the given ODE is performed using the explicit Runge-Kutta method with the limiter [10, 11].

2. DiamondTorre implementation algorithm

In the introduction of the paper the necessity of the proper algorithm of implementation for the constructed numerical scheme has been noticed. This paper is considered the DiamondTorre algorithm. Originally developed as an optimal locally-recursive non-locally asynchronous algorithm [12] for explicit numerical schemes with the stencil “cross”, in this paper DiamondTorre algorithm is being developed the RKDG scheme of the method for solving gas dynamics problems. Despite the fact that the stencil of the RKDG method itself is not a “cross”, each of its substage has a substencil “cross” [13].

The calculation of the problem using this algorithm is conveniently thought of as filling the computational area with towers. The essence of each brick of the tower with coordinates (x_i, y_j, t_k) is performing part of the calculation according to a numerical scheme over the entire segment (x_i, y_j, Nz, t_k) , it can be execution stages of calculation of dissipative members, Runge-Kutta or limiters. We will assume that the coordinates of the tower are the coordinates of its lower left brick in the xt plane. The parameter $NT \geq 1$ determines how many time steps are calculated with one iteration of the algorithm. In the xt plane each tower is built bottom up on the t axis, and for x in the direction of its slope. At each iteration of the algorithm filling the area in the xy plane goes from right to left, starting from the right border at x , and on each x_i , $i \in 0, \dots, Nx - 1$ towers are built through one along the y axis, while if at $x = x_i$ the towers were built only on even y , then at $x = x_{i-1}$ towers are built only on odd y . We use the fact that the substage calculation algorithms have all the pattern of type “cross”, with dependencies on the adjacent six cells.

The development of the fluid solver is made using the CUDA C++ technology. The DiamondTorre algorithm is friendly to CUDA programming tools as the Torres are evaluated by CUDA blocks and each z component inside the Torre is associated to each CUDA thread. Data copying between GPU and CPU is diminished.

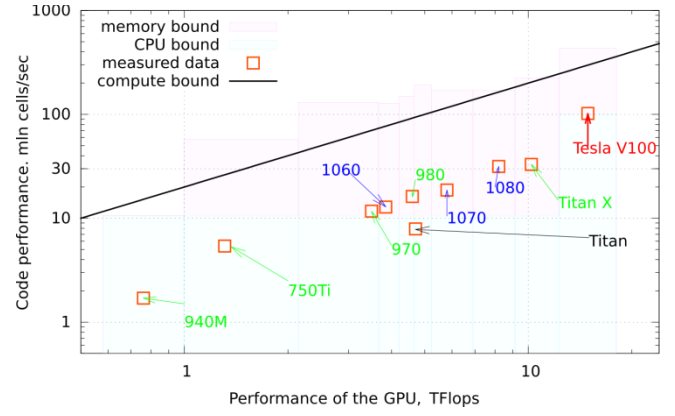


Fig. 1. The performance test of the developed software based on the DiamondTorre algorithm for different GPUs.

The performance tests show very good results. Gained speed is more than 10^8 cells per second on top-tier GPU. Full Navier-Stokes solver is considered in the examination. The results of testing on wide range of processors are shown in figure 1.

3. Validation

Several validation problems are considered: 1D, 2D and 3D.

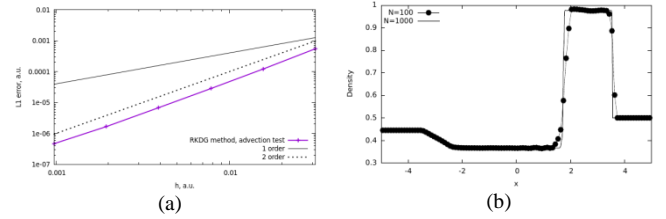


Fig. 2. (a) – the convergence of the solver for the 1D advection test; (b) – the results of density profile for 1D Sod problem.

In figure 2 the results of 1D testing are shown. Fig. 2a describes the convergence order of the RKDG scheme based upon linear basis and 2-stage Runge-Kutta method investigated using the pure advection setting. In the 2b one can see the results of solving the Riemann problem of Sod [9], showing good shock capturing and low dissipation of the scheme.

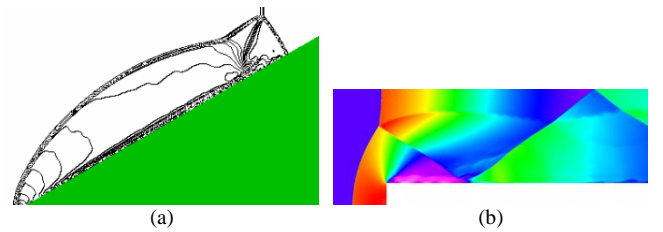


Fig. 3. (a) – 2D supersonic $M=10$ flow past a wedge, density levels drawn; (b) – density field for the 2D flow past a step obstacle, $M=3$.

In fig. 3 the widely used two-dimensional test problems of the flow past the wedge (fig. 3a) and the flow past the forward-facing step (fig. 3b). The good agreement with the known data is obtained.

Finally, the test of spherical Sod problem is considered [9]. The initial setting at the 3D Cartesian grid and the simulated density profile is shown in fig. 4.

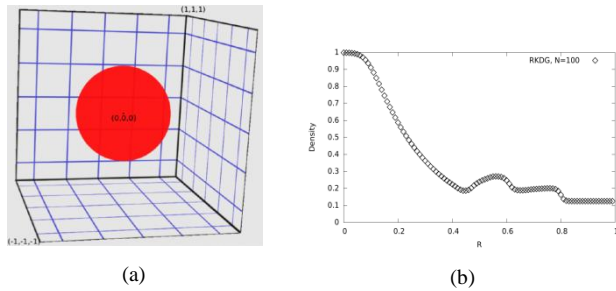


Fig 4. (a) – setting for the 3D spherical Sod problem; (b) – density profile.

Validation results show good quality of obtained solutions, allowing the application of the software for the practical problems.

4. Modeling results and discussion

The actual problems that researchers are usually faced with are complex flows of many components/phases and/or complex geometry. Due to the high performance of considered CFD solver, the “brute force” method of using extra-high grid resolution is possible to apply for these types of problems.

The first considered problem is the process of interaction between the shock wave and the heterogeneity. In fig. 5 the result of simulation of $M=2$ shock interacting with the high-density heterogeneity of complex initial shape (particularly inspired by letters *K* and *L*) is shown.

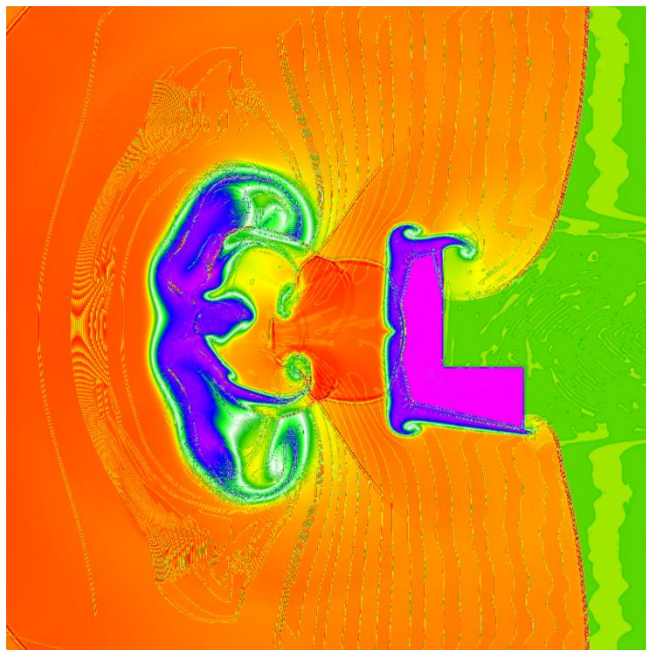


Fig 5. Interaction of a $M = 2$ shock with a high dense heterogeneity $At = 0.9$ of complex shape; density gradient field

From the knowledge of bubble-shock interaction problem, one can get that for the case of $At > 0$ the flow has unstable turbulent pattern [14], as proven by the current simulation.

The second problem concerns the secondary breakup of liquid droplets in the gas flow [15]. The following setup is used: $M = 0.3$ flow is given at initial time, the spherical droplet of incompressible fluid having surface tension force is put in the flow. The ratio between the kinetic energy of the flow and the Laplace energy of droplet (Atwood number At) describes the behavior of the droplet consistency. Experimental and numerical data shows that there are different regimes of the droplet breakup depending on the At number.

For this numerical experiment the current RKDG code for the gas is combined with the special GPU LBM solver for simulating non-compressible liquid. Gas simulation is much more computationally difficult, so the liquid solution is treated as the boundary condition for the gas at every time step. Simulation is performed using GeForce GTX 1080 GPU during several hours. Grid size is $256 \times 128 \times 128$ for each simulation.

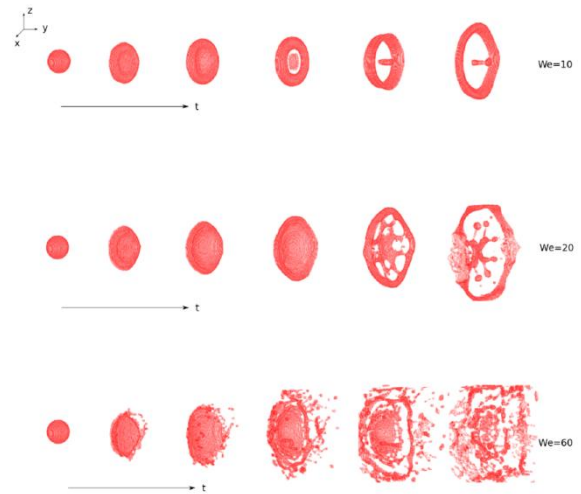


Fig 5. Combined RKDG and LBM simulation of liquid droplet breakup under the gas flow (Mach number $M=0.3$) at different Weber numbers: 10 (top line), 12 (middle), 60 (bottom). Droplet evolution at the time moments $t=0$ (left), $t=10, \dots, t=70$ microseconds (right) is shown.

We obtain the qualitative agreement with the known pattern of the droplet breakup [15, 16, 17].

5. Conclusion

The main results of the paper are following. In the framework of the work, a numerical scheme for solving Navier-Stokes equations for a three-dimensional Cartesian grid is created. For the scheme, the GPU algorithm implementation of DiamondTorre is developed. A software package using CUDA C++ is developed. Positive results of the program validation for the series 1D, 2D and 3D tests are obtained. Application of solver for solving complex engineering research problems of the interaction of the gas inhomogeneity with a shock and the disintegration of droplets in a gas stream is shown.

Acknowledgments

The work is supported by the Russian Science Foundation grant no.18-71-10004. Also Kintech Lab Company is gratefully acknowledged.

References

1. Flow simulation and high performance computing / T. Tezduyar [et al.] // Computational Mechanics. — 1996. — Vol. 18, no. 6. — Pp. 397–412.
2. Geller T. Supercomputing's exaflop target // Communications of the ACM. — 2011. — Vol. 54, no. 8. — Pp. 16–18.
3. Nickolls J., Dally W. J. The GPU Computing Era // IEEE Micro. — 2010. — Vol. 30, no. 2. — Pp. 56–69.
4. Hagen T. R., Lie K.-A., Natvig J. R. Solving the Euler equations on graphics processing units // International Conference on Computational Science. — Springer. 2006. — Pp. 220–227.
5. Brodtkorb A. R., Hagen T. R., Sætra M. L. Graphics processing unit (GPU) programming strategies and trends in GPU computing // Journal of Parallel and Distributed Computing. — 2013. — Vol. 73, no. 1. — Pp. 4–13. Metaheuristics on GPUs.

6. Batchelor G. K. An introduction to fluid dynamics. – Cambridge university press, 2000.
7. Abgrall R. How to prevent pressure oscillations in multicomponent flow calculations: a quasi conservative approach // Journal of Computational Physics. – 1996. – V. 125. – No. 1. – P. 150-160.
8. Cockburn B., Shu C.-W. The local discontinuous Galerkin method for timedependent convection-diffusion systems // SIAM Journal on Numerical Analysis. — 1998. — Vol. 35, no. 6. — Pp. 2440—2463.
9. Toro E. Riemann Solvers and Numerical Methods for Fluid Dynamics: A Practical Introduction. — Springer, 2009.
10. Krivodonova L. Limiters for high-order discontinuous Galerkin methods // Journal of Computational Physics. — 2007. — Vol. 226, no. 1. — Pp. 879—896.
11. Moe S. A., Rossmanith J. A., Seal D. C. A simple and effective high-order shock-capturing limiter for discontinuous Galerkin methods // arXiv preprint arXiv:1507.03024. — 2015.
12. Levchenko V. D., Perepelkina A. Y. Locally recursive non-locally asynchronous algorithms for stencil computation // Lobachevskii Journal of Mathematics. – 2018. – V. 39. – No. 4. – P. 552-561.
13. Korneev B. A., Levchenko V. D. Simulating three-dimensional unsteady viscous compressible flow on GPU using the DiamondTorre algorithm // Preprints of the Keldysh Institute of Applied Mathematics. – 2018. – . 105-17.
14. Korneev B., Levchenko V. Numerical simulation of increasing initial perturbations of a bubble in the bubble–shock interaction problem // Fluid Dynamics Research. – 2016. – V. 48. – No. 6. – P. 061412.
15. Hinze J. Fundamentals of the hydrodynamic mechanism of splitting in dispersion processes // AIChE Journal. — 1955. — Vol. 1, no. 3. — Pp. 289—295.
16. Taylor G. The shape and acceleration of a drop in a high speed air stream // The scientific papers of GI Taylor. — 1963. — Vol. 3. — Pp. 457—464.
17. Secondary breakup of a drop at moderate Weber numbers / M. Jain [et al.] // Proc. R. Soc. A. — 2015. — Vol. 471, no. 2177. – – P. 20140930.

IMPLICIT EULER TIME DISCRETIZATION AND FDM WITH NEWTON METHOD IN NONLINEAR HEAT TRANSFER MODELING

Ph.D. Filipov S.¹, Prof. D.Sc. Faragó I.²

¹ Department of Computer Science, University of Chemical Technology and Metallurgy, Bulgaria

² Department of Applied Analysis and Computational Mathematics, MTA-ELTE Research Group, Eötvös Loránd University, Hungary
 filipovstefan@yahoo.com, faragois@cs.elte.hu

Abstract: This paper considers one-dimensional heat transfer in a media with temperature-dependent thermal conductivity. To model the transient behavior of the system, we solve numerically the one-dimensional unsteady heat conduction equation with certain initial and boundary conditions. Contrary to the traditional approach, when the equation is first discretized in space and then in time, we first discretize the equation in time, whereby a sequence of nonlinear two-point boundary value problems is obtained. To carry out the time-discretization, we use the implicit Euler scheme. The second spatial derivative of the temperature is a nonlinear function of the temperature and the temperature gradient. We derive expressions for the partial derivatives of this nonlinear function. They are needed for the implementation of the Newton method. Then, we apply the finite difference method and solve the obtained nonlinear systems by Newton method. The approach is tested on real physical data for the dependence of the thermal conductivity on temperature in semiconductors. A MATLAB code is presented.

Keywords: HEAT CONDUCTION EQUATION, TEMPERATURE-DEPENDENT THERMAL CONDUCTIVITY, IMPLICIT EULER METHOD, BOUNDARY VALUE PROBLEM, FINITE DIFFERENCE METHOD, NEWTON METHOD

1. Introduction

We consider the one-dimensional unsteady heat conduction equation [1-3]

$$\rho c_p \frac{\partial u}{\partial t} = \frac{\partial}{\partial x} \left(\kappa(u) \frac{\partial u}{\partial x} \right), \quad (1)$$

where $u(x, t)$ is the temperature at position x and time t , ρ is the density, c_p is the heat capacity at constant pressure, and κ is the thermal conductivity of the media. We assume that ρ and c_p have constant values, but κ depends on the temperature u . This assumption is often justifiable for certain temperature range (e.g. for silicon [4]). Performing the differentiation in the right-hand side of (1) we get

$$\rho c_p \frac{\partial u}{\partial t} = \partial_u \kappa(u) \left(\frac{\partial u}{\partial x} \right)^2 + \kappa(u) \frac{\partial^2 u}{\partial x^2}. \quad (2)$$

When κ does not depend on u , i.e. $\partial_u \kappa(u) = 0$, then (2) is a linear (parabolic) partial differential equation. When $\partial_u \kappa(u) \neq 0$, then (2) is nonlinear. Equation (2) will be solved on the spatial interval $[a, b]$ subject to certain boundary and initial conditions:

$$u(a, t) = \alpha(t), \quad u(b, t) = \beta(t), \quad t > 0, \quad (3)$$

$$u(x, 0) = u_0(x), \quad x \in [a, b]. \quad (4)$$

The boundary conditions (3) give the temperature at the two ends as function of time. The initial condition (4) specifies the initial spatial distribution of the temperature.

2. Implicit Euler time discretization

For the linear problem ($\partial_u \kappa(u) = 0$), the numerical methods for solving (2)-(4) are well elaborated (finite difference, finite element methods, etc.). Usually, (2) is first discretized in space, whereby an initial-value (Cauchy) problem for first order ODE system is obtained. If the explicit Euler method is used to solve the Cauchy problem, then the method is stable only for $0 < \Delta t/h^2 \leq$

$1/2$, where $D = \kappa/(\rho c_p)$ is the thermal diffusivity, h is the discretization step in space, and τ is the discretization step in time.

Our approach is different. We first discretize (2) in time. Using a time-step τ , the time line $t \geq 0$ is partition by equally separated mesh-points:

$$t_n = n\tau, \quad n = 0, 1, 2, \dots \quad (5)$$

Then, using implicit Euler scheme [5], equation (2) is discretized on the mesh (5):

$$\rho c_p \frac{u_n - u_{n-1}}{\tau} = \partial_u \kappa(u_n) \left(\frac{du_n}{dx} \right)^2 + \kappa(u_n) \frac{d^2 u_n}{dx^2}, \quad (6)$$

where $u_n = u_n(x)$ and $u_{n-1} = u_{n-1}(x)$ approximate the values of $u(x, t_n)$ and $u(x, t_{n-1})$, respectively. Equation (6) approximates the partial differential equation (2). The error is $O(\tau)$, hence the discretization scheme is first-order accurate in time. The method is stable, unlike the explicit method, i.e. evaluating the right-hand side of (2) at u_{n-1} , which is only conditionally stable.

Solving (6) for the second spatial derivative of the temperature u_n we get

$$\frac{d^2 u_n}{dx^2} = f(u_n, v_n; u_{n-1}), \quad (7)$$

where $v_n = du_n/dx$ is the temperature gradient and f is the following nonlinear function:

$$f(u_n, v_n; u_{n-1}) = \frac{\phi(u_n, v_n; u_{n-1})}{\kappa(u_n)}, \quad (8)$$

$$\phi(u_n, v_n; u_{n-1}) = \rho c_p \frac{u_n - u_{n-1}}{\tau} - \partial_u \kappa(u_n) v_n^2. \quad (9)$$

Equation (7), together with the boundary conditions $u_n(a) = \alpha(t_n)$, $u_n(b) = \beta(t_n)$, constitutes a nonlinear two-point boundary value problem (TPBVP) for the unknown function u_n . If the function u_{n-1} is known (given) the problem can be solved by using some numerical technique for nonlinear problems. Thus, starting

from the initial condition u_0 we can solve successively (7) for $n = 1, 2, \dots$

3. Derivatives for the Newton method

The implementation of the Newton method requires the partial derivatives of $f(u_n, v_n; u_{n-1})$ with respect to u_n and v_n . Introducing the notation $f_n = f(u_n, v_n; u_{n-1})$, $\phi_n = \phi(u_n, v_n; u_{n-1})$ and denoting the derivatives by $q_n = q(u_n, v_n; u_{n-1})$, $p_n = p(u_n, v_n)$ we get:

$$q_n = \frac{\partial f_n}{\partial u_n} = \frac{1}{\kappa(u_n)} \left(-f_n \partial_u \kappa(u_n) + \frac{\partial \phi_n}{\partial u_n} \right), \quad (10)$$

$$p_n = \frac{\partial f_n}{\partial v_n} = \frac{1}{\kappa(u_n)} \frac{\partial \phi_n}{\partial v_n}, \quad (11)$$

where

$$\frac{\partial \phi_n}{\partial u_n} = \frac{\rho c_p}{\tau} - \partial_{uu}^2 \kappa(u_n) v_n^2, \quad (12)$$

$$\frac{\partial \phi_n}{\partial v_n} = -2 \partial_u \kappa(u_n) v_n. \quad (13)$$

4. Finite difference method

Since $\rho c_p / \tau$ grows to infinity as τ goes to zero (which effects IVP solutions), it turns out that the finite difference method (FDM) [6] is a better choice for the solution of the obtained TPBVPs than the shooting method [6,7]. Hence, we adopt the FDM. The interval $[a, b]$ is partitioned by N equally separated mesh-points:

$$x_i = a + (i-1)h, i = 1, 2, \dots, N, h = \frac{b-a}{N-1}. \quad (14)$$

Equation (7) is discretizes on the uniform mesh (14) using the FDM with the central difference approximation:

$$\frac{u_{n,i+1} - 2u_{n,i} + u_{n,i-1}}{h^2} = f(u_{n,i}, v_{n,i}; u_{n-1,i}), \quad (15)$$

$$i = 2, 3, \dots, N-1. \quad (16)$$

Correspondingly, everywhere in equations (8)-(13), we set $x = x_i$, and then replace the values of $u_n(x_i)$, $v_n(x_i)$, and $u_{n-1}(x_i)$ with their approximations $u_{n,i}$, $v_{n,i}$, and $u_{n-1,i}$ where

$$v_{n,i} = \frac{u_{n,i+1} - u_{n,i-1}}{2h}. \quad (17)$$

Equation (15) approximates (7) with error $O(h^2)$, i.e. it is second-order accurate in space. Equation (15) holds for the inner mesh-points. At the boundaries we apply the boundary conditions:

$$u_{n,1} = \alpha(t_n), u_{n,N} = \beta(t_n) \quad (18)$$

5. Solving the nonlinear system by Newton method

Introducing the column-vector $\mathbf{G}_n = [G_{n,1}, G_{n,2}, \dots, G_{n,N}]^T$ with components

$$G_{n,1} = u_{n,1} - u_a(t_n), G_{n,N} = u_{n,N} - u_b(t_n), \quad (19)$$

$$G_{n,i} = u_{n,i+1} - 2u_{n,i} + u_{n,i-1} - h^2 f_{n,i}, \quad (20)$$

$$f_{n,i} = f(u_{n,i}, v_{n,i}; u_{n-1,i}), \quad (21)$$

the system of nonlinear equations (15) and the boundary conditions (18) are written as one equation:

$$\mathbf{G}_n(\mathbf{u}_n) = 0, \quad (22)$$

where

$$\mathbf{u}_n = [u_{n,1}, u_{n,2}, \dots, u_{n,N}]^T. \quad (23)$$

Starting by some initial guess $\mathbf{u}_n^{(0)}$, the nonlinear system (22) can be solved by the Newton iterative method:

$$\mathbf{u}_n^{(k+1)} = \mathbf{u}_n^{(k)} - \left(\mathbf{L}_n^{(k)} \right)^{-1} \mathbf{G}_n(\mathbf{u}_n^{(k)}),$$

$$k = 0, 1, 2, \dots \quad (24)$$

where $\mathbf{L}_n^{(k)}$ is the Jacobian of \mathbf{G}_n with respect to \mathbf{u}_n evaluated at $\mathbf{u}_n^{(k)}$:

$$\mathbf{L}_n^{(k)} = \frac{\partial \mathbf{G}_n}{\partial \mathbf{u}_n}(\mathbf{u}_n^{(k)}). \quad (25)$$

Calculating the elements of the Jacobian we get:

$$L_{n(1,1)}^{(k)} = 1, \quad L_{n(N,N)}^{(k)} = 1, \quad (26)$$

$$L_{n(i,i)}^{(k)} = -2 - h^2 q_{n,i}^{(k)},$$

$$L_{n(i,i-1)}^{(k)} = 1 + \frac{1}{2} h p_{n,i}^{(k)},$$

$$L_{n(i,i+1)}^{(k)} = 1 - \frac{1}{2} h p_{n,i}^{(k)}, \quad (27)$$

$$q_{n,i}^{(k)} = q(u_{n,i}^{(k)}, v_{n,i}^{(k)}; u_{n-1,i}), p_{n,i}^{(k)} = p(u_{n,i}^{(k)}, v_{n,i}^{(k)}). \quad (28)$$

Iteration (24) is a one-step (two-level) iteration. Starting from some initial guess $\mathbf{u}_n^{(0)}$, we can find each next approximation $\mathbf{u}_n^{(k+1)}$, $k = 0, 1, 2, \dots$ using (24). If the sequence is convergent, then the limiting vector $\mathbf{u}_n = \lim_{k \rightarrow \infty} (\mathbf{u}_n^{(k+1)})$ is a solution to the nonlinear system (22). In practice, the iteration process is usually ended when

$$\|\mathbf{u}_n^{(k+1)} - \mathbf{u}_n^{(k)}\| < \epsilon. \quad (29)$$

This inequality is called a stopping criteria. The vector $\mathbf{u}_n^{(k+1)}$ is taken as approximate solution to (22). As an initial guess $\mathbf{u}_n^{(0)}$, we can use the solution \mathbf{u}_{n-1} found at the previous step.

6. Computer experiment

Consider a thin homogenous rod, along the x -axis between the points $x = 1$ and $x = 3$, without heat sources and without radiation. The density ρ and the heat capacity c_p are constant, but the thermal conductivity κ depends on the temperature as

$$\kappa = \kappa_0 \exp(\chi u). \quad (30)$$

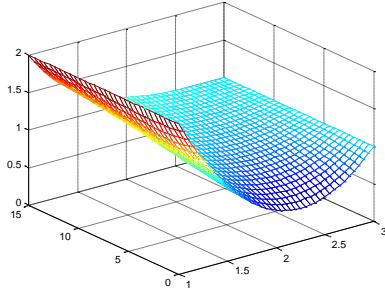
Such a temperature dependence actually occurs in real physical systems, e.g. for silicon [4]. We choose the following values of the constants: $\rho = 1$, $c_p = 1$, $\kappa_0 = 0.1$. The temperature at the two ends is kept constant:

$$u(1, t) = 2, u(3, t) = 1, t > 0. \quad (31)$$

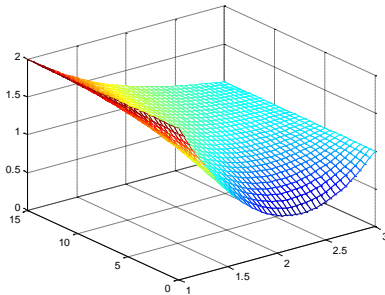
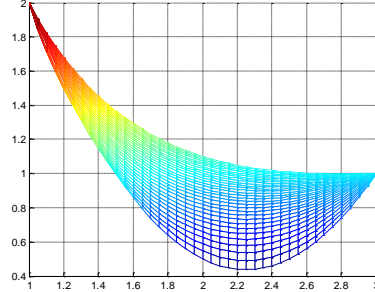
The initial temperature profile is

$$u(x, 0) = 2 - \frac{x-1}{2} + (x-1)(x-3), x \in [1, 3]. \quad (32)$$

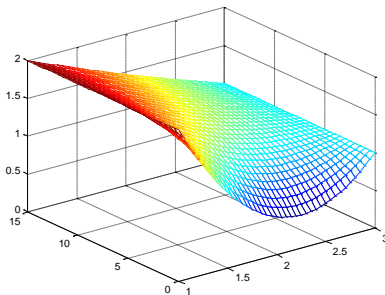
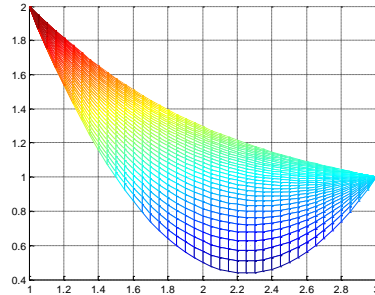
To find the time evolution of (32), we solve the partial differential equation (1) with boundary conditions (31) and initial conditions (32) by the method described in this paper. The equation is solved for $\chi = -1.0, -0.5, 0, 0.5, 1.0$. The step-size is chosen to be $\tau = 0.5$ with integration range $0 \leq t \leq 15$. The spatial interval $x \in [1, 3]$ is discretized by $N = 41$ mesh-points, i.e. $h = 0.05$. The results are shown in Fig. 1



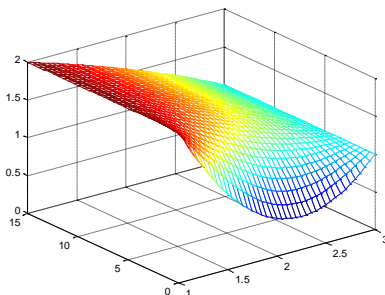
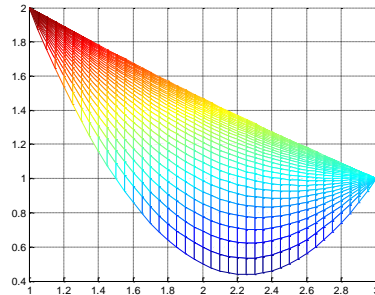
$\chi = -1.0$



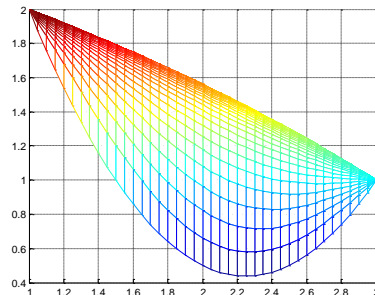
$\chi = -0.5$



$\chi = 0$



$\chi = 0.5$



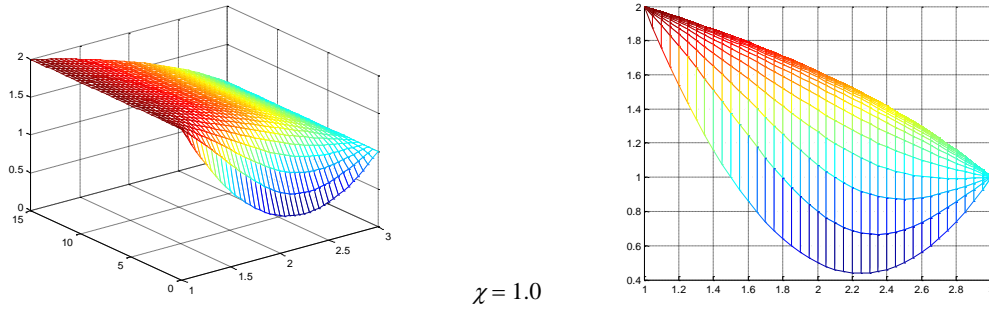


Fig. 1. Solving the heat conduction equation (1) for boundary conditions (31), initial condition (32), and thermal conductivity (30). In addition to the 3D view (left), a side-view u vs. x is also shown (right).

For $\chi = 0, 0.5$, and 1.0 the final temperature distribution reached in the experiment is practically the steady-state distribution. For $\chi = -1.0$ and -0.5 a little bit more time is needed. The steady-state distribution for $\chi = 0$ is, as expected, linear.

7. Conclusion

This paper considered heat transfer with temperature-dependent thermal conductivity. The one-dimensional unsteady heat conduction equation was solved numerically by using implicit time-discretization and FDM with Newton method for the solution of the arising nonlinear two-point boundary value problems. Data for the dependence of the thermal conductivity on temperature in certain semiconductors was used. The results obtained by the numerical computer experiments are consistent with the expected outcome. The proposed method is stable, unlike its explicit counterpart.

8. Appendix

A MATLAB code is presented for the numerical solution of the example provided in section 6.

```
function main
rho=1; Cp=1; kappa0=0.1; chi=0.5;
M=31; N=41;
tEnd=15; tau=tEnd/(M-1);
a=1; b=3; h=(b-a)/(N-1);
alpha=2; beta=1;
x=zeros(N,1);
u0=zeros(N,1);
for i=1:N
    x(i)=a+(i-1)*h;
    u0(i)=2-(x(i)-1)/2+(x(i)-1)*(x(i)-3);
end
t=zeros(M,1);
for n=1:M
    t(n)=(n-1)*tau;
end
u_1=zeros(N,1); u=zeros(N,1);
uNext=zeros(N,1); G=zeros(N,1);
L=zeros(N,N); L(1,1)=1; L(N,N)=1;
U=zeros(N,M); U(:,1)=u0;
for n=2:M
    u=U(:,n-1); u_1=U(:,n-1);
    eps=1;
    while(eps>0.0001)
        G(1)=u(1)-alpha;
        G(N)=u(N)-beta;
        for i=2:N-1
            k=kappa0*exp(chi*u(i));
            Dk=chi*k;
            D2k=chi*Dk;
            v=(u(i+1)-u(i-1))/(2*h);
            A=rho*Cp/tau;
            phi=A*(u(i)-u_1(i))-Dk*v*v;
            f=phi/k;
            q=(-f*Dk+A-D2k*v*v)/k;
```

```
p=-2*Dk*v/k;
G(i)=u(i+1)-2*u(i)+u(i-1)-h*h*f;
L(i,i-1)=1+0.5*h*p;
L(i,i)=-2-h*h*q;
L(i,i+1)=1-0.5*h*p;
end
uNext=u-L\G;
eps=sqrt(h*(uNext-u)*(uNext-u));
u=uNext;
end
U(:,n)=u;
end
mesh(x,t,U);
end
```

The mathematical quantities and the corresponding variables used in the MATLAB code are shown in Table 1.

Paper	MATLAB
ρ	rho
c_p	Cp
κ_0	kappa0
χ	chi
τ	tau
N	N
a	a
b	b
h	h
α	alpha
β	beta
x_i	x(i)
t_n	t(n+1)
u_0	u0
$u_n^{(k)}$	u
$u_n^{(k+1)}$	uNext
u_{n-1}	u_1
$u_{n,i}$	U(i,n+1)
$G_n(u_n^{(k)})$	G
$L_n^{(k)}$	L
$\ u_n^{(k+1)} - u_n^{(k)}\ $	eps
$u_n^{(k)}$	u(i)
$u_{n,i}^{(k)}$	
$\kappa(u_{n,i}^{(k)})$	k
$\partial_u \kappa(u_{n,i}^{(k)})$	Dk
$\partial_{uu}^2 \kappa(u_{n,i}^{(k)})$	D2k
$v_{n,i}^{(k)}$	v
$\phi(u_{n,i}^{(k)}, v_{n,i}^{(k)}, u_{n-1,i})$	phi
$f(u_{n,i}^{(k)}, v_{n,i}^{(k)}, u_{n-1,i})$	f
$q_{n,i}^{(k)}$	q
$p_{n,i}^{(k)}$	p

Table 1.

9. Acknowledgement

This research was carried out in the ELTE Institutional Excellence Program (1783-3/2018/FEKUTSRAT) supported by the Hungarian Ministry of Human Capacities, and supported by the Hungarian Scientific Research Fund OTKA, No. K112157 and SNN125119

10. References

- [1] R.B. Bird, W.E. Stewart, E.N. Lightfoot, Transport Phenomena, 2nd Edition, John Wiley & Sons, Inc., (2002)
- [2] H.S. Carslaw, J.C. Jaeger, Conduction of Heat in Solids, 2nd Edition, Oxford University Press, (1986)
- [3] S.L. Sobolev, Partial Differential Equations of Mathematical Physics, Dover Publications, (1989)
- [4] J. Lienemann, A. Yousefi, J.G. Korvink, Nonlinear Heat Transfer Modeling, In: P. Benner, D.C. Sorensen, V. Mehrmann (eds) Dimension Reduction of Large-Scale Systems, Lecture Notes in Computational Science and Engineering, 45 (2005) 327-331
- [5] U.M. Ascher, S.J. Ruuth, R.J. Spiteri: Implicit-Explicit Runge-Kutta Methods for Time-Dependent Partial Differential Equations, Appl Numer Math, vol. 25 (2-3) (1997)
- [6] U.M. Ascher, R.M.M. Mattheij, R.D. Russell, Numerical Solution of Boundary Value Problems for Ordinary Differential Equations, in: Classics in Applied Mathematics, vol. 13, SIAM, (1995)
- [7] S.M. Filipov, I.D. Gospodinov, I. Faragó, Shooting-projection method for two-point boundary value problems, Appl. Math. Lett. 72 (2017) 10-15
<https://doi.org/10.1016/j.aml.2017.04.002>

APPLICATION OF LAPLACE TRANSFORM IN FINANCE

Daci A. PhD, Tola S. PhD.

Faculty of Mathematical and Physical Engineering – Polytechnic University of Tirana

alfreddaci@gmail.com, saimir_tola@yahoo.com

Abstract: Laplace's transformation is an important chapter of Mathematical Analysis. At present it is widely used in various problems of signal theory, physics, mechanics, electro – techniques and economics. Laplace's transformation is the simplest and most economical method that leads directly to the required resolution of many of the various technical problems that arise when solving them. In this paper we will become acquainted with the basic concepts of operational mathematics and its application in economy. Not many analytic solutions exist for present discounted value problems but by using Laplace transform we can deduce some of the closed form solutions quite easily. There will be shown the connection between the current discounted value in finance and Laplace transformation.

Keywords: LAPLACE TRANSFORM, FINANCE, PRESENT VALUE, CASH FLOW, RATE, PERIOD.

1. Introduction

Before we consider the transformation of Laplace, we analyze the meaning of the integral of a complex function of the real argument.

Let it be $f(t)$ a complex function of the real t argument given in the segment $[a, b]$. As it is known, such a function may appear in the form: $f(t) = u(t) + iv(t)$

The integral of the function $f(t)$ in the segment $[a, b]$ with the definition is determined by the equation

$$\int_a^b f(t) dt = \int_a^b u(t) dt + i \int_a^b v(t) dt \quad (1)$$

Similarly, the infinite integral of that function is defined in $(0, \infty)$:

$$\int_0^{+\infty} f(t) dt = \int_0^{+\infty} u(t) dt + i \int_0^{+\infty} v(t) dt \quad (2)$$

provided that both right-side integrals are convergent.

Since the integral of a complex function of the real variable is defined by the equations (1) or (2) by two common integrals, then all the properties and the integration methods of the latter are true also for the integrals of the complex functions of the real argument.

Below we will be dealing with the integral of the forms (1) and (2). Considering the fact that the purpose of introducing the operational method is mainly the implementation direction of this method, we are not dwelling on the necessary conditions of convergence of such integrals but will be limited to the integral of the functions $f(t)$ that meets these conditions: [1], [2], [3], [4]

1. The function $f(t)$ is continuous in $(0, +\infty)$ combined with its derivatives up to any necessary order, with the exception of possibly a finite number of first type of critical points in each finite segment.
2. $f(t) = 0$ for $t < 0$.
3. The function $f(t)$ increases in absolute value no sooner than an exponential function. So there are numbers $M > 0$ and $S_0 > 0$ such that for each term t we have: $|f(t)| < Me^{S_0 t}$

The number S_0 that enjoys the above quality is called the growth indicator of the function $f(t)$. In particular when the function $f(t)$ is limited then it can be consider $S_0 = 0$. The fulfillment of the above conditions ensures the existence of many integrals of the

form (2) that we will consider below. We are now going to determine the transformation of Laplace.

Consider the product of the function $f(t)$ with the real argument t

$$e^{-pt} \cdot f(t) \quad (3)$$

Function (3) is again a complex function of the real argument:

$$e^{-pt} \cdot f(t) = e^{-(s+i\omega)t} \cdot f(t) = e^{-st} \cdot f(t) \cdot e^{-i\omega t} = e^{-st} f(t) \cos \omega t - ie^{-st} f(t) \sin \omega t$$

We will now show that when a function $f(t)$ meets the above conditions, then the integral

$$\int_0^{+\infty} e^{-pt} f(t) dt = \int_0^{+\infty} e^{-st} f(t) \cos \omega t dt - i \int_0^{+\infty} e^{-st} f(t) \sin \omega t dt \quad (4)$$

converges, even absolutely provided that: $\text{Re } p = s > S_0$.

According to the definition for the convergence of the integral (4), the existence of each of the right-side integrals is necessary and sufficient. Let's analyze the convergence of the first.

$$\begin{aligned} \left| \int_0^{+\infty} e^{-st} f(t) \cos \omega t dt \right| &< \int_0^{+\infty} |e^{-st} f(t) \cos \omega t| dt < \\ &< M \int_0^{+\infty} e^{-st} e^{S_0 t} dt = M \int_0^{+\infty} e^{-(s-S_0)t} dt = \frac{M}{s-S_0} \end{aligned}$$

Similarly, the second integral on the right side of (4) is evaluated.

The integral (4) converges to the entire complex plot area p extending to the right of the line $\text{Re } p = S_0$. The proving method also follows that only the real part of the number p determines the convergence of the integral (4).

Integral (4) defines a function of the parameter we mark $F(p)$, namely:

$$F(p) = \int_0^{+\infty} f(t) e^{-pt} dt.$$

The function $F(p)$, is called the Laplace image of function $f(t)$. The function $f(t)$ is called the original function.

As has been stated above, it follows that the fulfillment of the above three conditions is sufficient for the function $f(t)$ to be original. Below we will call original only the functions that meet those three conditions. This tightening of the class of originals is not very sensible from the practical point of view.

If $F(p)$, is a reflection of the function $f(t)$, then it says:

$$L\{f(t)\} = F(p) \quad \text{or} \quad F(p) \xrightarrow{\square} f(t)$$

Theorem. If the function $F(p)$, is an image, then:

$$F(p) \rightarrow 0 \quad \text{when} \quad \operatorname{Re} p = s \rightarrow +\infty$$

Truly, it is known that $|a + ib| = \sqrt{a^2 + b^2} \leq |a| + |b|$

$$\text{So:} \quad |F(p)| \leq \left| \int_0^{+\infty} e^{-st} f(t) \cos \omega t dt \right| + \left| \int_0^{+\infty} e^{-st} f(t) \sin \omega t dt \right|$$

or

$$|F(p)| \leq \frac{M}{s - s_0} + \frac{M}{s - s_0} \rightarrow 0 \quad \text{for} \quad s \rightarrow +\infty$$

Based on this theorem it can be said that the necessary condition for a given function $F(p)$, to be an image of a function $f(t)$ is to complete the reconciliation:

$$\lim_{\operatorname{Re} p \rightarrow +\infty} F(p) = 0$$

2. Finding the original when the image is rational

In the practice of the usage of the operational calculus, we often find it when the function $F(p)$, is rational. By the end of this paragraph we will deal precisely with the problem of finding the original when the image is rational:

$$F(p) = \frac{b_0 p^m + b_1 p^{m-1} + \dots + b_{m-1} p + b_m}{a_0 p^n + a_1 p^{n-1} + \dots + a_{n-1} p + a_n} = \frac{\phi(p)}{\psi(p)} \quad (5)$$

We note, first, that the rational fraction $F(p)$ should be regular because otherwise the condition is not met:

$$F(p) \xrightarrow{|p| \rightarrow \infty} 0$$

which is necessary for the function $F(p)$, to be an image. So we will have $m < n$.

In relation to the denominator $\psi(p)$ of the fraction (5) we distinguish these cases:

I. The function $\psi(p)$ has only simple roots (not repeated).

We mark the roots of the polynomial $\psi(p)$ with $\alpha_1, \alpha_2, \dots, \alpha_n$. Then it can be written in the form:

$$\psi(p) = (p - \alpha_1)(p - \alpha_2) \dots (p - \alpha_n)$$

while the function $F(p)$, can be expanded:

$$\frac{\phi(p)}{\psi(p)} = \frac{A_1}{p - \alpha_1} + \frac{A_2}{p - \alpha_2} + \dots + \frac{A_i}{p - \alpha_i} + \dots + \frac{A_n}{p - \alpha_n} \quad (6)$$

Since for the function $\frac{A_i}{p - \alpha_i}$ the original is $A_i e^{\alpha_i t}$, then

based on the property of linearity and equation (6) we will have:

$$\frac{\phi(p)}{\psi(p)} \xrightarrow{\bullet} A_1 e^{\alpha_1 t} + A_2 e^{\alpha_2 t} + \dots + A_n e^{\alpha_n t} \quad (7)$$

To find the coefficients we: multiply the two sides of (6) with $p - \alpha_1$ and using the fact that α_1 is the root of $\psi(p)$ i.e $\psi(\alpha_1) = 0$, the draw (6) takes the form:

$$(p - \alpha_1) \frac{\phi(p)}{\psi(p) - \psi(\alpha_1)} = A_1 + (p - \alpha_1) \left[\frac{A_2}{p - \alpha_2} + \dots + \frac{A_n}{p - \alpha_n} \right]$$

Now we get the limit on both sides of this draw for $p \rightarrow \alpha_1$. It is clear that the right-side borders will be A_1 . So we will have:

$$A_1 = \lim_{p \rightarrow \alpha_1} (p - \alpha_1) \frac{\phi(p)}{\psi(p) - \psi(\alpha_1)} = \lim_{p \rightarrow \alpha_1} \frac{\phi(p)}{\frac{\psi(p) - \psi(\alpha_1)}{p - \alpha_1}}$$

$$\text{from where} \quad A_1 = \frac{\phi(\alpha_1)}{\psi'(\alpha_1)}$$

In the role of α_1 it could be each of the roots $\alpha_2, \dots, \alpha_i, \dots, \alpha_n$, therefore in the general form we will have:

$$A_i = \frac{\phi(\alpha_i)}{\psi'(\alpha_i)} \quad (8)$$

Based on (7) and (8) we can write the operational relation:

$$\frac{\phi(p)}{\psi(p)} \xrightarrow{\bullet} \frac{\phi(\alpha_1)}{\psi'(\alpha_1)} e^{\alpha_1 t} + \frac{\phi(\alpha_2)}{\psi'(\alpha_2)} e^{\alpha_2 t} + \dots + \frac{\phi(\alpha_n)}{\psi'(\alpha_n)} e^{\alpha_n t}$$

or

$$\frac{\phi(p)}{\psi(p)} \xrightarrow{\bullet} \sum_{i=1}^n \frac{\phi(\alpha_i)}{\psi'(\alpha_i)} \cdot e^{\alpha_i t} \quad (9)$$

II. Among the roots of the denominator $\psi(p)$ there are such that are repeated.

Let $\alpha, \beta, \dots, \lambda$ be the roots of the polynomial $\psi(p)$, while the numbers a, b, \dots, l indicate how many times each of them is rooted. In this case, the polynomial $\psi(p)$ may appear in the form:

$$\psi(p) = (p - \alpha)^a (p - \beta)^b \dots (p - \lambda)^l$$

As it is known from the expansion of regular rational fractions into elemental fractions, each factor of the form $(p - \delta)^d$ corresponds d to the elemental fraction with denominator

$$(p - \delta)^d (p - \delta)^{d-1} \dots (p - \delta).$$

So the function $F(p) = \frac{\phi(p)}{\psi(p)}$ in this case will be presented in the form:

$$\left. \begin{aligned} \frac{\phi(p)}{\psi(p)} &= \frac{A_1}{(p-\alpha)^a} + \frac{A_2}{(p-\alpha)^{a-1}} + \dots + \frac{A_n}{p-a} \\ &+ \frac{B_1}{(p-\beta)^b} + \frac{B_2}{(p-\beta)^{b-1}} + \dots + \frac{B_b}{p-\beta} \\ &+ \frac{L_1}{(p-\lambda)^l} + \frac{L_2}{(p-\lambda)^{l-1}} + \dots + \frac{L_l}{p-\lambda} \end{aligned} \right\} \quad (10)$$

Let us now see how the decomposition coefficients that are marked with the same letter are counted, e.g. coefficients B . Similarly, coefficients that are written in other letters are calculated. Multiply both sides of the equation (10) with $(p - \beta)^b$:

$$(p-\beta)^b \frac{\phi(p)}{\psi(p)} = B_1 + B_2(p-\beta) + \dots + B_i(p-\beta)^{b-1} + (p-\beta)^b \cdot \sigma(p) \quad (11)$$

$\sigma(p)$ denotes the sum of all elementary expansions (10) that does not belong to coefficients B . There is no factor of the form $(p - \beta)$ in the denominator $\sigma(p)$, so the denominator is not canceled for $p = \beta$. Taking the limits of both sides of the equation (11) for $p \rightarrow \beta$ to find:

$$B_1 = \lim_{p \rightarrow \beta} \left[(p - \beta)^b \frac{\phi(p)}{\psi(p)} \right] \quad (12)$$

We now derive both sides of (11) in relation to p , then we have:

$$\frac{d}{dp} \left[(p-\beta)^b \frac{\phi(p)}{\psi(p)} \right] = B_2 + 2B_3(p-\beta) + \dots + b(p-\beta)^{b-1} \sigma(p) + (p-\beta)^b \sigma(p)$$

Considering again the limits of both sides for $p \rightarrow \beta$ we find:

$$B_2 = \lim_{p \rightarrow \beta} \frac{d}{dp} \left[(p - \beta)^b \frac{\phi(p)}{\psi(p)} \right]$$

Let k be any number from 1 to b . We derive both sides of (11) in relation to p , $k-1$ times and find:

$$\frac{d^{k-1}}{dp^{k-1}} \left[(p-\beta)^b \frac{\phi(p)}{\psi(p)} \right] = (k-1)! B_k + \dots + (b-1)(b-2) \dots (b-k+1) B_b (p-b)^{b-k-1} \\ + \frac{d^{k-1}}{dp^{k-1}} \left[(p-b)^b \sigma(p) \right]$$

We move to the limit for $p \rightarrow \beta$ on both sides of the above equation. It is clear that on the right side it will remain $(k-1)!B_k$ alone and if we divide it with the $(k-1)!$ we find:

$$B_k = \frac{1}{(k-1)!} \lim_{p \rightarrow \beta} \frac{d^{k-1}}{dp^{k-1}} \left[(p-\beta)^b \frac{\phi(p)}{\psi(p)} \right] \quad (13)$$

If instead of β we take another root of the polynomial $\psi(p)$, then according to the formula (13) we find coefficients that belong to that root. After finding the coefficients there is no difficulty in finding the original. As it is well known, each term of expansion (10) of the form

$$\frac{B_k}{(p - \beta)^{b-k+1}}$$

corresponds the original:

$$B_k \frac{t^{b-k}}{(b-k)!} e^{\beta t}$$

Then the original corresponding to the function $\frac{\phi(p)}{\psi(p)}$

deduced in form (10) is:

[illegible]

Remarks: If in formula (13) we get $b = 1$, then we will certainly have $k = 1$ and this formula results in the same formula (8). For this reason, if in the expansion of the polynomial $\psi(p)$ some roots are simple, then for finding the respective coefficients use the formula (9).

3. The Accumulated Value

If matured interest is added to the principal at the end of each period for which the interest is calculated and then this interest earns interest, it is said that the interest is compounded. The amount of initial principal and total interest is called the compound sum or accumulated value. [5]

¹ Let's note:

P = the initial principal or the discounted value of S

S = the sum of P's or accumulated value of P

t = total number of interest periods

 $r = \text{interest rate}$

Let P be the principal at the beginning of the first period and r the interest rate for the conversion period. We will calculate accumulated values at the end of consecutive periods of conversion for t periods.

At the end of the first period:

Interest matured

 $P \cdot r$

The accumulated value

$$P + P \cdot r = P(1 + r)$$

At the end of the second period:

Interest matured $[P \cdot (1+r)] \cdot r$

The accumulated value

$$P(1+r) + [P \cdot (1+r)] \cdot r = P(1+r)^2$$

At the end of the third period:

Interest matured $[P \cdot (1+r)^2] \cdot r$

The accumulated value

$$P(1+r)^2 + [P \cdot (1+r)^2] \cdot r = P(1+r)^3$$

Continuing this way we would get the accumulated values:

$$P(1+r), P(1+r)^2, P(1+r)^3, \dots$$

They form a geometric progression t whose term is:

$$S = P(1+r)^t \quad (15)$$

4. Relation Between Present Value and Laplace Transform

In business transactions it is usually necessary to determine the level of principal P today, that will be accumulated at a compound interest rate r in a given sum S on a given date (t interest period from that moment). By formula (15)

we have:

$$P = \sum_{t=1}^T \frac{S(t)}{(1+r)^t} \quad (16)$$

In other words, it is the amount that we would be willing to pay today in order to receive a cash flow or a series of them in the future. [6] Now by using an exponential series we can write equation (16) as,

$$P = \sum_{t=1}^T e^{-rt} S(t) \quad (17)$$

In the limiting case replacing summation to an integral, equation (17) can be written as

$$P = \int_0^T e^{-rt} S(t) dt \quad (18)$$

Again here T is some finite quantity. So if we consider as $T \rightarrow +\infty$, equation (18) will becomes

$$P = \int_0^{+\infty} e^{-rt} S(t) dt \quad (19)$$

Equation (19) is nothing other than the definition of Laplace's transformation, hence: [6]

$$P(r) = L\{S(t)\} \quad (20)$$

Suppose successive t payments are to be made, $k_1, k_2, k_3, \dots, k_t$

where: k_1 to be settled after a year, k_2 after two years and so on.

How much is the amount to be deposited today in one bank account in order to get enough savings to afford all future payments when the annual interest rate is r .

So what is the present value of all payments?

We start from formula (15) and apply it for the foregoing. To have the quantity k_1 after one year we have: $k_1 = P(1+r)$, from where,

the amount we need to deposit today is $P = \frac{k_1}{1+r}$. To have the

quantity k_2 after two years; $k_2 = P(1+r)^2 \Rightarrow P = \frac{k_2}{(1+r)^2}$, and

so on. The full amount that needs to be deposited today, so that all payments are covered is:

$$P_t = \frac{k_1}{1+r} + \frac{k_2}{(1+r)^2} + \frac{k_3}{(1+r)^3} + \dots + \frac{k_t}{(1+r)^t} \quad (21)$$

If the payments are the same, $k_1 = k_2 = k_3 = \dots = k_t = k$ then

$$P_t = \frac{k}{1+r} + \frac{k}{(1+r)^2} + \frac{k}{(1+r)^3} + \dots + \frac{k}{(1+r)^t} \quad (22)$$

This is nothing but a series of geometric progression at a time $\frac{1}{1+r}$ that;

$$P_t = \frac{k}{1+r} \cdot \frac{1 - \frac{1}{(1+r)^t}}{1 - \frac{1}{1+r}} = \frac{k}{r} \left[1 - \frac{1}{(1+r)^t} \right] \quad (23)$$

If we use Laplace transformation

$$L\{k\} = k \int_0^{+\infty} e^{-rt} dt = \frac{k}{r} \quad (24)$$

Example. Estimate the current value of a \$ 1000 instant spill series at the end of each year when the annual interest rate is 10%.

Solution: $P = \frac{k}{r} = \frac{1000}{10\%} = 10000\$$

4. Conclusions

- 1) Laplace transformation is the simplest and most economical method that leads directly to the required resolution of many of the various technical problems that arise when solving them.
- 2) Using the Laplace transformation we easily obtain a definitive analytical solution to the problems of the present discounted value where was shown the close relationship existing between the actual discounted value in finance and the transformation of Laplace. [6]
- 3) The result in this paper increases the practical benefits of Laplace transformation particularly in finance.
- 4) Laplace transformation is the major resource for discounted value functions to illustrate complex problems.

5. References

1. Jorgo Malita, *Analiza Komplekse*, Tiranë 2009.
2. Joel L. Schiff, *The Laplace Transform, Theory and Applications*, Springer 1999.
3. Marcel B. Finan, *Laplace Transforms: Theory, Problems, and Solutions*, Arkansas Tech University.
4. C.T.J. Dodson, *Introduction to Laplace Transforms for Engineers*, School of Mathematics, Manchester University.
5. Omer Stringa, *Matematika Financiare*, Pegi, Tiranë 2004.
6. N. A. Patil, Vijaya N. Patil, *Application of Laplace Transform*, Global Journals Inc. (USA), Online ISSN: 2249-4626 & Print ISSN: 0975-5896, Volume 12 Issue 12 Version 1.0 Year 2012.

INVESTIGATION OF CONVERGENCE OF ξ APPROXIMATIONS ON COMPLEX NUMBER PLANE

Assist. Prof. PhD. Işım Genç DEMİRİZ

Department of Mathematics, Davutpaşa Campus-Yıldız Technical University of İstanbul, Turkey

idemiriz@yildiz.edu.tr

Abstract: In this study, the convergence behaviour of the ξ approximants for the exponential operators is investigated on the entire complex plane. The purpose of this study is to develop an algorithm to observe how to transform a initial region on the complex plane defined by ξ approximants.

Keywords: LIE OPERATORS, COMPLEX RECURSIVE FUNCTIONS, EVALUATION OPERATORS

1. Introduction

In this study, the convergence behavior of the ξ approximants for the exponential operators is investigated on the entire complex plane.

Exponential operators play important roles in many branches of science and engineering. They can be constructed to characterize the solutions of various mathematically formulated problems. Exponential operators give quite accurate results for the short-term evolution but causes error accumulation for long-term evolution when they are employed through a numerical approximation scheme based on time discretization. Hence we need to evaluate exponential operators in a global and rapidly converging manner.

System with n degrees of freedom will be characterized by x_1, x_2, \dots, x_n complex variables, which are considered as the coordinates of a point or components of a vector in an n -dimensional complex vector space.

$\{x_1(t), x_2(t), \dots, x_n(t)\}$: System

x_1, x_2, \dots, x_n : Phase space vector components in this system.

Hence $Q(t_f, t_i)$ global evolution operator is defined as

$$x(t_f) = Q(t_f, t_i).x(t_i)$$

where t_i and t_f denote the initial and final states respectively. If factorization of evolution operators is considered as a sequence of rather simple global evolution operators then the evolution operator can be written as follows

$$Q(t_f, t_i) = e^{(t_f - t_i)S}$$

where S is defined through

$$S = \sum_{j=1}^N f_j(x_1, x_2, \dots, x_N) \frac{\partial}{\partial x_j}$$

so Q evolution operator can be assumed to be written as

$$Q = e^{t f(x) \frac{\partial}{\partial x}} = \prod_{j=1}^{\infty} e^{\sigma_j(t) x^j \frac{\partial}{\partial x}} \quad \sigma_j(t) = t f_j$$

where $L = f(x) \frac{\partial}{\partial x}$ and

$$f(x) = \sum_{j=1}^{\infty} f_j x^j \quad |x| < \rho$$

This equation is factorization formula for the one-dimensional case.

The definition of the evolution operators and their relations with the solutions of a differential equations are presented. Also the effects of the evolution operators on the functions is obtained as follows:

for $j = 0$

$$Q^{(0)} f(x) = e^{\sigma_0(t) x \frac{\partial}{\partial x}} f(x) = f(x + \sigma_0(t))$$

for $j = 1$

$$Q^{(1)} f(x) = e^{\sigma_1(t) x^2 \frac{\partial}{\partial x}} f(x) = f(e^{\sigma_1(t)} x)$$

for $j = n$ by $x = y^{\frac{1}{1-n}}$ transformation

$$Q^{(n)} f(x) = e^{\sigma_n(t) x^n \frac{\partial}{\partial x}} f(x) = f\left(\frac{x}{[1 - (j-1)x^{j-1}\sigma_j(t)]^{\frac{1}{j-1}}}\right) \quad j \geq 2$$

The essential approximation is to truncate

$$Q = \prod_{j=1}^{\infty} e^{\sigma_j(t) x^j \frac{\partial}{\partial x}} \quad \sigma_j(t) = t f_j$$

to a finite order. By this way it produces the following approximation.

$$\bar{\xi}_n(x, t) = \left\{ \prod_{j=1}^n Q^{(j)} \right\} x$$

If the infinite product representation of Q converges then the following result can be obtained:

$$\bar{\xi}(x, t) = Qx = e^{t f(x) \frac{\partial}{\partial x}} x = \lim_{n \rightarrow \infty} \bar{\xi}_n$$

A recursion relation for these approximants can be shown as follows:

$$\bar{\xi}_{n+1} = \left\{ \prod_{j=1}^n Q^{(j)} \right\} e^{\sigma_{n+1}(t) x^{n+1} \frac{\partial}{\partial x}} x$$

It can be clearly seen that this equation becomes

$$\bar{\xi}_{n+1} = \left\{ \prod_{j=1}^n Q^{(j)} \right\} \frac{x}{[1 - n\sigma_{n+1}(t)x^n]^{\frac{1}{n}}}$$

As a result we can easily obtain that

$$\bar{\xi}_{n+1} = \frac{\bar{\xi}_n(x, t)}{[1 - n\sigma_{n+1}(t) \bar{\xi}_n^n(x, t)]^{\frac{1}{n}}}$$

And this is a recursion relation with an initial member evaluated as follows:

$$\bar{\xi}_1(x, t) = e^{\sigma_1(t) x \frac{\partial}{\partial x}} x = x e^{\sigma_1(t)} = x e^{f_1 t}$$

Although this is a simple recursion relation, the existence of f_1 may not be suitable for numerical purpose depending on the value of f_1 . So we can normalize ξ -approximants as follows:

$$\bar{\sigma}_{n+1} = n\sigma_{n+1} e^{n f_1 t}$$

Then the final recursion relation becomes as follows:

$$\bar{\xi}_{n+1}(x, t) = \frac{\bar{\xi}_n(x, t)}{(1 - \bar{\sigma}_{n+1}(t) \bar{\xi}_n^n(x, t))^{\frac{1}{n}}}$$

The relation between the final and the previous approximants can be given as

$$\bar{\xi}_n(x, t) = \bar{\xi}_n(x, t) x e^{f_1 t}$$

In this study the convergence of the ξ -approximant sequences in the complex plane is main issue. The above transformation of ξ_n to $\bar{\xi}_{n+1}$ can be interpreted as applying some basic elementary transformations consecutively. For this reason the following transformations are presented

$$\begin{aligned} w_1 &= f_1(z) = z^n & 0 \leq r < \infty & \quad 0 \leq \varphi \leq \frac{2\pi}{n} \\ w_2 &= f_2(z) = -\sigma_{n+1} w_1 & 0 \leq r < \infty & \quad 0 \leq \varphi \leq 2\pi \\ w_3 &= f_3(z) = 1 + w_2 & 0 \leq r < \infty & \quad 0 \leq \varphi \leq 2\pi \\ w_4 &= f_4(z) = \frac{1}{w_3} & 0 \leq r < \infty & \quad -\emptyset \leq \varphi \leq \emptyset \\ w_5 &= f_5(z) = w_4 - 1 & 0 \leq r < \infty & \quad 0 \leq \varphi \leq 2\pi \end{aligned}$$

$$w_6 = f_6(z) = \frac{1}{\sigma_{n+1}} w_5 \quad 0 \leq r < \infty \quad 0 \leq \varphi \leq 2\pi$$

$$w_7 = f_7(z) = w_6^{\frac{1}{n}} \quad 0 \leq r < R \quad 0 \leq \varphi \leq 2\pi$$

As can be easily seen we get the main transformation function when we apply these consecutive transformations.

$$\begin{aligned} w_7 = w_6^{\frac{1}{n}} &= \left(\frac{1}{\sigma_{n+1}} w_5 \right)^{\frac{1}{n}} = \left(\frac{1}{\sigma_{n+1}} (w_4 - 1) \right)^{\frac{1}{n}} = \left(\frac{1}{\sigma_{n+1}} \left(\frac{1}{w_3} - 1 \right) \right)^{\frac{1}{n}} \\ &= \left(\frac{1}{\sigma_{n+1}} \left(\frac{1}{1 + w_2} - 1 \right) \right)^{\frac{1}{n}} = \left(\frac{1}{\sigma_{n+1}} \left(\frac{1}{1 - \sigma_{n+1} w_1} - 1 \right) \right)^{\frac{1}{n}} \\ &= \left(\frac{1}{\sigma_{n+1}} \left(\frac{1}{1 - \sigma_{n+1} \xi_n^n} - 1 \right) \right)^{\frac{1}{n}} \quad z \rightarrow \xi_n \\ &= \left(\frac{1}{\sigma_{n+1}} \left(\frac{1 - 1 - \sigma_{n+1} \xi_n^n}{1 - \sigma_{n+1} \xi_n^n} - 1 \right) \right)^{\frac{1}{n}} = \left(\frac{\xi_n^n}{1 - \sigma_{n+1} \xi_n^n} \right)^{\frac{1}{n}} = \frac{\xi_n}{(1 - \sigma_{n+1} \xi_n^n)^{\frac{1}{n}}} \end{aligned}$$

Here $\sigma_n(t)$ functions are assumed to be given and the ξ -approximants' nature are determined by these $\sigma_n(t)$ functions. The main purpose of the examination of this convergence is to give important information about the convergence of finite product sequences that appears during the factorization of these sequences.

The purpose of this study is to develop an algorithm to find out or observe how the above recursion relation defined via ξ -approximants transform a given initial region on the complex plane defined by ξ -approximants and a develop a computer program based on this algorithm. By this computer program we can expect to be able to examine the regional changes during the consecutive recursion transformations and to put forward some theorems by investigating this program outputs.

A singular point taken in the domain can carry us to infinity on the ξ_{n+1} -plane as can be noticed through

$$\xi_{n+1} = \frac{\xi_n}{(1 - \sigma_{n+1} \xi_n^n)^{\frac{1}{n}}}$$

Therefore one can obtain a singularity free initial region on ξ_n -plane by determining the locations of these singularities and discarding them from the domain.

In this study, the original contribution is the separation of the recursion relation between two consecutive ξ -approximants into basic simple consecutive transformations.

The other contributions are the construction of an algorithm that evaluates the region variations through the consecutive transformations and to develop a computer program to execute this algorithm. The computer program is written in C++ language and Mathematica is used for graphics.

2. Conclusion

In this study has shown for the $\sigma_n(t)$ sequences that shrink fast enough that the equivalent in the ξ_n -plane of a circular region without a singularity for the ξ_1 -plane will remain without singularity in the ξ_n series, regardless of n and time.

3. References

1. Feynman R.P., Phys. Rev., (1951)
2. Aizu K., Math. Phys., (1963)
3. Demiralp M., Rabitz H., Factorization of Certain Evaluation Operators Using Lie algebra: Formulation Method, J. Math. Chem., Vol.6., pp165-192, (1991)
4. Demiralp M., Rabitz H., Factorization of Certain Evaluation Operators : Convergence Theorems, J. Math. Chem., Vol.6., pp193-208, (1991)

A FUZZY APPROACH TO THE EMISSION ESTIMATION

Assoc. Prof. Ph.D. Filiz Kanbay¹

Department of Mathematics Davutpaşa Campus –Yıldız Technical University of İstanbul, Turkey ¹
fkanbay@yildiz.edu.tr

Abstract: In this study, emission amounts emitted from the transportation are examined by using fuzzy inference system in MATLAB. The effect of the speed and the traffic condition are taken into consideration in a fuzzy model.

Keywords: ESTIMATION, FUZZY, EMISSION, FUZZY INFERENCE SYSYTEM

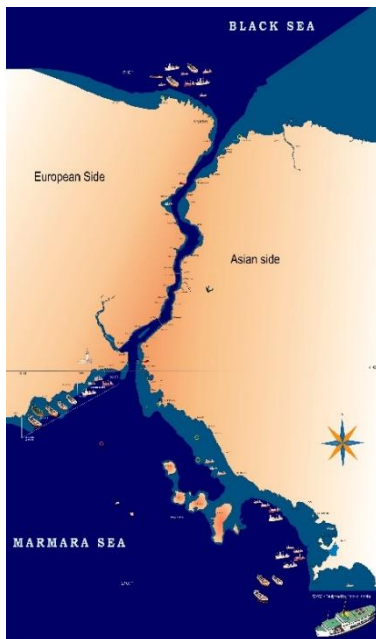
1. Introduction

It is known that air pollutants (e.g. carbon monoxide, sulfur oxides, nitrogen oxides, particulate matters) have harmful effects on the environmental and human health. Most air pollutants emitted from human-made sources: mobile sources such as transportation or stationary sources such as factories, power plants. Some air pollutants emitted from natural sources such as volcanic eruptions, forest fires (<https://www.epa.gov/>). Many researchers have been studying on the estimation of air pollutants and their effects by different methods. Some studies are about the different area of the world. For examples, emissions amounts for Tokyo Bay Area; NE Atlantic region; Tyrrhenian Sea; Turkish Straits; sea of Marmara; Dannish Ports were estimated by Onagawa [1]; Carlton [2]; Trozzi and Vaccaro [3,4]; Keskin and Vardar [5], Kanbay and Vardar[6]; Kılıç [7] and Deniz [8]; and Saxea and Larsena [9] respectively. On the other hand, Corbett and Fischbeck [10], Corbett and Koehler [11], Endresen [12] were estimated globally annual emissions.

In this study, as an example of the emission estimation; the estimation amounts NO_x emitted from transit vessels passing through the Bosphorus are calculated by using fuzzy inference system (FIS) in Matlab. Bosphorus (see Fig.1 it was taken from <http://www.bosphorusstrait.com/the-bosphorus-strait/map-of-bosphorus/>) connects Marmara sea and Black sea with the length 29.9 km. and the width ranges between 700 and 1500 meters.

Fig. 1 Bosphorus

2. Objectives and Method



The amounts NO_x emitted from transit vessels were calculated by using the methodologies explained in studies of Trozzi and Voccaro (see [3, 4]) and Kilic (see [7]). Amounts of emissions were calculated by the following equation;

$$E_i = t \cdot P \cdot (EF)_i \cdot [EngineLoad], \quad (1)$$

where i is the pollutant type, t is time, P is engine power in kilowatts (kW), $(EF)_i$ is emission factors of pollutant i , $[EngineLoad]$ is the percentage of full power of the engine. It is assumed that the engine runs 80 % load of the power of engine (Engine load is 0.8) and 4 generators work during the cruising time and run 75% load of the power of auxiliary engine. Due to the traffic and weather conditions, the cruising times are between $t_1 = 1.54$ hours and $t_2 = 2.42$ hours. The gross tonnages and engine powers are given according to the ship types on Tab.1 (see [7]). $(EF)_{NO_x}$ according to the ship and working types is presented on Tab. 2.

Table 1: The Ship Types and Engine Power

P Gross tonnage Ship Types	Engine Power (kW)					
	<500 grt	500 - 999 grt	1000 - 4999 grt	5000 - 9999 grt	10000 - 49999 grt	>50000 grt
Bulk Carrier	550	750	2700	5000	8800	17000
Cargo Ships	810	1181	3366	7516	13932	31471
Tanker	751	1003	2160	4854	10376	15997
Gross tonnage Ship Types	Auxiliary Engine Power(kW)					
	<500 grt	500 - 999 grt	1000 - 4999 grt	5000 - 9999 grt	10000 - 49999 grt	>50000 grt
Bulk Carrier	20	40	175	300	380	500
Cargo Ships	56	96	241	615	1396	1914
Tanker	52	65	153	300	425	761

Table 2: $(EF)_{NO_x}$ according to the ship and working types

SHIP TYPES	WORKING TYPE	$(EF)_{NO_x}$
Bulk Carrier	CRUISING	17.7
	HARBOUR	13.5
	MANOEUVRE	14.0
Cargo Ship	CRUISING	14.9
	HARBOUR	13.3
	MANOEUVRE	12.6
Tanker	CRUISING	14.0
	HARBOUR	12.3
	MANOEUVRE	12.2

By using the equation (1), the amounts of E_{NO_x} according to ship types and their gross tonnage for one ship are calculated. The results are presented on Tab. 3.

Table 3: E_{NOx} according to ship types and their gross tonnage for one ship

E_{NOx} (ton/year)						
Ship Types	<999 grt (Group 1)		1000-9999 grt (Group 2)		>9999grt (Group 3)	
	<500 Grt Subgroup 1-1	500-999 Grt Subgroup 1-2	1000-4999 Grt Subgroup 2-1	5000-9999 Grt Subgroup 2-2	10000-49999 Grt Subgroup 3-1	>50000 Grt Subgroup 3-2
Tanker	Min. 0.0163 Max. 0.0256	Min. 0.0215 Max. 0.0337	Min. 0.0471 Max. 0.0740	Min. 0.1031 Max. 0.1620	Min. 0.2064 Max. 0.3244	Min. 0.3251 Max. 0.5109
Cargo Ship	Min. 0.0187 Max. 0.0294	Min. 0.2828 Max. 0.4445	Min. 0.0783 Max. 0.1231	Min. 0.1803 Max. 0.2833	Min. 0.3518 Max. 0.5528	Min. 0.7094 Max. 1.1148
Bulk Carrier	Min. 0.0136 Max. 0.0214	Min. 0.0196 Max. 0.0308	Min. 0.0731 Max. 0.115	Min. 0.0790 Max. 0.1242	Min. 0.2229 Max. 0.3503	Min. 0.4115 Max. 0.6467

The number of ships (Tanker, general cargo and bulk carrier) passing through the Istanbul strait was recorded as 42553 in 2016 and the number of ships according to ship types are given on Tab. 4, (it was taken from the web-site of DTGM (2016): [https : //atlantis.udhb.gov.tr/istatistik/ gemigecis.aspx](https://atlantis.udhb.gov.tr/istatistik/gemigecis.aspx) of DTGM).

Table 4: Number of Ships Passed Bosphorus

The Total Number of Ships				
Ship Types	<999 grt (Group1)	1000-9999 grt (Group 2)	>9999 grt (Group3)	Total Number of Vessel
Tanker	110	7964	807	8881
Cargo Ships	320	23177	2354	25851
Bulk Carrier	92	7017	712	7821

Despite six groups vessels on Tab.3, the total number of ships are only three groups. On Tab. 3 all three groups are divided separately two sub-groups. The numbers of the ships of the subgroups are unknown. Hence the fuzzy inference system (FIS) could be appropriate solution method. The mamdani type FIS with various shaped fuzzy membership functions was created. The membership functions were experienced by taking into account the cruising time and the different gross tonnages possibilities (see Fig. 2, Fig. 3 and Fig. 4).

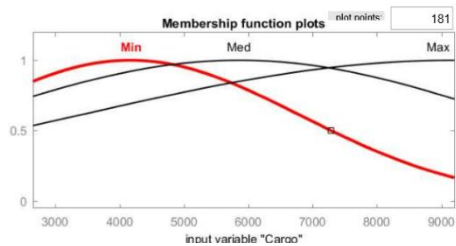


Fig. 2 Membership function plots of input variable “Cargo”.

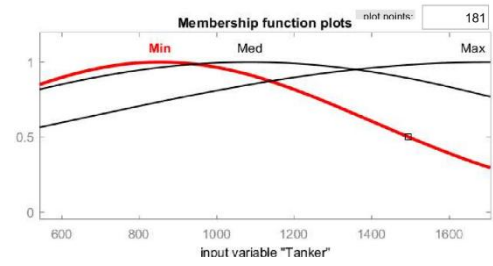


Fig. 3 Membership function plots of input variable “Tanker”.

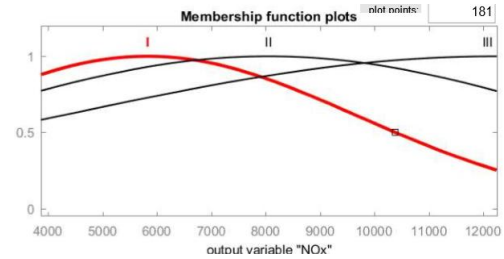


Fig. 4 Membership function plots of output variable “NOx”.

Seeing that the gross tonnages and cruising times of the transit vessels passing through the Bosphorus are different from each other. Total emission levels are different depending on gross tonnages and cruising times. The diversities of E_{NOx} are summarized on Table 5.

Table 5: The rules of the estimation E_{NOx} according to gross tonnage

Tanker	Tanker	Tanker	Cargo	Cargo	Cargo	Bulk	Bulk	Bulk	Total
Min	Med	Max	Ship	Ship	Ship	Carrier	Carrier	Carrier	Level
			Min	Med	Max	Min	Med	Max	
X			X			X			I
X			X				X		I
X			X					X	II
X				X		X			II
X				X			X		II
X				X				X	II
X					X	X			III
X					X		X		III
X					X			X	III
	X		X			X			II
	X		X				X		II
	X		X					X	II
	X			X		X			II
	X			X			X		II
	X			X				X	II
	X				X	X			III
	X				X		X		III
	X				X			X	III
		X	X			X			II
		X	X				X		II
		X	X					X	II
		X		X		X			III
		X		X			X		III
		X			X	X			III
		X			X		X		III
		X			X			X	III

3. Results

By using Fuzzy Inference System in Matlab, the variation of E_{NOx} values for different ship types according to the gross tonnage of the ships can be seen and the results are also illustrated by the surfaces (see Fig. 5).

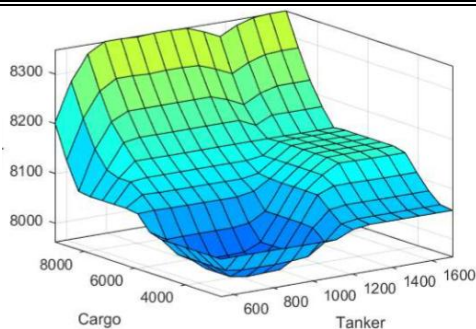


Fig. 5 The amount of NO_x for Tankers and Cargo Ships according to their gross tonnage

4. Conclusion

The Amount NO_x emission emitted from transit ships passing through the Bosphorus is estimated by using fuzzy inference system. Estimations were calculated for three different ship types. The effect of the gross tonnage and cruising speed changes of vessels were taken into consideration in the fuzzy model. It seems that the maximum amount of NO_x occurs from the cargo ships. The results is given as surface too.

5. References

1. Onagawa K., *Study on Impact of air pollutions emitted from Ships in Tokyo Bay Area*, Proceedings MARIENV'95. Vol.2, Japan, (1995), 824-829
2. Carlton J.S., Reynolds G.L., Wright A.A., Danton S.D., Webster A.D., *Marine Exhaust Emissions: Result from Shipboard Measurements and Regional Surveys*, Proceedings of ISME Yokohama'95, Vol.1 ,Japan, (1995) 57-67
3. Trozzi C., Vaccaro R., *Methodologies for Estimating Air Pollutant Emissions From Ships*, Techne Report MEET. (Methodologies for Estimating Air Pollutant Emissions from Transport) RF98 (1998)
4. Trozzi C., Vaccaro R., *Actual and Future Air Pollutant Emissions from Ships*, Transport and Air Pollution and Cost 319 – Final Conference – INRETS Graz, Austria 31 May – 2 June 1999
5. Kesgin U., Vardar N., *A study on Exhaust gas Emissions from Ships in Turkish Straits Atmospheric Environment* 35, (2001) 1863-1870.
6. Kanbay F., Vardar N., *On a Fuzzy Application of the Particulate Matters Estimation* Iranian Journal of Fuzzy Systems (Accepted)
7. Kılıç A., *Marmara Denizi'nde Gemilerden Kaynaklanan Egzoz Emisyonları*, BAÜ FBE Dergisi Cilt:11,Sayı:2, (2009) 124-134
8. Deniz C., Yalçın D., *Estimating Shipping Emissions in the Region of the Sea of Marmara*. Turkey Science of the Total Environment, 390(2008),
9. Saxea H., Larsena T., *Air Pollution from Ships in three Danish Ports*, Atmos Environ (38), (2004) 4057-4067.
10. Corbett J., Fischbeck P., Pandis S., *Global Nitrogen and Sulphur Inventories for Oceangoing Ships*, J Geophys Res 104 (1999) 3457-3470,
11. Corbett J., Koehler H., *Updated Emissions from Ocean Shipping*, J Geophys Res 108(D20) (2003).(9-1)-(9-13)
12. Endresen Φ., Sørsgard E., Sundet J.K., Dalsoren S.B., Isaksen ISA, Berglen T.F.,Gravir G., *Emissions from International*

OPTIMAL ERROR INDICATORS FOR CONVECTION DOMINATED PROBLEMS

Petr Lukáš

Charles University in Prague, Faculty of Mathematics and Physics,
Department of Numerical Mathematics
lukas@karlin.mff.cuni.cz,

Abstract: *In the talk we consider the numerical solution of the scalar convection–diffusion–reaction equation*

$$-\varepsilon \Delta u + b \cdot \nabla u + c u = f \text{ in } \Omega, u = u_b \text{ on } \Gamma_D \quad (1)$$

We present new results of an adaptive technique in finite element method based on minimizing a functional called error indicator $I_h : W_h \rightarrow R$, where W_h is a FE space for the discrete solution w_h of (1). The simplest form of such an indicator $I_h(w_h)$ is a residual based error indicator.

It is possible to enrich such an indicator by other terms which favor a less smeared solution to a diffuse one. One example of such an added term is $||\varphi(b^\perp \cdot \nabla w_h)||_{0,1,K}$, where φ is a function like square root (problems of the square root function and it's derivative around 0). The suitability of added terms depends on the particular problem.

The parameter we are changing in the optimization procedure is currently the parameter τ from SUPG (SDFEM) method and the parameter called epsilon in [2] for the SOLD method which adds diffusion in the crosswind direction (page 2205). In the talk we focus on a way to derive new indicators and optimizing those which are currently in use.

KEYWORDS: STABILIZED METHODS, SUPG, SDFEM, SOLD, ADAPTIVITY

References

- [1] V. John and P. Knobloch and S. B. Savescu A posteriori optimization of parameters in stabilized methods for convection-diffusion problems - Part I, Comput. Methods Appl. Mech. Engrg. 200 (2011), 2916–2929.
- [2] V. John, P. Knobloch On spurious oscillations at layers diminishing (SOLD) methods for convection-diffusion equations: Part I – A review, Comput. Methods Appl. Mech. Engrg. 196 (2007), 2197–2215.
- [3] P. Lukas, P. Knobloch Adaptive techniques in SOLD methods, Applied Mathematics and Computation 319 (2018), 24–30.

AIR SPACE ROUTING AND FLIGHTS PLANNING: A PROBLEM STATEMENT AND DISCUSSION OF APPROACHES TO SOLUTION

Assoc. Prof. PhD. Alieksieiev V.

Lviv Polytechnic National University, Lviv, Ukraine

Vladyslav.I.Alieksieiev@lpnu.ua,  <https://orcid.org/0000-0003-0712-0120>

Abstract: Air routing has become an important problem of recent years. Wide implementation of idea to use a free routing airspace (FRA) over the Europe and idea of exploiting FRA as a main airspace management resource to reduce air traffic problems revealed a necessity of a new look to a routing problem. Many previous solutions relied on predefined topology of airways and ability to exploit well-developed methods known in graph theory. Meanwhile the problem was current due to many factors needed to be involved in the airspace as a 3D-space: air management restrictions and different air spaces regulation rules, weather conditions, danger areas, aircraft's characteristics, pilots' preferences, etc. Moreover, the appearance of FRA has made it inappropriate to use previous algorithms. Most of these algorithms required a definite topology with known routing points connected with predefined edges, while the FRA may have only border points to fly into or fly out of the area and no definite edges inside. The task of constructing the route became the same difficult as obvious: any pilot can fly directly through the FRA, but the route should be built and confirmed prior to a take-off. Problem comes even more evident if considered for the unmanned flying vehicles (UFV) and the need for robots or AI systems to solve the routing problem by themselves. As a topping of the complexity of the problem, one may consider the upcoming difficulties of airspace congestion in FRA. Despite the problem is known for areas close to airports, it is still current to plan routes avoiding flights conflicts in the air and to avoid FRA high congestion. There are different researches on some particular problems and some approaches to solve these problems. Nevertheless, there is no complex problem statement yet. This research was focused on need of understanding the full scope of problems for air routing to understand the ability to build an efficient solution for the problem as a whole.

Keywords: ROUTING PROBLEM, AIR ROUTING, FLIGHTS MANAGEMENT, FLIGHTS OPTIMISATION, ALGORITHM ANALYSIS

1. Introduction

The problem of air routing nowadays comes with a few starting points:

- The main goal is to find route between departure and destination airports.
- The second goal typically is to have some reduce of fuel burn. Nevertheless, one should mention that there are estimates that optimal routes are able to give typically only 1–3% of fuel burn reduce.
- It is also assumed that all routes exist within the air space that can be predefined typically both by lateral dimension boundaries and altitude limits.
- It is assumed that there are many possible routes in airspace should exist and there are some routes that can be considered optimal (or at least one). Nevertheless, one can consider situation of reaching conditions that any of these routes are inappropriate for the particular type of aircraft (i.e. with respect to its fuel capacity and/or possible altitude limit).
- A longer route is expected to be closer to “straight” route (a great circle route).

Most researches on air routing problem are made with some of following assumptions:

- the most valuable optimization could be made within cruise stage (due to it is the main part of any flight with the most fuel burned, and climb/descend stages are much shorter or can not be optimized because of predefined fuel burn rates etc.);
- the problem of 3D routing is often reduced to 2D routing considering only cruise flight stage to be able to make notable influence;
- the problem of finding the shortest path is considered solvable with some graph algorithm like Dijkstra or A* (same as in on ground routing) without respect to vertical trajectories optimization and/or wind optimization (nevertheless these algorithms are less useful in FRA – Free Routing Area).

One recent research [1] showed the great decrease of algorithm running time with a wind optimized approach algorithm compared to classical shortest path search on graph (like Dijkstra and A* algorithms). Nevertheless, the algorithm does not consider so named 3D-routing. There are also some other researches dedicated to routing in FRA [2].

Some other researchers [3–4] offer considering both weather conditions (winds, temperature) and flight altitudes and they showed that it is more efficient to consider all conditions while building the path compared to step by step consideration of each type of conditions after initial shortest path search. There are also some similar direction researches [5–8].

However, most of approaches offered do not consider possible RADs (Route Availability Document) influence. This means there should be used a combined approach to be able to find a complex air route through both a FRA and a standard airspace (with a regular net of airways). One of possible solutions with respect to PRDs (Prohibited, Restricted and Dangerous areas) was offered in [9] based on China airspace experience.

2. Prerequisites and means for solving the problem

Now, the current airspace routing problem understanding includes a set of the following problems:

- *Path construction* – a problem to find a path between airports of departure and destination with respect to RAD constraints: avoid, mandatory, etc.
- *Path optimization* – a problem to have best path according to:
 - Length (shortest flight distance)
 - Time (fastest flight)
 - Fuel consumption (cheapest flight)
 - Weather conditions: wind, temperature, etc. (both fastest and cheapest flight)
- *Path compliance* – a problem to have an appropriate path including:
 - Vertical path profile (heights or flight levels distribution over the path)
 - Smoothness (pilot preferences compliant flight and smooth path) – pilot requested path options (waypoints, segments, areas, avoid areas etc.), ability to fly (matching aircraft technical abilities, avoiding sharp turns and impossible maneuvers, pilots and passengers convenient maneuvers).

Solving the problem requires a set of goals to be defined. It is obvious that a software should be developed also. The following goals in problem solution are ordered according to its importance decrease.

- 1) *100% success in route construction between departure and destination points.* Success rate must involve as a successful result a completely correct answer whether the path exists or not (this mean that if the route search failed then the customer should be completely convinced that there is no any possible route in given circumstances to fly).
- 2) *Build a set of fully optimized routes.* The set of resulting routes must include three offered routes (in some ideal circumstances this would be the same single route):
 - a. the shortest route – distance optimized only,
 - b. the fastest route – time & fuel optimized (evidently, with respect to weather conditions and fuel consumption),
 - c. the cheapest route – cost optimized (evidently, with respect to weather conditions, fuel consumption and FIR costs).
- 3) *Quickest delivery time for the first found route.* Possibly this time should not exceed 30 seconds. Next, the customer must see the progress in optimization, so each next optimized route (better than initial and each previous route) should be delivered in less than each next 30 seconds. Route delivery delay for more than 2 or 3 minutes should be considered as a long search and customer should be offered to decide whether to keep searching or to use the latest found route.
- 4) *Separate processing of route inexistence.* This should be a response to customer's request to perform totally route availability search, which may take a longer time. The decision whether to wait a longer time should be passed to customer.

Many researches still consider routing problem in air space as a plain problem. Nevertheless, it remains a 3D problem and according to restrictions and peculiarities of an air space, there is a set of task to be solved separately:

- Take-off / Climb and Landing / Descend. According to SID/STAR configuration there should be found a set of actual initial points to start routing. These points are evidently different to a departure and destination points of airports. This yields the path search between two sets of points (ADEP_SET and ADES_SET) instead of search between only two points (ADEP and ADES). Vertical profile for take-off (including direct climb and/or step-climb) and landing (descend) should be considered at current step. Regarding a set of flight levels one may expect up to 64 points on both ADEP_SET and ADES_SET ends for the routing (i.e. 3–8 FL × 4–8 take-off/landing edges = 12–64 initial routing points).
- Determined flight (flight via airways). According to known and predefined air routes, there should be a known solution to find route on a graph (a topology). The difficulty of the problem is due to restrictions set (like RADs) and combinatorial explosion (regarding a huge or fast growing number of involved waypoints and edges).
- “Free” flight (flight via FRA). Peculiarity of the problem for the general routing problem approach is that there are no predefined edges between waypoints and it requires a topology to be generated “artificially” to be able to solve the problem with the same algorithm like in case of flight via airways. This problem actually is a problem of connecting two sets of points: area fly-in and area fly-out. Despite of seeming simplicity of a free flight, the problem looks quite different and requires some kind of particular solution to be used.
- Short flight route. This could be considered as a special case of routing problem concerning only to build the shortest route, while the problem of optimization can be abandoned. The actual result of optimization can be less useful in most circumstances of a short flight. This can be yielded with a higher cost of optimization efforts compared to implementation of a simple direct flight (shortest path flight) or insignificant benefit of optimization.

One should remember to define, at least formally, a set of metrics to be able to understand finally if the route fits all the needs. These metrics may help to make both a better route during route construction procedure and allow a pilot to decide whether he is satisfied with a route offered. Among others, a set of metrics to understand the quality of routes should include following estimates:

- Successfulness – existence of a route
- Smoothness – calculation of route direction changes
- Duration – overall required time
- Cost – overall fuel consumption + FIR costs

3. Solution of the examined problem

There is set of a very interesting and promising approaches based on a so named “nature inspired approaches”. Those considered are mostly the optimization algorithms, like ant algorithm, artificial bee colony algorithm (used in [3]), blind naked mole rat algorithm [10], rolling swarm of locust model [11], and grasshopper optimization algorithm [12–13]. Nevertheless, some of these algorithms have not been applied to solve of an air space routing problem. Here in this paper I offer to exploit the idea of a locust swarm move due to its behavior similarity to aircrafts flights. First, a locust swarm acts as a space oriented unit – it moves in particular direction like having some target. Second, a locust swarm flies actually and it is vulnerable to winds – this is very similar to aircraft flights wind vulnerability. Third, the algorithm can be used both to construct and to optimize routes.

Let's consider an artificial locust swarm behavior as a model for multi-routing solution approach. Each single locust could be considered as a solution for routing problem. Each locust in a swarm of N species can act in a definite way: “jump & fly” or “land on & eat”.

“Jump & fly” should be made between waypoints $p_i \in P$ with number of waypoints $|P|$. These waypoints are considered to be a food source for locust. The initial food quantity at each waypoint can be eaten by a single locust or a group of locusts, so the number $q_i = q(p_i) \in [0..N]$ of locust species able to eat at particular waypoint could be measured also as a quantity of food at the waypoint. The number $q_i = q(p_i)$ may also define a maximum number of locust species able to stay at waypoint p_i . The set of $q(p_i) \in Q \subset \mathbb{N} \cup \{0\}$ can be included in set of parameters for the model. Each waypoint can be considered to have the same quantity of food $\forall \{i, j\} \subset \mathbb{N}, i \leq |P|, j \leq |P|: Q(p_i) = Q(p_j)$ or different quantity of food $\exists \{i, j\} \subset \mathbb{N}, i \neq j, i \leq |P|, j \leq |P|: Q(p_i) \neq Q(p_j)$. This should depend on problem specifics – the simplest approach to routing can be considered with $\forall i \in [0..|P|]: q_i = 1$.

After locust eat it have to move forward. The direction for the swarm can be generally defined by a vector \vec{D} from initial point to destination point. This vector also gives a line of attraction for the swarm (and each locust in a swarm, respectively). So, the swarm would have two attraction forces: swarm self-attraction force to keep swarm together and swarm direction vector attraction force.

According to eat action each locust will choose the next waypoint filled with a food. The hunger will force the locust and a swarm to move forward and not to return back to “empty” waypoints.

The jump is an act of movement from one waypoint to next waypoint. When a locust jumps to next waypoint with a food it may be considered mandatory to eat a portion of food – the quantity of food at the point to be decremented. Each locust can “decide” to stay and eat if there is still a food at the waypoint and the swarm attraction not forces it to move again. This “decision” can be implemented via act of zero-length jump (means to stay at a waypoint). All jumps should be made over the predefined topology edges (if there are airways topology) or to some neighboring waypoint (if there are no topology edges, like in FRA).

The fly action is a situation, when there are no vacant and non-empty neighboring waypoints. In case of predefined topology, some next to neighbor waypoint can be used with respect to swarm attraction force and swarm direction vector. In case of absence of predefined topology edges (FRA) the next waypoint can be selected only with respect to presence of food and attraction forces (swarm and direction). The fly distance should be regulated with a gravity force (the distance is shorter if the force is greater).

The swarm attraction force can be used also to find a way between and around obstacles. It is expected that there could be some waypoints on the border of each obstacle, and a part of a swarm should stick around an obstacle at each of such waypoints. This means the waypoints on the border of the obstacle is being saturated to prevent other locusts to stay at the waypoint. And when the swarm moves forward behind the obstacle the swarm attraction should force the locusts from behind to move and follow the swarm.

It may happen that the swarm can divide into two swarms, if the swarm attraction force for some part of locusts becomes low. But we leave this case for further consideration.

Swarm attraction force can be calculated as a vector from a single locust position to a middle point of all species locations: $\frac{1}{N} \sum_{n=1}^N p_n$. Alternatively, swarm attraction force can be understood as a swarm noise. Once a single locust finds a food it may be considered to keep quiet. Contrary, there can be a sound of locust flight, attracting all locust species left at the back to follow the swarm. This may affect the locusts from the back to choose direction to the swarm forward position and not to repeat some curved ways. So, the swarm attraction force should be calculated for each locust as a vector from its current position to the swarm "sound", produced with those species in-flight. If we have a subset of locusts performed a fly, then there is a flight vector for each flying/jumping locust defined with its initial and destination position and a sum vector of the swarm noise can be found. Nevertheless, this alternate approach requires more calculations instead of having only predefined waypoints position, and this may yield inappropriate computational difficulty of the algorithm.

4. Results and discussion

A custom software solution for the algorithm was developed using Microsoft Visual Studio 2015 in C++ programming language. Currently, an initial test of a locust swarm algorithm for solving routing problem was made as a plain routing with randomly generated topologies. Simulations were performed on a Dell Inspiron notebook (model no. 3737-5683) with Intel Core i7 processor. The results of simulations are presented in Table below.

Simulations were made for different topology sizes, described with number of waypoints and number of edges in a graph. Different sizes of the locust swarms were used to find out which swarm size could be enough to find best route. The number of steps is the number of waypoints between starting and finishing points. The time of each simulation is given in milliseconds. The route length is expected to be a dimensionless value according to random generated waypoints' coordinates.

As one can mention, swarm size was selected as a value compared to number of waypoints. Nevertheless, a test of a single locust ability to find a route was made. It was found, that in case of a large topology (250 and 1000 waypoints) a single locust was unable to find a route between starting and finishing point within a predefined limit of iterations. Other swarm sizes were calculated as a 1/10, 1/5, 1/4, 1/3, 1/2, 2/3, 3/4, 4/5 and 1/1 of number of waypoints.

For small topologies (30, 50 and 100 waypoints), the shortest route was found by the swarm with number of locusts in it not less than a half of number of waypoints (size of swarm ≥ 15 , ≥ 25 and ≥ 50 respectively). However, for bigger topologies (250 and 1000 waypoints) the size of the swarm needed to find the shortest route decreased (size of swarm ≥ 62 and ≥ 100) revealing that 1/4 or even

1/10 could be enough. This is a particularly interesting result with the algorithm implementation.

Among the cases considered, with the growth of a swarm size the number of steps in the algorithm can decreased faster compared to route length. For example, when the number of waypoints was 50 and the swarm size was 25, a route with 4 steps was found, but it was not the shortest one yet.

Table: Simulations results.

Waypoints	Edges	Swarm size	Steps	Time (ms)	Length
30	150	1	12	16	56.4299
		3	15	63	83.1392
		6	10	32	69.7788
		7	5	31	29.2127
		10	5	31	40.4625
		15	2	32	23.4546
		20	2	16	23.4546
		21	2	15	23.4546
		24	2	25	23.4546
		30	2	31	23.4546
50	500	1	45	94	537.526
		5	22	94	287.817
		10	10	77	136.194
		12	8	78	114.170
		16	6	78	96.4703
		25	4	93	80.5464
		32	4	78	60.4997
		36	4	134	60.4997
		40	4	127	60.4997
		50	4	144	60.4997
100	1 000	1	54	172	1322.46
		10	14	156	378.330
		20	8	230	229.159
		25	6	209	160.357
		33	6	313	195.650
		50	5	344	97.1437
		66	5	389	97.1437
		75	5	488	97.1437
		80	5	531	97.1437
		100	5	615	97.1437
250	2 500	1	—	—	—
		25	14	922	911.938
		50	8	1047	648.49
		62	6	1005	404.38
		83	6	1376	404.38
		125	6	2029	404.38
		166	6	2628	404.38
		186	6	2947	404.38
		200	6	3242	404.38
		250	6	4081	404.38
1 000	10 000	1	—	—	—
		100	6	5993	2131.7
		200	6	11981	2131.7
		250	6	15089	2131.7
		333	6	20211	2131.7
		500	6	30669	2131.7
		666	6	40544	2131.7
		750	6	45541	2131.7
		800	6	48540	2131.7
		1000	6	61203	2131.7

5. Conclusion

The problem of air space routing was discussed and some key features differing the problem from a known on-ground routing problem were defined. A set of nature inspired optimization approaches was analyzed and an approach of an artificial locust swarm was chosen as an appropriate one. The algorithm of an artificial locust swarm routing (ALSR) was offered and partly developed. First results of the simulations are very promising and expected to be enhanced and improved in further researches. Some "fine tuning" features for the algorithm would be implemented to fit all the requirements, including routing in FRA and giving an appropriate route smoothness. In addition, a weather forecasts and

avoidance areas should be involved in an algorithm to satisfy real flights requirements.

grasshopper-optimization-algorithm-for-constrained-and-unconstrained-test-functions-93308.html

6. Acknowledgement

RocketRoute Limited (London, United Kingdom) sponsored the whole research, including current problem analysis and a developed algorithm of an artificial locust swarm routing (ALSR). This research results and all rights for the objects of intellectual property will belong to RocketRoute Limited (London, United Kingdom). The publication of the paper is made by permission of RocketRoute Limited (London, United Kingdom).

7. Literature

1. Flight Planning in Free Route Airspaces / Casper Kehlet Jensen, Marco Chiarandini, and Kim S. Larsen // 17th Workshop on Algorithmic Approaches for Transportation Modelling, Optimization, and Systems (ATMOS 2017), 2017 – 14p.
2. Conflict Free and Efficient Flight Routes Planning In Free Route Airspace / Mariusz Krzyanowski // Prace Naukowe Politechniki Warszawskiej. Transport, 2013. – P.277-285
3. Four-Dimensional Aircraft En Route Optimization Algorithm Using the Artificial Bee Colony / Murrieta-Mendoza, Alejandro; Botez, Ruxandra Mihaela; Bunel, Audric // Journal of Aerospace Information Systems – Vol. 15 Issue 6, Jun. 2018 – P. 307-334.
4. Lateral Navigation Optimization Considering Winds and Temperatures for Fixed Altitude Cruise using the Dijkstra's Algorithm / Murrieta-Mendoza, Alejandro; Botez, Ruxandra // Proceedings of the ASME International Mechanical Engineering Congress and Exposition, Nov. 2014 – Vol. 1, 2015. – 9 p.
5. A Practical Approach For Optimizing Aircraft Trajectories In Winds / Ng, Hok K.; Sridhar, Banavar; Grabbe, Shon // IEEE/AIAA 31st Digital Avionics Systems Conference (DASC) Location: Williamsburg, VA, Oct. 14-18, 2012. – 14 p.
6. Generating Optimal Aircraft Trajectories with respect to Weather Conditions / B. Girardet, L. Lapasset, D. Delahaye, C. Rabut, and Y. Brenier. // ISIATM, 2013. – 12 p.
7. Optimizing Aircraft Trajectories with Multiple Cruise Altitudes in the Presence of Winds / Ng, Hok K.; Sridhar, Banavar; Grabbe, Shon // Journal of Aerospace Information Systems – Vol. 11, Issue 1, Jan. 2014. – P. 35-46.
8. Aircraft Path Planning under Adverse Weather Conditions / Xie Z. and Zhong Z.W. // MATEC Web of Conferences 77, 15001 (2016), ICMR 2016 – 4 p.
9. Air route network optimization in fragmented airspace based on cellular automata / Shijin Wang, Xi Cao, Haiyun Li, Qingyun Li, Xu Hang, Yanjun Wang // Chinese Journal of Aeronautics – No. 30 (3), 2017 – P. 1184–1195.
10. A novel meta-heuristic algorithm for numerical function optimization: blind, naked mole-rats (BNMR) algorithm / Mohammad Taherdangkoo, Mohammad Hossein Shirzadi, and Mohammad Hadi Bagheri. // Scientific Research and Essays – Vol. 7 (41), Oct. 2012 – P. 3566-3583 – Retrieved from: <https://academicjournals.org/journal/SRE/article-full-text-pdf/F02820F28755>
11. A model for rolling swarms of locusts / Topaz, C., Bernoff, A., Logan, S., Toolson, W. // The European Physical Journal Special Topics – Vol. 157, 2008. – P.93–109.
12. Grasshopper Optimisation Algorithm: Theory and application / Saremi S., Mirjalil S., Lewis A. // Advances in Engineering Software – Vol. 105, Mar. 2017 – P.30-47
13. Application of Grasshopper Optimization Algorithm for Constrained and Unconstrained Test Functions / A.G. Neve, G.M. Kakandikar, and O. Kulkarni // International Journal of Swarm Intelligence and Evolutionary Computation – Vol. 6, Issue 3, Art. No. 1000165, 2017. – 7 p. – Retrieved from: <https://www.omicsonline.org/peer-reviewed/papplication-of->

MODELING OF MAGNETIC HYSTERESIS UNDER WEAK MAGNETIC FIELDS AND TRIAXIAL STRESS STATE

Mushnikov A.N., Kryucheva K. D.

Institute of Engineering Science, Ural Branch of the Russian Academy of Sciences, Ekaterinburg, Russian Federation.

mushnikov@imach.uran.ru

Abstract: The magnetomechanical hysteresis models of Jiles-Atherton and its modifications by Sablik are extended to treat magnetic properties in the case of triaxial stress state. Unlike the previous version, it is focused on weak magnetic fields. Results of simulation are compared with experimental data.

Keywords: MAGNETIC HYSTERESIS, BULK STRESS STATE

1. Introduction

The problem of a theoretical description of changes in the magnetization of ferromagnets in external magnetic fields and mechanical stresses is associated with the need to take into account its total free energy, which depend in a complex way on internal factors (internal and applied stresses, magnetic anisotropy, dislocations, non-equilibrium point defects and inclusions, phase composition). One of the popular mathematical models of magnetic hysteresis of ferromagnetic materials was developed by Jiles and Atherton [1] and then was supplemented by the other scientists. The Jiles-Atherton model (JA-model) has a higher computational performance compared with Preisach phenomenological model and the Stoner-Wolfart hysteresis model [2]. And taking into account modifications, important advantages of the JA-model are the connection with the actual physical parameters of the ferromagnetic material, the calculation of major and any minor hysteresis loops on the same model parameters, the simulation of the materials with isotropic and anisotropic properties, the calculation of the effect of mechanical stresses on magnetization.

The hysteresis model for the triaxial (bulk) stress state [3] was based on modifications of the JA-model [4, 5]. However, it turned out to be insufficiently suitable for describing processes in weak magnetic fields.

In the present paper, we refine the model for better describing the magnetization in weak fields, nevertheless maintaining adequate calculations in strong fields.

2. Mathematical formulation

The ideal (but impractical) experiment include triaxial stretching a cube with measuring magnetic characteristics simultaneously. In this paper, the bulk stress state is achieved by combining such types of loading as uniaxial tension/compression, torsion, and internal pressure. Listed types of loadings separately maybe not typical for some structures. They must be considered as the possibility of creating a stress state with independent changes in all three main stresses. The mechanical formulation was described in detail in [6].

Specimens are affected by axial load F , torque T and internal pressure p .

Normal stresses are calculated as:

$$(1) \quad \sigma_z = \frac{F}{\pi(R_{out}^2 - R_{in}^2)},$$

where R_{in} – internal radius of specimen, R_{out} – outer radius of specimen.

The volume-averaged values of the tangential stresses are equal to:

$$(2) \quad \tau = \frac{(R_{out} + R_{in})}{\pi(R_{out}^4 - R_{in}^4)} T.$$

Under the action of internal pressure, tensile circumferential stresses σ_r and compressive radial stresses σ_θ are occurring. Their values, as functions of radius r , can be written as:

$$(3) \quad \begin{cases} \sigma_r = \frac{R_{in}^2}{R_{out}^2 - R_{in}^2} \left(1 - \frac{R_{out}^2}{r^2} \right) p, \\ \sigma_\theta = \frac{R_{in}^2}{R_{out}^2 - R_{in}^2} \left(1 + \frac{R_{out}^2}{r^2} \right) p \end{cases}$$

In the general case, the stress tensor in a cylindrical coordinate system is defined as:

$$(4) \quad A = \begin{pmatrix} \sigma_r & 0 & 0 \\ 0 & \sigma_\theta & \tau \\ 0 & \tau & \sigma_z \end{pmatrix}.$$

By solving the characteristic equation, we find the values of the main stresses averaged over the volume:

$$(5) \quad \begin{cases} \sigma_{j_1} = \frac{1}{R_{out} - R_{in}} \int_{r=R_{in}}^{R_{out}} \sigma_r dr \\ \sigma_{j_2} = \frac{1}{R_{out} - R_{in}} \int_{r=R_{in}}^{R_{out}} \frac{\sigma_\theta + \sigma_z + \sqrt{(\sigma_\theta + \sigma_z)^2 + 4(\tau^2 - \sigma_\theta \sigma_z)}}{2} dr \\ \sigma_{j_3} = \frac{1}{R_{out} - R_{in}} \int_{r=R_{in}}^{R_{out}} \frac{\sigma_\theta + \sigma_z - \sqrt{(\sigma_\theta + \sigma_z)^2 + 4(\tau^2 - \sigma_\theta \sigma_z)}}{2} dr \end{cases},$$

where indexes j_1 , j_2 and j_3 take values 1, 2, 3 from condition $\sigma_1 \geq \sigma_2 \geq \sigma_3$.

To determine the directions of the main stresses, found main stresses are alternately substituted into the system of equations:

$$(6) \quad \begin{cases} (A - E\sigma_j) \vec{n}_j = 0, \\ n_{rj}^2 + n_{\theta j}^2 + n_{zj}^2 = 1 \end{cases},$$

where \vec{n}_j is a vector with components n_{rj} , $n_{\theta j}$ and n_{zj} , ($k = 1..3$), E is identity matrix. In this system of equations, three of the four equations are linearly independent. Thus, having solved three systems, we obtain direction cosines of the main stresses. The angles corresponding to them are denoted by ψ_j .

The JA-model is constructed in two steps: on the first, the anhysteretic magnetization is calculated, then the hysteresis is simulated using a system of differential equations, taking into account changes in the external magnetic field. Anhysteretic magnetization is a magnetization obtained by the simultaneous action of a constant field and an alternating field with an amplitude decreasing to zero. Often, a modified Langevin function is used to describe the anhysteretic magnetization of isotropic materials:

$$(7) \quad M_{an} = M_s \left[\coth\left(\frac{H_e}{a}\right) - \frac{a}{H_e} \right].$$

But it has a singularity at $H_e = 0$ and therefore is not well suited for weak magnetic fields. To find a better function, we carried out an experiment to measure the anhysteretic magnetization curve of structural chromium-nickel steel 15KhN4D.

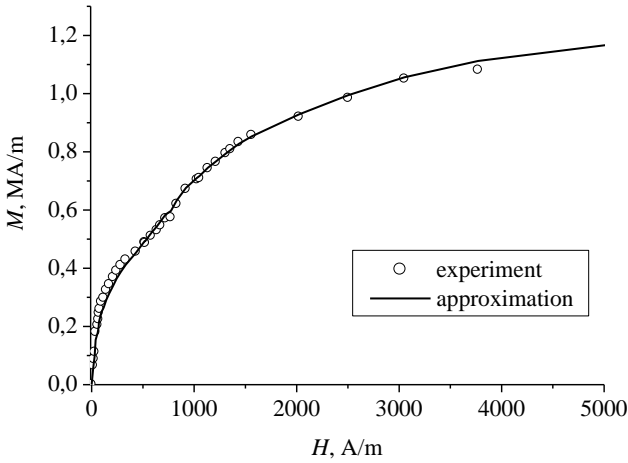


Fig. 1 Anhysteretic magnetization curve and its approximation.

This made it possible to choose a more suitable function that describes anhysteretic magnetization in weak magnetic fields with sufficient accuracy, and at the same time leads it to M_s when $H \rightarrow \infty$:

$$(8) \quad M_{an} = \frac{2}{\pi} M_s \arctan\left(\frac{H_e}{a}\right)$$

M_{an} is a function of effective field H_e :

$$(9) \quad H_e = H \cos \beta + \alpha M + H_\sigma,$$

where β is an angle between the direction of the external field and the vector of the resulting magnetization.

The basic equation of the JA-model, describing the change in total magnetization M , without separating it into reversible and irreversible components can be written as:

$$(10) \quad \frac{dM}{dH} = \frac{c}{1+c} \frac{dM_{an}}{dH} + \frac{1}{1+c} \frac{M_{an}(H) - M(H)}{\delta k - \alpha(M_{an}(H) - M(H))}.$$

Magnetoelastic energy under the action of three orthogonal mechanical stresses consists of three independent parts. The formula proposed previously [3] significantly increases the complexity of calculations because it includes a derivative of magnetostriction which depending on the M . So, as the first approximation for weak fields, we use the more simple form:

$$(11) \quad H_\sigma = \sum_{j=1}^3 \left[(b_{j1} + b_{j2} \sigma_j) \frac{M_{an}(H)}{M_s} (\cos^2 \varphi_j - \nu \sin^2 \varphi_j) \right].$$

Angles φ_j are solutions of three equations:

$$(12) \quad \frac{d}{d\varphi_j} \left[\frac{1}{2} \alpha \mu_0 M^2 - \mu_0 H M \cos(\arccos n_{zj} - \varphi_j) \right] = 0$$

for $j=1..3$.

The angle β between the direction of the external field and the magnetization vector, which is necessary to calculate the effective field (9), can be expressed in terms of the angles that were found above.

$$(13) \quad n_r^* = \sum_{j=1}^3 \cos\left(\frac{\varphi_j}{\psi_j} \arccos(n_{rj})\right)$$

$$(14) \quad n_\theta^* = \sum_{j=1}^3 \cos\left(\frac{\varphi_j}{\psi_j} \arccos(n_{\theta j})\right)$$

$$(15) \quad n_z^* = \sum_{j=1}^3 \cos(\psi_j - \varphi_j)$$

Then angle β is determined by the expression:

$$(16) \quad \beta = \frac{1}{|n^*|} \arccos n_z^*,$$

where $|n^*| = \sqrt{(n_r^*)^2 + (n_\theta^*)^2 + (n_z^*)^2}$. And also we take into account that $\cos \psi_j = n_{zj}$ are known values calculated by (6).

3. Results and discussion

Thus, the simulation of magnetic hysteresis in the bulk stress state must be performed in the following steps:

1. Calculating main stresses (5) and their directions (6).
2. Choosing range of H and the increment dH .

3. Solving the differential equation (10) at each step of H . Considering that anhysteretic magnetization is defined by equation (8), where effective field is given by expressions (9) and (11); angles between the magnetization vector and the directions of action of the main stresses (φ_1 , φ_2 and φ_3) are the solutions of the system of three equations (12); the angle β between the magnetization vector and the direction of external magnetic field is defined by the formula (16).

Experimental studies were conducted on the hollow cylindrical and continuous flat specimens of structural steel 15KhN4D. Permeameter magnetic measurements were made under applied loading. The tests were performed in the elastic strain region. A magnetic field was applied along the axis of the sample.

Although all the parameters of the JA-model have a physical meaning, their experimental determination is not a trivial problem. More practical are the methods of selecting the values of parameters which give a hysteresis loop, with sufficient accuracy reproducing the loop obtained in the experiment. M_s was directly obtained from the experimental major magnetic hysteresis loop. The difference between absolute saturation and the state of technical saturation (in a field of 60 kA/m) can be considered insignificant. To find the optimal parameters, the residuals R are minimized over all unknowns:

$$(17) \quad R = \sum_{i=1}^n (M_i^{\text{exp}} - M(H_i))^2,$$

where (H_i, M_i^{exp}) are experimental points "field-magnetization", n is a number of points in all hysteresis loops. For each set of parameters and for each point, the values $M(H_i)$ are calculated according to the mathematical model described in the previous section.

Analysis of the obtained loops with different stress variations showed that use of parameters b in (11) is not enough. Improving the fit between the experimental and calculated hysteresis loops was received by modifying the parameter k , which was previously considered as a constant:

$$(18) \quad k_\sigma = \left(\xi + (1 - \xi) \exp\left(-\frac{\sigma}{\varsigma}\right) \right) k,$$

where ξ and ς are additional constants for material.

As examples, Figure 2 shows some series of calculated and experimental minor hysteresis loops of the investigated steel. The difference between experimental and calculated values does not

exceed 15%. Figure 2a represents hysteresis loops (only the first quadrant) at various values of the maximum magnetic field. Magnetic fields that are close to the geomagnetic field almost do not create irreversible part of magnetization.

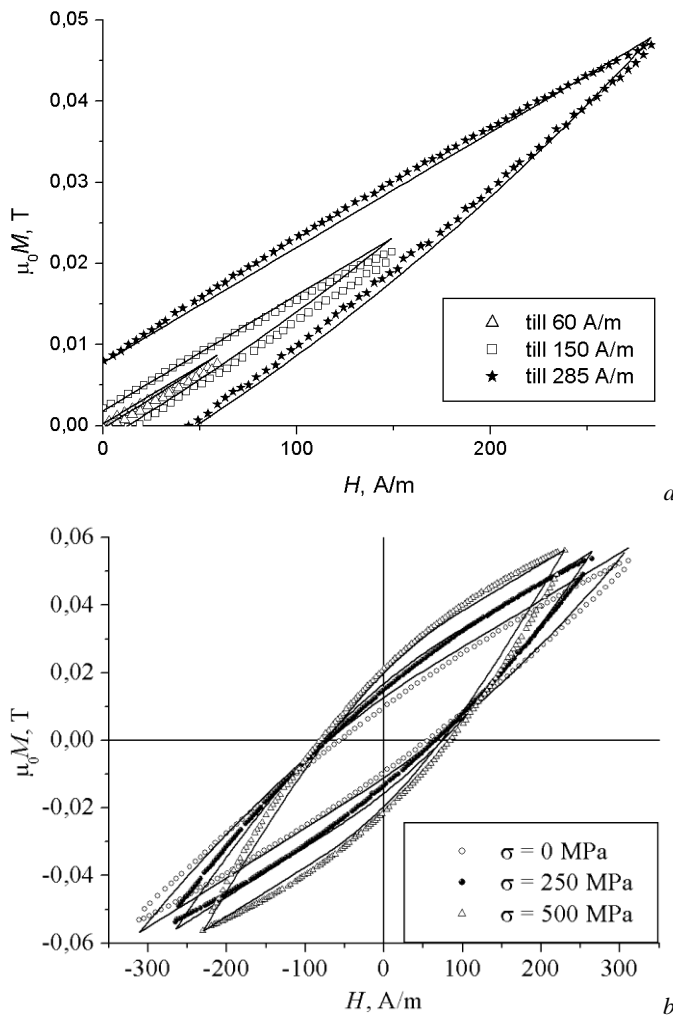


Fig. 2 Comparison of mathematical model and experimentally obtained minor loops. Points from experiments; lines are the model.

Figure 2b shows the effect of mechanical stresses on minor hysteresis loops obtained under magnetization up to the maximum induction of 0.05 T. Tensile stresses lead to the formation of a magnetic texture facilitating magnetization along the specimen axis. The minor loops measured in weak fields grow wider with increasing tensile stresses, their initial portion being steeper.

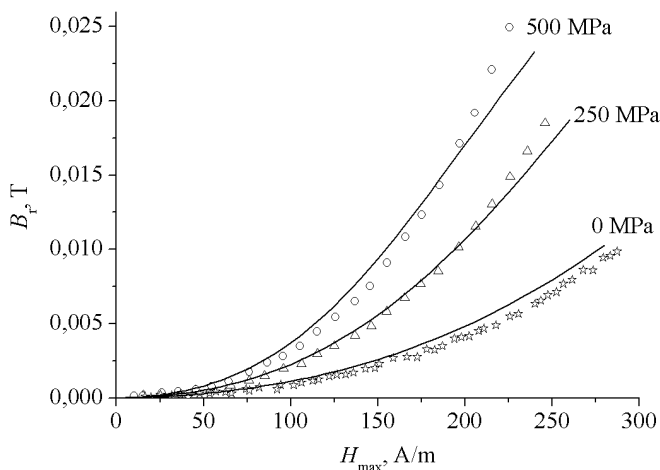


Fig. 3 Residual induction as a function of mechanical stresses and the maximum value of the external magnetic field.

A slight increase in coercive force is also observed. So in a magnetic field of a given strength, growing tensile stress is accompanied by an increase in the relative magnetized volume of the ferromagnetic material.

In details, figure 3 represents changes of residual induction B_r for various minor loops under mechanical stresses. The experiment was carried out on samples of the same grade of steel but from another melting. For this reason, the difference in the integral magnetic characteristics, which are calculated from major hysteresis loops, reaches 10%. In spite of this, for weak magnetic fields, the model rather accurately describes changes of the residual magnetization at the same parameters.

4. Conclusion

A modification of the mathematical model of hysteresis of Jiles-Atherton was proposed for the case of a bulk stress state and weak magnetic fields. It also includes some simplification for increase calculation speed. Comparison of calculated results with experimental data of structural steel showed the adequacy of the model.

5. Acknowledgements

The research was done within the state assignment, theme No. 0391-2016-0005. The experiments were carried out with the use of the equipment of the Plastometriya collective use center affiliated to IES UB RAS.

6. References

1. Jiles D. C., Atherton D. L. Theory of ferromagnetic hysteresis // Journal of Applied Physics, 1984, Vol. 55, p. 2115-2120.
2. Liorzou F., Phelps B., Atherton D. L. Macroscopic Models of Magnetization // IEEE Transactions on Magnetics, 2000, Vol. 36, № 2, p. 418-428.
3. Mushnikov A.N., Putilova E.A. Mathematical Model of Magnetic Hysteresis Under Triaxial Stress State // MATHMODEL'17 Proceedings, p. 55-58.
4. Sablik M.J., Rubin S.W., Riley L.A., Jiles D.C., Kaminski D.A., Biner S.B. A model for hysteretic magnetic properties under the application of noncoaxial stress and field. - Journal of Applied Physics, 1993, v. 74, №1, p. 480-488.
5. Sablik M.J., Riley L.A., Burkhardt G.L., Kwun H., Cannell P.Y., Watts K.T., Langman R.A. Micromagnetic model for biaxial stress effects on magnetic properties. - Journal of Magnetism and Magnetic Materials, 1994, v. 132, №1-3, p. 131-148.
6. Gorkunov E.S., Zadvorkin S.M., Mushnikov A.N., Smirnov S.V., Yakushenko E.I. Effect of Mechanical Stresses on the Magnetic Characteristics of Pipe Steel // Journal of Applied Mechanics and Technical Physics, 2014, Vol. 3, p. 530-538.

MATHEMATICAL MODELS OF CALCULATIONS OF PARAMETERS OF CRYSTALLIZATION OF BINARY ALLOYS BY MEANS OF COMPUTER THERMAL ANALYSIS

Ass. Prof., Dr. Eng. Donii O.¹, Ass. Prof., Dr. Eng. Khristenko V.¹, Omelko L.², Ass. Kotliar S.¹

National Technical University of Ukraine "Kyiv Polytechnic Institute named after Igor Sikorsky" - Kyiv, Ukraine¹
Physical Technological Institute of Metals and Alloys, National Academy of Science of Ukraine²

Email: dosha@iff.kpi.ua

Abstract: Mathematical models of crystallization of binary metal alloys crystallizing in the temperature range are proposed. These models are intended for use in the composition of quality control systems for cast alloys based on computer thermal analysis. The proposed models make it possible to calculate the time dependences of the relative amounts of the solid and liquid phases using the data of the cooling curve, as well as to determine the intensity of the increase of the amount of the solid phase. The method of determining the temperature dependences of the specific heat and latent crystallization heat using the data on the temperature-concentration dependences of the free energies of the phases forming the system under study was used.

KEYWORDS: THERMAL ANALYSIS, CRYSTALLIZATION, ENTHALPHY, GIBBS ENERGY, HEAT CAPACITY

1. Introduction

The final level of service properties of cast parts is laid down during the smelting and crystallization of alloys. It is at the stage of crystallization the "primary" structure of the solid metal is formed, which essentially determines the properties of the final product. Therefore, the creation of systems for operational control and management of the state of alloy, as well as control and management of crystallization phase of the melt is relevant.

The operation of many systems for monitoring of the state of metal melts is based on thermal analysis, which provides information on the thermal effects accompanying cooling of sample [1-7]. On the cooling curves (dependences of temperature on time $T = f(t)$), the thermal effects accompanying the formation of the cast metal structure are especially pronounced. Therefore, it seems promising studying the kinetics of crystallization and prediction of the service properties of metals in the solid state from the results of the analysis of cooling curves. The information which is obtained by this way (especially in the express mode) is necessary for making operational decisions on management of casting technological processes [5, 6].

In [8, 9], mathematical models were developed that describe the solidification of pure metals based on computer thermal analysis in the subsystem of quality control of casting melts. They describe the crystallization of a small sample of metal (for sufficiently small values of the Biot criterion: $Bi \ll 1$). When they were created, it was assumed that the specific heat (c) and latent heat of crystallization (L) are constants. Indeed, during the crystallization of pure metals, the specific latent heat of crystallization L is a constant value, while specific heat capacities of the liquid and solid phases differ (for example, for aluminum - by about 20%). It should be noted that these models were also used to describe the crystallization of alloys [8 - 10]. However, the crystallization of alloys occurs in the temperature range with changes in the composition of both the liquid and solid phases. Therefore, the values of the specific heat c and the specific latent heat of crystallization L depend on the composition and temperature of the liquid-solid medium, which, in turn, changes with time. Therefore, in the mathematical models of crystallization, intended for use in thermal analysis, it is necessary to make appropriate corrections.

The purpose of this work is to develop mathematical models of crystallization of multicomponent metal melts, which are crystallized in the temperature range, and are intended to interpret the results of computer thermal analysis.

2. Solution of the problem under consideration

Considering the solidification of a small casting, when the condition $Bi \ll 1$ is satisfied (which is typical for thermal analysis), we can write the heat balance equation [8]:

$$dQ = dQ_c + dQ_L, \quad (1)$$

where dQ is the amount of heat given by the alloy to the

environment; dQ_L - the amount of heat released as a result of the

formation of a solid phase; dQ_c - the amount of heat released as a result of temperature changes during the cooling of the metal.

Such a record of the heat balance equation (1) assumes that the temperature gradient over the cross section of the casting is neglected, and the casting is a homogeneous material point with mass m_0 .

In [6, 8 - 10], the well-known calorimetric relations were substituted in (1):

$$dQ_c = -cm_0dT(t), \quad (2)$$

$$dQ_L = Ldm(t), \quad (3)$$

and the intensity (speed) of heat removal to the environment was described by the law of total heat transfer:

$$\frac{dQ}{dt} = fS[T(t) - T_e] + \sigma\epsilon S[T^4(t) - T_e^4], \quad (4)$$

where $T(t)$ is the function of the dependence of the temperature of the metal sample on time (cooling curve of thermal analysis); T_e is the ambient temperature; c is the specific heat, L is the specific latent heat of crystallization; m_0 is the mass of the metal under study; $m(t)$ is the mass of the metal which have been crystallized to the moment of time t ; f is the heat transfer coefficient; S is the surface of the area from which heat is removed to the environment; ϵ - is the degree of blackness of the sample's surface; σ is the Stefan - Boltzmann constant.

Taking into account that the thermophysical parameters of alloys in the crystallization process are changed, it seems appropriate to determine the temperature-concentration dependences of the heat capacities of the phases $c(x, T(t))$ and the specific latent heat of crystallization $L(x, T(t))$ in the temperature range of crystallization for the particular alloy under study (here x is the content of the second component in the melt).

In [11], a method was proposed for determining of the dependences of interest from analytical expressions for the temperature-concentration dependences of the molar free energies of the phases. The calculation is based on the assumption that the values of enthalpy, entropy and isobaric-isothermal potential are interconnected through the heat capacity C_p :

$$\left. \begin{aligned} H &= \int c_p dT, \\ S &= \int \frac{c_p}{T} dT, \\ G &= H - TS = \int c_p dT - T \int \frac{c_p}{T} dT. \end{aligned} \right\} \quad (5)$$

where G is the Gibbs free energy; H - is enthalpy; S - entropy. For many metallic systems data on the temperature-concentration dependences of the Gibbs free energy of the phases forming the system under consideration are given in the literature. For example, for the case of a two-component system, the temperature-concentration dependence of the Gibbs molar energy of the phase is defined as:

$$G(x, T) = G_A(T) \cdot (1 - x_B) + G_B(T) \cdot x_B + G_{mix}(x, T) + RT \cdot (x_A \ln x_A + x_B \ln x_B), \quad (6)$$

where $G_A(T)$, $G_B(T)$ are the molar free energies of the pure components A and B in the phase at temperature T ; $x_A = 1 - x_B$, x_B - are content of components A and B in the phase (molar fractions); $G_{mix}(x, T)$ - is excess molar free energy of mixing in the phase of composition x at temperature T ; R - is the universal gas constant.

If the temperature-concentration dependence of the molar heat capacity $c_p(x, T)$ of the phase is expressed as a polynomial

$$c_p(x, T) = z_3(x) + z_4(x)T + \frac{z_5(x)}{T^2} + z_6(x)T^2 + z_7(x)T^3 + \dots, \quad (7)$$

then, in accordance with (5):

$$G(x, T) = z_1 - z_2T + z_3(x)T(1 - \ln T) - \frac{z_4(x)T^2}{2} - \frac{z_5(x)}{2T} - \frac{z_6(x)T^3}{6} - \frac{z_7(x)T^4}{12} + \dots, \quad (8)$$

where z_1 and z_2 are the integration constants.

The dependence of the heat capacity on the composition can be taken into account by presenting the coefficients in (7) in the form of polynomials

$$z_k(x) = z_{k,1}(x) + z_{k,2}(x)x + z_{k,3}(x)x^2 + \dots \quad (9)$$

Therefore, by presenting the temperature-concentration dependences of the free energies of the phases (6) in the form of polynomials (8) (for example, using the polynomial regression), one can obtain the desired temperature-concentration dependences of the heat capacities of the phases $c(x, T(t))$.

Taking into account (5), the temperature-concentration dependences of the enthalpies of the phases take the form:

$$H(x, T) = z_1 + z_3(x)T + \frac{z_4(x)T^2}{2} - \frac{z_5(x)}{T} + \frac{z_6(x)T^3}{3} + \frac{z_7(x)T^4}{4} + \dots, \quad (10)$$

Changes of the enthalpy of the system during the transition from the melt to the solid solution, calculated as the difference between the enthalpies of the liquid and solid phases (taken with the appropriate sign), are nothing else but the desired temperature-concentration dependences of the specific heat of crystallization $L(x, T(t))$.

Having determined by this way the temperature-concentration dependences $c(T(t))$ and $L(T(t))$ and substituting them in (2) and (3), equation (1) can be reduced to the form:

$$\frac{dV(t)}{dt} = \frac{c(T(t))}{L(T(t))} \frac{dT(t)}{dt} + \frac{k_{co}}{L(T(t))} [T(t) - T_e] + \frac{k_{ra}}{L(T(t))} [T^4(t) - T_e^4], \quad (11)$$

$$V(t) = \frac{m(t)}{m_0}, \quad (12)$$

$$k_{co} = \frac{fS}{m_0}, \quad (13)$$

$$k_{ra} = \frac{\sigma \varepsilon S}{m_0}, \quad (14)$$

where $V(t)$ is the relative amount of solids.

The solution of equation (11) can be obtained by direct integration:

$$V(t) = \int_w^t \frac{c(T(t))}{L(T(t))} \frac{dT(t)}{dt} dt + \int_w^t \frac{k_{co}}{L(T(t))} [T(t) - T_e] dt + \int_w^t \frac{k_{ra}}{L(T(t))} [T^4(t) - T_e^4] dt. \quad (15)$$

The under integral functions in (15) are complex non-linear dependencies. However, taking into account the fact, that the result of thermal analysis is the cooling curve $T(t)$, which is a time series with constant time intervals [9], the integrals in expression (15) are easily calculated by numerical methods. The calculation uses the initial condition:

$$V(t_{cr}) = 0, \quad (16)$$

showing the absence of a solid phase at the onset of crystallization.

3. Results and discussion

The proposed mathematical model (16) allows to determine the amount of the solid phase $V(t)$ at any time of crystallization using the cooling curve obtained by thermal analysis. Although the same information can be obtained from the alloy state diagram, due to the non-equilibrium crystallization conditions, its use leads to significant calculation inaccuracies. Beside this, the usage of a state diagram does not allow to estimate the intensity (rate) of the formation of a solid phase $V'(t)$. But this is namely that parameter which is used for prediction of mechanical properties of alloys [5, 6].

For practical calculations of the amount of the solid phase and the intensity of its formation using expressions (11) and (16), first of all it is necessary to determine the time derivative of the temperature $T'(t)$ from the cooling curve and calculate the coefficients k_{co} and k_{ra} . Calculation of $T'(t)$ is easily implemented using the numerical differentiation formulas. However, in many cases, pre-filtering of the cooling curve is required [9]. To determine the values of the coefficients k_{co} and k_{ra} from the cooling curve, one can use the method of determining of the coefficients k_1 and k_2 , given in [9]. In [9], they are calculated by linearizing the portions of the cooling curve before and after crystallization, followed by the using of the least squares method. The coefficients k_{co} and k_{ra} are related to k_1 and k_2 as follows:

$$k_{co} = k_1 c_{Li}, \quad (11)$$

$$k_{ra} = k_1 c_{So}, \quad (12)$$

where c_{Li} , c_{So} are the specific heat values of the studied alloy in the liquid and solid states.

The above mentioned methodology can also be used in the development of mathematical models of crystallization of alloys with eutectic. Models for such alloys are given in [10], where temperature dependences of thermal parameters are not taken into account.

4. Conclusions

In this paper, we developed a method for constructing of

mathematical models of crystallization of binary metal alloys which are crystallized in the temperature range. A characteristic feature of the proposed models is to take into account the dependence of the specific heat and latent heat of crystallization on temperature. For this purpose, the temperature-concentration dependences of the free energies of the phases forming the system under study are used. The proposed models make it possible to calculate the time dependences of the relative amounts of the solid and liquid phases from the cooling curves obtained by using of computer thermal analysis, as well as to determine the intensity of formation of the solid phase.

5. References

1. Apelian D., Sigworth G.K., Whaler K.R. Assessment of grain refinement and modification of Al-Si foundry alloys by thermal analysis // Trans. Amer. Foundrymen's Soc. - 1984. - 92. - p. 297-307.
2. Argyropoulos S., Closset B., Gruzelski J.E., Oger H. Quantitative Kontrolle der verdellung von Al-Si gublegierungen unter anwendung eine thermoanalysetechnik // Giesser. Prax. - 1985. No11. - s. 173-180.
3. Argyropoulos S., Closset B., Gruzelski J.E., Oger H. The quantitative control of modification in Al-Si foundry alloys using thermal analysis technique // Transact. Amer. Foundrymen's Soc. - 1983. - 91. - p. 351-358.
4. Shumikhin V.S., Vitusevich V.T., Kornienko G.L. Comprehensive quality control of cast iron by thermal analysis // Foundry. - 1984. - No2. - P. 3-5 (Russian)
5. Bialik OM, Donii A.N., Pikovsky V.S., Shapoval A.I. The usage of the computer system for quality control of melts - "Foundry", 1996, No. 2, pp.28-30. (Russian)
6. Bialik OM, Donii A.N., Shapoval A.I., Kulinich A.A. System of computer thermoanalysis of silumin - "Foundry production", 1998, №7, p.41-42. (Russian)
7. Borisov G. P., Smulsky A. A., Semenchenko A. I. Express-control of the melt and prediction of the properties of a future casting at the stage of preparation of a liquid metal based on an improved method of thermal analysis // Casting processes. - 2007. - № 1-2. - p. 19-22. (Russian)
8. Bialik OM, Mentkovsky Yu.L. Questions of the dynamic theory of solidification of metal castings. - Kiev: Vishcha school, 1983. - 111 p. (Russian)
9. Donii O.M. Mathematical models for calculating of the parameters of crystallization and preliminary filtration of the cooling curve during computer thermal analysis // Bulletin of SevNTU. Vip 110: Mechanics, energy, ecology: zb. sciences. pr. Sevastop. nat tech. un-t - Sevastopol: View of SevNTU, 2010. - p. 193-197. (Ukrainian)
10. Donii O.M. . Mathematical models of hardening of alloys with eutectic for calculation of parameters of crystallization based on data of the cooling curve in computer thermal analysis // Bulletin of SevNTU. Vip 110: Mechanics, energy, ecology: zb. sciences. pr. Sevastop. nat tech. un-t - Sevastopol: View of SevNTU, 2011. - p. 126 - 131. (Ukrainian)
11. Khristenko V., Omelko L., Donii O. Calculation of temperaure dependence of thermal effects at cooling of metal alloys // Machines. Technologies. Materials. - 9. - 2018. - P.374 - 377.

APPLYING QUEUE THEORY AT STUDY OF REFUSALS OF REQUESTS RECEIVED IN UNIVERSAL AUTOMOTIVE SERVICE

Assist. Prof. Grozev D. PhD.¹, M.Sc. Georgiev I. PhD.², , Assist. Prof. Milchev M. PhD.¹
 Faculty of Transport –University of Ruse “Angel Kanchev”, Bulgaria ¹
 Faculty of Natural sciences and education –University of Ruse “Angel Kanchev”, Bulgaria ²
 dgrozev@uni-ruse.bg

Abstract: The refusal of requests received in a universal automotive service workshop in the city of Rousse was investigated. The present work analyses the average monthly requests from the workshop customers. The number of the actual repairs was also determined. The work in the service have been seen as a mass service system with a non-stationary mid-month incoming stream with queries. The basic values of the system parameters were calculated under non-stationary conditions and Mat Lab application was created. After the model has been validated, a service conversion option was proposed to reduce the refusals. The proposed approach can serve as a methodology for analysing and optimizing of the activity of other universal automotive service.

Keywords: queue theory, refusals of requests, modelling, universal automotive service, correction, operating mode, work organization

1. Introduction

In the maintenance of transport equipment the main objective is the technical condition of the fleet to be always correct, using minimal resources. This can be achieved with different strategies and methodologies. The most modern trends used in the maintenance of vehicles is the development of different methods and methodologies for predicting the technical condition change [13].

Outsourcing the maintenance of vehicles is the most widely used method. The most common reasons for using this are:

- freeing resources for core business activities;
- improving productivity and quality;
- saving of funds;
- use of external competencies;
- transfer of the risks [10].

Using outsourcing has a number of drawbacks. The first is related to the employment of the service itself, which is the time for repair of the damaged vehicle (the time for order / order processing). The second disadvantage is related to the quality of the performed repairs / service.

The full query processing time includes the queue time and the time for processing the query itself. Queue is directly dependent on the time required for the query to be processed, i.e., the shorter the processing time for the query is, the queue is the smaller as well.

According to the online business catalog "bussines.bg" there are 30 vehicle workshops in the town of Rousse [3]. The average number of working posts in these workshops is 7, which means that the working posts for servicing and repairing cars in Rousse are 210. In 2009, 90 871 cars were registered in city of Rousse [4]. From what has been written here follows that there will be a chronic shortage of working posts in the city. A queue of damaged cars will be produced in the workshops. For many workshops, getting big queues leads to denial of potential customers and financial losses. The purpose of this report is to provide a practical solution to this problem by researching a specific workshop.

The goal will be achieved by setting and solving the following tasks:

- collecting and processing statistical information from the services of a universal automotive workshop based on previous periods;
- defining the type of mass-service system;
- input modelling.
- solving the system of differential equations;
- defining the main features of the system;
- preparing proposals for adjusting the regime or organization of work in the workshop.

2. Exposition

In order to describe the operation mode of the car service, considered as a mass service, it is necessary to know the characteristics of the incoming flow of cars considered as a

stochastic process, the service intensity, the maximum length of the tail and the number of service units [6, 11].

For the inbound flow of freight we can make the following assumptions:

- ordinary flow - The probability of two or more cars occurring for an elementary time interval is infinitely small compared to the probability of occurrence of only one car. The normality feature means that the cars come as single, not in group of two, three and so on at the same time.

- flow without consequences - the number of cars arriving in the system for time interval Δt does not depend on how many vehicles have already arrived, i.e. does not depend on the history of the studied phenomenon (the flow without action afterwards (Poisson flow)).

- stationarity / non-stationarity of the flow [8, 13] - for sufficiently long periods of time - 1 month, 6 months, 1 year, etc. it is possible to assume the steady-state of the incoming stream, that is to say, with certain conventions. the probability of occurrence of a certain number of cars in a given, sufficiently long interval depends only on the length of that interval. Generally, in arbitrary periods, the λ stream is non-stationary $\lambda = \lambda(t)$. This non-stationarity is clearly distinguishable over a period of one business year (about 300 working days).

For service intensity data by the service owner, it is known that the service time of a vehicle is a relatively constant quantity and is about half a working day (4 hours) based on a plan, $\mu = \text{const}$. Regarding the number of service channels (servers), if necessary it can reach up to 3 ($1 \leq n \leq 3$). Two installers are needed to ensure continuous work for 8 hours on one channel. Again, according to the owner's data with more than $m = 12$ waiting in the queue, he refuses the order of the day, or the client renounces himself. To test the system's operation, it is necessary to find the probability that the system will have a number of cars at the time t when operating the n server [7, 2]

$$P_k(t) = ?, k = \overline{0, n+m}, t \in [1, T], 1 \leq n \leq 3, \quad (1)$$

where for one period T is taken one full working month $T = 1$ of 12 months. The beginning of the first working month $t = 1$ coincides with the astronomical beginning of the year, and the end of the last working month $t = T = 12$, with the end of the astronomical year.

For the queue theory model, the following can be summarized: a non-stationary stream of requests with density $\lambda(t)$, supplied to a mass service system with n serving channels. Request service time is a random variable with an indicative distribution and parameter $\mu = \text{const}$. A car arriving at a busy time stands in the waiting line and "patiently" waits for service, unless there is more than $m = 12$ in the service queue. a limited waiting system and a limited number of cars in the queue. The main indicator will be the intensity of returned requests, and at what time of year these peaks are the highest, as well as the average number of underserved queries in those peaks.

From everything told above so far, it can be said that the system is of type (M / M / s) in non-stationary mode. To describe a system of this type, the following system of differential equations of Kolmogorov (Erlang-Kolmogorov) [mitrofanova] is in effect [1, 7]:

$$\begin{aligned} \frac{dp_0}{dt} &= -\lambda P_0(t) + \mu P_1(t) \\ &\dots\dots\dots \\ \frac{dp_k(t)}{dt} &= \lambda P_{k-1}(t) - (\lambda + k\mu)P_k(t) + \mu(k+1)P_{k+1}(t) \\ &\dots\dots\dots(0 \leq k \leq n-1)\dots\dots\dots \\ \frac{dp_n(t)}{dt} &= \lambda P_{n-1}(t) - (\lambda + n\mu)P_n(t) + n\mu P_{n+1}(t) \\ &\dots\dots\dots \\ \frac{dp_{n+s}(t)}{dt} &= \lambda P_{n+s-1}(t) - (\lambda + n\mu)P_{n+s}(t) + n\mu P_{n+s+1}(t) \\ &\dots\dots\dots(0 \leq s < m)\dots\dots\dots \\ \frac{dp_{n+m}(t)}{dt} &= \lambda P_{n+m-1}(t) - n\mu P_{n+m}(t) \end{aligned} \quad (2)$$

n is the number of channels and the maximum queue length when all servers are occupied. In some cases (with endless waiting) the differential equation system is open and for the numerical decision it is necessary to take the extra algebraic condition $\sum_{i=0}^{\infty} P_i(t) = 1$ for normality. In the more general case, the maximum length of the queue is large. The computational features associated with a system (2) following the possible introduction of an algebraic equation are as follows:

- a large-scale system (generally)
- the system is differential-algebraic
- the system is of the "rigid system" type.

This can be summarized as followed: a system of rigid, differential-algebraic equations in some large-scale slashes. Numerical methods have been developed to overcome these difficulties. A Matlab program was developed to solve a system (2), using the built-in "solver" ode15s, implementing the Gir method. When entering $\lambda(t), \mu, n, m$, the application returns a numerical solution to $P_k(t)$. Artificially, the precision is greater than the default for the solver – from 10^{-6} to 10^{-9} to absolute error from 10^{-3} to 10^{-5} to relative error [3, 12].

Input stream $\lambda(t)$, generally every day, is different, and some seasonality is also highlighted. The following table 1 gives statistics for the applications received over a period of 3 years between 2015 and 2017.

Tab. 1 Distribution of orders in researched automotive Service by Month

Month\Year	2015	2016	2017
1	139	145	144
2	102	106	108
3	149	145	148
4	137	152	148
5	155	162	160
6	165	168	172
7	187	188	184
8	190	186	184
9	169	175	176
10	130	122	128
11	130	128	132
12	119	118	120

To model $\lambda(t)$, it is advisable to select a relatively elementary function who have a periodicity. This is appropriate given the seasonal fluctuations. To approximate the average values for the

period 2015-2017. two methods are used - least squares method and minimax method. The use of the minimax method is motivated by the fact that the biggest error is minimal.

The model should be as simple as possible but reflects the most characteristic behavior of the real stream. For a model, the following trigonometric line is selected, non-linear to the quoted ratios:

$$\lambda(t) = a_0 + a_1 \cos(wt) + b_1 \sin(wt) \quad (3)$$

the coefficients a_0, a_1, b_1, w , calculated by the least squares method are:

$$a_0 = 154.734311, a_1 = -2.134153, b_1 = -31.383019, w = 0.660038. \quad (4)$$

The coefficient of determination is $R^2=0.8132$ (statistically significant).

The coefficients a_0, a_1, b_1, w , estimated by the minimax method are:

$$a_0 = 154.760396, a_1 = -12.684669, b_1 = -30.630357, w = 0.647557 \quad (5)$$

Figures 1 and 2 show the graphs of $\lambda(t)$ with coefficients calculated by least squares method and minimax method.

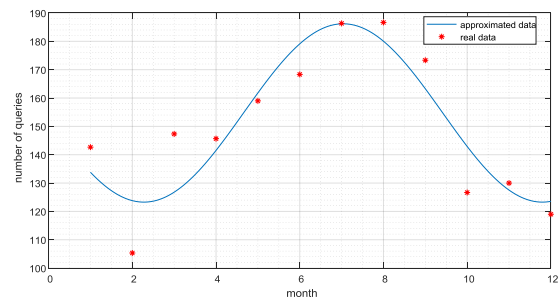


Fig. 1 The function $\lambda(t)$ with coefficients found by least squares method

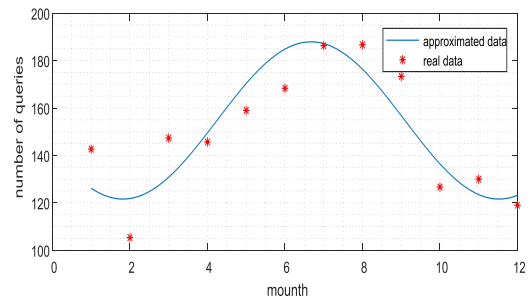


Fig. 2 The function $\lambda(t)$ with coefficients found by the minimax method

For the service intensity of one channel - μ , taking into account the service time of one car from one channel (we consider the working month for 25 days), we receive a $\mu = 50$ cars a month from a single channel for a month.

The starting state of the system $P_k(t_0)$ is unknown. It is known that these types of processes are persistent and after a long period of time they enter into regular mode of operation. Therefore, an initial state may be taken arbitrarily. The integration of the system needs to be done not for a period of time but for a sufficient number of periods. In this way, probability functions $P_k(t)$ begin to bend to their regular values. After repeated integration with different end times it was found that only after 5-6 periods the $P_k(t)$ functions enter the regular mode (for two adjacent periods, remain the same). Accuracy is also increased here, with integration being done over 20 periods, with the difference of all $P_k(t)$ in the last and penultimate periods being less than 10^{-8} for each t . Taking into account the proximity of $\lambda(t)$ calculated by the coefficients of (4) and (5), all calculations are further made at $\lambda(t)$ by coefficients of (5) (minimax method).

The following graphs reflect the results of the system decision (2) at the following values:

$\lambda(t)$ calculated with coefficients of (5) $\mu = 50, n = 3$ (3 running servers), $m = 12$ (up to 12 in the queue).

Figure 3 illustrates the probability of having exactly $k \in [0; 3]$ cars in the system. It is noteworthy that the most likely values for a

small or zero number of cars are between 5 and 9 months (May-September).

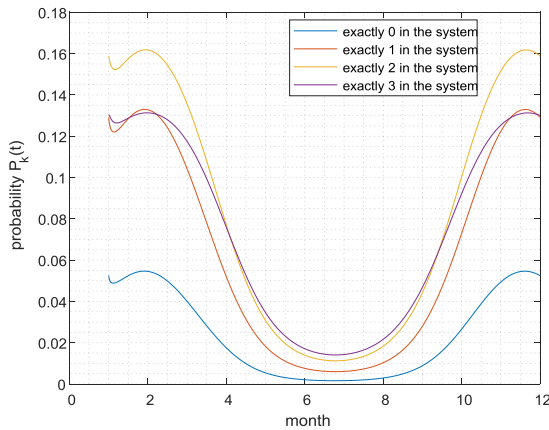


Fig. 3 Graph of the probability of having exactly the $k \in [0; 3]$ vehicle in the system

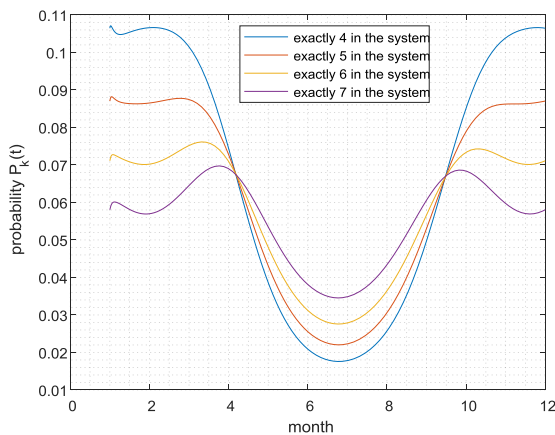


Fig. 4 Graph of the likelihood of having an exact $k \in [4; 7]$ vehicle in the system

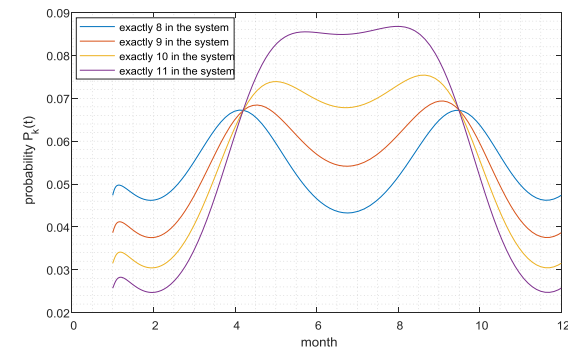


Fig. 5 Graph of the likelihood of having an exact $k \in [8; 11]$ vehicle in the system

In Fig. 6 shows that shortly after the fourth to the middle of the ninth month the probabilities of a big queue grow at high speed, with a peak coming just before the seventh month.

The probability of rejection is given by $P_{n+m}(t)$, i.e. all channels and places in the queue are busy and the arrived request will be denied (in Figure 6 the curve with purple color). It is also essential to know the density of declined queries. They are given with:

$$P_f(t) = \lambda(t)P_{n+m}(t) \quad (6)$$

Fig. 7 reflects the density of failures. Again, it is noticeable that in Fig. 7 the density of failures strongly starts to increase after the fourth month. The highest value is about 7 months after it starts to decrease. The volumes of returned requests V_f calculated between arbitrary times t_1 and t_2 are given by:

$$V_f = \int_{t_1}^{t_2} \lambda(t)P_{n+m}(t)dt = \int_{t_1}^{t_2} P_f(t)dt \quad (7)$$

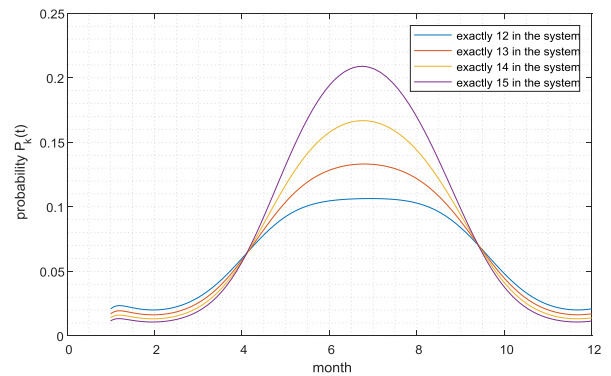


Fig. 6 A graph of the probability of having an exact $k \in [12; 15]$ vehicle in the system with $\lambda(t)$, calculated by the coefficients of (5)

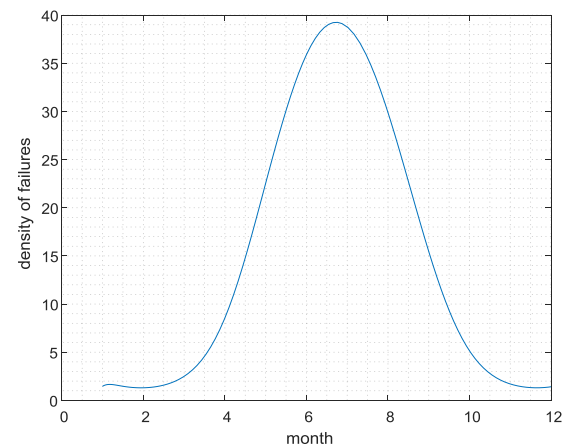


Fig. 7 Graph of the density of failures

The average volume of returns for the entire period is about 163.24. Also interesting are the volumes between 4-6 months, 6-8 months, 8-10 months, and in the busiest period between 5 and 9 months. After numerical solving of the integral (7), the results are shown in Table 2

Tabl. 2 Results of the calculations

Months	Average number of returns	% from all returns
4-6	44.26	27.11
6-8	74.83	45.84
8-10	30.92	18.94
5-9	125.51	76.89

Table 2 shows that almost 77% of the returned applications are for a period of 4 months - from the beginning of May to the beginning of September.

Research shows that with constant work of 3 channels (6 people) there is a marked unevenness in the main indicators of the system. The ineffective mode of operation of the system leads to the need to take adequate measures to optimize it. According to the data from the owner of the garage, the hire of an additional third worker on each channel i.e. a 50% increase in the workforce would not lead to a linear decrease in service time by 50%, and a working day (4 hours) for repair, the time would fall to about 3 hours. Hiring more people from three people per channel does not lead to a decrease in service time.

There is a variant in which three additional people are appointed for a period of 4 months from the beginning of May until the beginning of September. The service speed of $\mu = 50$ will increase for this period at $\mu = 66,667$, with the other indicators not changing.

In Fig. 8 is a graph of the density of failures when hiring a supplementary labour for a period of 4 months. It appears that in the troubled period, returns have substantially decreased. There are also two large peaks, around the beginning of the year and after the beginning of the fourth month. They can be neutralized in a similar way, but it is not always possible to hire a workforce for a short time.

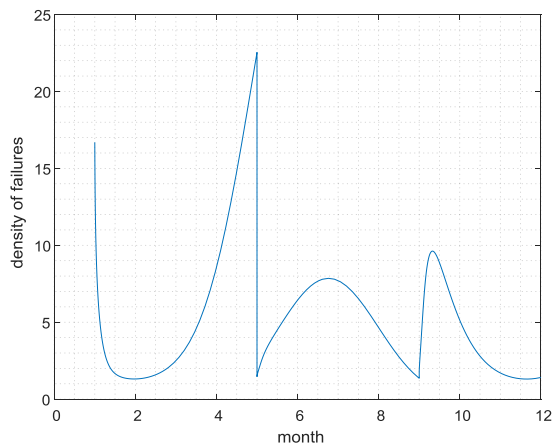


Fig. 8 Graph of the density of failures in μ different during the season whit high intensity of orders

In the proposed option to improve system performance the returned orders are 57.32, which is 2.85 times less than the original volume.

The study described in this report is also applicable to other repairers because of the similarity of organization of work in them, which is similar to the inputs of the system.

3. Conclusion

1. The theoretical results obtained are intended to clarify the behavior of the system at any time of the day for periods of approximately equal non-stationary intensity (accuracy to constant) of arrival and service.

2. A way is proposed to approximate the input flow density by the most general average statistics.

3. A methodology has been proposed for modeling and testing of the characteristics of a universal car service with similar non-stationary behavior as well as universal car service with a number of service units.

4. When system characteristics are unsatisfactory, the theoretical results will determine what adjustments in service intensity and / or number of channels are to be made for better performance. This would save time and problems of the "trial and error" type.

5. For the study, given the average behavior of intensity, the "average tail length" characteristic is sufficiently synchronized with the theoretical predictions (Table 1 and Figure 8). With sufficient statistics and measurements (a fairly accurate approximate intensity) for other universal car repair shops, it will provide theoretical characteristics that are close enough to the real ones.

6. Improvements can be made at no extra cost (for example opening new positions). This can be done by organizing a job involving more workers. This organization of working time will have the necessary effect in minimizing and adjusting the waiting time and the number of failures. This would result in a much more efficient way of working for the system itself. The waiting time will be approximately the same regardless of the arrival of the cars. The total average waiting time will also be reduced.

The study was supported by a contract of University of Ruse "Angel Kanchev", № BG05M2OP001-2.009-0011-C01, "Support for the development of human resources for research and innovation at the University of Ruse "Angel Kanchev". The project is funded with support from the Operational Program "Science and Education for Smart Growth 2014-2020" financed by the European Social Fund of the European Union.

References:

1. A. Mitrofanova, Continuous times Markov chains. Poisson process. Birth and death process, (New York University, 2007)
2. H. Taha, Operations research, an introduction, New York (J. Wiley and Sons, 1993)
3. L. Shampine, M. Reichelt, The MATLAB ODE Suite, SIAM Journal on Scientific Computing, 18, 1-22 (1997)
4. L. Norov, D. Akbarov, Customs – time for a change, Problems of Economic Transition, 52(2), 47-60 (2009)
5. M. Fitzmaurice, Optimization plan for freight movements at key commercial border crossings, Report compiled by Transport Logistics Consultants, August (2009)
6. M. Zukerman, Introduction to queueing theory and stochastic teletraffic models, EE Department, City University of Hong Kong (2016)
7. N. Gautam, Analysis of queues: Methods and applications (CRC Press, 2012)
8. S. Ross, Introduction to probability models, (Elsevier, 2007)
9. R. Markov, Transport corridors South-North in Southeastern Europe. Sustainable development of Lower Danube regions. Variant "Son – 2" of Rousse – Veliko Tarnovo Motorway, Sofia (2017)
10. Robert Klepper, Wendell O. Jones, Outsourcing information technology, systems and services, Prentice-Hall, Inc. Upper Saddle River, NJ, USA ©1998, ISBN:0-13-281578-8
11. J. Sztrik, Basic Queueing Theory, GlobeEdit, OmniScriptum GmbH, KG, Saarbrücken, Germany (2016)
12. V. Todorov, I Georgiev, Optimization methods with MATLAB, (Avangard print, 2016)
13. Wallace R.B., D. N. Prabhakar Murthy, Case studies in reliability and maintenance, Wiley-interscience, 2003
14. <https://www.business.bg/k-586/avtomobilni-servizi/c-191/ruse.html>, Бизнес каталог „business.bg“, (22.08.2018)
15. <http://www.nsi.bg/bg/content/606/basic-статистика-на-европейските-градове-град-русе, брой на регистрираните в гр. Русе автомобили>

COMPUTER MODELLING OF RADIAL-SHEAR ROLLING OF AUSTENITIC STAINLESS STEEL AISI-321

D.t.s., prof. Naizabekov A.B.¹, c.t.s. ass. prof. Lezhnev S.N.¹, PhD Arbuz A.S.², PhD Panin E.A.³, d.t.s. Koinov T.A.⁴

¹Rudny industrial Institute, Rudny, Kazakhstan; ²Nazarbayev University, Astana, Kazakhstan

³Karaganda state industrial University, Temirtau, Kazakhstan; ⁴University of Chemical Technology and Metallurgy, Sofia, Bulgaria

E-mail: sergey_legnev@mail.ru

Abstract: In this paper the results of modelling of radial-shear rolling process of austenitic stainless steel AISI-321 are presented. The simulation in Simufact Forming program complex was performed. The conditions of simulation for radial-shear mill SVP-08 of Rudny industrial Institute were adopted. The various parameters of stress-strain state (effective plastic strain, effective stress, mean normal stress and Lode-Nadai coefficient) and also microstructure evolution with rolling force were considered. It is revealed that radial-shear rolling is an effective process for obtaining of high quality round billets from stainless steels of austenitic class.

Keywords: RADIAL-SHEAR ROLLING, SIMULATION, STRESS-STRAIN STATE, AUSTENITIC STAINLESS STEEL

1. Introduction

Despite the current level of development of virtual computing technologies, the main method of research of any technological process is a physical experiment. Since only in natural experiment it is possible to take into account all parameters that affect the investigated process. At the same time, conducting only physical experiments is a very irrational task that requires a lot of effort, time and material resources.

The ideal compromise is the use of software systems of virtual modeling, which allow to simulate the investigated process, to take into account almost all parameters that affect it, as well as to optimize the process, i.e. to determine the values of all the dependent parameters at which the process will be the most stable. After that, when conducting a physical experiment with optimal values, the result will be the most successful, without rejection of the workpiece or equipment failure.

The aim of this work is the study of radial-shear rolling process of austenitic stainless steel based on computer simulation. For computer simulation the program Simufact Forming was chosen, which along with the traditionally used Deform program allows to simulate the processes of pressure treatment of any complexity. However, Simufact Forming has certain advantages over Deform: it has more flexible options for building finite element meshes, including different mesh builders; it also has an additional database of materials Matilda, with which it is possible to simulate the evolution of the microstructure.

2. Preparation of model

To create a model of radial-shear rolling, it was decided to use the parameters of the existing SVP-08 mill installed at Rudny industrial institute. The initial billet with a diameter of 30 mm and a length of 150 mm was rolled on the mill with a compression of 3 mm. The billet material is stainless austenitic steel AISI-321 (0.08% C, 17-19% Cr; 9-11% Ni; 2% Mn; 0.8% Si; 0.5-0.7% Ti). Since the initial temperature of recrystallization or diffusion annealing for the selected steel grade is 1020 °C [1], the heating temperature of the steel was 1000 °C, as the maximum possible to eliminate the recrystallization process; the rolling speed was 50 rpm, as the nominal value at the mill SVP-08. The coefficient of friction at the contact of the workpiece and the rolls was taken to be 0.3, as the recommended value for hot rolling [2].

In the course of modeling the obtained model was correct (Figure 1). Here the workpiece was captured by the rolls of the mill SVP-08 and completely rolled in them with a diameter of 30 mm to 27 mm. The final dimensions of the workpiece after rolling were as follows: diameter 27 mm and length 185.2 mm.

In the study of any metal forming process, the main position before the laboratory experiment is the study of the stress-strain state (SSS) [3]. This makes it possible to identify the distribution of stresses and strains in the deformable workpiece, as well as to determine their critical values, which will make it possible to test the working tool for strength.

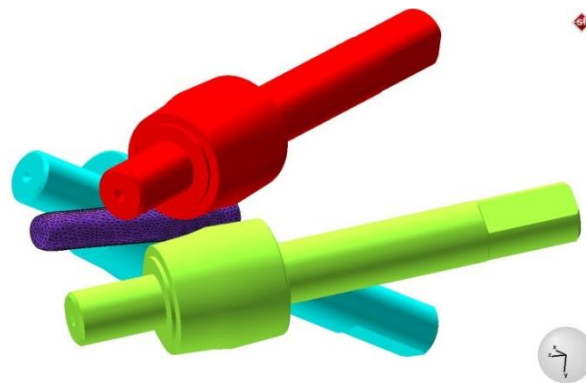


Fig. 1 Model of radial-shear rolling

To determine the stress and strain values, it is necessary to find the values of the components of the corresponding tensors, which is a very difficult task for the three-dimensional flow of metal. Therefore, usually when considering the parameters of the SSS use simple indicators of strain intensity and stress, or the so-called effective strain and effective stress.

To study the parameters of the SSS it is necessary to study the parameters that allow to estimate the share of tensile and compressive stresses in the deformation zone. These are the main stresses σ_1 , σ_2 and σ_3 . All three main stresses together represent the average hydrostatic pressure (stress mean).

Also, to determine the level of processing of the initial structure of the metal, the average grain size was determined, the initial size of which was equal to 40 microns.

3. Study of strain state

Effective strain is often mentioned in many sources as "accumulated strain". The reason for this is that this is a cumulative parameter, i.e. after removing the load, this parameter is not reset, unlike the stress.

Since the radial-shear rolling refers to the transverse type of rolling, the study of effective deformation is advisable to carry out not only in the longitudinal but also in the cross section of the workpiece – this will allow to evaluate not only the numerical values of the parameter, but also the nature of its distribution over the cross section during deformation. In the analysis of effective deformation (Figure 2), it was found that the distribution of this parameter is fully consistent with the transverse type of deformation when the workpiece makes a rotational movement around its axis, because in the cross section clearly visible annular zones of processing. It can be noted that the distribution of this parameter in the radial direction is rather large. In the axial zone (0÷35% of the radius from the center) the level of deformation is about 0.45. In the peripheral zone (35÷80% of the radius from the center) the shear deformation intensity increases, here the deformation level is 0.5÷0.55. In the surface area (80÷100% of the radius from the center) the maximum action of shear deformation is observed, here the deformation level is 0.6÷0.65.

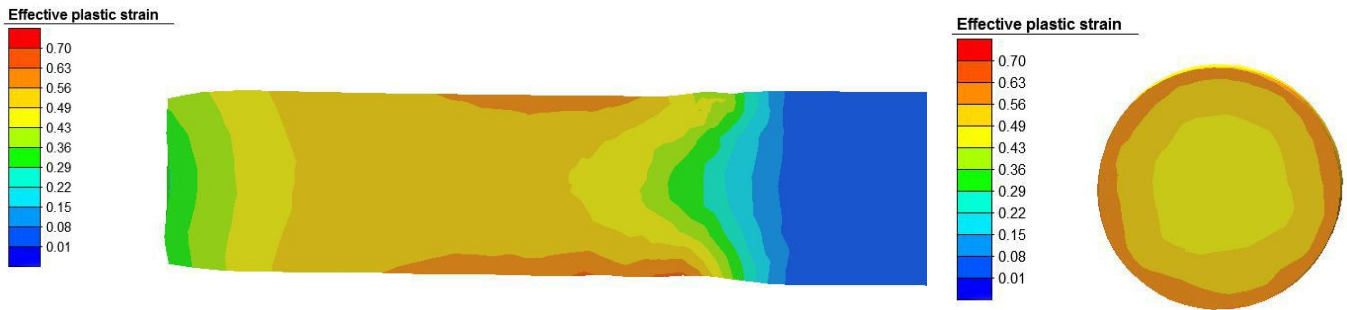


Fig 2 Effective strain

4. Study of stress state

When considering the effective stress, it should be understood that this parameter does not show what stress is acting at a particular point – tensile or compressive. As a fully-rooted expression, its value is always positive. It shows the intensity of the stress, i.e. whether there is a stress at a given point or not. Its value characterizes the average value of all stresses acting at a given point. It is also necessary to understand that the stress state components, in contrast to the previously considered effective strain, are characterized by the absence of cumulative, i.e. they occur only in the places of application of loads, in other areas they are absent. Therefore, it is advisable to consider the stress state directly in the deformation zone.

In the analysis of the effective stress (Figure 3), it was noted that due to the simultaneous action of compression and shear strains in radial-shear rolling, the entire cross section of the workpiece is covered by the action of stresses. In this case, the maximum stress values are observed in the areas of direct contact of the metal with the rolls. In these areas, the effective stress reaches 140 MPa, gradually decreasing to 90 MPa towards the center of the workpiece. In contact-free zones the effective stress is much lower and reaches 70 MPa.

When considering the average hydrostatic pressure, it is

possible to determine which type of stress acts at a given point – tensile or compressive. It was found that compressive stresses prevail in the entire cross section of the workpiece during radial-shear rolling (Figure 4). The maximum values of compressive stresses are observed in the areas of contact between the metal and the rolls. In these areas their value reaches -300 MPa, gradually decreasing to -120 MPa towards the center of the workpiece. In contact-free zones, the compressive stress is much lower and reaches -55 MPa.

In addition to these parameters, it was decided to use the Lode-Nadai coefficient [4]. This coefficient allows to assess the nature of the resulting deformation in the workpiece, i.e. to determine what type of deformation is realized at a particular point – tension, compression or shear. The value of the coefficient varies from -1 to 1. The value from 0.2 to 1 corresponds to compression; from -0.2 to -1 corresponds to tension; the coefficient value in the range of -0.2÷0.2 corresponds to the shear.

When considering this parameter (Figure 5), it was found that in the surface areas, at the contact of the metal with the rolls, the Lode-Nadai coefficient is 0.95, which corresponds to the compression. Immediately after leaving the rolls, the effect of compressive stresses decreases, shear strains act here and the Lode-Nadai coefficient is 0.15÷0.2.

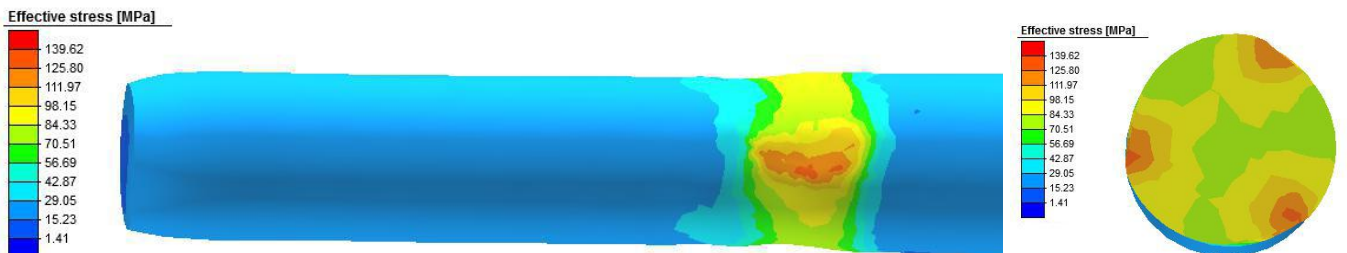


Fig 3 Effective stress

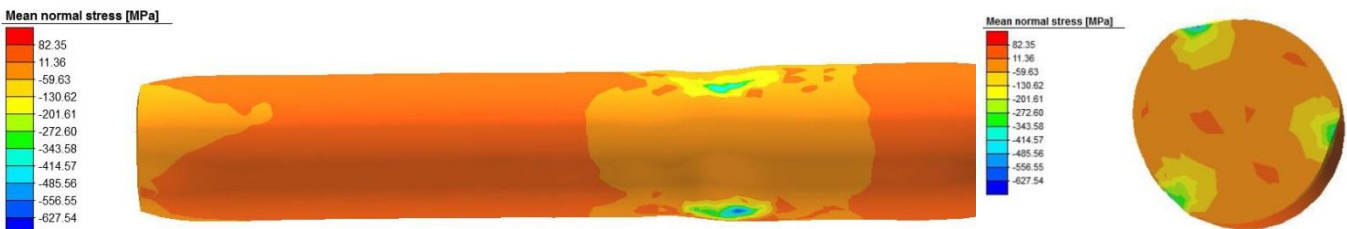


Fig 4 Average hydrostatic pressure

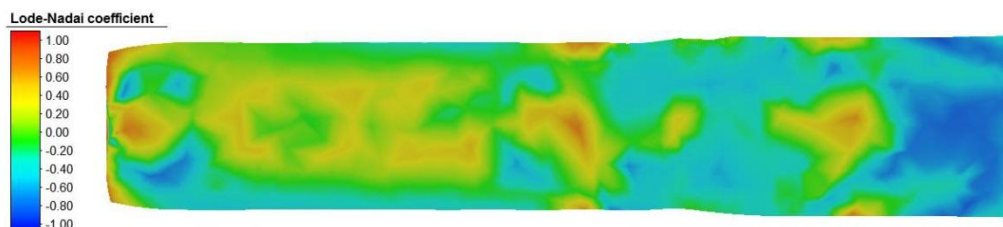


Fig 5 Lode-Nadai coefficient

5. Study of microstructure evolution and rolling force

When considering the microstructure evolution, it was noted that radial shear rolling is a very effective way of processing austenitic stainless steel AISI-321 (Figure 6). After one pass, the grain size decreased from 40 μm to 30 μm in the axial zone; in the peripheral zone, due to the intensification of shear deformations, the grain size was about 27 μm . The minimum grain size of 25 μm was recorded in the surface area, where the influence of shear strains and compressive stresses on the side of the rolls are the most intense.

Grain size in m-6

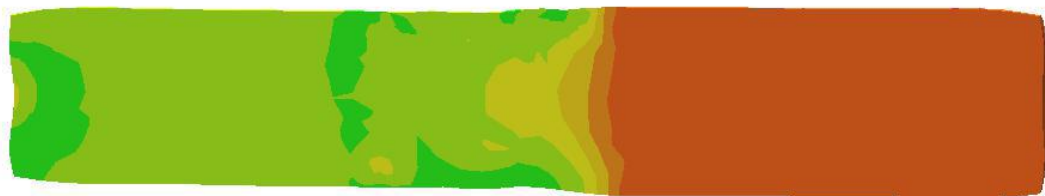
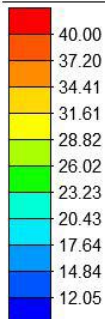


Fig 6 The change of grain size

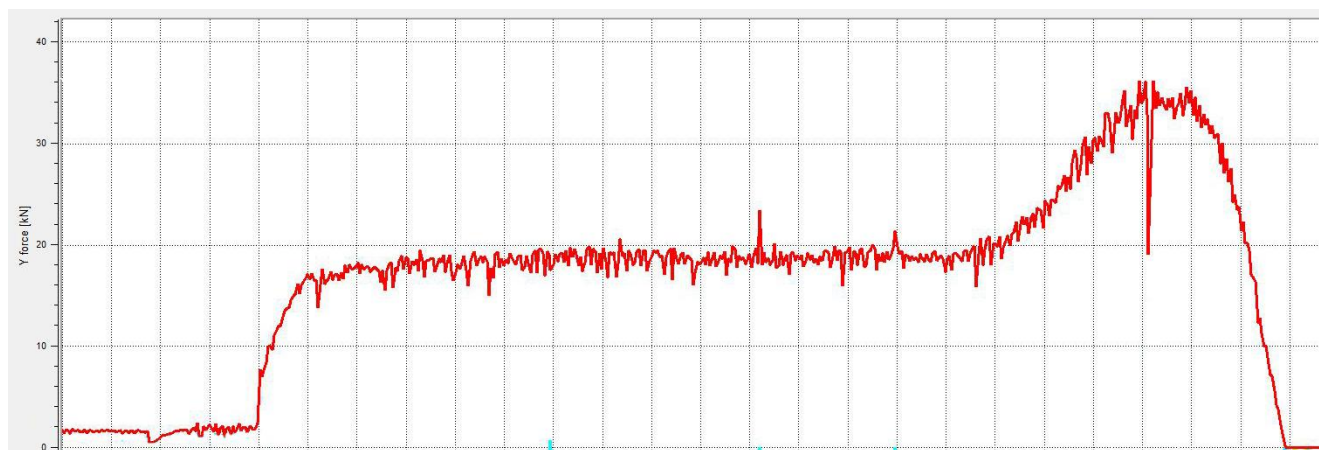


Fig 7 Rolling force diagram

6. Study of multi-pass deformation process

Despite the fact that the considered model is successful from the point of view of the emerging picture of the stress-strain state and the deformation force, it does not provide an UFG structure in the processed material. To achieve this goal, the workpiece must be processed with a much higher level of deformation. The used mill SVP-08 allows rolling blanks with a diameter of 9 mm. Taking into account the fact that the radial-shear rolling can not set the same level of compression in one pass, as in the longitudinal rolling, it was decided to increase the compression through 3 mm. As a result, it was found that for the workpiece with an initial diameter of 30 mm in this mill it is necessary to conduct 7 cycles of deformation (table 1.1). During simulation of all 7 passes the strain state study after each passage was performed. As a result, the following data were obtained (table 2).

Table 1 - Pass compression modes

	1 pass	2 pass	3 pass	4 pass	5 pass	6 pass	7 pass
Initial diameter, mm	30	27	24	21	18	15	12
Final diameter, mm	27	24	21	18	15	12	9

The last studied parameter was the rolling force on the rolls (Figure 7). Analysis of the force graph showed that radial-shear rolling process on the SVP - 08 mill proceeds quite stable. With the steady-state rolling process, the force value is about 20 kN, increasing to 35 kN at the time of exit of the rear end of the workpiece from the deformation zone. Given the fact that the allowable force on the roll, according to the technical documentation, is not more than 100 kN, this mill can deform austenitic stainless steel AISI-321, heated below the recrystallization temperature.

As can be seen from the data of table 2, in the axial zone the necessary level of deformation for the formation of the UFG structure (more than 4) is achieved only after 7 passes. This suggests the need for all 7 cycles of deformation at any temperatures and strain rates.

Table 2 - Effective strain by passes

	1 pass	2 pass	3 pass	4 pass	5 pass	6 pass	7 pass
Axial zone							
Effective strain	0,45	0,92	1,42	1,95	2,55	3,25	4,07
Peripheral zone							
Effective strain	0,52	1,07	1,66	2,28	2,94	3,77	4,65
Surface zone							
Effective strain	0,63	1,27	1,93	2,72	3,54	4,42	5,4

Analysis of the stress state in multi-pass deformation showed the following:

1) in all 7 cycles of deformation the nature of the stress distribution is completely identical. The reason for this is that in all passes the load application circuit remains constant.

2) as the number of passes increases, the stress values gradually increase. Despite the same amount of absolute compression in all passes, this is due to the fact that the workpiece cools during deformation, thereby reducing the ductility of the metal.

Similar results were obtained in the analysis of forces, but here the nature of the increase is less. The reason for this is that the force depends not only on the stress that increases, but also on the area of the contact surface of the metal with the rolls, which decreases with increasing number of passes. The common results of the analysis of power parameters are given in tables 3 and 4.

From the data in table 3 it can be seen that in all passes in the cross section of the workpiece in the deformation zone compressive stresses are formed, which is the most favorable factor for the study of the original structure. Analysis of the force values showed that the implementation of 7 cycles of deformation with the parameters of the basic model of excess load on the rolls is not observed, which leads to the conclusion about the possibility of deformation of this steel grade on the mill SVP-08 with the specified parameters.

Table 3 – Values of stress state by passes

	1 pass	2 pass	3 pass	4 pass	5 pass	6 pass	7 pass
Effective stress, MPa							
In the contact area, at the surface	140	147	155	164	189	204	224
In the contact area, periphery	90	94	97	108	116	131	147
In contact-free areas closer to center	70	74	80	90	102	118	130
Average hydrostatic pressure, MPa							
In the contact area, at the surface	-300	-312	-327	-344	-365	-378	-394
In the contact area, periphery	-120	-137	-145	-161	-180	-193	-210
In contact-free areas closer to center	-55	-67	-82	-94	-112	-126	-144

Table 4 - Values of rolling forces by passes

	1 pass	2 pass	3 pass	4 pass	5 pass	6 pass	7 pass
Average value, kN	20	22	25	28	32	36	41
Peak value, kN	35	37	40	44	47	54	62

When considering the evolution of the microstructure along the passages (table 5), the following was noted:

1) as the number of passes increases, the grain size values in all three zones decrease continuously. This is primarily due to the increase in the accumulated equivalent strain.

2) as the deformation level increases, the grain size difference between the axial and surface zones gradually decreases. This is due to the fact that during the deformation of the workpiece is lengthened and its cross-section is reduced. As a result, the action of compressive stresses in the axial zone becomes more intense, which leads to an increase in the study of this zone.

Table 5 – Values of the grain size by passes

	1 pass	2 pass	3 pass	4 pass	5 pass	6 pass	7 pass
Axial zone, μm	30	28	25	22	17	14	11
Peripheral zone, μm	27	26	21	19	14	11	9
Surface zone, μm	25	22	19	15	12	9	7

7. Conclusions

In this paper the results of modelling of radial-shear rolling process of austenitic stainless steel AISI-321 were presented. The conditions of simulation for radial-shear mill 14-40 of Rudny industrial Institute were adopted. The analysis of strain state by effective plastic strain was showed that there is a rather large uneven distribution of this parameter in the radial direction (from 0.45 in axial zone to 0.65 in surface zone). The analysis of stress state by effective stress, mean normal stress and Lode-Nadai coefficient was showed that during radial-shear rolling in the entire cross section of the workpiece compressive stresses are dominated. Studies of microstructure evolution and rolling force were showed that radial shear rolling is a very effective and energy-saved way for obtaining of high quality round billets from stainless steels of austenitic class.

8. Acknowledgment

Work is performed under the state budget-funded theme № AP05131382 "Research and development of the technology for obtaining ultrafine-grained materials with improved mechanical properties and increased radiation resistance for their use as materials of the first wall of thermonuclear reactors and in nuclear power engineering" with the program "Grant financing of scientific researches on 2018-2020" (Customer - the Ministry of education and science of the Republic of Kazakhstan).

9. References

1. V.G. Sorokin, A.V. Volosnikova, S.A. Vyatkin, HandBook of steels and alloys, M.: Mashinostroenie, 1989.
2. www.Simufact.com - Simufact Forming manual
3. ASM Metals HandBook Vol. 19 - Fatigue and Fracture. ASM International, 2002.
4. V.M. Segal, V.I. Reznikov, V.I. Kopylov, D.A. Pavlik, V.F. Malyshev, Processes of plastic structure formation of metals, Minsk: Science and technology, 1994.

Evaluation of robustness in ASR for different ‘Front-End’ methods

Tola S. PhD., Daci A. PhD,
Faculty of Mathematical and Physical Engineering – Polytechnic University of Tirana

saimir_tola@yahoo.com; alfreddaci@gmail.com

Abstract: Some feature extraction methods suffer performance degradation in different environments. So it has become a necessity to search for new methods that perform better in different types of conditions. Therefore we can make a comparison of the new found methods to evaluate their performance and to determine which is best in multi-condition tests in order to have a more robust ASR system.

Keywords: FEATURE EXTRACTION, DEGRADATION, PERFORMANCE, ASR.

1. Introduction

Speech recognition, is commonly known as automatic speech recognition (ASR), is the process of converting an acoustic signal, captured by a microphone or a telephone, to a text. The main goal of speech recognition is to get effective ways for mankind to communicate with computers, for example, voice-controlled personal computers. A speech recognizer can be divided mostly in two parts: ‘front-end’ and ‘back-end’. The general structure of a speech recognizer is shown as below.

The purpose of the ‘Front-End’ is to extract feature vectors from a speech signal. The feature vectors can capture the important

characteristics of an utterance. When an unknown utterance is presented a feature vector is obtained. In this paper we study three major feature extractions ‘Front-End’ in order to get an overview of the situation in which we are studying.

These methods consist in: Gammatone Filter Cepstral Coefficients (GFCC) [1], Mel Frequency Cepstral Coefficient (MFCC) [2], and Perceptual Linear Prediction Coefficients (PLPC) [3]

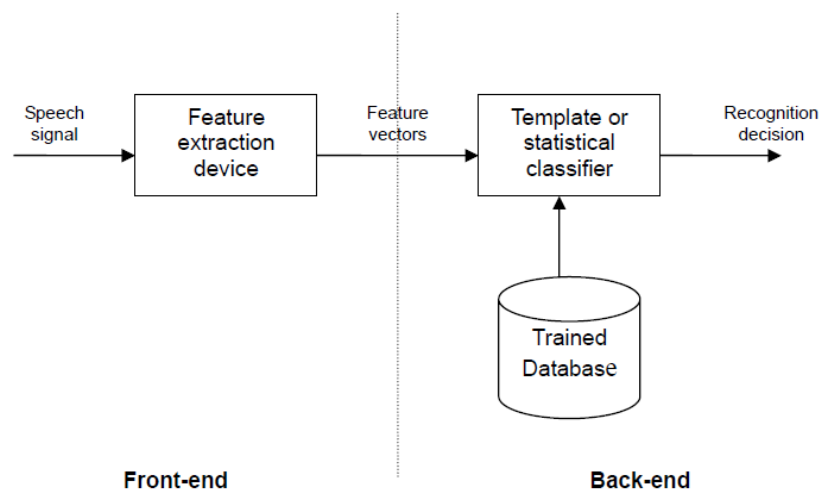


Fig. 1 Common structure of a speech recognizer

2. Data Description

One of the major factor that leads to degradations in the performance of ASR systems is the presence of noise in the environment. Such degradations in performance can be due to the mismatch between the conditions in which the systems are trained and the ones in which they are operated.

Some speech enhancement approaches are found really well to deal with unknown noise and filtering such as, Spectral Subtraction, Spectral Normalization. We will see and deal with the parameters that affect the ASR like: pitch, intensity, duration, voice quality, voice strength and the signal to noise ratio [4].

Based on it, data descriptions are shown below:

Type of recognition system: Speaker-independent continuous speech recognition

Front-ends: PLPCC, MFCC, GFCC,

Back-end: Hidden Markov Modelling (HMM) with context-dependent 4-mixture triphone HMMs

Number of coefficients in a vector: 39 (13 static + 13 delta + 13 delta-delta coefficients; Static coefficients include 12 coefficients+ log energy coefficient)

Window size (sec): 20 ms

Step size (sec): 10 ms

Sampling rate: 16kHz

Speech Database: IEEE, Aurora-4

Training set: 4578 utterances spoken by 546 speakers

Test set: 1258 utterances spoken by 134 speakers

Noise Type: White Gaussian noise

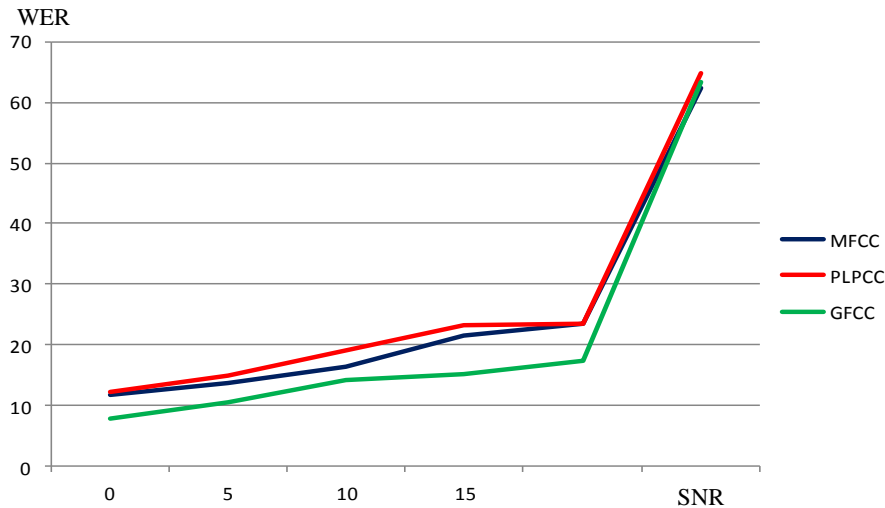
SNR range: 0dB, 5dB, 10dB, 15dB, 20dB, clean

3. Experimental Results

To evaluate the performance of the ASR System we will use the WER (Word Error Rate) algorithm. Below we will show the results of our experiment in Table 1 and Fig.2:

Table 1. The results in percentage of correctly recognized phonemes in various SNR environments

WER	SNR (dB)					
	0 dB	5 dB	10 dB	15 dB	20 dB	clean
PLPC	10.72	13.61	18.32	21.44	23.57	62.33
MFCC	12.12	14.97	19.02	23.21	23.57	64.72
GFCC	7.71	10.44	14.21	15.22	17.34	63.31


Fig. 2 Graphical presentation of the results in the in various SNR environments

4. Conclusions

Amongst the three conventional feature extraction front-ends (MFCC, PLPC and GFCC), it is obvious that PLCC is the worst performing front-end. All of them have up to 62% accuracy in clean environment. Also, the recognition rate of PLPCC in adverse environment is lower than GFCC and MFCC. In noisy conditions (0-20dB SNR), LPCC performs approximately 2-5% worse than PLPCC and MFCC.

Between PLPC and MFCC, MFCC performs slightly better than PLP in general. In all of the above three plots, MFCC performs approximately up to 2% better than PLP, except for the static feature at 5dB SNR, where MFCC is 2% worse than PLP.

GFCC is either performing equally to or better than the three conventional front-ends. In clean, 20dB and 0dB conditions, GFCC has approximately the same recognition rate as MFCC. In all other conditions, GFCC outperforms MFCC by 4-5%.

This method can also be applied in improvement of the measurement uncertainty at reference [5]

Issues (IJCSI), 8(5), 440-449 (2011)

5. Klodian Dhoska, Saimir Tola, Agus Pramono, Indrit Vozga, Evaluation of measurement uncertainty for the determination of the mechanical resistance of the brick samples by using uniaxial compressive strength test, Int. J. Metrol. Qual. Eng. 9, 12 (2018)

5. References

1. Aniruddha Adiga, Mathew Magimai, Chandra Sekhar Seelamantula. Coefficients for Robust Speech Recognition, TENCON conference, pp. 01-04, (2013)
2. Davis, S. and Mermelstein, P., Comparison of parametric representations for monosyllabic word recognition in continuously spoken sentences, IEEE Trans. ASSP-28, pp 357-366, (1980).
3. Hermansky, H., Perceptual linear predictive (PLP) analysis for speech, J. Acoust. Soc. Am., pp.1738-1752, (1990).
4. Urmila Shrawankar, Vilas Thakare. The Adverse Conditions and ASR Techniques for Robust Speech User Interface International Journal of Computer Science

OPTIMAL HYDRO-THERMAL COORDINATION WITH A MAXIMUM RES POWER UTILIZATION STRATEGY CONSTRAINTS MODEL

M.Sc. Trashlieva V. PhD.¹, M.Sc. Radeva T. PhD.¹

Department of Electrical Power Engineering – Technical University of Sofia, Bulgaria
vesselina.trashlieva@gmail.com

Abstract: This paper presents a formal and practical approach onto the short-term evaluation of the impact of the different RES power generation technologies. All these are considered stochastic and basically unreliable in the active power balance but they also seem to be an irreplaceable part of the electric power generation in the future. Here a generalized hydro-thermal coordination optimization model is presented aiming to help a day-ahead power balance impacts analysis and some further risk assessment to the EPS security and resilience.

Keywords: OPTIMIZATION MODELING, HYDRO-THERMAL COORDINATION, RES POWER GENERATION

1. Introduction

The contemporary environmental requirements for the operation of the EPS lead to an increase in the installed nature-friendly renewable power resources (RES) production [1-5]. The model presented in this paper aims to assesses and evaluate the impact of increased RES generation in the EPS in a short-term power production planning when a certain strategy for max RES power production is aimed as well as evaluating on one side the different RES producers and on the other the implicit financial impact they introduce in the production power planning. A major feature of these plants is that the peaks of renewable production are often in periods of low system load, which in turn affects the overall management of the EPS. In such periods it might be necessary to reject part of the renewable production. The another purpose of the planning optimization model is to reduce the amount of unused renewable energy [3] by optimizing the combined operation of the thermal power plants and the PHPS storage capacities and to achieve minimum values for the costs of the production activity. The model is constructed for the general case of an EPS with generally nonlinear thermal, HPS and PHPS.

The production of HPPs is determined by the available inlet water quantities. If there is a possibility of accumulation (sufficient useful volume of the tank), the HPP can produce energy when needed (under the circumstances of energy shortages). In many countries worldwide, at a peak load periods, HPPs are mainly used as peak, regulating and reserving capacities. Pumped storage power plants (PSP) possess the potential to accumulate the processed water quantities (presence of a lower reservoir) and are used for balancing loads, being practically the most flexible and multifunctional elements of the EPS. In the peak load periods PHPSs operate in generator (turbine) mode, and in low load periods and in the inability to reduce the power output of other generating units, they operate in pumping mode by pumping water from the bottom into the upper tank as controllable loads. In addition to importing the requested extra load into the system, they accumulate part of the surplus electricity, which is later attributed to the peak periods at a higher price. This reversible cycle (turbine-pump, load-generator) helps to prevent frequent and multiple stops and starts of thermal units or prevents changes in the output levels of the nuclear and thermal generators [6-11].

The criterion for the efficient operation of PHPP is the financial income from the plant's operation that is generally determined by the difference between the sold electricity production and the purchased electricity consumed in the operation of the pumps [5,12]. From an economic point of view the accumulation process is a "cost with recovery in the future". If the accumulated energy is not sold in the future periods at better prices (this condition guarantees a positive revenue), these costs will also include the cost of the lost economic benefits as the unit was idle and waited for the corresponding economically advantageous period. Thus the energy accumulation may prove itself technically necessary from the point of view of the EPS but economically unprofitable for the PHPS owner. Sometimes it may be necessary to release water from the

above reservoir (primal energy resource waste) to turn on the load in future period according the major EPS balance requirements, and in this case there must be a mechanism to stimulate the PHPS owner. Energy storage is economically justified when the cost of the electricity used by the pumps is less than the electricity generated and sold, taking into account the accumulation-production cycle losses.

The system load changes with daily, weekly and seasonal patterns and these changes lead to the respective changes of the generating plants power outputs. When PHPPs are available system operators accumulate cheaper energy produced during low load periods and inject it into the grid during peak periods when the process is cost-effective. Where there is an opportunity to accumulate energy (large dams are built), the power injections may be postponed, having in mind that this is not a "surplus" energy storage but it can later participate in energy production or balance market. Power plant using RES (exception of HPPs of stored water) generally are considered as incapable of storing their primal energy source [13] (water, solar radiation, etc.) and when aiming to use the whole availability of these stochastic RES power plants they usually increase the EPS balance problems [5,12,14].

With the increase of the share of renewable wind and solar generally uncontrollable stochastic power plants, PHPPs become an indispensable element in the EPS operation that assures the balance as a buffer to reconcile the specifics of the renewable generation and consumer load schedules[15-18]. This is extremely important most of the contemporary EPS as optimization of the coordinated work of the three different generating types are involved in order to minimize the total operation costs in the EPS and preserve the active power balance. The model presented in this paper aims to optimally model the functioning and operation of HPPs and PHPPs as an active power balance tool in order to minimize the total EPS costs with different origin of the RES power production and also with the respective attention to the specifics of the different hydro-power plants under consideration, generally at limited water availability circumstances.

Hydro-power generation is known for many ears and the HPPs have a considerably long exploitation period, some of them more than 50 years. So hydro-power plants are build in different moments and in different terrain thus leading to different efficiency of each plant. Many power plants also struggle from limited water quantities or tank volumes that further limit their operation. In some terrains the processed primal water resource of a HPS may be used again by another HPS that is below the first one, making a hydro-power cascade and thus optimizing the utilization of the limited water resource. Cascades lead to other problems in the optimization modeling.

The importance of energy storage increases with the increased RES power generation penetration [16,17,19]. Energy storage is applied for smoothing short-term fluctuations in the power generation of wind and solar plants due to wind gusts or clouds, for electric power source for longer periods of RES generation intersections (at night or when it is windless), as a back-up power

source, for example a in case of a main network failure, or as a main or auxiliary energy source for vehicles, etc. So depending on their purpose, the energy storages are considered system-general, in the distribution network or local [17]. The former are a tool of the Electricity System Operator for tertiary frequency control and cross-border exchanges. They are powerful facilities, predominantly connected to the power transmission network of hydro-power stations, with the possibility of storing water in an upper tank. The second is a device whose capacity is proportional to the load of a distribution line. These are installed in distribution substations or transformer stations. The third ones are in scale with the load of an individual consumer who needs to be fed when the primary source drops out. They are installed in the user's property.

When combining conventional thermal power generation and water a separate class of EPS optimization problems emerge - those of optimal hydro-thermal coordination. [5,7,9,19-21].

The hydro-thermal optimal coordination model presented here is a high-dimensional non-linear mixed-integer model because of the presence of reversible accumulation-generation power plants. HPPs with their responsiveness to meet load changes and speed are the top balance and peak sources for most EPS. Taking into account the fact that the costs of the water as a primary energy resource is practically inconsistent with those of conventional thermal power plants, HPPs have a significant impact on the total EPS operating and production costs, usually in the direction of their reduction [1,20-22].

2. Model Formulation

The presentation here models the formation of an optimal strategy for combined thermal and hydro power generation when a significant power is injected in inappropriate moments from renewable power generators. Active power balance should be satisfied at any moment and the possible alternative for renewable power generation rejection has to be properly presented and evaluated. No start or stop of a thermal unit is allowed in the optimization horizon so if the max RES power utilization strategy is adopted optimal operation plan for systems controllable loads (pumps) has to be elaborated thus leading total costs reduction, peak shaving and steady thermal power operation. In the model formulation a certain nomenclature is used and it is given below.

FORECASTED VALUES USED IN THE MODEL:

D_j - load forecast

P_{Wj} and P_{Sj} - forecasts for the wind and solar production

$P_{Resj} = P_{Wj} + P_{Sj}$ - expected summary renewable production

$L_{Res,j}$ - resulting load in a time interval j

NOMENCLATURE FOR THE THERMAL GENERATION UNITS

i – thermal unit,

c_i - price for fuel for 1 MWh for a thermal unit i

P_{ij} , P_{imin} , and P_{imax} – power output level, minimal and maximal admissible values of the thermal unit's i operational range in MWh i in a unit interval j

The work of a thermal unit i is the function $f(P_{ij})$ and the total costs for its operation for the whole planning horizon is $\sum c_i f(P_{ij})$

NOMENCLATURE FOR THE HPS AND PHPS:

r - reservoirs

k - power stations (HPS and PHPS)

m_k - available number of pumps in a k -th PHPS with similar operation values, that in the fixed level of the pump $P_{P,mk}^F$

$V_{r,Usable}^{\min}, V_{r,Usable}^{\max}$ - minimal and maximal usable water reservoir r volume

$V_{r,j}$ - water reservoir r volume at the end of the time interval j

$F_{r,j}$ - water flow in r during a unit interval j

$R_{r,j}$ - unprocessed water from r in a unit interval j . Unprocessed water quantity includes controllable water release as well as uncontrollable losses such as evaporation.

$P_{Pk,j}$ - power used by the pumps of k in a unit interval j

$P_{Pmk,j}$ - power used by the pump m_k in a unit interval j

$P_{Hk,j}$ - power produced by the turbines of k in j

$P_{P,k}^{\min}, P_{P,k}^{\max}$ - minimal and maximal pump capacity of k

$P_{P,mk}^F$ - available (fixed) pump level of a pump m_k

$0 \leq n_{k,j} \leq m_k$ and integer is the number of pumps working in j

$P_{H,k}^{\min}, P_{H,k}^{\max}$ - minimal and maximal generating capacity of plant k

φ_{Hk} and φ_{Pk} - water consumption (m^3/MWh) for plant k in both generation and accumulation mode

η_k - efficiency coefficient for a PHPS plant k

$v_{k,j}$ - artificial binary variable for the operation mode of a PHPS k . $v_{k,j} = 1$ if the mode is pumping in j

$w_{mk,j}$ - artificial binary variable for the operation mode of a pump m_k . $w_{mk,j} = 1$ if pump m_k is working at a fixed level P_{Pmk}^F in j

The operational curve of a HPS with neglecting the water head may be expressed via the following linear functions:

$Q_{Hk,j} = \varphi_{Hk} P_{Hk,j}$ - processed water quantity by the turbines of plant k in a unit interval j

$Q_{Pk,j} = \varphi_{Pk} P_{Pk,j}$ - processed water quantity by the pumps of plant k in a unit interval j

c_{Hk} and c_{Pk} - costs for the operation of hydro plants may be introduced in the model. These costs might include a complex structure like constant and variable components. In the current model formulation operation costs of hydro power plants are neglected

δ_i - permissible change of the output generation of a thermal unit i between two successive time intervals

α_j and β_j - rejection of renewable power for a time interval j , $0 \leq \alpha_j \leq 1$ and $0 \leq \beta_j \leq 1$

The model aims to minimize the total operation costs in a short-term (day-ahead) interval of an EPS consisting of continuously operating i thermal units (within their operation range $[P_{imin}, P_{imax}]$), renewable stochastic generation from wind and solar power plants and k PHPS as peak generators with a strategy of maximum RES penetration.

$$\min_P J = c_i \sum_{ij} f(P_{ij}) \quad (1)$$

The balance constraint (2) will guarantee that the total production of both controllable and uncontrollable units and loads will equal the load forecasts for each time interval in the planning horizon:

$$\sum_j P_{ij} + \sum_j P_{H,kj} - \sum_j P_{P,kj} = L_{Res,j} \text{ for each } j \quad (2)$$

The right-hand side of the balance constraint is the resulting load has to be covered from the working controllable generation units:

$$L_{Res,j} = D_j - (1 - \alpha_j)P_{w,j} - (1 - \beta_j)P_{s,j} \quad (3)$$

It is clear that in some periods with peak RES production the resulting load will be less than the total minimum of operating thermal plants. In these periods excess renewable power should be rejected in order to sustain the power balance or this excess power has to be accumulated for further periods.

In order to avoid the modeling of the water balance constraints which is redundant and exhaustive for a short-term optimal coordination problem a single efficiency constraint for each PHPS k may be introduced.

$$\eta_k \sum_j P_{p,k} = \sum_j P_{H,k} \quad \text{for each } k \quad (4)$$

Water balance constraints (5) have to be formulated if not all hydro units are reversible or if a PHPS and a HPS use same water reservoirs. Further reduction of the number of the water balance constraints is achieved by formulating such constraints for those r that limit the hydro units operation in the given horizon (i.e. the limiting reservoir that is the smaller one). (5) is a general form of a water balance constraint for each reservoir r with modeling the work of all interconnected to r generators a pumps (feed-in and feed-out) as well as controllable and non-controllable inflows and outflows:

$$\begin{aligned} V_j = & V_{j-1} - \sum_{k \in \Gamma_{from}} \varphi_{Hkj} P_{Hkj} + \sum_{k \in \Pi_{in}} \varphi_{Pkj} P_{Pkj} + \\ & + \sum_{k \in \Gamma_{from}} \varphi_{Hkj} P_{Hkj} - \sum_{k \in \Pi_{in}} \varphi_{Pkj} P_{Pkj} + Q_{Rj} + \\ & + \sum_{q \in \Pi_{in}} L_{R,qj} - L_{Rj} - R_{Rj} \end{aligned} \quad (5)$$

Γ_{from} and Π_{from} are the sets of plants (with their pumps and turbines) that drain water from r during j . Γ_{in} and Π_{in} are the sets of plants that feed in water in r during j .

The following constraints model the physics of the accumulation-generation cycle, namely that no pumping and generation are possible simultaneously in a single time interval j :

$$P_{p,kj} - v_{kj} P_{p,k}^{\max} \leq 0 \quad (6)$$

$$P_{Hk} - (1 - v_{kj}) P_{H,k}^{\max} \leq 0 \quad (7)$$

Constraint (6) implies that the summary of the pumps is a controllable load whose power can be linearly controlled in a certain interval. Most pumps are considered controllable loads with a fixed power consumption. In order to model such particularity the following changes in the model may be introduced:

If using the number of pumps as groups (8) should be added:

$$P_{p,k,j} - \sum_{mk} n_{k,j} P_{p,mk}^F = 0 \quad (8)$$

If using a respective modeling for each pump with a fixed level (6) will change because the summary pump consumption is determined by the work of each pump, i.e. $P_{p,kj} = \sum_{mk} P_{p,mkj}$ thus becoming (9) and adding (10) to keep each pump in the allowed power level (one of 0 and $P_{p,mk}^F$):

$$\sum_{mk} P_{p,mkj} - v_{kj} P_{p,k}^{\max} \leq 0 \quad (9)$$

$$P_{p,mkj} - w_{mk,j} P_{p,mk}^F = 0 \quad (10)$$

Ramp-up and ramp-down constraints for the thermal units:

$$|\Delta P_{ij}| \leq \delta_i \rightarrow \begin{cases} P_{ij} - P_{ij-1} \leq \delta_i \\ P_{ij} - P_{ij-1} \geq -\delta_i \end{cases} \quad \text{for each } i \text{ and } j \quad (11)$$

If the duration of a unit time interval is greater than 30 minutes the ramp up and down constraints might be neglected, because most of the large thermal units can reach maximal operating value within 30 minutes.

Operation range for the thermal units is modeled with simple bounds:

$$P_{i,\min} \leq P_{ij} \leq P_{i,\max} \quad (12)$$

The following simple bounds for the water reservoirs and the controllable outflows are introduced if water balance constraints (5) are implied in the model. The volume of each reservoir in every unit interval must be within the actual water level limits:

$$V_{r,Usable}^{\min} \leq V_{r,j} \leq V_{r,Usable}^{\max} \quad (13)$$

Values for the first ($j=1$) and last interval ($j=j_{\max}$) might be provided for the water level maintenance cycle:

$$V_{r,j=1} = V_{r,1} \quad \text{and} \quad V_{r,j=j_{\max}} = V_{r,N} \quad (14)$$

Thus this model allows for the analysis of the impact of different RES production in a short-term power balance as well as presenting in an appropriate way the specifics of hydro-power plant under consideration.

3. Conclusion

A model for optimized combined operation of thermal, PHPP and RES is formulated for short-term planning in the absence of the possibility of starting and stopping of the thermal generating units, resulting in a uniform operation of the base thermal plants and realization of the ideas of Energy Demand Management. The introduction of price indicators for the operation of storage capacities is justified from the point of view of the development and maintenance of these facilities, thus modifying investments in improving the installed facilities or their investments return policies. Differences in PHPSs may be modeled appropriately as general constraints using the efficiency coefficient for each storage plant or using water balance equations that allow for the estimation of natural resources in periods of high water and drought, as well as the quantitative and cost recovery of unprocessed water. Further the problem with the fixed operation level of pumps is discussed and appropriately solved in the model. It is built on a strategy for maximum production and utilization of RES energy, which is in line with environmental requirements as 100% RES power utilization, reduces the negative environmental impact of the thermal power plants. These models are especially useful in the case of generating power from renewable energy sources, which have a random nature of the generated electric power (wind turbines and photovoltaic power plants) and large amplitudes in the load schedules. In these cases, the optimal coordinated of conventional thermal power plants and storage capacities allows for an increase in the share of renewable production and hence the ecological operation of base power plants at small deviations. Without manageable loads and peak power, the balance of the EPS will be severely hampered. The approach of this model formulation to the different renewable stochastic resources allows for a deep analysis of the impact of the different RES production strategies and production/energy market penetration as well as it is a useful tool for the EPS optimization and development problems.

4. Bibliography

[1] Gjelsvik A., Mo B., Haugstad A., Long- and Medium-term Operations Planning and Stochastic Modeling in Hydro-dominated Power Systems Based on Stochastic Dual Dynamic Programming, Handbook of Power Systems I, 2010, p. 33-55

- [2] Usaola J., Castronuovo E. D., Wind Energy in Electricity Markets with High Penetration, Nova Science Publishers Inc, ISBN: 978-1-60741-153-6, 2009
- [3] Lee K.Y., Ortiz J.L., Mohtadi M.A. and Park Y.M, Optimal Operation of Large Scale Power Systems, (1998) IEEE TPS Vol. 3, No. 2, p. 413-420
- [4] King, T. D., El Hawary, M. E., El Hawary, F., OPTIMAL ENVIRONMENTAL DISPATCHING OF ELECTRIC POWER SYSTEMS VIA AN IMPROVED HOPFIELD NEURAL NETWORK MODEL, IEEE Transactions on Power Systems, Vol. 15, No.3,2000
- [5] El-Hawary M. E., Electrical Energy Systems, Second Edition, CRC Press, ISBN 978-0849321917, 2000, 384 Pages
- [6] Vieira F., Ramos H. M., Hybrid solution and pump-storage optimization in water supply system efficiency: A case study, Elsevier Energy Policy, ISSN: 0301-4215, Volume 36, Issue 11, November 2008, Pages 4142-4148
- [7] Etwire C.J., Twum S.B., Optimal Hydrothermal Energy Generation for Ghana, International Journal of Scientific & Technology Research, Vol. 3, Issue 12, Dec. 2014 ISSN 2277-8616, p.65-74
- [8] Etwire C.J., Twum S.B., Sensitivity Analysis of a Mixed Integer Linear Programming Model For Optimal Hydrothermal Energy Generation For Ghana, International Journal of Scientific & Technology Research Vol. 4, Issue 03, March 2015, p. 129-141
- [9] Happ, H. H., Johnson, P. C., Wright, W. J., Large Scale Hydro-Thermal Unit Commitment - Method and Results, IEEE Transactions on Power Apparatus and Systems, Vol. PAS-90, May/June 1971, pp. 1373-1384
- [10] Stoilov D., Kaneva M., Syltan F., Optimal Operation Planning of Mosul Hydro Power Complex - Part I: Mathematical Models, Proceedings of Int. Conf. ELMA '2008, Sofia, Bulgaria, 2008, (in English);
- [11] Syltan F., Stoilov, D., Optimal Operation Planning of Mosul Hydro Power Complex - Part II: Simulation Results and Analyses, Proceedings of Int. Conf. ELMA'2008, Sofia, Bulgaria, 2008, (in English);
- [12] Mazer A., Electric Power Planning for regulated and deregulated markets, Arthur Willey 2007 ISBN 978-0-470-11882-5, 313 pages
- [13] Stanev R., "A primary power control of small hydro power plants in autonomous, micro and minigrids", XVIIIth International Symposium on Electrical Apparatus and Technologies SIELA 2014, 29 – 31 May, 2014, Bourgas, Bulgaria
- [14] Shaqiri R., Bogdanow D., Nasufi E., Model for estimation the effects of new generators connected to existing distribution network of Kosovo, 2016 19th International Symposium on Electrical Apparatus and Technologies (SIELA), 2016, DOI: 10.1109/SIELA.2016.7543041
- [15] Wang J., Botterud A., Miranda V., Monteiro C., Sheble G., Impact of Wind Power Forecasting on Unit Commitment and Dispatch, <http://citeseerx.ist.psu.edu/viewdoc/download?doi=10.1.1.470.5813&rep=rep1&type=pdf>
- [16] Кънева М., Попов З., Стоилов Д., Балансиране на активните мощности в електроенергийни системи със значително използване на вятърни електростанции, Списание Екологично инженерство и опазване на околната среда, 2013г., брой 1, стр. 60-66, ISSN 1311-8668
- [17] Kaneva M., Popov Z., Stoilov D., Power balancing in electric power system with considerable wind power penetration, Proceedings of the conference COFRET 2012, p. 309-314, Sozopol, June 11-13, 2012, ISBN 978-619-460-008-3
- [18] Mabel M. C., Edwin Raj R. E., Fernandez E., Analysis on reliability aspects of wind power, Renewable and Sustainable Energy Reviews, Vol. 15, Issue 2, February 2011, ISSN: 1364-0321, pages 1210-1216
- [19] Snergiev D., Valiev R., Eroshenko S., Khalyasmaa A., Functional Assessment System of Solar Power Plant Energy Production, 2017 International Conference on ENERGY and ENVIRONMENT (CIEM), DOI: 10.1109/CIEM.2017.8120862
- [20] Chen H., Cong T.N., Yang W., Tan C., Li Y., Ding Y., Progress in electrical energy storage system: A critical review, Progress in Natural Science, Vol. 19, Issue 3, 10 March 2009, p. 291-312 [15] 100 Wei H., Sasaki H., Kubakowa J., Yokoyama R., Large Scale Hydrothermal Optimal Power Flow Problems Based on Interior Point Nonlinear Programming, IEEE TRANSACTIONS ON POWER SYSTEMS, Vol. 15, February 2000, p. 396 - 403
- [21] Rajan C.C.A, Hydro-thermal unit commitment problem using simulated annealing embedded evolutionary programming approach, International Journal of Electrical Power & Energy Systems, ISSN: 0142-0615, Vol. 33, Issue 4, May 2011, pages 939-946
- [22] Wei H., Sasaki H., Kubakowa J., Yokoyama R., Large Scale Hydrothermal Optimal Power Flow Problems Based on Interior Point Nonlinear Programming, IEEE TRANSACTIONS ON POWER SYSTEMS, Vol. 15, February 2000, p. 396 - 403

OPTIMAL HYDRO-THERMAL COORDINATION WITH A MAXIMUM RES POWER UTILIZATION STRATEGY CONSTRAINTS: RESULTS AND ANALYSIS

M.Sc. Trashlieva V. PhD.¹, M.Sc. Radeva T. PhD.¹

Department of Electrical Power Engineering – Technical University of Sofia, Bulgaria
vesselina.trashlieva@gmail.com

Abstract: In this paper results for the optimal hydro-thermal coordination optimization problem is presented. The EPS power production structure under consideration consists of thermal, hydro and renewable power plants. The solution analysis shows the impact of different RES power production onto the EPS balance and resilience. A practical analysis of the marginal values of the right-hand sides of the balance model's constraints is also given.

Keywords: OPTIMIZATION MODELING, HYDRO-THERMAL COORDINATION, RES POWER GENERATION

1. Introduction

Since electric power supplies became problematic in some isolated areas alternatives for power feeding of such consumers are considered. Further bigger installations for RES power generation are built mainly to satisfy such problems in electric power distribution in larger isolated regions (like isles) [1-3] and also to address the current environmental requirements for the operation of the EPS. No matter of the case, wind and solar power prove themselves as variable and uncertain power generators which steadily leads to a huge the interest in the challenges this stochastic power generation brings to the EPSs [4-8]. A model presented in [9] aims to assesses and evaluate the impact of increased RES generation in the EPS in a short-term power production planning. A strategy for maximal RES power production is aimed as well as evaluating this same impact caused by different RES producers and its influence on EPS reliability and cost effectiveness. The model formulated in [9] allows for the inclusion of stochastic generating sources such as wind power and photovoltaic power plants as well as the presentation of each power plant separately, thus allowing for an evaluation of a change in the priority list that commits the power generators at a first place.

This model is also designed to evaluate the impact in the power balance of different sources of the renewable power production. This impact gains larger significance in both EPS planning and real-time operation because of the difficulties it causes due to increased EPS reliability. Reserves of controllable loads and peak generators have to be evaluated as well as limit values of the right-hand sides of the balance constraints.

2. Parameters and Results

The goals and benefits of the model is illustrated with a typical power load forecast for a shiny summer day in three scenarios for the origin of the renewable power generation:

Scenario I: RES production is solely from wind power plants,

Scenario II: RES production is solely from solar power plants,

Scenario III: RES production is a combination of wind and solar power plants.

Table 1: Thermal units parameters

	$P_{i, min}$	$P_{i, max}$	δ_i	c_i
Thermal 1	980	1 000	10	15,30
Thermal 2	620	1 550	110	24,00
Thermal 3	268	670	120	24,50
Thermal 4	252	630	120	45,00
Thermal 5	420	840	120	48,00
Thermal 6	630	1 260	130	53,00

24-hour forecasts for the system load and renewable generation are used. The load profile (Figure 1) shows two distinguishable peaks, the evening has a greater absolute value than the morning. In all three scenarios the renewable generation peaks are in periods with lower system load (Figures 2, 3 and 4).

Table 2: PHPS parameters

		PHPS 1	PHPS 2
Turbine	$P_{Hk, min}$	0 MW	0 MW
	$P_{Hk, max}$	864 MW	375 MW
	c_{Hk}	\$ 0,00 /MWh	\$ 0,00 /MWh
	ϕ_{Hk}	595 m ³ /MWh	600 m ³ /MWh
Pump	$P_{Pk, min}$	0 MW	0 MW
	$P_{Pk, max}$	784 MW	104 MW
	c_{Pk}	\$ 0,00 /MWh	\$ 0,00 /MWh
	ϕ_{Pk}	510 m ³ /MWh	475 m ³ /MWh
	$V_{Lk, max}$	4,7.10 ⁶ m ³	0,375.10 ⁶ m ³

The optimal solution aims at optimal operation day-ahead planning of 6 thermal power plants and 2 PHPSs as both peak plants are reversible. The parameters of the thermal and hydro power plants under consideration are given in Tables 1 and 2. The i/o curves are considered linear for simplification of the results presentation but the general model formulation allows for non-linear curves as well as linear approximations. The two PHPSs use a common upper water reservoir whose volume is more than 10 times bigger than the lower reservoirs. So it can be considered that the operation of both PHPSs is limited by only one (lower) tank, which is represented by its usable volume.

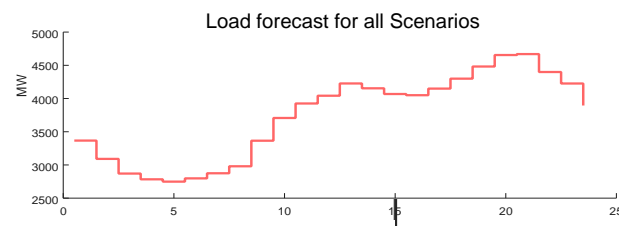


Fig. 1: Load forecast for all Scenarios

Uncontrollable inflows and outflows in both volumes Q_{Rj} and R_{Rj} are neglected due to the short-term planning horizon as well as the unprocessed water quantities L_{Rj} and L_{Rqj} so $Q_{Rj} = 0$ and $R_{Rj} = 0$ and $L_{Rj, max} = 0$ and $L_{Rqj, max} = 0$. Pumps are considered as a variable power controllable load, not a fixed power level ones. Also their consumption is evaluated as a generalized variable according the nomenclature in [9]. Water balance constraints are formulated for the limiting lower reservoirs for both PHPSs. In all three scenarios, a strategy for maximum utilization of RES energy is formulated.

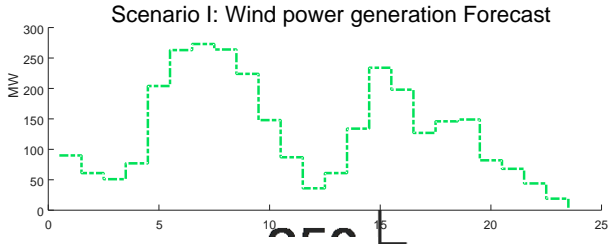


Fig. 2: Wind power generation for Scenario I

Figure 1 shows the forecast of the load used in all three scenarios and the forecasts for renewable generation. In the first case (Scenario I), the impact of wind power production on the performance of the EPS is analyzed.

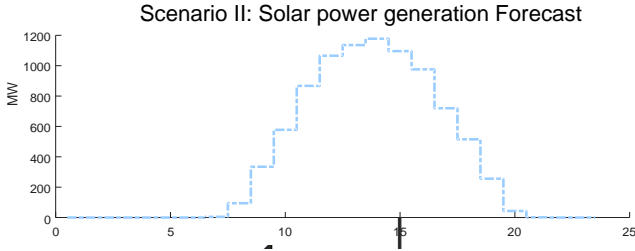


Fig. 3: Solar power generation forecast for Scenario II

There are two peaks in the forecast for the wind generation (Figure 2) - in the morning and afternoon hours, which coincide with the reduced load hours of the EPS (Figure 1).

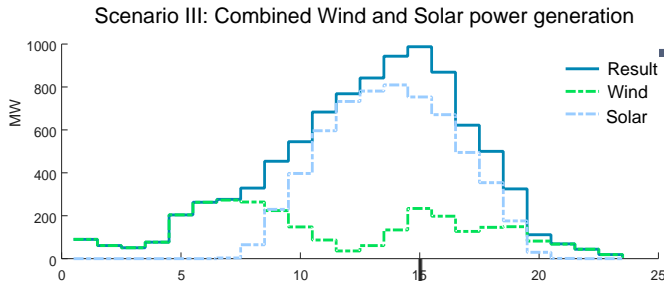


Fig. 4: Combined wind and solar power generation for Scenario III

For Scenario II the renewable production is solely from a solar power plant, whose peak is in the early afternoon hours (Figure 3) when there is a reduced system load again.

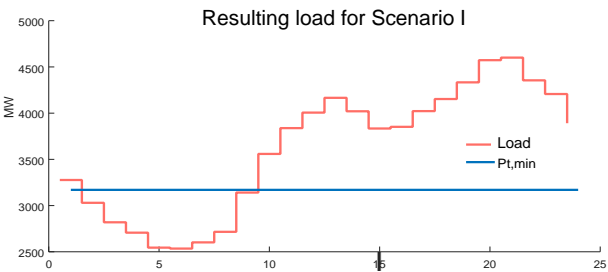


Fig. 5: Resulting load for the 1st scenario

When the renewable energy production plants include both wind and solar power generation, according to the used forecasted data (Scenario III), the peak of RES is in the afternoon (Figure 4) when the system load is low. The equivalent (summary) total renewable generation forecast is shown with dark blue color on Figure 4.

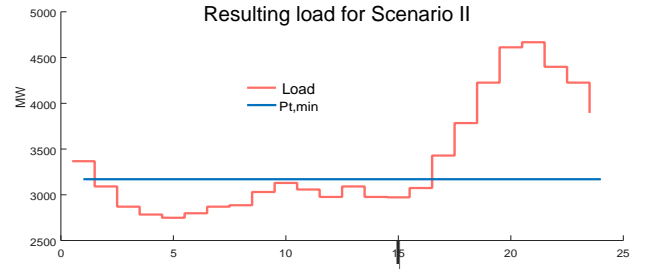


Fig. 6: Resulting load for the 2nd scenario

According to constraints (2) and (3) in [9], with available forecasts for the renewable generation, the electric power that has to be produced by the thermal and hydro power plants is formed as the difference between the load forecast and the RES generation forecast.

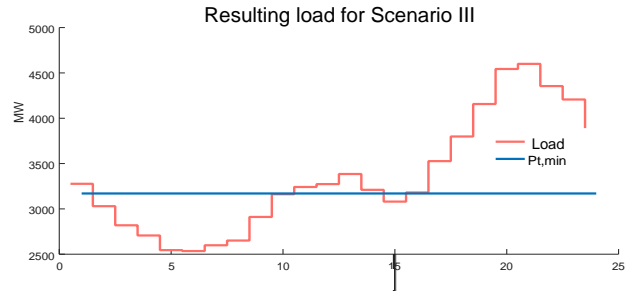


Fig. 7: Resulting load for the 3rd scenario

Figures 5, 6 and 7 illustrate this difference as a "resultant load" and show the periods in which its values are below the minimum possible total output from the thermal plants, shown with a straight line. In these periods, the EPS could not function without additional controllable loads (Figures 8, 9 and 10).

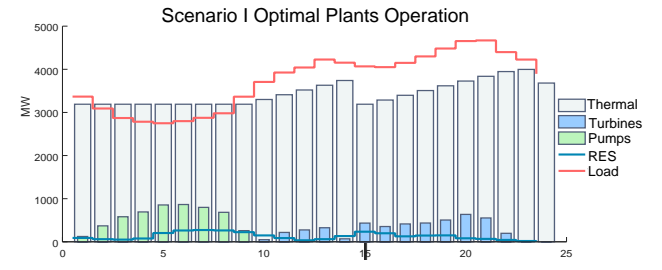


Fig. 8: Optimal operation of hydro and thermal plants for Scenario I

Solution will be infeasible for Scenario I because from 1 am to 9 am, the resulting load is less than the minimum output power of the committed thermal units. In these periods wind power may be rejected ($\alpha_j > 0$) or accumulated by the pumps. The minimal system load that can be covered is given by $\sum_i P_{i\min} - \sum_k P_{P,k}^{\max}$, so

whenever the difference $D_j - (1 - \alpha_j)P_{w_j}$ is greater than the minimal possible system load the rejection parameter will be non-basis, i.e. zero valued in the optimal solution:

$$\alpha_j = 0 \text{ for } D_j - (1 - \alpha_j)P_{w_j} > \sum_i P_{i\min} - \sum_k P_{P,k}^{\max}$$

$$\alpha_j = 1 \text{ for } D_j = \sum_i P_{i\min} - \sum_k P_{P,k}^{\max}$$

Pumps will be charged with excess renewable generation when the resulting system load considering full utilization strategy for

values of the resulting load less than the possible minimal output of
thermals: $(D_j - P_{w_j})|_{\alpha_j=0} \in [\sum P_{i,min} - \sum P_{P_k}^{max}; \sum P_{i,min}]$

Same assumption about the rejection variable is made in the case when the renewable generation in the EPS is given by solar energy (Scenario II).

$$\beta_j = 0 \text{ for } D_j - (1 - \beta_j)P_{s_j} > \sum_i P_{i,min} - \sum_k P_{P_k}^{max}$$

$$\beta_j = 1 \text{ for } D_j = \sum_i P_{i,min} - \sum_k P_{P_k}^{max}$$

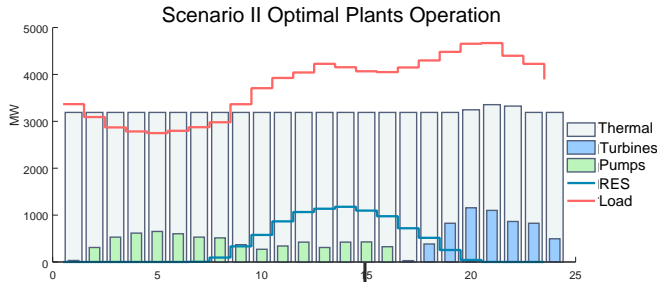


Fig. 9: Optimal operation of hydro and thermal plants for Scenario II

So according to these considerations given the resulting system load shown on Figures 5, 6 and 7 pumps will have to work from 1 am to 10 am for Scenario I, from 1 am to 4 pm for Scenario II and from 1 am to 10 am and again for an hour at 3 pm to provide a feasible solution, i.e. assure the EPS power balance.

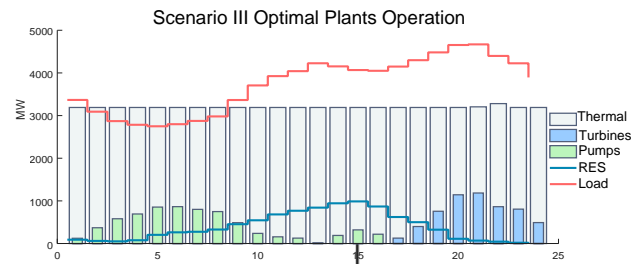


Fig. 10: Optimal operation of hydro and thermal plants for Scenario III

In the first case (Scenario I, Figure 8), the pumps work from 0 am to 10 am. In the second case Scenario II (Figure 9) and pumps work from 0 am to 4 pm. In the third case Scenario III (Figure 10) pumps also work from 0 am to 4 pm. In the hours when the resulting load is below the total sum $P_{i,min}$ pumps are working on the **resilience** of the EPS, as the model does not allow the thermal units to be shut down.

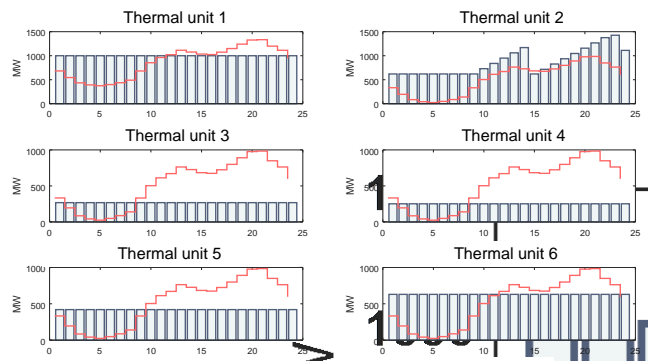


Fig. 11: Thermal power plants operation in Scenario I

In the third case, pumps continue to operate at time intervals where the resulting load is not below the minimal thermal line. In these intervals they are charged for energy storage. The accumulated power is then generated by the turbines mainly in peak evening hours the system load reaches its maximum forecasted values. I.e. PHPSs play *two* separate but *important* roles: to assure the active power balance and to increase total profits by reducing the costs associated with the operation of the thermal power plants.

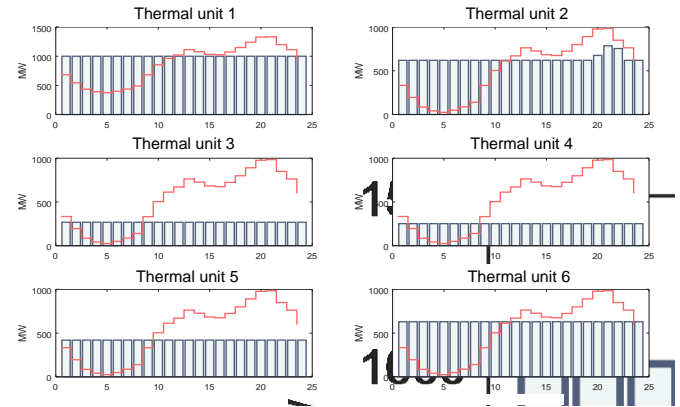


Fig. 12: Thermal power plants operation in Scenario II

In all three scenarios the pumps work in times of low EPS load and turbines generate power in periods with peak electric power demand levels (Figures 8, 9 and 10). In scenarios II and III, the plants of the thermal power plant work at almost constant power (Figures 9 and 10 and Figures 12 and 13).

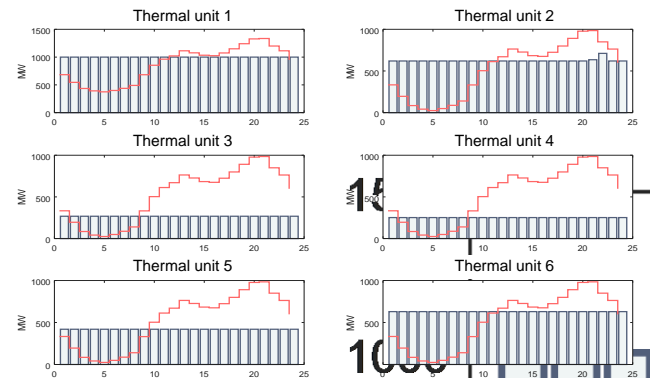


Fig. 13: Thermal power plants operation in Scenario III

The production costs of thermal unit 1 have the lowest weight (Table 1) in the cost function therefore it works at full power throughout the whole optimization horizon. Thermal plants 3, 4, 5 and 6 are expensive (Table 1) and this is why they operate at minimum power levels when possible in all three scenarios (Figures 11, 12 and 13).

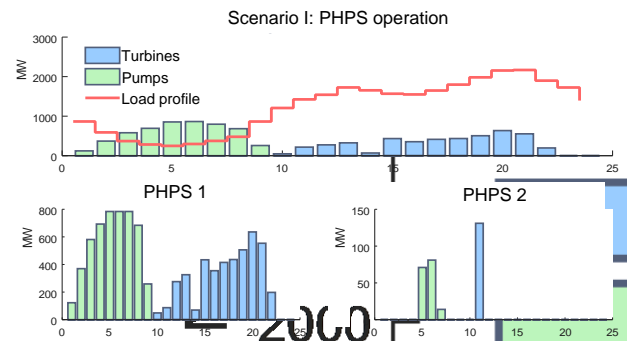


Fig. 14: PHPS operation within Scenario I

TPP 2 has the largest operating range (Table 1) and takes the second lowest price place (also in the priority list) so it is the sole thermal power plant whose output power takes an active role in the changes of the system load. This is most evident in Scenario I (Figure 11) and less - in Scenario III (Figure 13).

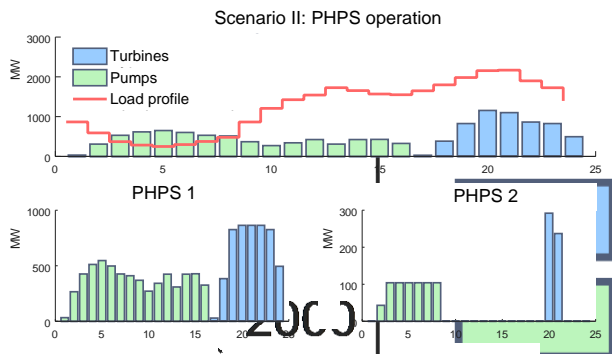


Fig. 15: PHPS operation within Scenario II

The optimal coordinated operation of thermal plants and PHPSs allows the operation of thermal units with small output deviations in two consecutive time intervals (Figures 11 - 13) so that the load is satisfied in all periods with maximum utilization of the available renewable energy (that is the rejection variables α_j and β_j are of a zero value in all time intervals) such as PHPSs are peak generators in the EPS and controllable loads.

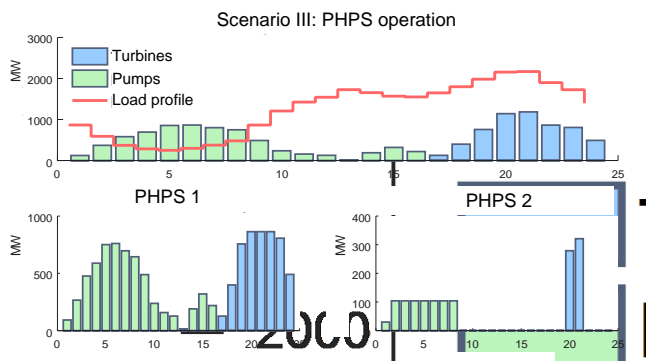


Fig. 16: PHPS operation within Scenario III

Such economic and efficient work of the thermal power plants is possible only in the case of optimal coordinated work with PHPS. Figures 14, 15 and 16 illustrate the operation of the two PHPS together and separately for the three scenarios.

4. Conclusion

The model presented in [9] aims to help a day-ahead evaluation of the impact of different RES power generators in the EPS power balance and resilience. In this paper a hydro-thermal coordination is considered with three different scenarios for the renewable generation. The results presented here show that the EPS under consideration needs controllable loads to be able to adopt all the forecasted nature-friendly generation. Results also show the margins for this production whenever it will be possible to preserve power balance. Both wind and solar power generation peaks occur in periods of low system load. The controllable loads here presented by PHPS demonstrate an important role in the power balance as they operate to assure the EPS's active power balance and to increase total profits by reducing the costs associated with the operation of the thermal power plants. The latter are able to work within the most effective, thus economic, power ranges that generally means with minimal deviations of their output power in the consecutive time intervals. Flexible and controllable loads also assure a maximum RES power production utilization thus increasing the ecological impact.

5. Bibliography

- [1] Anagnostopoulos J.S., Papantonis D.E., Pumping station design for a pumped-storage wind-hydro power plant, *Energy Conversion and Management*, Vol. 48, Issue 11, November 2007, p. 3009-3017
- [2] Castronuovo E. D., Lopes J. A. P., Optimal operation and hydro storage sizing of a wind-hydro power plant, *International Journal of Electrical Power & Energy Systems*, Vol. 26, Issue 10, December 2004, Pages 771-778
- [3] Dinglin L., Yingjie C., Kun Z. , Ming Z., Economic evaluation of wind-powered pumped storage system, *Systems Engineering Procedia*, Vol. 4, 2012, Pages 107-115
- [4] Holttinen H., Wind integration: experience, issues, and challenges, *Wiley Interdisciplinary Reviews: Energy and Environment*, Volume 1, Issue 3, November/December 2012, p. 243-255
- [5] Gonzalez-Aparicio, A. Zucker, Impact of wind power uncertainty forecasting on the market integration of wind energy in Spain, *Elsevier APPLIED ENERGY*, ISSN: 0306-2619, DOI: 10.1016/j.apenergy.2015.08.104, vol. 159, 2015, p. 334-349
- [6] Gomes B. A., Saraiva, J. T., Dealing With Load and Generation Cost Uncertainties in Power System Operation Studies: A Fuzzy Approach *Handbook of Power Systems I*, ISBN 978-3-642-02492-4, 2010, p. 209 - 234
- [7] Daoxin L., Lingyun L., Yingjie C., Ming Z., Market Equilibrium Based on Renewable Energy Resources and Demand Response in Energy Engineering, *Systems Engineering Procedia*, Vol. 4, 2012, p. 87-98
- [8] Mabel M. C., Edwin Raj R. E., Fernandez E., Analysis on reliability aspects of wind power, *Renewable and Sustainable Energy Reviews*, Vol. 15, Issue 2, February 2011, ISSN: 1364-0321, pages 1210-1216
- [9] Trashlieva V., Radeva T., Optimal Hydro-Thermal Coordination with a maximum RES Power Utilization Strategy Constraints Model, *International Scientific Conference "Mathematical Modeling"*, 12-15.12.2018, Borovets, Bulgaria

ON A MATHEMATICAL MODEL OF LAND-USE CHANGE

Assoc. Prof. M.Sc. Kolev M. PhD.¹, M.Sc. Urumova A.¹, Assoc. Prof. M.Sc. Kolev B. PhD.¹
 Faculty of Mathematics and Natural Sciences – South West University “Neofit Rilski”, Blagoevgrad, Bulgaria¹

mkkolev@abv.bg, aneliaaneli@abv.bg

Abstract: The paper is devoted to a mathematical model of land-use change proposed by Dobson et. al. We formulate and investigate some quantitative properties of the corresponding Cauchy problem. We construct a numerical algorithm for approximate solution of the problem and present some of the numerical results. Their meaning is explained and discussed.

Keywords: LAND-USE, MATHEMATICAL MODEL, CAUCHY PROBLEM, NUMERICAL SIMULATIONS

1. Introduction

In the distant past people had practically no potential to influence the nature. However since the early 19-th century (the beginning of the Industrial Age) and especially since the rapid increase in the number of inhabitants of the Earth the technological potential for changing the natural resources has multiplied many times. The main cause of all problems is undoubtedly the increase in the world's population – more than 7 billion now, which means that it increased around 7-fold since the year 1800. Another several billion newcomers are expected by 2050, even with all the cataclysms and epidemics that can kill millions and depopulate entire regions. These epidemics (such as AIDS, for example) are a reality now in large areas of Africa and Asia, unlike Europe and North America where, despite their absence, population growth is about zero or negative. Six countries are currently "responsible" for over half of the annual human growth on Earth by 80 million people – India, China, Pakistan, Nigeria, Bangladesh and Indonesia [1].

If their economic (industrial) development follows their population growth at the same pace and their standard of living is close to that of the US and the European Union, this would mean almost immediate depletion of most resources such as oil, minerals, arable land and water. The Earth, which is currently suffocate under the burden of its inhabitants, will have to absorb a new amount of carbon dioxide and harmful emissions.

The need of more and more resources (water, food etc.) for the continuously increasing amount of people worldwide leads to deforestation, related with clearance of forests for agriculture, building of cities, the fragmentation of forests, where large forest areas appear to be fragmented on numerous smaller plots located in agricultural lands or developing cities, which definitely affects forests and dependent species [2]. The deforestation leads to serious problems because the forests are very important to the health status of the environment. Forests provide numerous and vital ecosystem services for the environment and the climate. They help, for example, to regulate our climate and keep the river basins in a sustainable state by providing us with clean water. Forests contribute to purifying the air we breathe. The growth of the forest fund often helps capture large amounts of carbon dioxide from the atmosphere. This also helps to maintain and preserve biodiversity, as many species live in and depend on forests. The forests are also an important economic resource not only for the production of wood but also for other raw materials used for medicines and other products. Thus, forests have important functions for people's well-being and rest.

Methods of mathematical modeling are widely used for the study of complex processes, allowing mathematical description and an opportunity for performing numerical experiments. Investigation and modeling of complex phenomena are preceded by phenomenological observations and experimental work. After collecting the experimental data the investigation continues with interpretation and prediction of the behaviour of the system by identifying areas of independent variables, selection of the state parameters and definition of the parameters of the system under study. Thus one comes to the formulation of a model or to the

description of the unknown and known variables and the relationships between them.

An interesting example of mathematical modeling is the work of Thomas Malthus "Essay on the principle of population" (1798) [3]. There Malthus mentioned the conflict between the growing population and the limited capacity of the environment, which has to satisfy the continuously increasing needs of natural resources. Due to Malthus, in certain moment of population development, its aspiration for growth should transform into "fight for survival". The theory of Malthus had strong impact on Charles Darwin and his book "On the origin of species" [4] devoted to the theory of survival of the most adaptive individuals. In the early 20-s of the 20-th century Pearl [5], Lotka [6] and Volterra [7] separately developed mathematical models for studying populations. These models provoked conducting a series of experimental studies on predator-prey interactions, competitive relationships between species and the regulation of populations.

The aim of the present paper is to study a model proposed in [8]. It describes the temporary change of land-use in particular situations. We formulate the model and study some of its properties. Further we perform numerical experiments and give some of their results.

2. Mathematical model of land-use dynamics

Here we present a model of land-use dynamics proposed by Dobson et al. [8]. The usefulness of such models follows from the high rate at which natural habitats can be converted to other uses. For example, pristine or almost pristine habitats may be colonized by humans and transformed into agricultural land. Moreover, the agricultural land can be converted into degraded land or into housing developments, cities etc. [8]. In some situations conversion to agricultural land can be partially reversible. For example: the conversion of forests into farmlands can be followed by regeneration of forests over substantial areas after abandoning of the farms (transformations observed in some countries [8]).

The model proposed by Dobson et al. [8] describes the dynamics of the size of human population supported by agriculture, denoted by W , the amount of land under agriculture, denoted by Y , the amount of degraded land (in recovery), denoted by V , and the amount of pristine or recovered land (undisturbed forest), denoted by X .

The model is the following system of four ordinary differential equations:

$$(1) \quad \frac{dX}{dt} = sV - dWX$$

$$(2) \quad \frac{dY}{dt} = dXW + bV - aY$$

$$(3) \quad \frac{dV}{dt} = aY - (b + s)V$$

$$(4) \quad \frac{dW}{dt} = rW \frac{Y - hW}{Y}$$

The meaning of the variables and of the parameters of the model is the following. The variable X denotes the area of pristine forest habitat, which can be converted to agriculture land (area Y). Agriculture land transforms into unused land (denoted by V) after a time period $1/a$. It is also assumed that the unused land can be restored to agriculture land after an interval of time $1/b$. The variable W denotes the number of people that use the land. The parameter r denotes the growth rate of human population. Its dynamics is described by logistic expression with carrying capacity proportional to the land amount h needed to support one human. The parameter d denotes the rate of transformation of forests into agriculture land, while the parameter s denotes the rate of recovery of degraded land to forest.

The parameters of the model are assumed to be non-negative. The problem has to be supplemented by corresponding initial conditions.

We study the Cauchy problem related to the model (1) – (4). The following theorems can be easily proved.

Theorem 1.

If the Cauchy problem (1)-(4) with non-negative initial conditions possess a continuously differentiable solution, then this solution is non-negative for every time $t \geq 0$.

Theorem 2.

The system (1) – (4) with non-negative initial conditions possess a unique continuously differentiable solution for every $t \in [0, T]$,

where T is an arbitrary positive constant.

3. Numerical simulations

We solved the model numerically by using the code `ode15s` from the Matlab ODE suite. `Ode15s` is a multistep solver using numerical differential formulae [9].

We used the following values of parameters:

$$s = 1, b = 0.2, a = 0.05, p = 0.2, r = 0.5, h = 0.9$$

and initial values:

$$X(0) = 10000, Y(0) = 0.1, V(0) = 0.1, W(0) = 30.$$

We have analyzed the role of parameter d for the dynamics of the system.

The result of the numerical solutions are presented in Fig. 1 – Fig. 4. In Fig. 1 we present the system dynamics for $d = 0.00005$, in Fig. 2 – for $d = 0.0001$, in Fig. 3 – for $d = 0.001$ and in Fig. 4 – for $d = 0.05$.

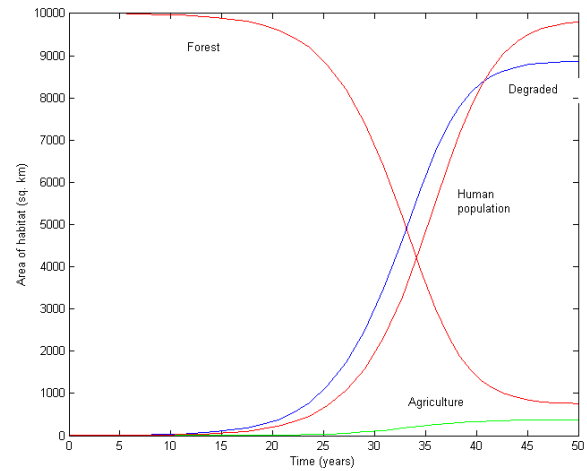


Fig. 1. Dynamics of the system for $d = 0.00005$

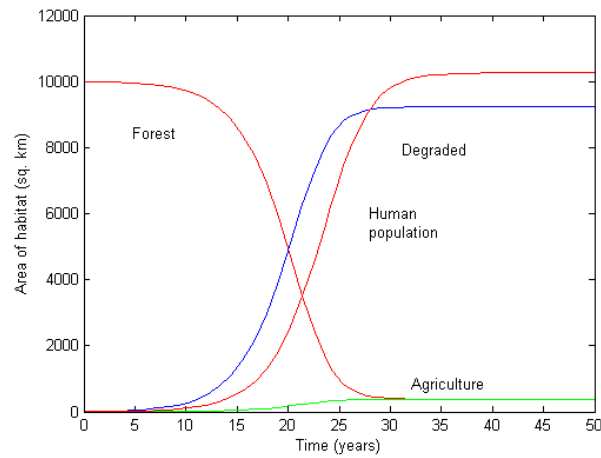


Fig. 2. Dynamics of the system for $d = 0.0001$

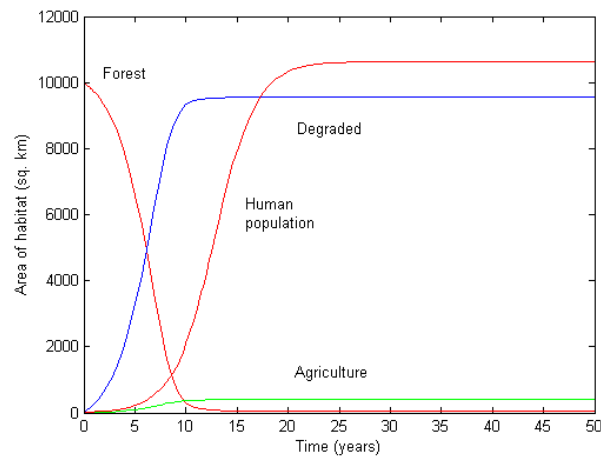


Fig. 3. Dynamics of the system for $d = 0.001$

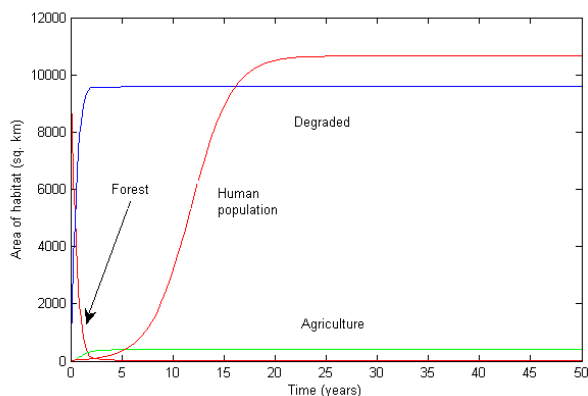


Fig. 4. Dynamics of the system for $d = 0.05$

The numerical solution shows that when the initial patch of pristine forest is invaded by 30 people starting to use land for agriculture, whose area increases, the area of pristine forest declines, while the area of unused land increases. When the value of parameter d is very small (e.g. Fig. 1, Fig. 2), the speed of these transformations is very small and it needs more time in comparison with situations with higher values of this parameters (e.g. Fig. 3, Fig. 4).

CONCLUSIONS

The presented model can be useful for prediction of the temporary dynamics of the various types of land and their change. Our future work will address the problem of estimation of parameters values by using specific field data.

BIBLIOGRAPHY

- [1] Roser M., Ortiz-Ospina E. (2018) - "World Population Growth". Published online at OurWorldInData.org. Retrieved from: 'https://ourworldindata.org/world-population-growth'
- [2] Koomen E., Stilwell J., Bakema A., Scholten H. (eds.). Modelling Land-Use Change. Springer, 2007.
- [3] Malthus T. (1798) *Essay on the principle of population* (reprinted Macmillan, London, 1926)
- [4] Darwin, Ch (1859) *On the origin of species*, J. Murray, London.
- [5] Pearl R. (1928) *The rate of living*. Knopf, New York.
- [6] Lotka, A.J. (1925) *Elements of Physical Biology*, Williams and Wilkins, Philadelphia.
- [7] Volterra, V (1926) *Variations and fluctuations of the numbers of individuals in animal species living together*. Reprinted 1931 in R.N. Chapman, *Animal Ecology*, McGraw-Hill, New York.
- [8] Dobson A., Bradshaw A., Baker A. (1997) Hopes for the future: Restoration ecology and conservation biology. *Science* 277: 515-521.
- [9] Shampine, L, Reichelt, M (1997): The Matlab ODE suite. *SIAM J. Sci. Comput.* 18: 1-22.

RESEARCHING THE CAPABILITIES OF INFORMATION TECHNOLOGIES FOR EDUCATION IN DESIGN, 3D MODELING AND VISUALIZATION OF THE WORKING OF COMPLEX MECHANISMS

ИЗСЛЕДВАНЕ НА ВЪЗМОЖНОСТИТЕ НА ИНФОРМАЦИОННИТЕ ТЕХНОЛОГИИ ЗА ОБУЧЕНИЕ ПО ПРОЕКТИРАНЕ, СЪЗДАВАНЕ НА 3D МОДЕЛИ И ВИЗУАЛИЗАЦИЯ НА ДЕЙСТВИЕТО НА СЛОЖНИ МЕХАНИЗМИ

S. Il. Antonov

Artillery, Air Defense and CIS Faculty – Shumen, “Vasil Levski” National Military University, Bulgaria
stamantonov@abv.bg

Abstract: This report explores modern means for researching automation of design and construction methods of engineering analysis and integrated production systems. The report is fully adapted for the need of knowledge and skills in the future work of engineering specialists in the field of machine-engineering.

Keywords: INFORMATION SYSTEMS, CLASSIFICATION, CAD SOFTWARE

1. Introduction.

The automation of the design is the systematic use of computer equipment and software in the process of engineering work (research, design, technological design, experimentation, planning and management of production processes) in the scientifically technical distribution of functions between the specialists and the electronic computing equipment (ECE). Additionally, including reasonably chosen methods for computer calculation of engineering tasks.

This means that the specialist is always leading in the design process. He solves the tasks that are creative. The ECE is tasked with the tasks that can be algorithmized i.e. provided with programs whose solving with the computer would be significantly more effective than manual execution.

As a creative process designing is an alternation of the mentally-creative and mentally-formal activities of the engineer. Formal types of activities are for example: information storage and search; processing the results of experiments; drawing up documentation, etc. These activities in the total design time balance can take up to 40-70% and are relatively easy to automate with the help of the ECE and appropriate software[13].

For a thorough study of modern means of automation of design and construction methods of engineering analysis and integrated production systems it is necessary to acquire knowledge in the fields of Materials Science and Mechanics, Mechanics, Resistance of Materials, Elements, Fluid Mechanics, Theory of Mechanisms and Machines, Methodology of Design, Technology of Mechanical Engineering, Engineering Graphics, Informatics.

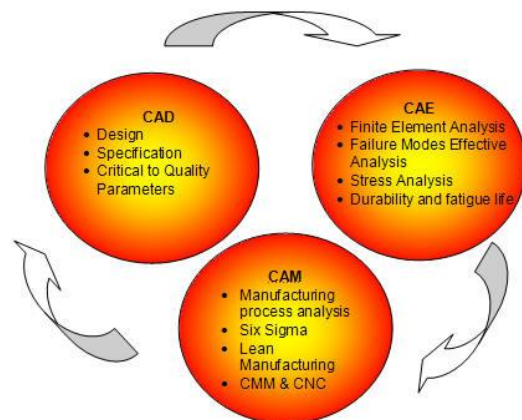
2. Researching the capabilities of information technologies for education in design.

Modern digital controllers (CNCs) offer advanced capabilities to increase productivity quality and implement an individual approach to each technical assignment. The programming and communication software based on a dialogue principle is the main focus. Undoubtedly the best form of organization of automated designing in the course of design training, 3D modeling, and visualization of the characteristic elements of armament are the automated design and manufacturing systems called Computer Aided Design (Computer Manufacturing), fig. 1.

Information Systems for Computer Design and Engineering (CAD/CAE) with their capabilities facilitate the acquisition of knowledge and practical habits in working with engineering

databases, engineering methods for calculation and analysis and simulation modeling in machine engineering.

The information support of the design and visualization of the distinctive armament elements is a set of activities for the creation and implementation in the work of machine-building organizations of computer networks and systems as well as various high-tech technical means (numerically controlled metal cutting machines, sensors, 3D printers, etc.) with corresponding information and programming capabilities in order to increase the efficiency and effectiveness of the management process and the life cycle of products.



CNC - computer (or computerized) numerical control

CMM - Coordinate Measuring Machines

Fig. 1 Connections between automated design systems modules of engineering.

The information support of the life-cycle management of the armament in the conceptual stage of designing of its individual details and mechanisms is expressed in assisting the engineering and designing activity by defining, forecasting and registering activities by assessing the suitability, feasibility and eligibility of the specified variants for the geometric description of digital models and computer simulation through the use of information systems[14].

The essence of the information systems in the private sector related to the maintenance of engineering solutions in the design of distinctive elements of the armaments in an organizational aspect can be defined as organizational-technical unification (complex) of bodies, automated workplaces, information resources (forces, means and systems), specialized peripherals, procedures and documents to ensure the handling, storage and provision of engineering support information at the design stage.

At this stage, there are many CAD/CAM/CAE systems that serve various functional areas of teams involved in the armament design process. The following section of the report presents the most used products for computer-engineered analysis and design.

2.1. Software products of Allplan Deutschland GmbH, Germany [1]:

- Allplan Engineering - integrated BIM / CAD design software.
- Allplan Architecture - object-oriented BIM/CAD software for designing all types of buildings.

2.2. Products of Altium, USA [2]:

- Altium Designer - CAD/EDA product for designing electronic circuits, embedded software, simulations, PCBs.

2.3. Autodesk Products, USA [3]:

- AutoCAD 2018 - a popular product for 2D and 3D design and construction on a global scale. The program offers innovations that provide more effective design and documentation that enables safer more accurate and seamless sharing of projects and drawings.

- AutoCAD LT 2018 - 2D drawing and detail design software with a focus on continuous productivity gain. Its comprehensive set of tools allows you to create, modify, and share drawings accurately and effectively. Using the original DWG file format ensures stability and interoperability when communicating with customers and colleagues.

- Autodesk AutoCAD Architecture 2018 - Special Software for Architects. Includes all the functionality of the standard 3D AutoCAD and adds specially designed architectural design tools that automate frequently recurring tasks and speed up the workflow. The DWG file format ensures seamless communication with colleagues and teams. Included visualization tools help ensure realistic presentation and early approval of the project.

- AutoCAD MEP 2018 - specialized CAD software for creating drawings in the water, electricity and HVAC section. Automates repetitive tasks by allowing engineers to create accurate documentation faster and communicate seamlessly with colleagues thanks to the DWG format.

- Advance Steel 2018 - a specialized product for designing structures. It allows the creation of BIM (Building Information Modeling) models and drawings of steel structures with integrated libraries and tools. Works as an AutoCAD upgrade. Version 2018 also includes AutoCAD 2018.

- Autodesk Revit - includes 3 modules with architectural, building and construction features:

- Autodesk Revit Architecture Module 2018 - BIM for architects providing integrated tools for building design and analysis. Shows each distinctive view, drawing, 2D, and 3D view from the same database, automatically coordinating changes at all stages of project design and deployment. Helps to make more informed decisions in the early stages of the project.

- Autodesk Revit MEP 2018 Module - BIM for SIP, HVAC and HVAC Engineers. Provides special tools for design and analysis of building installations.

- Autodesk Revit Structure Module 2018 - a BIM-based design solution that provides custom-designed design, analysis, and documentation tools. BIM helps coordinate drawings, reduce

mistakes, and improves collaboration between the engineering and architectural team.

- Autodesk Revit 2017 includes Revit Architecture, Revit MEP, and Revit Structure as a single product for all majorities.

- Autodesk Robot Structural Analysis Professional 2018 - professional software for calculating building structures of all kinds. It offers functionality for thousands of analyzes, both static and dynamic, earthquake resistance analysis and hurricane winds.

- AutoCAD Plant 3D 2018 - 3D software for designing, modeling and documenting factory processes and industrial facilities (pipelines, equipment, bearing structures and other plant components, industrial buildings and wastewater treatment plants).

- Autodesk ReCap 2018 - Laser scanning data processing software initiated in digital CAD or BIM environments for building and refining specialized design software for renovation, reconstruction and rehabilitation projects.

- Autodesk Navisworks Simulate 2018 - combines design data from various specialists, including BIM and digital prototypes (DPs), in an integrated model that allows analysis and visualization of the project, as well as simulation of building processes for timely detection of errors.

- Autodesk Navisworks Manage 2018 - includes project review tools and more effective communication that combine multidisciplinary design data, including BIM or digital prototypes. Helps to detect inconsistencies prior to the construction phase, which reduces the cost and time to process the project.

- AutoCAD Mechanical 2018 [4] - Includes all the features of AutoCAD, as well as comprehensive automation tools for mechanical engineering tasks such as machine tool generation, sizing and distinctive of materials. AutoCAD Mechanical has a library of over 700,000 standard elements, supports multiple international drafting standards, and allows users to create details and documents using Autodesk Inventor-created digital prototypes. AutoCAD Mechanical makes engineers more competitive by helping them save hours of effort they can use for innovation rather than drawing. AutoCAD Mechanical for machine design offers users up to 70% faster performance than AutoCAD.

- AutoCAD Electrical 2018 [5] - a specialized version of AutoCAD designed distinctively for electrical engineering and automation, AutoCAD Electrical incorporates all AutoCAD tools plus a complete set of CAD design features for electrical design. Extensive libraries with ready-made components and tools for automating tasks in electrical engineering and automation help save hours of effort to allow engineers to devote more time to innovation.

- Autodesk Inventor Professional 2018 - 3D Parametric Modeling Tool. The only product on the market that has a 100% garnet relationship with two-dimensional drawings in original DWG format. It enables the creation of a complete digital prototype allowing the machine to be tested and optimized before it is produced. Inventor provides a vast array of tools for easy 3D design, error elimination and machine and detail optimization. Provides users with tools for dynamic simulation, cable, tracking, and pneumatics in 3D, as well as the ability to create and test tooling. With Inventor's capabilities, you can be more effective, reduce errors and create innovative projects at times faster.

- Autodesk Fusion 360 - Cloud-based platform for 3D CAD, CAM and CAE design of machines and products. Fusion 360 combines mechanical design capabilities, simulations, tools to improve collaboration, and the ability to prepare components for CNC machines. The Fusion 360 works in iOS for Mac and Windows PCs, allowing the use of the client's preferred operating system. Fusion 360 TM is part of the AutoDesk product family for machine and product design and one of the core products in the Product Design Collection software package.

- Autodesk Vault Family 2018 - The Vault Series products help support teamwork as well as individual designers. Autodesk Vault works directly from Autodesk applications, such as AutoCAD and Inventor, allowing for secure storage of engineering data, sharing and sharing, retaining previous versions, approving changes, and more.

- Autodesk Nastran In-CAD 2018 - is a built-in CAD module for simulations using the Finite Elements method. Taken from Autodesk Nastran® Solver, this product offers users multiple analytics, including linear and non-linear stresses, dynamic simulations, and heat exchange. The product is available through network licensing, providing users with trouble-free work, eliminating the need for multiple individual simulation software. It delivers high-quality simulations in the CAD environment so you can test and create great products.

- Autodesk Inventor HSM is a solution that works in addition to Inventor Professional software and provides users with an integrated CAM system with 2.5 and 5-axis processing for CNC machines.

- Autodesk Alias 2018 - Product Designed for Machine Building and Product Design. Alias is used by 99% of all automotive manufacturers to create complex surfaces and shapes. In machine building, this program combines perfectly with the parametric model of Inventor and serves as a tool for modeling difficult by traditional methods such as propellers, screws, spirals,

- Autodesk Moldflow 2018 - Specialized Plastic Product Simulation Software, part of Autodesk's Digital Prototyping solution. This software offers tools that help manufacturers of plastics to test, optimize and validate their products and related manufacturing processes. Many companies use Autodesk Moldflow Adviser and Autodesk Moldflow Insight to reduce the need for costly prototypes, reduce the risk of potential manufacturing defects, and generally shorten the production process and bring their products to the market.

- Autodesk CFD 2018 - Specialized fluid simulation software - heat pumps, streams, swirling, etc. Designed for designers in their day-to-day work with a menu in familiar AutoCAD and Inventor environments. Autodesk CFD offers the ability to make calculations both on a local computer and in Autodesk Cloud Space. Works with models from all three dimensional CAD formats.

2.4. Autodesk Manufacturing products that provide effective control over a wide range of NC machines - lathes, 2-5 axis milling centers, wire erosion machines, Swiss lathes, robots [6]:

- PowerMILL - a high-end control system for milling NC machines.

- FeatureCAM - control of milling, lathe, lathe and wire erosion machines.

- PowerSHAPE - modeling system for surface and solid geometric objects.

- PowerINSPECT - Product Inspection Product and Equipment.

- ArtCAM - a system for modeling and production of artistic forms.

2.5. Bentley Systems, USA [7]:

- MicroStation (MicroStation, MicroStation PowerDraft, Bentley View) - one of the most popular global 3D CAD / GIS infrastructure design solutions.

2.6. Products of Dassault Systemes, France [8]:

- CATIA - high-end engineering solutions for 3D design and manufacture. They allow users to simulate the whole cycle of industrial process modeling, from the original idea, through product design to virtual assembling.

- 3DEXPERIENCE - an engineering and business platform for managing development and production projects. Provides access to project information through regulations for all project participants (constructors, production technologists, economists, project managers) as well as centralized storage and controlled information management.

- SIMULIA - high-end simulations.

- ENOVIA - Lifecycle and Management of Products.

- DELMIA - Production Management.

2.7. Products of Dassault Systemes Solidworks Corp., USA [9]:

- SOLIDWORKS - SOLIDWORKS 'CAD solutions cover all aspects of a product development process with a seamless, integrated workflow - design, verification, communication and data management. The main SOLIDWORKS software applications are as follows:

PRODUCT DATA MANAGEMENT (PDM): Allows you to easily find and redirect files, details and drawings, automate workflow, and secure production with the correct version of the tech. product data.

ELECTRICAL DESIGN: Combines the functionality of electrical circuits from SOLIDWORKS Electrical Schematic with 3D design capabilities of SOLIDWORKS Electrical 3D.

SIMULATION: Allows you to simulate a different real environment for pre-production product testing in the virtual environment of the program.

3D EXPERIENCE: SOLIDWORKS Mechanical Conceptual Makes Conceptual Design Your Business Advantage. Innovation in an instinctive, powerful modeling environment that allows for freedom in design.

2.8. Products of DP Technology Corp [10]:

- Esprit CAM - Automated, reliable and easy to use high-speed 3-axis and 5-axis CAM software. Using the knowledge of material handling, residual material, integrated simulation and ESPRIT testing provides fast, safe, and reliable CAM software for a wide variety of 3D operations. ESPRIT's high performance and capabilities include processing of any kind of solid geometry (Solid, Surface or Wireframe), universal postprocessors generate a G code for any machine on the market, the ability to simulate and verify programs gives optimal quality and integrity detail. ESPRIT is 100% compatible with Windows and provides a convenient and familiar environment for maximum productivity.

2.9. Products of EPLAN Software & Service GmbH & Co. KG

- EPLAN Electric P8 - an electrotechnical CAD system for designing circuits in electrical design and automation. The product covers all the needs of the electric designer when preparing the technical and installation documentation. The program can be designed with multiple automated functions, has large array of macros and technical information for products that are used in such projects.

2.10. Products of HCL Technologies

- CAMWorks - a fully integrated SOLIDWORKS CAM control system for all types of CNC machine tools.

2.11. Products of SIEMENS PLM Software [11]:

- NX - a high-end CAD / CAE / CAM solution for 3D modeling, engineering analysis, CNC and CMM control. NX encompasses and accelerates the whole process chain in the creation and production of end-to-end products - design, design and system engineering, design, FEM / FEA simulation and optimization, production drawings, technical preparation, off-line programming CNC machines, measurement procedures and robotized production.

- NX CAM2PART & MOLD - a comprehensive solution for machining parts, including CNC and robot programming, CNC machining simulation and CNC program validation, DNC and integrated metrology control.

- Solid Edge - Provides 3D CAD/CAE/PDM technologies from product design: Convergence Modeling, Reverse Design, Integrated Fluid Analysis, 3D Printing Tools. Synchronous technology for direct editing of own and external models. Solid Edge ST10 has built-in product data control (PDM) and Cloud collaboration.

- Tecnomatix - software for simulation and management of manufacturing processes and programming of robots. A complete portfolio of digital production solutions that enables product engineering, production engineering and manufacturing to be synchronized.

- Teamcenter - a software platform for digitization of businesses in manufacturing enterprises. Teamcenter centralizes product data management, manages team collaboration, and automates processes throughout the product's lifecycle - from conceptual ideas, through design, technical preparation to service servicing, and recycling of materials.

- SIMCENTER 3D - Provides a unified, scalable, open and expanded environment for 3D CAE simulations and engineering analysis with links to design, simulation, testing and data management. Simcenter speeds up the simulation process by combining the best-in-class associative geometry modeling tools with a wide range of FEM / FEA / CFD simulations. Helps engineers use the available 3D CAD geometry to quickly prepare the analysis. Unique management architecture in Simcenter 3D allows more efficient creation, assembly and management of large models, even with 3D details from multiple CAD systems, incl. CATIA, SOLIDWORKS, PRO-E / CREO, INVENTOR, STEP and IGES.

- PROCESS / TOOL SIMULATION PORTFOLIO - Operating alone or integrated with Solid Edge, NX, Catia, SolidWorks, PTC and other CAD solutions, these products extend the scope of engineering engineering beyond the typical CAD / CAM / CAE boundaries and ensure the most important competitive advantages for a manufacturing company: shorter time to realization of the order; lower cost of production; higher quality and reliability.

2.12. Products of Vectorworks, Inc., USA:

- Vectorworks Fundamentals - a basic CAD package that provides excellent 2D and 3D modeling capabilities combined with an intuitive and easy-to-use interface.

- Vectorworks Designer - gives you the freedom to design without the need for additional applications. The program provides a competitive advantage by offering a wide range of modeling tools in an intuitive interface.

- Vectorworks Architect - software for designers, architects and designers, providing creative freedom throughout the whole process - from idea / sketch to complete BIM (Digital Model Building). Unlimited 2D and 3D modeling is complemented by solid BIM functionality, excellent documentation and various intelligent tools such as the world-famous Parasolid 3D and Cinema 4D.

2. 13. Autodesk CAE (USA) [3]:

- Autodesk Robot Structural Analysis Professional - software for static and dynamic analysis of building structures using the finite element method, sizing, constructing, detailing and generating drawings and reports. It offers engineers tools for in-depth BIM analysis and design, for easier understanding of the work patterns of different constructions and verification of compliance codes. The product uses BIM technology and supports a two-way connection with Autodesk Revit.

2.14. Additive manufacturing technologies and 3D printing of 3D SYSTEMS [12]:

- ProX - the production and professional 3D printers offer the benefits of additive technology to produce a wide range of functional prototypes, spare parts, small and medium series of plastic details, dental and surgical products, and more. The 3D printing capabilities in metal, with solid, thermoplastic plastics and elastomers offer a real alternative to manufacturers looking for competition. 3D Printers ProX Direct Metal Printing produces metal parts and nodes with high precision and high metal density (96% - 100%) of a wide range of metallic powders with proven mechanical properties. The ProX DMP 100, 200 and 300 printers include the most flexible industry parameter control settings. The ProX DMP 320 complements the range of metal printers with the ability to build large-scale titanium alloy models and manage from one controller the parallel operation of 3 printers.

- Creaform's 3D scanners for reverse engineering and inspection

- 3D Stratasys printers - designed for conceptual design, prototyping and direct production, based on FDM and PolyJet technologies.

3. Conclusion.

The analysis of the listed products for computer-engineered analysis and design gives reason to summarize that different CAD/CAM products provide a variety of management databases, system and application software. However, they are compatible (or have integration capabilities) with Microsoft products as well as MS Project and MS SharePoint products, and this facilitates training, training and the work of engineering staff.

4. Bibliography:

1. <https://www.allplan.com/en/>
2. <https://www.altium.com/>
3. <https://www.autodesk.eu/>
4. <https://www.autodesk.com/products/autocad/included-toolsets/autocad-mechanical>
5. <https://www.autodesk.com/products/autocad-electrical/overview.1>
6. <https://www.autodesk.com/solutions/manufacturing>
7. <https://www.bentley.com/en>
8. <https://www.3ds.com/>
9. <https://www.solidworks.com/sw/globalsites.htm>
10. <http://www.espritcam.com/>
11. <https://www.plm.automation.siemens.com/global/en/>
12. <https://www.3dsystems.com/>
13. Лилев И. „Приложение на линейното оптимизиране в управлението на системите за информационна сигурност“, 4^{-та} Международна научно-техническа конференция „Техника. Технологии. Образование. Сигурност“, В. Търново, 2016 г.
14. Hutov I, Lilov I “Numerical model for simulation of the velocity fields for the explosively formed penetrator”, 1-ва Международна Научна Конференция "Mathmodel 2017", 13-16.12.2017, Боровец, България, International Scientific Journal Mathematical Modeling Print ISSN 2535-0978; Online ISSN 2603-2929; <https://stumejournals.com/journals/mm/2017/4>.

MATHEMATICAL MODELLING OF PIEZOELECTRIC DISK TRANSFORMER WITH RING ELECTRODES IN PRIMARY ELECTRICAL CIRCUIT

Dr. Bazilo C., PhD.

Faculty of Electronic Technologies and Robotics – Cherkasy State Technological University, Ukraine
b_constantine@ukr.net

Abstract: Thanks to its unique properties piezoceramics has applications in various fields of engineering and technology. Disk piezoelectric devices are widely used in the elements of information systems. Mathematical model of piezoceramic disk transformer with ring electrode in primary electrical circuit is constructed. An estimate is obtained and calculated and experimental curves of the frequency dependence of the modulus of transformation coefficient of piezoceramic disk transformer with ring electrode in primary electrical circuit are compared in the work. As a result of research of real device's mathematical model a set of geometrical, physical and mechanical and electrical parameters of a real object can be determined which provides realization of technical parameters of piezoelectric functional element specified in technical specifications. The cost of the saved resources is the commercial price of the mathematical model.

Keywords: PIEZOELECTRIC DISK ELEMENT, PHYSICAL PROCESSES, AMPLITUDE-FREQUENCY RESPONSE

1. Introduction

Thanks to its unique properties piezoceramics has applications in various fields of engineering and technology. The relevance of the use of various functional elements of piezoelectronics in radio electronics, information and power systems is explained by their high reliability and small dimensions, which solves the problem of miniaturization of such systems. Piezoelectric disks with surfaces partially covered electrodes are often used to create various functional piezoelectronic devices. Disk piezoelectric devices are widely used in the elements of information systems. In disk piezoelectric elements with surfaces partially covered by electrodes we can simultaneously excite oscillations of compression-tension and transverse bending vibrations. Manipulating the geometric parameters of electrodes and their location relative to each other, you can have a significant effect on the energy of oscillatory motion particular type of material particles of piezoelectric disk volume. It should be especially noted that this piezoelectric element has compatibility with microsystem technology, so it can be made as microelectromechanical structures (MEMS) [1]. One of the main elements of functional piezoelectronics is piezoelectric transformer (PT). Research has shown that PTs can compete with traditional electromagnetic transformers on both efficiency and power density [2-4]. PTs are therefore an interesting field of research [5]. The favorable attributes of the PT are low weight and size and potentially low cost. One additional important characteristic is the high voltage isolation of the ceramic materials used to build PTs [6]. In addition, a piezoelectric transformer is more suitable for mass production than traditional, coil-based transformers [7].

The **purpose** of this paper is to set out the principles of mathematical models construction that are sufficiently adequate to real devices and occurring physical processes using the simplest example of axially symmetric radial oscillations of the piezoelectric disk.

2. Calculation of transformation ratio of piezoelectric transformer with ring electrode in primary electrical circuit

Let us consider a disk piezoelectric transformer (Fig. 1), primary electrical circuit of which consists of electric potential difference generator $U_1 e^{i\omega t}$ (where U_1 is an amplitude value of electric potential difference; $i = \sqrt{-1}$ is an imaginary unit; ω is an angular frequency; t is a time) with output electrical impedance Z_g and ring electrode (position 1 in Fig. 1). The secondary electrical circuit consists of an electrode in the form of a circle (position 2) with connected electronic circuit to it with input electrical impedance Z_n , on which an electric potential difference $U_2 e^{i\omega t}$ is formed. The primary and secondary circuits of piezoelectric transformer do not have a galvanic connection. The energy exchange between the primary and secondary circuits is

carried out by means of axisymmetric radial vibrations of the piezoceramics material particles in the volume of thickness polarized disk (position 3 in Fig. 1).

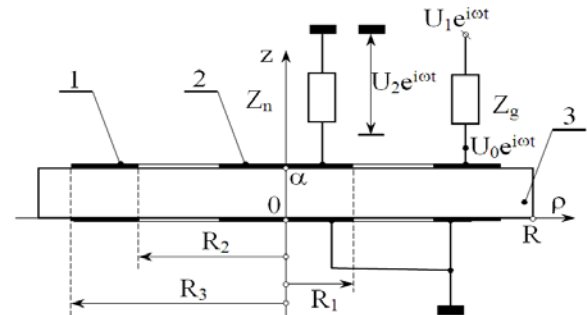


Fig. 1. Calculation scheme of disk piezoelectric transformer

It is obvious that the work of function piezoelectronic element, which is schematically shown in Fig. 1, is fully described by transformation ratio $K(\omega, \Pi) = U_2/U_1$ (Π is a set of geometrical and physical and mechanical properties of the piezoelectric transformer), which is a mathematical model of the device under consideration. Scheme of construction of piezoelectric transformer's mathematical model is outlined in [8].

Methodology for calculating the transformation ratio of piezoelectric transformer with ring electrode in primary electrical circuit is shown in [9]:

$$K(\omega, \Pi) = \frac{U_2}{U_1} = \frac{K_2(\Omega, \Pi)}{1 - i\omega C_0^\sigma Z_g K_3(\Omega, \Pi)}, \quad (1)$$

where

$$K_2(\Omega, \Pi) = \frac{2f_1(\omega) K_{31}^2 A_{12} [J_1(\Omega R_1/R)/(\Omega R_1/R)]}{1 - 2f_1(\omega) K_{31}^2 A_{11} [J_1(\Omega R_1/R)/(\Omega R_1/R)]};$$

$K_{31}^2 = (e_{31}^*)^2 / (c_{11} \chi_{33}^\sigma)$ is a squared electromechanical coupling coefficient for the mode of radial oscillations of thickness polarized piezoceramic disk material particles; e_{31}^* and χ_{33}^σ are material constants and dielectric permittivity for planar stress-strain state of the polarized across the thickness piezoceramic element; c_{11} is a modulus of elasticity for the mode of axially symmetric radial oscillations of the piezoceramic disk material particles; $f_1(\omega)$ is a switching on function or load characteristic of the output ring electrode of the piezoelectric transformer; $f_1(\omega) = \frac{i\Omega^*}{1 - i\Omega^*}$,

$\Omega^* = \omega \tau_n$ is a dimensionless quantity; $\tau_n = C_1^\sigma Z_n$ is a time constant of secondary electrical circuit; $C_1^\sigma = \pi R_1^2 \chi_{33}^\sigma / \alpha$ is a static electrical capacitance in secondary electrical circuit;

$$K_3(\Omega, \Pi) = \frac{2K_{31}^2}{1 - \beta^2} \left\{ [K_2(\Omega, \Pi)A_{41} + A_{42}]J(\Omega) + \right. \\ \left. + [K_2(\Omega, \Pi)A_{51} + A_{52}]N(\Omega) \right\} - 1; \\ J(\Omega) = [J_1(\Omega R_3/R) - \beta J_1(\beta \Omega R_3/R)] / (\Omega R_3/R); \\ N(\Omega) = [N_1(\Omega R_3/R) - \beta N_1(\beta \Omega R_3/R)] / (\Omega R_3/R);$$

$\beta = R_2/R_3$ is a geometrical parameter of the ring; $J_1(\Omega)$ and $N_1(\Omega)$ are Bessel and Neumann functions of the first order; Ω is a dimensionless wave number; coefficients A_{ij} are defined in [9].

All calculations are performed for piezoceramic disk with radius $R = 33 \cdot 10^{-3}$ m and thickness $\alpha = 3 \cdot 10^{-3}$ m, made of thickness polarized PZT type piezoceramics with following parameters: $\rho_0 = 7400$ kg/m³; $c_{11}^E = 112$ GPa; $c_{12}^E = 62$ GPa; $c_{33}^E = 100$ GPa; $e_{33} = 20$ C/m²; $e_{31} = -9$ C/m²; $\chi_{33}^E = 1800\chi_0$; $\chi_0 = 8,85 \cdot 10^{-12}$ F/m is a dielectric constant; $Q_M = 100$ is a quality factor of piezoceramics.

In Fig. 2 it is shown the calculated (solid line) and the experimentally obtained (dashed line) curves of the frequency dependence of the modulus of piezoceramic ring-dot disk transformer's transformation coefficient. Naturally, the dimensions of the disk transformer in the calculation and experiment are chosen to be the same, i.e., the radius $R = 33 \cdot 10^{-3}$ m, the thickness $\alpha = 3 \cdot 10^{-3}$ m and $R_1/R = 12/25$, $R_2/R = 15/25$, $R_3/R = 0,999$. The values of the modulus of transformation coefficient of the piezoceramic disk transformer are plotted along the ordinate axis, and the frequency f (dimensionless value $\Omega = \omega\tau_0$, where $\tau_0 = R/\sqrt{c_{11}/\rho_0}$ is a time constant of piezoceramic disk) on the abscissa axis. The frequency $f = 15206$ Hz corresponds to the value $\Omega = 1$.

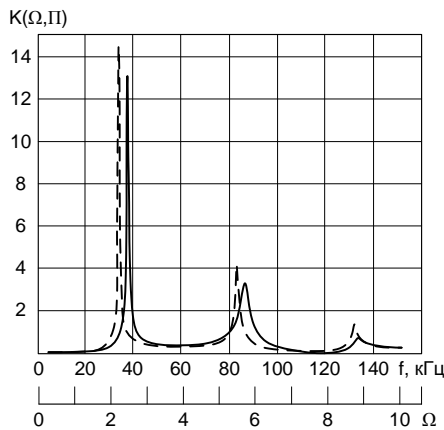


Fig. 2. Calculated (solid line) and experimentally obtained (dashed line) curves of the frequency dependence of the modulus of piezoceramic ring-dot disk transformer's transformation coefficient

When building the model, it was assumed that the thickness of the electrodes located on the surfaces of the disk is very small in comparison with the thickness of the disk α . In other words, the thickness of the electrodes, which, as a rule, does not exceed 15 μ m, was not taken into account for constructing a mathematical model of piezoelectric transformer based on piezoceramic thin disk ($\alpha/R \ll 1$). It should also be noted that mathematical model (1) was built for ring-dot piezoelectric transformer (see Fig. 1) with surfaces partially covered by electrodes (area 1, $\rho \in [0, R_1]$, and area 3, where $\rho \in [R_2, R_3]$) and in the areas where there are no

electrodes (area 2, where $\rho \in [R_1, R_2]$, and area 4, where $\rho \in [R_3, R]$).

As expected, the absolute values of the frequencies of resonances in calculation and experiment differ from each other. So, following the calculation, the frequencies of the first second and third electromechanical resonances are respectively equal to $f_{r1} = 37193$ Hz, $f_{r2} = 88194$ Hz and $f_{r3} = 135330$ Hz; the frequency ratio $\zeta = f_{r2}/f_{r1} = 2.371$.

The experimental values of the same quantities are, respectively, $f_{r1} = 34491$ Hz, $f_{r2} = 83728$ Hz, $f_{r3} = 132325$ Hz and $\zeta = f_{r2}/f_{r1} = 2.428$. If the experimental data are assumed to be true, the error in determining the frequency ratio is $\Delta\zeta = 2.3\%$. The obtained results are explained very simply. The numerical values of the frequencies of resonances s are determined by the dimensions and physicomechanical parameters of the material of disk element. The ratio of the resonances frequencies of the same disk is determined practically only by its dimensions. For this reason, a very satisfactory match between the theoretically and experimentally determined resonance frequency ratios is observed. The discrepancy between the absolute values of the resonance frequencies is explained by the discrepancy between the physicomechanical parameters of the piezoceramics, which were incorporated into the calculation and which are inherent in the experimentally investigated object. Comparing the curves, we can conclude that the quality factor of the material of the experimentally investigated sample is at least 1.2 times larger than included in the quality factor calculation.

3. Discussions and Conclusions

It can be asserted that the character of the variation of both curves, shown in Fig. 2, in a fairly wide frequency range coincides with accuracy to details. This means that the qualitative content of the expression (1) is adequate to the processes that occur in real object. In other words, expression (1) is a mathematical model of piezoelectric ring-dot transformer with ring electrode in primary electrical circuit and sufficiently adequate to the real object and the processes occurring in it. The latter allows us to assume that the mathematical description of the stress-strain state of the disk transformer also corresponds quite well to the real state of things.

Main results of this work can be formulated as follows: mathematical model of piezoelectric transformer with ring electrode in the primary electrical circuit is constructed; calculated and experimentally obtained curves of frequency dependence of modulus of piezoceramic ring-dot disk transformer's transformation coefficient are estimated and compared.

4. References

- [1] Varadan V., Vinoy K., Jose K. RF MEMS and their applications. Moscow: Technosphaera, 2004, 528 p..
- [2] Bove T., Wolny W., Ringgaard E., and Breboel K. New type of piezoelectric transformer with very high power density. Applications of Ferroelectrics, 2000, Vol. 1, pp. 321-324.
- [3] Flynn A. M. and Sanders S. R. Fundamental limits on energy transfer and circuit considerations for piezoelectric transformers. IEEE Transactions on Power Electronics, 2002, Vol. 17, pp. 8-14.
- [4] Shao W., Chen L., Pan C., Liu Y., and Feng Z. Power density of piezoelectric transformers improved using a contact heat transfer structure. IEEE Transactions on Ultrasonics, Ferroelectrics and Frequency Control, 2012, Vol. 59, pp. 73-81.
- [5] Andersen T., Andersen M. A. E., Thomsen O. C. Simulation of Piezoelectric Transformers with COMSOL. Proceedings of the 2012 COMSOL Conference in Milan. URL:

- https://www.comsol.dk/paper/download/151765/andersen_paper.pdf
- [6] Ivensky G., Shvartsas M., and Ben-Yaakov S. Analysis and Modeling of a Piezoelectric Transformer in High Output Voltage Applications. URL: http://cbucc.com/glecture_file/2002060132032.pdf
- [7] Huang Y.-T., Wu W.-J., Wang Y.-C., Lee C.-K. Multilayer Modal Actuator-Based Piezoelectric Transformers. IEEE Transactions on Ultrasonics, Ferroelectrics, and Frequency Control, 2007, Vol. 54, No. 2.
- [8] Tikhonov A.N. Mathematical model. In *Mathematical Encyclopedia*, 1982, Vol. 3, Soviet encyclopedia, Moscow, pp. 574–575.
- [9] Petrishchev O.N., Bazilo C.V. Mathematical model of piezoelectric disk transformer with ring electrode in primary electrical circuit. Herald of Cherkasy State Technological University, 2016, No. , pp.14–27.

ИЗСЛЕДВАНЕ НА КРЕНА НА АВТОМОБИЛ ПОСРЕДСТВОМ МОДЕЛ НА ПРУЖИННО ОБЪРНАТО МАХАЛО

STUDY THE VEHICLE ROLL MOTION BY SPRING INVERTED PENDULUM MODEL

гл. ас. д-р инж. Павлов Н. Л.

Факултет по транспорта, Технически университет - София, България

npavlov@tu-sofia.bg

Abstract: This paper describes a spring inverted pendulum dynamic model of a commercial vehicle. The differential equation of roll motion is worked out. Numerical simulations with given disturbance caused by the centrifugal force when the vehicle corners are carried out in program field of MATLAB. The graphical results of the roll angle are shown.

Keywords: COMMERCIAL VEHICLE, INVERTED PENDULUM, ROLL ANGLE, CORNERING

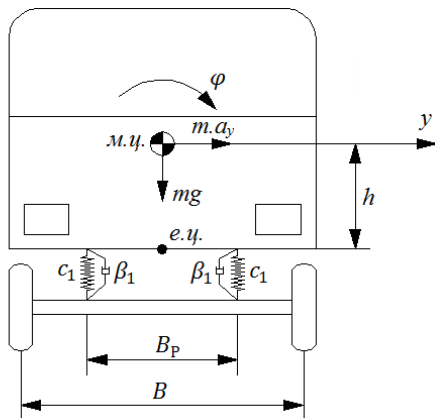
1. Увод

При движение на автомобила в завой, под действието на страничен вятър или напречен наклон на пътя, възниква странична сила, действаща в масовия му център [1]. Тази сила предизвиква напречно наклоняване на каросерията на автомобила. Ъгълът на напречен наклон на автомобила се нарича „крен“ по аналогия с възприетата първоначално терминология в теорията на кораба [2], а в последствие и в теорията на въздухоплавателните средства [3] и в теорията на автомобила [4]. Различни по сложност механо-математични модели за изследване на крена се срещат в различните литературни източници [1, 5, 6]. Един от най-простите модели използвани за определяне на крена на автомобилите е представен в [7], а в работа [8] е използван като част от модел за определяне на влиянието на крена върху собствените честоти на автомобила около вертикалната му ос. Моделът представлява обърнато махало с ъглови еластичен и демпфиращ елемент.

Целта на настоящата работа е да се състави динамичен модел на пружинно обърнато махало с подходящи параметри, чрез който да се изследва крена на товарен автомобил. Да се проведат числени симулации за определяне на крена при движение на автомобила в завой.

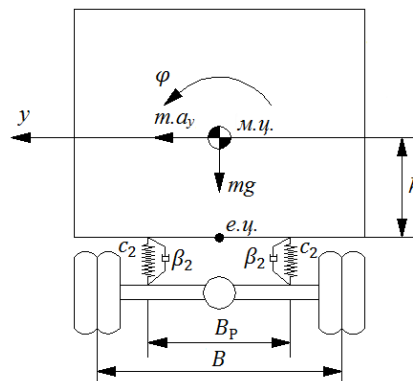
2. Механо-математичен модел

За по-лесно съставяне на динамичния модел първо ще бъдат разгледани схеми на предната и задната част на товарен автомобил (фиг. 1 и 2).



Фиг. 1. Схема на предната част на товарен автомобил.

От тези схеми може да се определят ъгловата еластичност и ъгловото съпротивление на окачването. Едностранно разположените еластични елементи от предното и задното окачване при крен работят като паралелно свързани пружини.



Фиг. 2. Схема на задната част на товарен автомобил.

Тогава за ъгловата еластичност може да се запише:

$$(1) \quad c_\varphi = 2(c_1 + c_2) \left(\frac{B_p}{2} \right)^2 = 0,5(c_1 + c_2) B_p^2$$

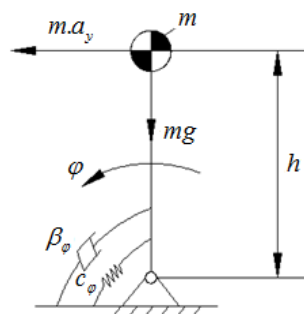
където c_1 коефициент на еластичност на един еластичен елемент (ляв или десен) от предното окачване; c_2 – коефициент на еластичност на един елемент от задното окачване; B_p – ресорна колея.

Същото важи и за ъгловото съпротивление на окачването:

$$(2) \quad \beta_\varphi = 2(\beta_1 + \beta_2) \left(\frac{B_p}{2} \right)^2 = 0,5(\beta_1 + \beta_2) B_p^2$$

където β_1 и β_2 са коефициенти на съпротивление на един амортизатор съответно от предното или задното окачване.

Механо-математичният модел на автомобила като пружинно обърнато махало се състои от динамичен модел и диференциално уравнение на движение. Динамичният модел е представен на фиг. 3.



Фиг. 3. Динамичен модел на товарен автомобил, като пружинно обърнато махало в напречната равнина.

Представеният модел е с една степен на свобода, следователно движението ще се описва с едно уравнение [7]:

$$(3) \quad J_x \ddot{\varphi} = m a_y h \cos \varphi + m g h \sin \varphi - c_\varphi \varphi - \beta_\varphi \dot{\varphi}$$

Където J_x е осов инерционен момент, спрямо оста на ротация на махалото. В случая това е оста, пресичаща еластичния център на окачването в напречно направление. За определянето на J_x се използва теоремата на Хюйгенс-Щайнер която гласи: „Инерционният момент на произволно тяло спрямо произволна ос е равен на сумата от инерционния момент на тялото спрямо ос, успоредна на разглежданата и минаваща през масовия му център и произведението от масата на тялото и квадрата на разстоянието между тези две успоредни оси“ [9]. Следователно:

$$(4) \quad J_x = J_{0x} + m h^2$$

където J_{0x} е инерционният момент спрямо надлъжна ос, минаваща през масовия център на автомобила;

m - масата на автомобила;

h - разстоянието от еластичния център до масовия център в напречната равнина.

За малки ъгли може да се приеме [10]:

$$(5) \quad \sin \varphi \approx \varphi; \quad \cos \varphi \approx 1$$

Тогава за уравнение (3) може да се запише:

$$(6) \quad J_y \ddot{\varphi} = m a_y h + m g h \varphi - c_\varphi \varphi - \beta_\varphi \dot{\varphi}$$

За да може да се извърши числено решаване на диференциалното уравнение в средата на MATLAB е необходимо привеждането му чрез подходящи субституции, към диференциално уравнение от първи ред. Тази операция се нарича канонизиране на диференциалното уравнение [11]. За целта се правят следните субституции:

$$(7) \quad x(1) = \varphi; \quad dx(1) = x(2) = \dot{\varphi}; \quad dx(2) = \ddot{\varphi};$$

Каноничната форма на диференциалното уравнение е:

$$(8) \quad dx(2) = \frac{1}{J_x} (m a_x h + m g h x(1) - c_\varphi x(1) - \beta_\varphi x(2))$$

3. Числени изследвания

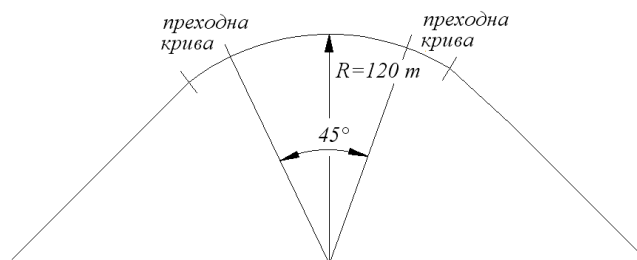
Числените изследвания са извършени в програмната среда MATLAB. Параметрите и техните числените стойности са дадени в табл. 1.

Таблица 1: Параметри на динамичния модел

Parameter	Sym bol	Value	Dimension
Маса на автомобила	m	5000	kg
Инерционен момент	J_{0x}	7442	kg.m ²
Еластичност на преден еластичен елемент	c_1	83300	N/m
Еластичност на заден еластичен елемент	c_2	115312	N/m
Съпротивление на преден амортизатор	β_1	4760	Ns/m
Съпротивление на заден амортизатор	β_2	6150	Ns/m
Разстояние от е.ц до м.ц.	h	1,0	m
Ресорна коlea	B_p	1,6	m
Коlea	B	2,1	m

Числените изследвания са проведени при смущение, съответстващо на движение на автомобила в участък, включващ движение в прав участък, преминаващ в движение в завой с радиус $R=120$ m. Преминаването от права в крива и обратно се извършва чрез преходна крива (клотоида).

Дължината на дъгата на окръжността е 94,3 m, а на преходните криви в началото и края по 17 m. Ако автомобилът се движи със 40 km/h то за изминаване на тези разстояния са необходими по 1,5 s на всяка преходна крива и 8,5 s за преодоляване на циркулярната крива с радиус $R=120$ m (фиг. 4).



Фиг. 4. План на пътният участък, за който са проведени числените изследвания.

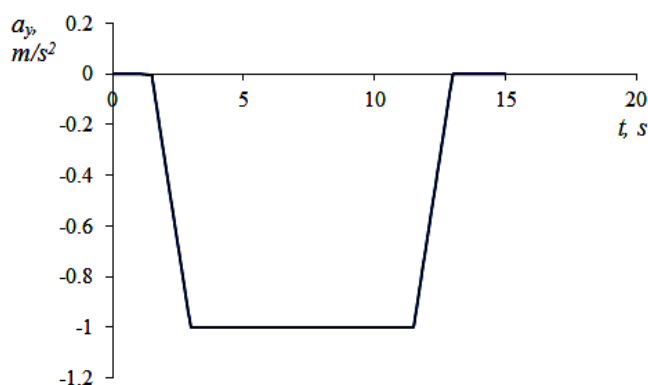
Центробежната сила е:

$$(9) \quad F_y = m \frac{v^2}{R} = m a_y$$

Следователно страничното ускорение при движение по циркулярната крива може да се определи като:

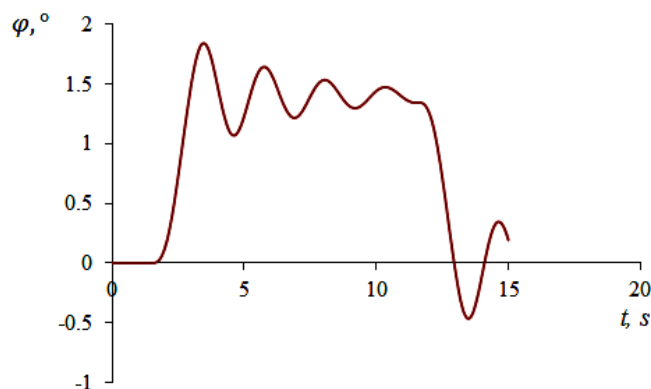
$$(10) \quad a_y = \frac{v^2}{R} = \frac{11,1^2}{120} = 1 \text{ m/s}^2$$

Съгласно тези разсъждения, а също и ако се приеме, че ускорението при движение по преходните криви нараства и съответно намалява по линеен закон, то смущението може да се представи графично по следния начин (фиг. 5):



Фиг. 5. Закон на изменение на страничното ускорение.

Получените резултати за крена на автомобила при това въздействие са показани на фиг. 6.



Фиг. 6. Изменение на крена на автомобила.

На фигурата се вижда, че трептенията на каросерията след началото на завоя, когато е приложен началният смущаващ импулс, бавно затихват, същото се забелязва и след излизане от завоя. Това означава, че демпфиращите параметри на окачването могат да бъдат повишени до граници ненарушаващи комфорта – т.е. вертикалните трептения. Ако няма такава възможност, тогава може да се повиши само ъгловата еластичност на окачването посредством пасивен или активен напречен стабилизатор и тогава при малки начални ъгли на крена, ще има и по-малки амплитуди на затихващите трептения.

4. Заключение

Представеният модел дава възможност за изследване на крена на автомобила. Получени са резултати за изменението на крена при преминаване от движение в прав участък от пътя към движение в завой чрез преминаване през преходните криви на завоя. Моделът може да се използва за оптимизиране на параметрите на окачването и оценка на необходимостта от използване на стабилизатор на напречна устойчивост. При подходящо задаване на смущаващия закон, моделът може да се използва за изследване на влиянието и на други видове смущения върху крена на автомобила. Например движение по страничен наклон, слалом, движение с престрояване, лосов тест и др. Някои от тези типове смущения ще бъдат включени в бъдещите изследвания на автора.

Литература

- [1] Ротенберг, Р. Подвеска автомобиля. Колебания и плавность хода. Москва, Машиностроение, 1972.
- [2] Войткунский, Я. Справочник по теории корабля. Том 2. Статика судов. Качка судов. Ленинград, Судостроение, 1985.
- [3] Тодоров, М. Динамика на полета I. Технически университет – София, 2015.
- [4] Димитров, Й. Теория на автомобила, трактора и кара. Технически университет – София, 1991.
- [5] Семенов, Н., В. Ролле. Расчет параметров подвески автомобиля с учетом поперечно-угловых колебаний кузова. Научно-технические ведомости СПбПУ. с. 152-156, 2011.
- [6] Павлов, Н. Активни напречни стабилизатори и избор на управляващи параметри за тях. Транспорт, екология - устойчиво развитие: научно-техническа конференция с международно участие ЕКО: сборник доклади. - Варна: Техн. унив., с. 13-27, 2011.
- [7] Goodarzi A., A. Khajepour. Vehicle Suspension System Technology and Design. Morgan & Claypool Publ, USA, 2017.
- [8] Sakai, H. Prediction of yaw natural frequency taking roll motion into account. The Dynamics of Vehicles on Roads and Tracks (IAVSD 2017), vol. 1, pp. 335-340, 2018.
- [9] Илиев, Л. и др. Механика: Лабораторен практикум. Университетско издателство „Св. Климент Охридски“, София, 2009.
- [10] Ангелов, И. Матрична механика: кинематика. Авангард прима, София, 2011.
- [11] Тончев, Й. Matlab 6, 7: част II. Преобразувания, изчисления, визуализация. Техника, София, 2006.

ИЗСЛЕДВАНЕ НА ДИФЕРЕНТА НА АВТОМОБИЛ ПОСРЕДСТВОМ МОДЕЛ НА ПРУЖИННО ОБЪРНАТО МАХАЛО

STUDY THE VEHICLE PITCH MOTION BY SPRING INVERTED PENDULUM MODEL

гл. ас. д-р инж. Павлов Н. Л.

Факултет по транспорта, Технически университет - София, България

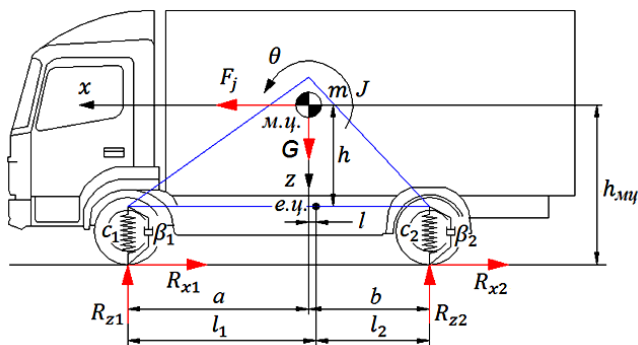
npavlov@tu-sofia.bg

Abstract: This paper describes a spring inverted pendulum dynamic model of a commercial vehicle. The differential equation of pitch motion is worked out. Numerical simulations with given disturbance caused by the inertial force when the vehicle brakes are carried out in program field of MATLAB. After conducting road tests of a truck in road conditions, the spring inverted pendulum model is validated.

Keywords: COMMERCIAL VEHICLE, INVERTED PENDULUM, PITH ANGLE, BRAKING

1. Увод

При спиране на автомобил в масовият му център действа инерционната сила. В процеса на спиране тя се явява движеща сила, на която силите създадени от спирачките на автомобила трябва да противодействат. Тъй като еластичният център на окачването на автомобила в повечето случаи се намира под масовия му център, то действието на инерционната сила води до надлъжно наклоняване на каросерията на автомобила. Надлъжният наклон е прието да се нарича диферент – съгласно терминологията на теорията на кораба [1] или тангаж – съгласно терминологията в динамика на полета [2]. Тъй като инерционната сила е насочена обратно на ускорението, то при спиране ускорението е отрицателно и следователно инерционната сила е насочена по посока на движението. Следователно при спиране се донатоварват колелата на предната ос на автомобила, а тези от задната се разтоварват, като при екстремно спиране може дори да загубят контакт с пътната повърхност. При изследване на това явление обикновено се използва равнинен модел на автомобила в надлъжната равнина [3, 4]. Такъв модел е използван и от автора на настоящата публикация в някои негови предишни изследвания на надлъжния наклон и деформациите в окачването на предната и задната ос на транспортните средства [5, 6]. Примерен модел на товарен автомобил в надлъжната равнина е показан на фиг. 1.



Фиг. 1. Равнинен модел на товарен автомобил [6].

Означения използвани на фиг. 1, необходими за моделирането посредством модела на пружинно обърнато махало са дадени в публикацията по-долу в таблица 1.

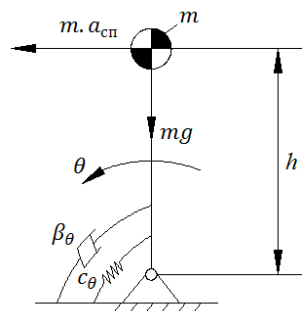
За изследване на напречния наклон на каросерията (кренът) на автомобилите при движение в завой, се предлага моделът на пружинно обърнато махало в различни литературни източници [7, 8]. На автора не са му известни работи по изследване на диферента на автомобил чрез такъв модел.

В тази връзка целта на настоящата работа е да се представи динамичен модел на пружинно обърнато махало, отчитащ масовите, еластичните и демпфиращите параметри на ъгловото преместване на товарен автомобил при спиране. Да се изведе

диференциалното уравнение на движение на махалото и да се проведе числено симулационно изследване на ъгъла на диферента на автомобила при спиране. Получените резултати от численото изследване ще бъдат сравнени с резултати от реален пътен експеримент, проведен от изследователски екип, под ръководството на автора.

2. Механо-математичен модел

Механо-математичният модел на товарен автомобил като пружинно обърнато махало се състои от динамичен модел и диференциално уравнение на движение. Динамичният модел е представен на фиг. 2.



Фиг. 2. Динамичен модел на товарен автомобил, като пружинно обърнато махало в надлъжна равнина.

Представеният модел е с една степен на свобода, следователно движението ще се описва с едно уравнение [8]:

$$(1) \quad J_y \ddot{\theta} = m a_{cn} h \cos \theta + m g h \sin \theta - c_{\theta} \dot{\theta} - \beta_{\theta} \ddot{\theta}$$

Където J_y е осов инерционен момент, спрямо оста на ротация на махалото. В случая това е оста, пресичаща еластичния център на окачването. За определянето на J_y се използва теоремата на Хюйгенс-Щайнер: „Инерционният момент на произволно тяло спрямо произволна ос е равен на сумата от инерционния момент на тялото спрямо ос, успоредна на разглежданата и минаваща през масовия му център и произведението от масата на тялото и квадрата на разстоянието между тези две успоредни оси“ [9]. Следователно:

$$(2) \quad J_y = J_{oy} + m h^2$$

където J_{oy} е инерционният момент спрямо напречна ос, минаваща през масовия център на автомобила;

m - масата на автомобила;

h - разстоянието от еластичния център до масовия център.

Известно е, че за малки ъгли може да се приеме:

$$(3) \quad \sin \theta \approx \theta; \quad \cos \theta \approx 1$$

Тогава за уравнение (1) може да се запише:

$$(4) \quad J_y \ddot{\theta} = m a_{cn} h + m g h \theta - c_{\theta} \dot{\theta} - \beta_{\theta} \dot{\theta}$$

Ъгловата еластичност на окачването е:

$$(5) \quad c_{\theta} = c_1 a^2 + c_2 b^2$$

където c_1 е еластичността на окачването на предната ос на автомобила; c_2 - еластичността на окачването на задната ос.

Аналогично ъгловото съпротивление на окачването е:

$$(6) \quad \beta_{\theta} = \beta_1 a^2 + \beta_2 b^2$$

където β_1 е съпротивлението на амортизаторите от предното окачване; β_2 - съпротивлението на амортизаторите от задното окачване на автомобила.

За численото решаване на диференциалното уравнение в средата на MATLAB е необходимо то да се приведе чрез подходящи субституции, към диференциално уравнение от първи ред. Тази операция се нарича канонизиране на диференциалното уравнение [10]. За целта се правят следните субституции:

$$(7) \quad x(1) = \theta; \quad dx(1) = \dot{\theta}; \quad dx(2) = \ddot{\theta};$$

Каноничната форма на диференциалното уравнение е:

$$(8) \quad dx(2) = \frac{1}{J_y} (m a_{cn} h + m g h x(1) - c_{\theta} x(1) - \beta_{\theta} x(2))$$

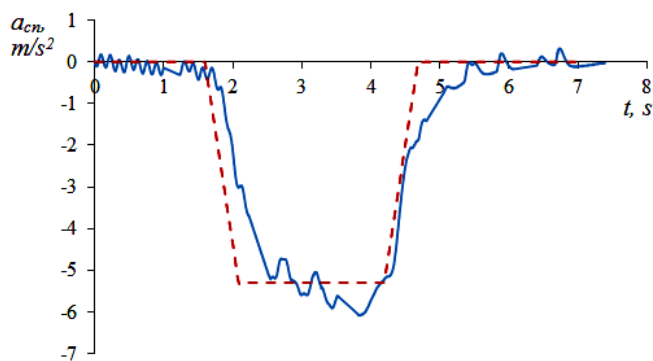
3. Числени изследвания. Валидиране на модела

Числените изследвания са извършени посредством MATLAB. Числените стойности на параметрите са дадени в табл. 1.

Таблица 1: Параметри на динамичния модел

Parameter	Symbol	Value	Dimension
Маса на автомобила	m	5000	kg
Инерционен момент	$J_{\theta y}$	20808	kg.m ²
Еластичност – предна ос	c_1	166600	N/m
Еластичност – задна ос	c_2	230625	N/m
Съпротивление – предна ос	β_1	9520	Ns/m
Съпротивление – задна ос	β_2	12300	Ns/m
Разстояние от е.ц до м.ц.	h	1,0	m
Разстояние от м.ц. до предната ос	a	1,53	m
Разстояние от м.ц. до задната ос	b	2,72	m

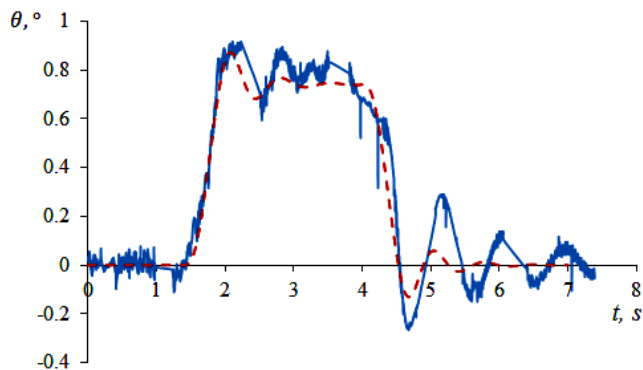
Числените изследвания са проведени при отрицателно спирачно ускорение (спирачно закъснение), изменящо се по трапецовиден закон.



Фиг. 3. Спирачно ускорение при числени симулации (---) и пътни експерименти (—).

За да бъде валидиран моделът, продължителността на спирането, максималната стойност на ускорението и времената на нарастването и намаляването му са подобни на тези, получени по време на пътния експеримент с товарен автомобил със същите параметри (фиг. 3).

Диферента при спиране в реалния експеримент се определя посредством изчисляване на резултатите, получени за деформациите на предното и задното окачване от сензори за преместване. Резултатите от числената симулация и пътния експеримент са показани на фиг. 4.



Фиг. 3. Ъгъл на диферента при числени симулации (---) и пътни експерименти (—).

Вижда се, че има добра съпоставимост на резултатите през целия период на спирачния процес. При пътните експерименти освен основните трептения се забелязват и допълнителни хармоници, вероятно поради пътните неравности, които не се отчитат в дадения модел, както и от допълнителни смущения. Такива смущения могат да бъдат пулсираща спирачна сила следствие на лошо техническо състояние на спирачните механизми или нееднородна пътна настилка по отношение на коефициента на сцепление. Пулсации предизвикани от работата на антиблокиращата спирачна система, пулсации на вятъра и др.

4. Заключение

Представеният модел може да се използва за изследване на диферента при спиране на автомобила. Получените резултати от числената симулация имат добра съпоставимост с тези от експеримента, проведен в реални пътни условия. Като недостатък на модела може да се отбележи невъзможността му да се използва за изследване на деформациите в предното и задното окачване по отделно, тъй като обикновено те имат различни еластичности. При изследване на ъгъла на крена този проблем не съществува поради това, че еластичните и демпфиращите елементи от двете страни на автомобила при изправно окачване имат еднакви характеристики. Също така не може да се използва и за изследване на комбинирано смущение от спиране и пътни неравности. Ако се интересуваме само от диферента, предизвикан от инерционната сила при спиране или потегляне моделът на пружинното обърнато махало е за предпочитане поради неговата простота.

Литература

- [1] Войткунский, Я. Справочник по теории корабля. Том 2. Статика судов. Качка судов. Ленинград, Судостроение, 1985.
- [2] Тодоров, М. Динамика на полета I. Технически университет – София, 2015.
- [3] Карапетков, С., М. Михайлова, С. Пехливанов, И. Монева. Моделиране на автомобил при спиране с отчитане на колебанията му спрямо масовия център. Известия на съюза на учените – Сливен. том 11, кн. 2, с. 70-71, 2006.
- [4] Енаев, А. Колебания автомобиля при торможении и применение их исследования в проектных расчетах, технологии испытаний, доводке конструкции. Автореферат, Братск, 2002.

[5] Павлов, Н. Числено изследване на движението на мотоциклет при спиране с отчитане на деформацията в окачването. Транспорт, екология - устойчиво развитие: научно-техническа конференция с международно участие ЕКО: сборник доклади. - Варна: Техн. унив., с. 214-223, 2017.

[6] Pavlov, N. Possibilities for Control of Semi-active Shock Absorbers in order to Reduce Cases of Suspension Jounces when Braking. INTERNATIONAL Scientific Journal Trans Motauto World. - Sofia: Scientific Technical Union of Mechanical Engineering Industry 4.0, Iss. 1, pp. 19-20, 2018.

[7] Sakai, H. Prediction of yaw natural frequency taking roll motion into account. The Dynamics of Vehicles on Roads and Tracks (IAVSD 2017), vol. 1, pp. 335-340, 2018.

[8] Goodarzi A., A. Khajepour. Vehicle Suspension System Technology and Design. Morgan & Claypool Publ, USA, 2017.

[9] Илиев, Л. и др. Механика: Лабораторен практикум. Университетско издателство „Св. Климент Охридски“, София, 2009.

[10] Тончев, Й. Matlab 6, 7: част II. Преобразувания, изчисления, визуализация. Техника, София, 2006.

COMPLEX SPATIAL MODELLING POSSIBILITIES OF THE SOCIO-ECONOMIC CHANGES OF HUNGARY - POTENTIAL APPROACHES AND METHODS

PhD Lennert J.

Institute for Regional Studies, CERS HAS (MTA KRTK Regionális Kutatások Intézete), Hungary

E-mail: lennert.jozsef@krtk.mta.hu

Abstract: *The paper overviews the possible methodological and practical approaches which can be used to create a custom-made toolset for the complex spatial modelling and forecasting of the socio-economic processes of Hungary for the 21st century. The author already participated in projects concerning land cover change and demographic modelling and gathered valuable experience in creating isolated models. In his three-year post-doctoral research programme, the author plans to take a more holistic approach with combining the elements of demography, economy and land use to create an integrated model with feedbacks between the consisting parts. The proposed methodology relies heavily on a scenario-based approach, creating a range of different forecasts from the business-as-usual ones to the highly improbable ones to explore the outer edges of future possibilities. Both local and global future assumptions will be considered during the formulation of the scenarios. An additional goal is to make the prepared modelling tool publicly available.*

KEYWORDS: AGENT-BASED MODELLING, SPATIAL MODELLING, FORECAST, SCENARIO, HUNGARY, DEMOGRAPHY, ECONOMY, LAND COVER

1. Introduction

In the light of the looming challenges of the 21st century, the significance of socio-economical modelling and forecasting cannot be overstated. Besides global level, this need has been recognised in Hungary as well, and different sectoral predictions were prepared (Polónyi and Timár 2002, Király 2015, Koós 2015, Tagai 2015, Vaszócsik 2017, Obádovics 2018).

I've also participated in some projects concerning land cover change modelling and demographic modelling (Long-term Socio-Economic Forecasting for Hungary – 2015, the further development of NATÉR (KEHOP) – the possible effects of climate change on internal migration processes (2017-2018), and the further development of NATÉR (KEHOP) – the methodological improvement of land cover modelling (2017-2018) (Farkas and Lennert 2015, 2016). During these research contributions, I've gathered valuable experience in creating isolated models, and I've also become familiar with the limitations of this approach. In my ongoing postdoctoral research project (PD 128372, from 2018.09.01 to 2021.08.31), focusing on the complex spatial modelling possibilities of the socio-economic changes of Hungary for the 21st century, I'd like to move toward a more holistic direction. The modelling toolset will constitute of three main components (demography, economy, and land use) forming an integrated model and thus provide more possibilities for feedback than the isolated ones. With heavily relying on a scenario-based approach, I want to extend the timescale of the forecast farther than before – and to explore the challenges and limits for Hungary in the 21st century. In order to achieve this, I am going to elaborate a custom modelling tool fit for my purposes. The existing professional software can be used to model the selected phenomenon (e.g. land use change) more or less universally – and I do not wish to compete with that feature. However, general applicability has a price – it cannot handle the regional/national irregularities of the investigated phenomena well, and it is hard (or impossible) to alter an existing toolset. However, if I build the modelling framework taking these regional characteristics into consideration from the beginning, I get much less generally applicable software as a result, but more fit to my purpose: the modelling of the selected socio-economic processes of Hungary. The aimed interconnectivity of the components also calls for a custom design.

Naturally, with these intentions, a marketable product cannot be prepared (the socioeconomic modelling needs of a single middle-sized country cannot be considered even as a niche market).

However, I still intend to make the prepared modelling tool publicly available in the suitable platforms (a dedicated website, and/or GitHub), in the hopes that the stakeholders and professionals can freely experience with the different scenarios and their territorial consequences, and to generate further research contributions.

The research project is still in the stage of conceptualisation (with results coming in 2021), so in the next pages, I'd like to summarise my previous experiences in modelling and forecasting, and present the insights that contributed to the conceptualisation of the recent research.

2. Results and discussion

In the project of the Long-term Socio-Economic Forecasting for Hungary, I created a land cover modelling and forecast with my colleague, Jenő Farkas. For the procedure, the Land Change Modeler for ArcGIS software was used and the Corine Land Cover maps were served as basemaps (1990 and 2006). According to the meta-analysis of Schroyen et al. and his colleagues, all simulation models of land use are based on at least one of the following four principles: continuation of historical development, suitability of land, result of neighbourhood interaction and result of actor interaction.

Also, they distinguished the following methodological concepts, which can be used for land use change modelling: cellular automata, statistical analysis, Markov chains, artificial neural networks, economic based models, agent based models (Schroyen et al. 2011).

For predicting the amount of future land cover transformation, the LCM relied on Markov chains and on the historical trends (represented by the two basemaps). From the possible options for locating the sites of the transformations, we selected the Multilayer Perceptron neural network method, which uses a neural network, the basemaps explanatory variables (with the same spatial dimension) to determine the probability of change between each modelled land cover category. The available variables mostly emphasised the expression of the principles of suitability of land and neighbourhood interaction. Additionally, it was also possible to declare spatial constraints and incentives for certain transitions, which helps the expression of actor interaction.

With the software, two types of predictions were produced, a hard prediction showing the land cover for 2030 and a soft prediction depicting the probability of change, which can be considered valid for a longer period. The results indicate an increase in the share of forests, artificial surfaces and vineyards and fruit cultivations, and a

decrease in the area of arable land, grasslands and complex agricultural surfaces. According to the soft prediction, the probable transition hotspots include the rural-urban fringe of Budapest, and also the diverse but environmentally vulnerable landscapes of Kiskunság and Nyírség.

During the execution of the research, we could identify several limitations. In its default setting, the volume of future change is exclusively based on the rate of change between the two uploaded basemaps, and possible changes in the driving forces are dismissed. Also, without a feedback between the determination of the transition locations and the total amount of change, suitability does not necessarily translate to viability. In case of a shortage from a certain land use category, transitions will occur even in the highly improbable locations (except if absolute constraints had been declared). Generally, the Land Change Modeller software produces the best results in case long-term changes with few well identifiable location factors (like tropical deforestation and urban sprawl).

The planned recent research will take these limitations into consideration. The integrated execution with the demographic and economic component will make it possible to follow a more supply and demand based approach instead on relying on historical trends. And while the previous research experiences proved that Corine Land Cover is a good starting point for creating a basemap for modelling, but because of the presence of some unique features in Hungary (e.g. scattered farms and garden zones), some of the categories need revision (e.g. complex cultivation patterns).

In case of the preceding demographic modelling research (the further development of NATÉR – the possible effects of climate change on internal migration processes), I used a self-developed modelling toolset coded in Python. The model integrates a lot of different theoretical-practical approaches of demographic modelling (e.g. cohort-component method, Lee's push-pull theory, neoclassical theories, value-expectancy model, life course approach of migration, Enyedi's urbanisation stages), but from methodological viewpoint, it can be considered as an agent-based model, which handles each inhabitant as an individual decision making agent. During each five-year modelling cycle, every person undergoes a multiple-step decision tree with seven possible outcomes (passes away, gives birth, participates in university student migration, participates in labour migration, participates in suburbanisation, participates in amenity migration, remains in his/her former location without taking part in any of the former ones). The attractiveness of the areas are defined independently for each migration type, and probability for the actors to take part in either of the natural or migration movement depends on the age, sex and the socioeconomic status of the inhabitant. The model gives stochastic results.

During the research 33 scenarios were prepared, which differ from each other in three aspects: their fertility and mortality assumptions, the integrated climatic scenarios, and in their socioeconomic assumptions about transport, commuting, and the prevalence of atypical work.

The results indicate that (further) natural decrease of the population of Hungary seems unavoidable, but the scenarios vary between moderate to drastic loss. Due to the current age structure, an increase in life expectancy can play a more significant role in reducing population loss than an increase in fertility. As a consequence, higher projected population number means a less favourable old-age dependency ratio.

The results also point out, that the predicted changes will further increase the spatial differences of Hungary. While the agglomeration ring of Budapest will continue to grow, the larger

part of Hungary faces significant to severe depopulation. The rate of decrease is average in the urban, below average in the commutable rural, and higher than average in the remote rural areas.

The different introduced climate scenarios only had minimal effect on the predicted migration patterns, while the differences in the socio-economic path caused more substantial alterations. The results also indicate that the effect of climate change on the internal migration patterns will depend more on the share of population who is able and willing to take the climatic parameters into account when changing residence than on the exact changes in the climatic parameters.

The created custom modelling tool provides a good starting point for the current modelling procedure. However, it still has three important shortcomings of which I plan to address this time.

The first concerns the agents: while they were created together with individual age and gender data from the population census of the starting year, municipality level data was used to describe their socioeconomic status – which affects their migration preferences and probabilities. This decision was a necessity stemming from the lack suitable data. While it provided acceptable results, it hindered the expression of the life-course approach. Also, the presence of different social strata within the same settlement is an important driving factor for some migration types (e.g. involuntary economic migration). These migration types could not be included without individually declared economic situation before, but the current project will remedy this. As the 0th step of the project, a more detailed database connected to agents will be assembled with the inclusion of socioeconomic data (the lack of suitable database still persists, so in some cases, I will have to rely on estimations based on cross-sectioned data).

The partial overlook of the meso-theories of migration shows a somewhat opposite shortcoming. While the previous one focused on the improvement of individual agents, the meso-theories emphasise the role of social connections in the migration decisions, especially family ties. In order to comply with this approach, the agents has to be formulated together with their respective relationship network (with the help of census data), and in some cases, migration decisions have to be taken in family level.

The importance of feedback was already emphasized between components. Within the demographic component, the changes of housing prices will also provide an important (usually negative) feedback, making migration from the depressed areas less probable. In the previous research, this phenomenon was taken into account using the settlement development level, but this time I aim for a more dynamic implementation. This will also help the inclusion of involuntary economic migration subtype to the model. To achieve this, a dynamic housing database has to be assembled, and joined to the agents. Also, the economic component has to take the housing market into consideration.

Without previous research experience, the elaboration of the economic component is the least certain. Economic actors (currently existing and potential fictional) determining the changes of the labour market (and thus the migration flows) surely have to be declared. The most important economic actor of Hungary is naturally the central government. It will be elaborated as a half-autonomous agent, with predefined preferences and condition-action rules which depend on the selected scenario.

3. Conclusion

The project aims to create projections till the end of the century. While it is a daunting aspiration, the previous research experiments pointed out its necessity. If we want the introduced socio-economic

paradigm shifts to play out in their full scale and create significant divergences from the business-as-usual scenarios, we have to consider a longer modelling period than a few decades. Naturally, it increases the uncertainty of the projections. However, as the previous research results have pointed out, uncertainty appears in a spatially uneven pattern. While some settlements and regions face with a rather undetermined future, the fate of other areas seems to be more certain due to their path-dependency. Even without providing unquestionable predictions, the mapping of uncertainty is a valuable result in itself.

Acknowledgement

Project no. PD 128372 has been implemented with the support provided from the National Research, Development and Innovation Fund of Hungary, financed under the PD_18 funding scheme.

References

- Farkas J. Zs, Lennert J. A földhasználat-változás modellezése és előrejelzése Magyarországon. In: Czirfusz M, Hoyk E, Suvák A. (eds) Klímaváltozás - társadalom - gazdaság: Hosszú távú területi folyamatok és trendek Magyarországon, Publikon Kiadó, Pécs, 2015, p 193–221.
- Farkas J. Zs, Lennert J. A földhasználat-változás modellezése és előrejelzése Magyarországon, Geográfus hírlevél, 41, 2016, p 13–15.
- Király G. A magyarországi népesség „status quo” morbiditási és mortalitási jövőképe 2016 és 2051 között. In: Czirfusz M, Hoyk E, Suvák A. (eds) Klímaváltozás - társadalom - gazdaság: Hosszú távú területi folyamatok és trendek Magyarországon, Publikon Kiadó, Pécs, 2015 p 167–178.
- Koós B. A deprivációs folyamatok területi képe Magyarországon. In: Czirfusz M, Hoyk E, Suvák A. (eds) Klímaváltozás - társadalom - gazdaság: Hosszú távú területi folyamatok és trendek Magyarországon. Publikon Kiadó, Pécs, 2015, p 179–191.
- Obádovics Cs. A népesség szerkezete és jövője. In: Monostori J, Őri P, Spéder Zs. (eds) Demográfiai portré 2018, KSH Népességtudományi Intézet, Budapest, 2018, p 271–294.
- Polónyi I, Timár J. A népesség, a gazdasági aktivitás és a nemzetközi migráció távlatai Magyarországon, 1950–2050, Közgazdasági szemle, 11, 2002, p. 960–971.
- van Schrojenstein Lantman J, Verburg P H, Bregt A, Geertman S. Core principles and concepts in land-use modelling: a literature review. In: Koomen E, Borsboom-van Beurden, J, (eds) Land-Use Modelling in Planning Practice, Springer Netherlands, 2011, p. 35–57.
- Tagai G. Járási népesség-előreszámítás 2051-ig. In: Czirfusz M, Hoyk E, Suvák A. (eds) Klímaváltozás - társadalom - gazdaság: Hosszú távú területi folyamatok és trendek Magyarországon, Publikon Kiadó, Pécs, 2015. p. 141–166.
- Vaszócsik V. Meddig nőhetnek a városok? – A területhasználat-változási folyamatok modellezése, Területi Statisztika 2, 2015, p. 205–223.

COMPARISON OF APPROACHES TO ESTIMATION OF TRANSITION MATRIX FOR THE TERRORIST THREAT MARKOV MODEL

Ing. Martin Tejkal, Doc. RNDr. Jaroslav Michálek, CSc.
University of Defence, Brno, Czech Republic
martin.tejkal@unob.cz, jaroslav.michalek@unob.cz

Abstract: Markovian models are often used in modelling a time development of random phenomena. When modelling real world scenarios it is reasonable to assume that the respective phenomena may not be time homogeneous. Based on the sociological and security research, it can be assumed that there is a link between a destabilisation of a society of a given geographical region and the acts of terrorism. This link is utilised in construction of a model for description of the intensity of a terrorist threat based on given determinants/indicators of societal stability. The model is based on the theory of discrete non-homogeneous Markov chains. The theory of generalised linear models (GLMs) is used in the estimation of the probabilities of the categorised level of the terrorist threat. In the contribution the use of different estimates of the categorised level of terrorist threat probabilities is studied. The estimates are determined by GLMs with different input parameters. The influence of the resulting estimate on the transition matrix of the non-homogeneous Markov chain is assessed. Additionally, a real world example utilising the data from Global Terrorism Database of University of Maryland and Organisation for Economical Cooperation and Development is presented.

Keywords: MARKOV CHAIN, NON-HOMOGENEOUS, POISSON GLM, MULTINOMIAL LOGIT GLM, RISK, TERRORISM

1 Introduction

In recent years the mathematical models are finding more and more applications in the field of social sciences. Due to current geopolitical events the ability to asses and predict the risk of terrorism has become topical.

The model discussed in this paper aims to describe the evolution of the categorised level of terrorist threat in time. From mathematical viewpoint this might be seen as a time development of random events. In other fields, mathematical models based on the theory of Markov chains are often used to model random events time development, when some categorisation is involved. The markovian framework provides a good compromise between computational feasibility of the model and taking into account the real world dependencies. The finite or countable state space of the chain is particularly suitable to model the considered categories. Such models are often used in economics and finance. Quite common is the application by banking institutions to model the credit risk, i. e. the risk of default (see [1], [2], [3]).

The problematic of modelling of time development of categorised level of terrorist threat bears some resemblance to the credit risk models. For that reason the framework of Markov chains is utilised in this paper as well.

For some particular events a connection to a set of explanatory variables might be found. For example, it is reasonable to believe that the ability of the companies to fulfil their obligations to the credit institution is influenced by the economical development. Thus, it is reasonable to assume a dependence of the level of the terrorist threat on some economical variables, like gross domestic product etc. Some authors have considered models utilising this additional information provided by the covariates (see [4], [5], [6]).

When it comes to modelling the threat of terrorism, a sociological research suggests, that the level of terrorist threat within a given society (country, etc.) may be connected with an overall stability of the studied society (see [7]). There are numerous indicators of stability of a given society. The authors of this paper have already proposed a model utilising this link connecting the terrorist threat with selected indicators (see [8]). The link was used in the estimation of the transition matrix of the Markov chain. In this paper the research is taken a step forward by providing a different and possibly more suitable way of estimation of the transition matrix as well as a comparison of the two approaches.

2 Prerequisites and means for solving the problem

2.1 Markov Chains

The model presented in this paper is based as well as the model presented in [8] on the theory of Markov chains. The formal description does not differ from the one presented in [8]. For the

reader's convenience, the authors will recall the key points in this subsection.

A sequence $M = \{M_n : n = 0, 1, 2, \dots\}$ of random variables, that attains values from a finite set S is called a Markov chain with finite state space S if

$$(1) \quad \begin{aligned} \mathbb{P}[M_{n+1} = l | M_n = k, M_{n-1} = k_{n-1}, \dots, M_1 = k_1, \\ M_0 = k_0] \\ = \mathbb{P}[M_{n+1} = l | M_n = k]. \end{aligned}$$

for each $l, k, k_{n-1}, \dots, k_0 \in S$. The equation (1) is the well known Markov property.

In the model presented in this paper, the elements $k \in S$ of state space will correspond to the L categories of the level of the terrorist threat.

Out of convenience, henceforth it will not be differentiated between a state of the Markov chain and a category of a level of the terrorist threat. Thus, when we say that the process moved into category k in time step from n to $n + 1$, we actually mean that the process jumped into k -th state in time step from n to $n + 1$ and so on. Furthermore, from the interpretational point of view, the states (categories) denoted by larger values of integers are considered to be the ones of higher level of terrorist threat (i. e. state (category) $k = 3$ denotes higher level of threat than state (category) $k = 1$).

The transition probabilities are defined as follows

$$(2) \quad \pi_{kl}(n, n + 1) = \mathbb{P}[M_{n+1} = l | M_n = k],$$

for each $k, l \in S$. The transition probability is the probability the process jumps into state l (the level of the categorised threat changes to l) in the time step from n to $n + 1$, provided it was in a state k in time n .

Transition probabilities of a homogeneous Markov chain do not depend on time step n , i. e. $\pi_{kl}(n, n + 1) = \pi_{kl}$. In this model, however, it is assumed, that the numbers of terrorist attacks are dependent in each time instant n on a set of m indicator variables $\mathbf{X} = (X_1, \dots, X_m)$. These variables vary in time step n , and hence the notation $\mathbf{X} = \mathbf{X}_n = (X_{n1}, \dots, X_{nm})$ is used. Thus, the resulting Markov chain is non-homogeneous. The transition probabilities of the Markov chain with L states are collected in the transition matrix $\mathbf{P}_{n,n+1}(\mathbf{X}_n)$ of a type $L \times L$ given by

$$(3) \mathbf{P}_{n,n+1}(\mathbf{X}_n) = \begin{pmatrix} \pi_{11}(n, n + 1; \mathbf{X}_n) & \dots & \pi_{1L}(n, n + 1; \mathbf{X}_n) \\ \dots & \dots & \dots \\ \pi_{L1}(n, n + 1; \mathbf{X}_n) & \dots & \pi_{LL}(n, n + 1; \mathbf{X}_n) \end{pmatrix}.$$

The notation $\mathbf{P}_{n,n+1}(\mathbf{X}_n)$ is used to further stress out the fact, that the transition matrix depends on the indicator variables.

The properties of the transition matrix are discussed more in detail in [8] or any classical book on Markov theory (e. g. [9]).

Given the state vector $\mathbf{p}_0 = (p_{1,0}, \dots, p_{L,0})$ in time 0, where $p_{k,0} = \mathbb{P}[M_0 = k]$ for $k \in S$, it is possible to obtain a state vector $\mathbf{p}_n = (p_{1,n}, \dots, p_{L,n})$, where $p_{k,n} = \mathbb{P}[M_n = k]$ for some $n \in \mathbb{N}_0$ in the following way

$$(4) \quad \mathbf{p}_n = \mathbf{p}_0 \mathbf{P}_{0,1}(\mathbf{X}_1) \mathbf{P}_{1,2}(\mathbf{X}_2) \dots \mathbf{P}_{n-2,n-1}(\mathbf{X}_{n-1}) \mathbf{P}_{n-1,n}(\mathbf{X}_n).$$

The transition matrices $\mathbf{P}_{0,1}(\mathbf{X}_1), \dots, \mathbf{P}_{n-1,n}(\mathbf{X}_n)$ need to be estimated.

2.2 Multinomial Response Generalised Linear Models

Generalised linear model (GLM) is used to connect the categorised level of terrorist threat with the indicator variables. The GLM is used to obtain an estimate of the transition matrix row by row. In the paper [8], a Poisson GLM is utilised. Here the use of the multinomial response generalised linear models is proposed (see [10], [11]).

Let M_n for $n \in \mathbb{N}$ be a nominal scale response variable with L categories. The multicategorical model used in this paper to obtain the estimates of the transition probabilities in k -th category is the multinomial logit model (see [10], [11]), that is given by

$$(5) \quad \log \left(\frac{\mathbb{P}[M_n=l]}{\mathbb{P}[M_n=L]} \right) = \beta_{l0,k} + \mathbf{x}_{n,\bullet,k} \boldsymbol{\beta}_{l,k},$$

where $\beta_{l0,k}$ and $\boldsymbol{\beta}_{l,k} = (\beta_{l1,k}, \dots, \beta_{l(L-1),k})$ are unknown parameters, which correspond to state $k = 1, \dots, L-1$. For the baseline category $l = L$, set $\beta_{L0,k} = 0$ and $\boldsymbol{\beta}_{L,k} = \mathbf{0}$. The $\mathbf{x}_{n,\bullet}$ are the values of the indicator variables \mathbf{X}_n at the time step n .

3 Solution of the examined problem

The multinomial logit GLM was used repeatedly in sequence for each state $k \in \{1, \dots, L\}$ the process visited. In this way a vector $\hat{\pi}_{k,\bullet} = (\hat{\pi}_{k1}, \dots, \hat{\pi}_{kL})$ of probability estimates was obtained, such that the respective probability estimates correspond to the k -th row of the desired transition matrix estimate.

3.1 Transition Matrix Estimation Using Multinomial Logit GLM

The multinomial logit GLM described in the Subsection 2.2 is computed for each category $k \in \{1, \dots, L\}$. Hence, for each category $k \in \{1, \dots, L\}$, the estimate $\hat{\boldsymbol{\beta}}_k = (\hat{\beta}_{10,k}, \hat{\boldsymbol{\beta}}_{1,k}^T, \dots, \hat{\beta}_{L0,k}, \hat{\boldsymbol{\beta}}_{L,k}^T)$ of the vector of parameters of the GLM is obtained.

For the multinomial logit GLM for each category $k \in \{1, \dots, L\}$ the estimates of $L-1$ fitted values $\hat{\pi}_{k1}(\mathbf{x}_{n,\bullet}), \dots, \hat{\pi}_{k(L-1)}(\mathbf{x}_{n,\bullet})$, given the vector of covariates $\mathbf{x}_{n,\bullet} = (x_{n1}, \dots, x_{nm})$ for some $n \in \mathbb{N}$ are obtained through a formula

$$(6) \quad \hat{\pi}_{kl}(\mathbf{x}_{n,\bullet}) = \frac{\exp(\hat{\beta}_{l0,k} + \mathbf{x}_{n,\bullet,k} \hat{\boldsymbol{\beta}}_{l,k})}{1 + \sum_{r=1}^{L-1} \exp(\hat{\beta}_{r0,k} + \mathbf{x}_{n,\bullet,k} \hat{\boldsymbol{\beta}}_{r,k})},$$

where $l = 1, \dots, L-1$. For $l = L$ we then have

$$(7) \quad \hat{\pi}_{kL}(\mathbf{x}_{n,\bullet}) = 1 - \sum_{r=1}^{L-1} \hat{\pi}_{kr}.$$

The estimate of the probability of transition from state k to state l in time instant from n to $n+1$ for $n \in \{1, \dots, s\}$ is then defined as $\hat{\pi}_{kl}(n, n+1; \mathbf{X}_n) = \hat{\pi}_{kl}(\mathbf{x}_{(n+1),\bullet})$.

3.2 Transition Matrix Estimation Using Poisson GLM

The detailed description of the method of obtaining the estimates of the transition matrix using the Poisson GLM is provided in the paper

[8]. The key points will be recalled here.

The response in this case are the numbers of terrorist attacks. These are split into categories together with the corresponding observations of explanatory variables, based on whether the value of the observation of the response lies between a selected bounds of the respected category.

The Poisson GLM is given by

$$(8) \quad \log(\lambda_n) = \beta_0 + \mathbf{x}_n \cdot \boldsymbol{\beta},$$

where the expectation λ_n (the average number of terrorists attacks in the given category) depends on unknown parameters $\beta_0, \boldsymbol{\beta}$ and on the values \mathbf{x}_n of the indicator indicator variables \mathbf{X}_n at the time step n .

This model is again applied for each category $k = 1, \dots, L$ in order to obtain vector of estimates $\hat{\alpha}_k = (\hat{\beta}_{0,k}, \hat{\boldsymbol{\beta}}_k^T)$ of the parameters $\alpha_k = (\beta_{0,k}, \boldsymbol{\beta}_k^T)$.

The estimate $\hat{\lambda}_{nk}$ of the parameter λ_{nk} for each category $k = 1, \dots, L$ is then obtained via the formula

$$(9) \quad \hat{\lambda}_{nk} = e^{\hat{\beta}_{0,k} + \mathbf{x}_n \cdot \hat{\boldsymbol{\beta}}_k}.$$

Then a random variable Z_k with Poisson distribution with the value $\hat{\lambda}_{nk}$ as an expectation parameter is defined for each category $k = 1, \dots, L$. The transition transition from a category k into a category l , $k, l \in S$ is then defined as the probability of the random variable Z_k attaining values between the lower and upper bound of the category.

4 Results and discussion

4.1 Real Data Example

The approaches proposed in this paper and in paper [8] were applied to estimate a transition matrix using a real dataset. The dataset consisted of quarterly numbers of terrorist attacks in France between the years 1981 and 2018 obtained from the Global Terrorism Database of University of Maryland, and two indicator explanatory variables, the gross domestic product and the unemployment rate obtained from the Organisation for Economical Development. Detailed description of the dataset is provided in [8]. For the readers convenience the authors will present figures of the dataset in question.

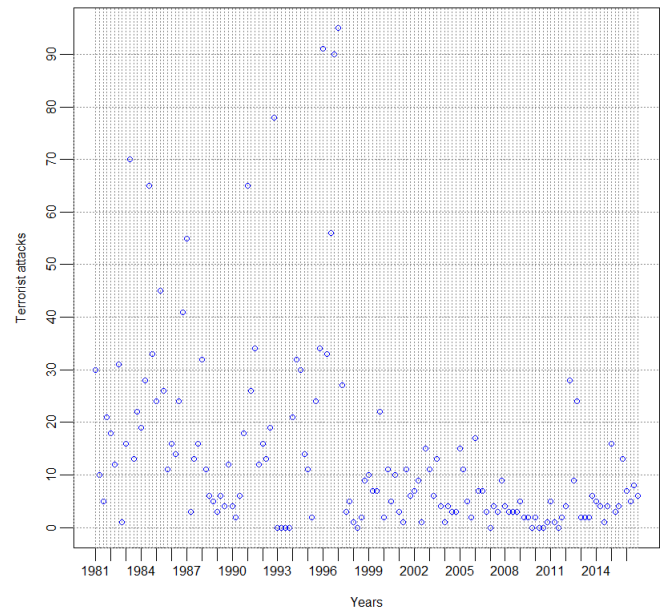


Fig. 1: Time series of quarterly observations of the numbers of terrorist attacks

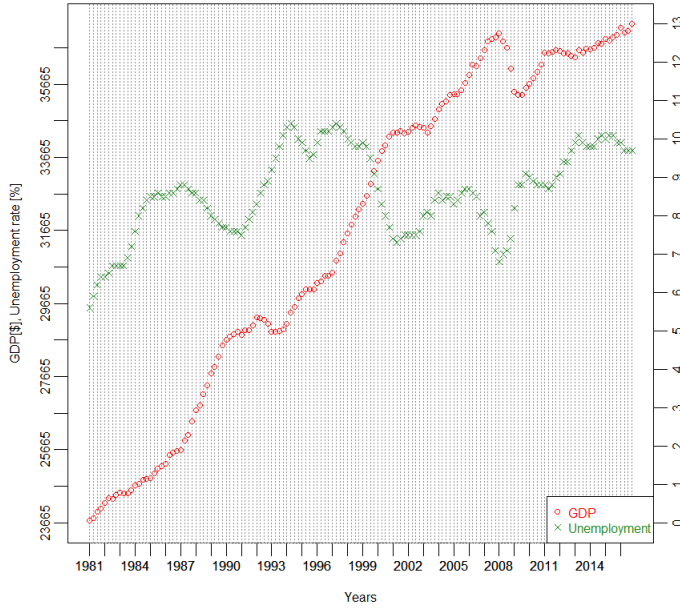


Fig. 2: Time series of quarterly observations of GDP in constant prices of US Dollar (left horizontal axis) and of unemployment rate in percentage of labour force (right horizontal axis)

From the Fig 2 one can see that, the gross domestic product grew in average over time, while the unemployment rate stagnated or increased slightly. This development might be considered still more or less optimistic scenario. It should be noted, that there might be a relation between the two explanatory variables (see Fig 2). The last available observation of the explanatory variables in the year 2016 was taken as the “future” observation.

Categorisation of the data was carried out in the following manner. Into the first category were placed observations greater or equal to 0 and lesser than 6, into the second observations greater or equal to 6 and lesser than 13. Into the third category were placed observations greater or equal to 13. The transition matrix estimate obtained using the Poisson GLM described in [8] is the following:

$$(10) \quad \hat{\mathbf{P}}_{0,1;Po}(\mathbf{X}) = \begin{pmatrix} 0.990 & 0.010 & 0.000 \\ 0.335 & 0.636 & 0.029 \\ 0.000 & 0.007 & 0.993 \end{pmatrix}.$$

The matrix obtained using the multinomial logit GLM described in this paper is

$$(11) \quad \hat{\mathbf{P}}_{0,1;Mult}(\mathbf{X}) = \begin{pmatrix} 0.812 & 0.095 & 0.093 \\ 0.361 & 0.530 & 0.109 \\ 0.457 & 0.453 & 0.090 \end{pmatrix}.$$

The transition matrix estimated using the multinomial logit GLM reflects the optimistic development of responses, favouring the category with the least terrorist threat. This is not entirely true about the transition matrix obtained via the Poisson GLM described in [8]. In the estimate (10) the probabilities $\hat{\pi}_{kk}(0,1)$ on the diagonal attain large values, while the further we move in the row away from the diagonal entry, the lower the estimated probability (compare $\hat{\pi}_{12}(0,1)$ and $\hat{\pi}_{13}(0,1)$ in (10). Additionally, the probability $\hat{\pi}_{33}(0,1)$ of staying in the third category of the highest terrorist threat seems to be unreasonably high, given the optimistic scenario. In [8] it was

suggested, that this might rather be due to the properties of the Poisson GLM itself, and does not reflect the reality very well.

Note, that the size of real input dataset is rather small, in addition the observations of terrorist attacks contain a large number of very small observations and a small set of relatively high values (see Fig. 1). This, altogether with the particular choice of the bounds of the categories further worsens the effect that the Poisson model has on the estimates of the entries on the diagonal.

The problem of unreasonably high values on the diagonal seems not to be present in the estimate (11). The probability is more evenly distributed among the respective categories, while at the same time reflecting the positive development scenario. For the first and the third row we have $\hat{\pi}_{kl} > \hat{\pi}_{kr}$ for k fixed and $l < r$. The exception is the second row, where the probability jumping from the second state back to the second state is the highest.

The link between the response observations and the covariates was weak when modelled via the Poisson GLM. Only for the category $k = 3$ the tests for each parameter rejected the null hypothesis $H_0: \hat{\beta}_{j,k} = 0$ for $j = 0,1,2$. In the case of multinomial logit GLM the link between the response and the covariates was weak as well. Additionally, no matter the choice of the baseline category, a separation occurred for some logits (see [10]), rendering the tests of significance for the respective parameters impossible.

5 Conclusion

The paper [8] presents a non-homogeneous Markov chain model for prediction of a categorised level of terrorist threat. The non-homogeneity of the Markov chain stems from the assumption that the categorised level of the terrorist threat and thus the transition matrix of the chain is dependent on a set of indicators of destabilisation of a society, that vary in time. A Poisson GLM is used to connect the categorised level of terrorist threat with the indicator covariates and estimate the transition matrix row by row. This paper proposes a modified approach using multinomial logit GLM instead of the Poisson one. A comparison of the two approaches is carried out on a real dataset.

The estimates of the transition probabilities on the diagonal of the transition matrix obtained via the Poisson GLM tend to attain large values. This is assumed to be rather a property of the Poisson GLM, that does not reflect the real situation. Especially unexpected is the large value of the probability of staying in the category of the largest terrorist threat in case of an optimistic development scenario. This effect is not present, when the multinomial logit GLM is applied instead. The transition probabilities tend to be more evenly distributed among the respective categories, while reflecting the character of the scenario (for the rather optimistic scenario given by the real data the transition to the categories of lower threat tend to be higher than the ones to the categories of higher threat).

It should be noted, however, that in general the connection between the responses and the covariates regardless of the used GLMs was weak. Additionally, the size of the currently available real data sample proved to be insufficient. The proposed multinomial logit model did not share the diagonal values-increasing effect of the Poisson model, and thus seems to be more suitable, in further research however, it would be necessary to choose different set of indicators to further study the model. Additionally, a way to generate the datasets for a thorough simulations study would need to be developed. In order to increase the sample size a panel data approach may be considered. That is however, beyond the scope of this paper.

References

- [1] Jarrow, R.A., Lando, D., Turnbull, S.M., A Markov model for the term structure of credit risk spreads. The Review of Financial Studies 10 (2), 1997, 481–523.

[2] Altman, E. I. and Kao, D. The implications of corporate bond rating drift. *Financial Analysts Journal*, 48(3), 1992, 64–75.

[3] Carty, L. V. and Fons, J. S. Measuring Changes in Corporate Credit Quality, *Journal of Fixed Income*, 4(1), 1994, 27–41.

[4] Nickell, P., Perraudin, W. and Varotto, S. Stability of rating transitions. *Journal of Banking & Finance*, 24(1–2), 2000, 203–227.

[5] Koopman, S. J. and Lucas, A. Business and default cycles for credit risk. *Journal of Applied Econometrics*, 20(2), 2005, 311–323.

[6] Gavalas, D. and Syriopoulos, T. Bank Credit Risk Management and Rating Migration Analysis on the Business Cycle. *International Journal of Financial Studies*, 2(1), 2014, 122–143.

[7] Svoboda, I. and Hrbata, M. Extremism and Terrorism as

Destabilizing Factors of Society, *Vojenské rozhledy*, 23 (55), N. 1, p., 2014, 33 - 41 (In Czech)

[8] Tejkal, M. and Michálek, J. Markov Model for Description of Intensity of Terrorist Threat. Abstracts of XXXII International Conference Problems of Decision Making under Uncertainties (PDMU-2018) , July 3-9, 2018, Prague, Czech Republic.

[9] Resnick, S. I., *Adventures in stochastic processes*, Boston: Birkhäuser, 1992.

[10] Agresti, A., *Categorical data analysis*, 3rd ed. Hoboken, NJ: Wiley, 2013.

[11] Fahrmeir, L. and Tutz G. *Multivariate statistical modelling based on generalized linear models*. New York, Springer-Verlag, 1994.

USE OF ICT RESOURCES IN THE HUMANITARIAN SUBJECTS IN BULGARIAN SCHOOLS

M.Sc. Boneva Y.¹, Assist. Prof. PhD. Paunova-Hubenova E.¹, Assist. Prof. Terzieva V.¹, PhD. Dimitrov S.¹

Institute of Information and Communication Technologies – Bulgarian Academy of Science, Bulgaria¹

boneva.yordanka@gmail.com, eli_np@hsi.iccs.bas.bg, valia@isdip.bas.bg, sdimitrov85@abv.bg

Abstract: Modern technologies are a part of contemporary life, and they have been part of the educational process in Bulgarian schools for a while. There is no doubt that computer competencies are a necessity, and therefore they are taught as a separate subject at school. However, the use of Information and Communication Technologies (ICT) resources is not limited only to this dedicated subject, these tools also support teaching all other matters. They are used during each stage of school education as well. For exploring the implementations of ICT in an educational environment, an online-based survey aimed at students and teachers was conducted. This paper presents a comparison of the frequency of use of ICT in Bulgarian schools according to different educational stages and subjects with the focus on the humanitarian ones. The current research shows the statistical analysis of the data and a comparison between the answers of students and teachers.

Keywords: SCHOOL EDUCATION, SURVEY-BASED STUDY, ICT RESOURCES, HUMANITARIAN SUBJECTS

1. Introduction

With the introduction of ICT in everyday life, the ordinary teaching methods are increasingly difficult to attract students' attention. The traditional teaching process in the classrooms becomes a real challenge for teachers. It is necessary to integrate new and upgrade the existing technology resources so that they be a tool for the transfer of knowledge, not an obstacle.

There are many studies on the use of information technologies in the Humanitarian classes in different countries. For language learning often used resources are educational videos and games. The authors of [1] present an approach for Computer Assisted Language Learning by means of designing serious games. Another study [2] presents methods for automatic changes of playback speed which can affect the score for learning in the second language. The potentials of using digital educational games for English foreign language learning are discussed in [3]. Many aspects of the usage of technology in foreign language teaching, as well as different types of case studies, are presented in [4].

The authors of [5] discuss the value of hypervideos in presenting historical artifacts in museums. In the framework of the APOGEE project [6], an innovative platform intended for teachers to create adaptive educational maze games in the domain of History is designed. An online educational game in Geography is presented in [7].

According to the number of researches, students can learn from multisensory information quickly and thoroughly. So, for example, something new can be learned much easier with technology-supported lessons than in the traditional way. That is why the authors have started a project that aims to explore the real use of ICTs in teaching practice in Bulgarian schools.

The focus of this research is the implementation of ICT resources in teaching humanitarian subjects in Bulgarian school education. The next section presents the used methodology and the respondents' profile. The results are described in the third section, and their statistic distribution – in the fourth one. The last section presents the analysis of the results and conclusions.

2. Methodology

In this paper, the authors explore the quantitate parameters of the use of ICT resources and tools in the Humanitarian educational context through a quantitative research methodology. The study is based on a comprehensive anonymous online survey that covers many issues, which offer an opportunity for detailed processing and classifying the findings [8]. The survey comprises four different questionnaires – three for students of different age groups and one for teachers [9]. Thanks to the personal efforts of researchers and the cooperation of regional educational authorities the survey was spread via e-mails to the majority of schools in Bulgaria, so the

results can be considered as a national representative. Moreover, the study population covers more than 1600 teachers and 8000 students from all stages of school education in Bulgaria.

In particular, the focus here is on the frequency of usage of different types of innovative pedagogical instruments in each of school stages – primary, low secondary and high secondary. Thus the results from the four different surveys are examined and compared. For in-depth interpretation and analysis of the survey data, the authors use quantitative statistical methods and calculations of indicators such as frequencies, means, and standard deviations. Generally, the developed detailed questionnaires give an opportunity to differentiate the variety of manners for the integration of ICT into the teaching practice. The inclusion of field for comments in each question was of particular importance to gain respondents' opinions and valuable extra information when analyzing data.

For a more accurate analysis of the data, the teachers' profile should be taken into account. In many Bulgarian schools, especially the small ones, the teachers have classes in more than one stage and/ or subject. In such cases, their answers are considered in more than one group, and thus, the sum of the different types of teachers can be higher than the total number of respondents.

The total number of respondent teachers is 1652 from the three school stages, distributed as follows: 605 – primary, 622 – low and 776 – high secondary school teachers. From those the Humanitarian teachers that participate in the survey are 414. Table 1 presents the number of Humanitarian teachers classified according to the school stage and learning subject. The primary teachers are not divided by this criteria, because usually, one person teaches most of the subjects for the earliest stage.

Table 1: Teachers' distribution according to school stage and learning subject.

Teachers in subject \ Stage	Bulgarian language & Literature	Foreign language & Literature	Geography & History	Philosophy
High secondary	74	109	57	12
Low secondary	72	71	71	–
Primary	605 (all subjects)			

3. Results and discussion

The researchers collected and analyzed the data for the use of different types of e-resources by teachers according to the school stage and subject. Here, besides for primary school teachers, the results are also presented for teachers in the humanitarian subjects such as Bulgarian language and literature (BLL), foreign languages

and literature (FLL), History and Geography, and Philosophy. The survey explores what types of ICT resources employ teachers in their practices. The respondents have to choose between five predefined options – very often (almost every day), often (at least ones a week), rarely (at least ones a month), never and do not give answers. The obtained results for different groups of respondents are presented on figures 1 to 7. The missing parts to 100% in the graphics are for those who did not answer (in some cases about half).

Teachers in primary schools

Primary school teachers (see Fig. 1) usually use often and very often presentations (69%), e-textbooks (54%), educational videos (58%) and additional e-resources (37%). All these resources attract pupils' attention easily, so it is worth the efforts to integrate them into lessons. As a whole, there are not many available specialized software and process simulations intended for primary school students, so they are seldom used.

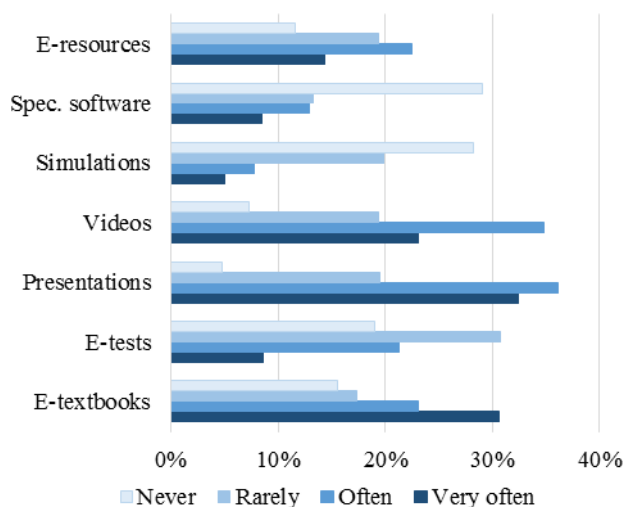


Fig. 1 Primary school teachers – frequency of usage of ICT resources

Teachers in low and high secondary schools

Fig. 2 shows the findings concerning teachers in Bulgarian language and literature in secondary schools. Again, for more than half of respondents, presentations are the most used technology resources, followed by videos and e-textbooks. It should be mentioned that their use prevails in low secondary schools compared to high secondary. E-tests follow the same tendency, but only for about a quarter of teachers.

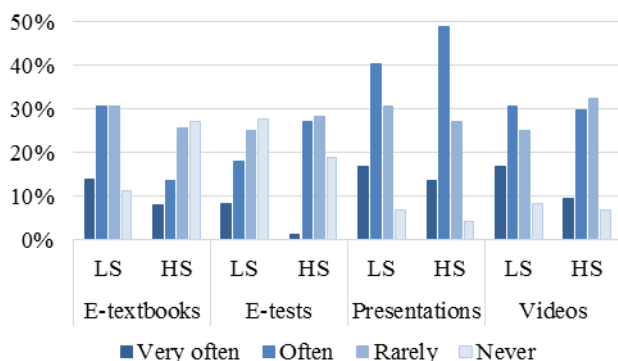


Fig. 2 Low (LS) and High secondary (HS) school teachers in BLL

Almost the same is the situation when considering answers of teachers in foreign languages and literature (Fig. 3). The main difference here is in an almost twice number of teachers who use

very often e-textbooks – 20% and 23% for low and high secondary schools respectively.

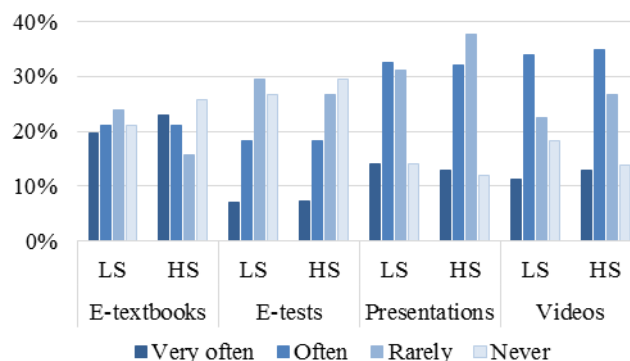


Fig. 3 Low (LS) and High Secondary (HS) school teachers in FLL

The graphics on Fig. 4 compare the frequency of use of simulations, specialized software and other types of e-resources. The latter, usually different kind of web-based resources, are most often employed in language teaching. They are usually used every day by 11% of teachers in a foreign language in high secondary schools and teachers in the Bulgarian language in low secondary schools. Between 16% - 27% of teachers enrich lessons with such resources at least once a week. Simulations and specialized software usually are rarely used (mainly because of their lack), while virtual laboratories are not appropriate in general.

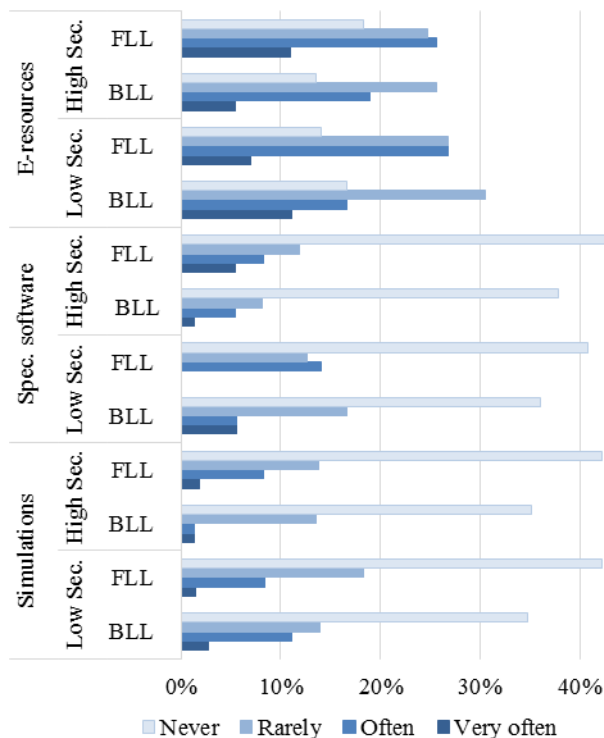


Fig. 4 Low and High Secondary school teachers in BLL and FLL subjects

Generally, in the survey, teachers in foreign languages pointed as usual sources of e-resources the digital versions of textbooks and workbooks that are provided by the publishers as well as various popular electronic dictionaries.

Following the general tendency, as it is shown in Fig. 5, the majority of teachers in Geography and History usually use often and very often presentations, educational videos and e-textbooks. The first two types of resources have more frequent usage in high secondary schools, while the e-textbooks seems to be more popular

in low secondary schools. Only a few of the teachers (11% - 12%) check the students' knowledge by e-tests very often.

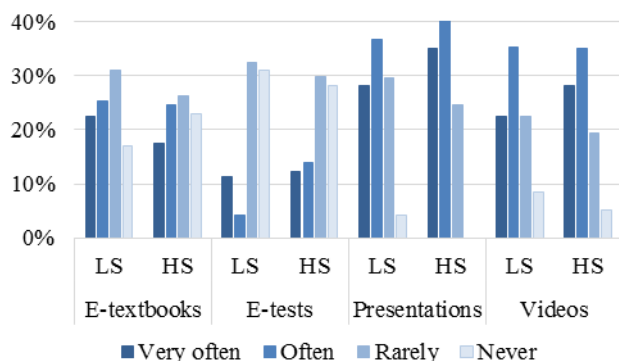


Fig. 5 Low and High Secondary school teachers in Geography and History subjects

The graphics on Fig. 6 shows the comparison by usage frequency of more elaborated technology tools – process simulations, specialized software and different types of e-resources. The latter is quite often integrated into lessons by a third of teachers. Besides no much availability of appropriate learning resources of the other two types, these require additional preparation and efforts to be utilized. Thus they are only used by few teachers in both low and high secondary schools.

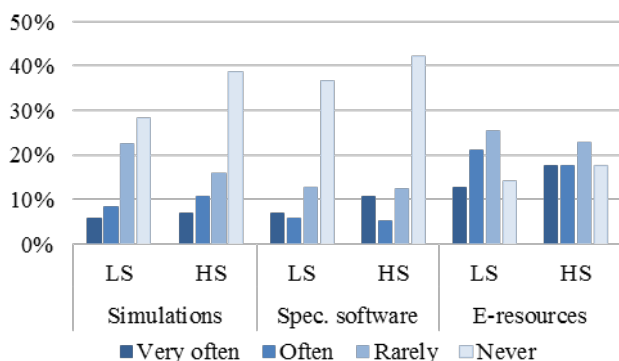


Fig. 6 Low and High Secondary school teachers in Geography and History subjects)

The majority of teachers in Philosophy subjects, like their colleagues, most frequently integrate presentations and educational videos in the lessons. As Fig. 7 shows, about 42% of them use these resources almost every day or every week. Digital textbooks and e-tests present in the pedagogical practice of a third and a quarter of teachers, respectively. The other types of e-resources are not very usual for these learning subjects.

To sum up, in the survey, teachers usually pointed as traditional sources of e-resources the popular platforms with e-lessons such as Uchase, Khan Academy, Kahoot, etc.

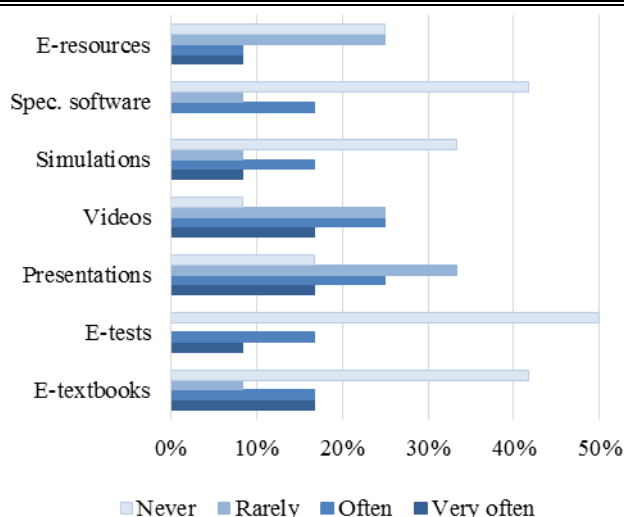


Fig. 7 Low and High Secondary school teachers in Philosophy subjects.

4. Statistical Analysis of Results

Based on the survey findings for usage frequency of different ICT resources, the research explores their appropriateness in teaching humanitarian subjects. The common statistics such as mean values, standard deviation, standard error, difference between M and p-value for the three groups of school subjects are presented in tables 2, 3 and 4. For that purpose the answers are transformed in a 4-level Likert scale from 1 – very rarely/ never use to 4 – very often use (almost every day). These tables compare values corresponding to the answers of low secondary and high secondary teachers.

For Bulgarian language and literature (Table 2) the differences in the means M are statistically significant with a p-value of less than 0.05 only for e-textbooks. The reason is trivial – there are digital versions of textbooks only for students in low secondary classes. The answers for the other ICT-based educational resources are very similar for both low and high secondary school teachers, so the p-value is greater than 0.05.

Table 3 shows that for foreign language teachers the differences are negligible and not statistically significant where the p-value is much greater than 0.05. The same goes for the teachers in geography and history (Table 4). Therefore, according to the teachers, the diverse types of e-resources are equally appropriate for both low and high secondary school students.

The educational games are not very popular resources in all humanitarian subjects in both low and high secondary schools as it is seen from the statistics. Their average use is rare – about once a month, where the most frequently they are used in foreign language teaching and in low secondary Bulgarian language classes.

Table 2: Average frequency of usage of ICT resources in Bulgarian language and literature

Value	Low secondary teachers (N=72)			High secondary teachers (N=74)			Difference	
Answers	M	SD	SE	M	SD	SE	ΔM	P
E-textbooks	2.333333	0.236519	0.118260	1.770270	0.082960	0.041480	0.563063	0.004861
E-tests	1.861111	0.078874	0.039437	1.864865	0.273878	0.136939	-0.003754	0.749578
Presentations	2.611111	0.383771	0.191885	2.648649	0.493012	0.246506	-0.037538	0.649976
Videos	2.361111	0.233544	0.116772	2.202703	0.238194	0.119097	0.158408	0.340418
Simulations	1.444444	0.223952	0.111976	1.202703	0.323249	0.161625	0.241742	0.075947
Virtual Labs	1.125000	0.358212	0.179106	1.054054	0.396467	0.198233	0.070946	0.248554
Spec. software	1.444444	0.216951	0.108476	1.229730	0.317118	0.158559	0.214715	0.175170
E-resources	1.972222	0.074471	0.037235	1.797297	0.136939	0.068469	0.174925	0.827064
Games	1.819444	0.118412	0.059206	1.540541	0.214839	0.107420	0.278904	0.245018

Table 3: Average frequency of usage of ICT resources in foreign languages and literature

Value	Low secondary teachers (N=71)			High secondary teachers (N=109)			Difference	
Answers	M	SD	SE	M	SD	SE	ΔM	P
E-textbooks	2.253521	0.163950	0.081975	2.266055	0.233934	0.116967	-0.012534	0.894641
E-tests	1.873239	0.119251	0.059626	1.853211	0.101645	0.050822	0.020028	0.882591
Presentations	2.380282	0.264694	0.132347	2.403670	0.293184	0.146592	-0.023388	0.878495
Videos	2.239437	0.267304	0.133652	2.348624	0.286321	0.143160	-0.109187	0.572808
Simulations	1.394366	0.240547	0.120274	1.357798	0.255649	0.127825	0.036568	0.901278
Virtual Labs	1.211268	0.330086	0.165043	1.110092	0.367910	0.183955	0.101176	0.199650
Spec. software	1.408451	0.266119	0.133059	1.449541	0.220040	0.110020	-0.041091	0.764238
E-resources	2.014085	0.194747	0.097374	2.091743	0.148216	0.074108	-0.077659	0.954470
Games	1.760563	0.189847	0.094924	1.844037	0.147985	0.073992	-0.083473	0.426237

Table 4: Average frequency of usage of ICT resources in Geography and History subjects

Value	Low secondary teachers (N=71)			High secondary teachers (N=109)			Difference	
Answers	M	SD	SE	M	SD	SE	ΔM	P
E-textbooks	2.492958	0.257861	0.128930	2.280702	0.167128	0.083564	0.212256	0.428567
E-tests	1.746479	0.192345	0.096173	1.947368	0.068370	0.034185	-0.200890	0.380963
Presentations	2.873239	0.437527	0.218764	3.105263	0.562550	0.281275	-0.232024	0.161917
Videos	2.605634	0.343901	0.171950	2.736842	0.411066	0.205533	-0.131208	0.324485
Simulations	1.563380	0.164968	0.082484	1.578947	0.157651	0.078825	-0.015567	0.763189
Virtual Labs	1.225352	0.312151	0.156076	1.228070	0.322182	0.161091	-0.002718	0.812073
Spec. software	1.450704	0.225435	0.112717	1.543860	0.214509	0.107255	-0.093155	0.840805
E-resources	2.056338	0.079985	0.039992	2.105263	0.108148	0.054074	-0.048925	0.916665
Games	1.661972	0.221243	0.110622	1.789474	0.089886	0.044943	-0.127502	0.496901

5. Conclusion

The survey findings show that nowadays when ICTs enter classrooms, they penetrate into the teaching-learning process in many forms not always even have been imagined. The technology can offer quality educational resources, but it is not only because of the technology itself. Teachers need focused knowledge on technology-enhanced pedagogy to make the best of these innovative tools in the classrooms. The educational authorities need to take into account research like the presented here that demonstrates the degree of incorporating a variety of technologies into learning environments so that to create an effective policies to further development in this direction.

The results show that Bulgarian teachers in the humanitarian subjects use mainly educational videos and presentations, followed by e-textbooks and additional e-resources. The least used resources are the virtual labs, specialized software and process simulations which are not appropriate or the teachers do not know about such resources for their subjects.

Acknowledgements

This work has been partly supported by project M02/1 of the Bulgarian National Science fund: "Learning data analytics for ICT resource integration in Bulgarian schools", contract DM 02/1, 13.12.2016.

References

[1] Meyer B. and B. Sørensen, Designing Serious Games for Computer Assisted Language Learning – a Framework for Development and Analysis. Design and Use of Serious Games. Springer, Vol. 37, 2009, pp. 69 - 82

[2] Kishi Y., J. Kim, T. Tachino, Design of Automatic Playback Speed Control System for Learning in Second Language Using Online Videos, in: Proceedings of 10th International Conference EDULEARN18, Palma de Mallorca, Spain, 2nd-4th July 2018, pp. 7023-7029.

[3] Wang X., J. Dostál, Using Digital Educational Games For English Foreign Language Learning, in: Proceedings of 10th International Conference EDULEARN18, Palma de Mallorca, Spain, 2nd-4th July 2018, pp. 144-148.

[4] Motteram, G. (Ed.) Innovations in Learning Technologies for English Language Teaching, London: British Council, 2013.

[5] Rußwurm L., Knowledge Transfer In Museums: Hypervideos As a Way to Present and Communicate Historical Artifacts, in: Proceedings of 10th International Conference EDULEARN18, Palma de Mallorca, Spain, 2nd-4th July 2018, pp. 2767-2776.

[6] Bontchev, B. and Vassileva, D., "Affect-based adaptation of an applied video game for educational purposes", Interactive Technology and Smart Education, Vol. 14, No. 1, 2017, pp. 31-49.

[7] Paunova E., K. Stoilova. Comparative Characteristics of Serious Games. Mathematics and Education in Mathematics, in: Proceedings of the 43rd Spring Conference of the Union of Bulgarian Mathematicians, April 2–6 2014, Bulgaria, pp. 186-191

[8] Terzieva, V., E. Paunova-Hubenova, S. Dimitrov, and Y. Boneva, ICT in STEM Education in Bulgaria, in: Proceedings of 21th International Conference ICL'18, 25-28 September 2018, Kos Island, Greece, pp. 1232 – 1243.

[9] Survey of Teachers in Google Forms (in Bulgarian): <https://docs.google.com/forms/d/1VCOj3r2OPbu7goQTM7QMXf7f20iP5c6Qiv6WF3IBBY>

AUTOMATIC GENERATION OF A NATIONAL DIABETES REGISTER FROM OUTPATIENT RECORDS

Dimitar Tcharaktchiev¹, Zhivko Angelov², Svetla Boytcheva³, Galia Angelova³

Medical University Sofia and University Specialized Hospital for Active Treatment of Endocrinology "Acad. I. Penchev" Sofia, Bulgaria¹
ADISS Lab Ltd., Sofia, Bulgaria²

Institute of Information and Communication Technologies, Bulgarian Academy of Sciences, Sofia, Bulgaria³

galia@lml.bas.bg

Abstract: *In this paper, we present the construction of Bulgarian National Diabetes Register, using pseudonymized outpatient records submitted to the Bulgarian National Health Insurance Fund. The automatic generation facilitates the construction because it does not burden any medical experts with additional paper work. The Register is a healthcare system integrating natural language processing in large scale and analytics functionalities that provide new views to the information concerning Diabetes Mellitus and diabetic patients in Bulgaria. This successful approach encouraged the authors to initiate a research programme in eHealth focused on collection and analysis of patient data, with the intention to assess the feasibility of secondary patient record use in evaluation of healthcare quality.*

Keywords: HEALTHCARE SYSTEMS, BIG DATA IN HEALTHCARE, AUTOMATIC ANALYSIS OF CLINICAL TEXTS

1. Introduction

Diabetes prevention and cure in Europe have improved after 2008 because less people die [1]. Patient awareness is raising, self-monitoring becomes easier, and the variety of medications is growing. However, still a very high number of diabetic patients are undiagnosed and half of the European countries cannot provide reasonably good data concerning procedure indicators. It is claimed that “as long as important data is not systematically reported and transformed into methodology, diabetes care will remain inefficient and, at worst, haphazard” [1].

The Euro Diabetes Index 2014 lists seven European countries that support diabetic registers: Sweden, Denmark, Norway, Netherlands, UK, Switzerland, and Hungary [1]. Data input to the registers is ensured either by self-registration or by burdening medical professionals with additional documentation tasks. Practically, self-registration means that a significant percent of the patients remains unregistered. Even in Sweden, which is the country with the best diabetes care delivery in Europe according to the Euro Diabetes Index 2014, the register was constructed by self-registration. During its development phase 2001-2005 the self-registration rate of patients gradually increased and reached 75%, which in 2010 still remains stable and is one of the highest in the country [2]. No information is available about the procedures for register update and maintenance.

Availability of relevant data is of primary importance in diabetes prevention and treatment (“no data, no cure” according to the Euro Diabetes Index 2014). However, high-quality data is hard to collect. Information about diabetic patients is often not collected nationally but rather in hospitals or at regional level, with limited comparability of collected indicators. Moreover, data often come from isolated national projects or EU-funded initiatives with fixed duration. After the project ends, no strategic plans are built by the respective political or governing institutions and in this way projects that started and proved to be successful remain feasibility studies without practical effects.

All countries in Europe have national plans for discovery, treatment and prevention of Diabetes [3] but one hardly finds information about the execution of these plans, monitoring of various plan measures and evaluation of their success. Positive health outcomes are difficult to assess too, moreover this needs to be done dynamically at national level in order to improve the treatment plans. From a technological point of view, the general impression is that healthcare authorities lack understanding about the potential of modern Information and Communication Technologies (ICT) as an enabling tool that facilitates data collection, monitoring of indicators, knowledge discovery, early alerting and automatic sending of feedbacks, evaluation of updated indicators and automatic preparation of aggregated recaps.

Surprisingly, no attempts for automatic extraction of Registers from available Electronic Health Records (EHR) repositories are mentioned in the Euro Diabetes Index 2014. A recent book about secondary use of EHR [4] lists three types of users that utilize information from patient records: clinicians searching data for their daily work; clinical researchers who need to extract patient groups or cohorts, or patients with specific diseases for their research; and finally the hospital management that needs to gather statistics and predict the future of the hospital activities. The book [4] states: “Generally when asking users what type of systems they want, they do not know”. The suggested approach is to develop a prototype and show it to the users who give feedback. Thus, it somehow becomes clear that, apart from archiving purposes, the application of nation-wide EHR repositories is still limited and their potential as content repositories is not fully understood and exploited by the community of medical professionals.

In this paper, we sketch our approach to generate automatically an anonymous Diabetic Register from outpatient records, submitted to the only health insurance fund in Bulgaria – the National Health Insurance Fund. The construction took place in 2015 and later the Register has been updated. We show how the Register is used today, together with the underlying repository of pseudonymized outpatient records. Finally, we present ideas for future work in secondary use of patient records, to be performed within the National Research Programme ‘eHealth’ funded by the Bulgarian Ministry of Education and Science in 2018-2021.

2. Generation of the Diabetes Register

The mandatory health insurance was introduced in Bulgaria in 1998. The National Health Insurance Fund (NHIF) was founded in 1999 with the mission to deal with the obligatory health insurance in the country. All General Practitioners and Specialists from Ambulatory Care produce reimbursement requests (Outpatient Records) whenever they contact patients and submit these requests to the NHIF. The Outpatient Records are semi-structured XML files with numerous fields containing structured and coded information about the patient and the examining medical expert, and sufficient clinical data to summarize the case. Many indicators in the Diabetic Register copy the structured data submitted to NHIF: (i) date and time of the visit; (ii) pseudonymized personal data, age, gender; (iii) pseudonymized visit-related information; (iv) diagnoses in ICD-10; (v) NHIF drug codes for medications that are reimbursed; (vi) a code if the patient needs special monitoring; (vii) a code concerning the need for hospitalization; (viii) several codes for planned consultations, lab tests and medical imaging.

The Outpatient Records contain also values of clinical tests and lab data, presented in the free text fields. Using software extractors for automatic text analysis of Bulgarian texts, which have been developed in our previous projects, we mine these values from four

free text fields: (i) *Anamnesis*: summarizes case history, previous treatments, often family history, risk factors; (ii) *Status*: summary of patient state, height, weight, body-mass index BMI, blood pressure etc.; (iii) *Clinical tests*: values of clinical examinations and lab data; (iv) *Prescribed treatment*: free text descriptions of drugs that are not reimbursed by NHIF. The focus was placed mostly on extraction of numeric values that are important for diabetes like values of blood sugar and measurement time, glycated hemoglobin, BMI, blood pressure etc. More details about the construction of the Register are given in [5, 6]. Knowledge discovery using original data mining techniques is presented in [7].

NHIF delivered pseudonymized outpatient records to the University Specialized Hospital for Active Treatment of Endocrinology (USHATE), Medical University Sofia, which was authorized by the Bulgarian Ministry of Health to host the information. The Register was constructed iteratively: at first using data for 2010-2014 and then updated twice with outpatient records for 2015 and 2016. The repository behind the Register currently contains more than 262 million pseudonymized outpatient records submitted to the NHIF in 2010-2016 for more than 7.3 million citizens (more than 5 million citizens yearly), including 483,836 diabetic patients. This repository contains also information about patients, who are not formally diagnosed with Diabetes Mellitus. This allows to study particular groups of citizens in pre-diabetes condition.

The internal Register interface in USHATE provides functionalities to authorized medical experts to track disease history of individual patients (Fig. 1). The public web interface¹ generates on the fly aggregated statistics about key factors related to the Diabetes Mellitus and provides monitoring and assessment at regional level (Fig. 2).

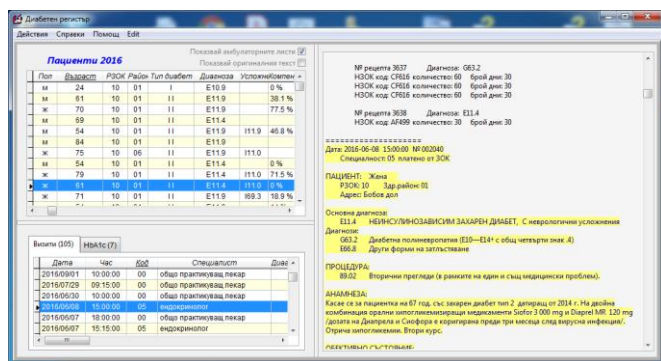


Fig. 1 Diabetes Register interface in USHATE – a general view

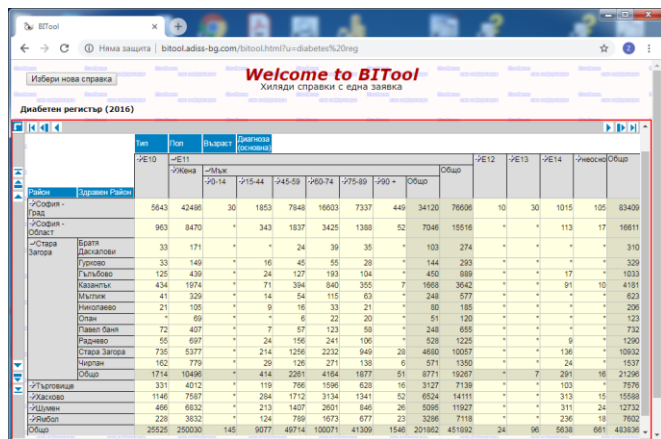


Fig. 2 Diabetes Register Web interface – public generalized and aggregated data enhanced with OLAP technology

3. Present Use of the Register

The main objectives of the National Diabetes Register are [5]:

- Assessing Diabetes Mellitus morbidity in Bulgaria;
- Providing views to patient care in long-term;
- Improving prevention by Diabetes risk stratification;
- Improving Diabetes patient care by comprehensive analysis of comorbidities, studies of Diabetes Mellitus complications and treatment side effect.

Here we show how the objectives listed above are met in various studies performed on patient groups.

Diabetes Mellitus morbidity assessment (Fig. 3) shows the trend of a steady gradual increase of prevalence of Diabetes Mellitus in the majority of Bulgarian demographic regions. The most significant increase (Fig. 3 – dark red) is observed in the regions with the poorest population and low quality of life. The average percentage 9.47% for Bulgaria looks relatively good in the European context. The distribution of patients per ICD-10 codes of diagnosis (Fig. 4) shows that in 2016 about 93.4% of the patients have Diabetes Mellitus Type 2 and approximately 5.28 % - Diabetes Mellitus Type 1.

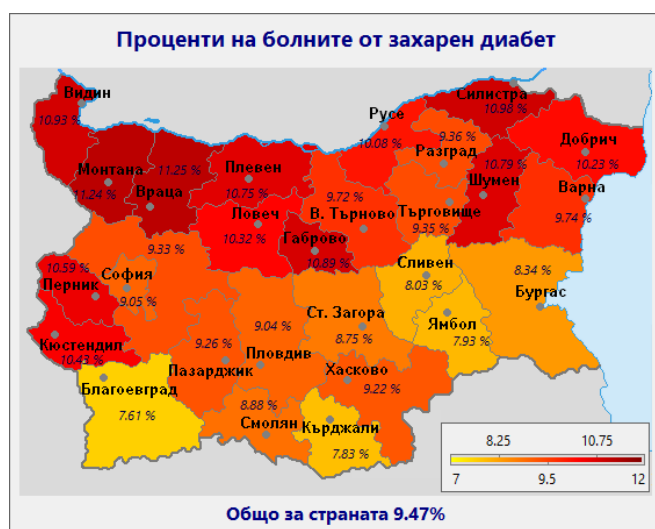


Fig. 3 Prevalence of Diabetes Mellitus type 2 in demographic regions of Bulgaria in 2016

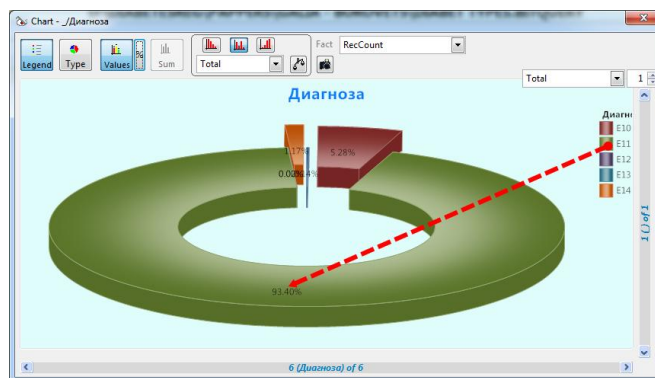


Fig. 4 Ratio of patients with different ICD-10 codes related to Diabetes Mellitus in 2016

Long-term studies of patient care have both economic and healthcare impact. They cover tasks like:

- Monitoring of treatment effect for new drugs and various combined therapies;
- Evaluation of Diabetes Mellitus glycemic control etc.

Treatment with new drugs like incretins achieves good effect on Diabetes glycemic control for most patients (Fig. 5). The statistical data show that the most popular combined treatment includes two types of Insulins and analogues for injection (Fig. 6). Three types of drug combinations are most popular for combined peroral therapy

¹ <https://usbale.org/bg/register-zaharen-diabet/>

(Fig. 7). The overall evaluation of the Diabetes Mellitus compensation per age groups is shown on Fig. 8.

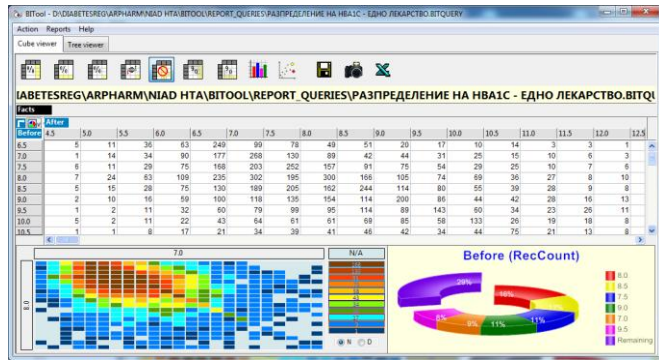


Fig. 5 Treatment effect monitoring for selected drugs – HbA1c levels before and after incretins treatment

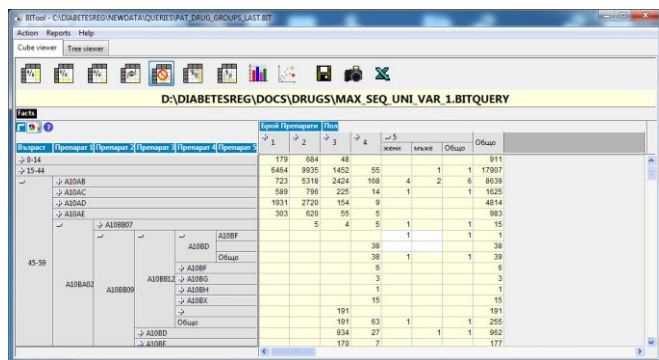


Fig. 6 Patients with combined therapy of Diabetes Mellitus grouped by number of drugs included in the therapy and ATC codes of drugs per age groups

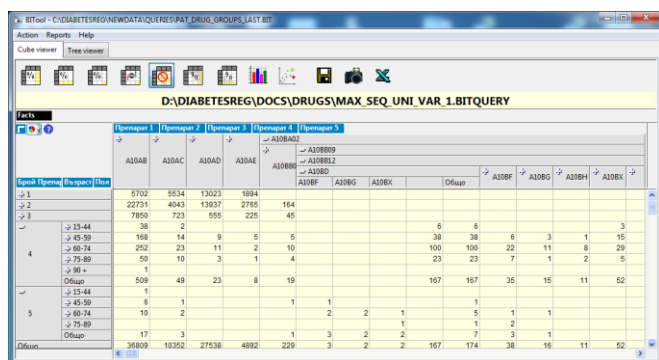


Fig. 7 Patients with combined therapy of Diabetes Mellitus grouped by different ATC drugs codes in the therapy, and number of drugs included in the therapy per age groups

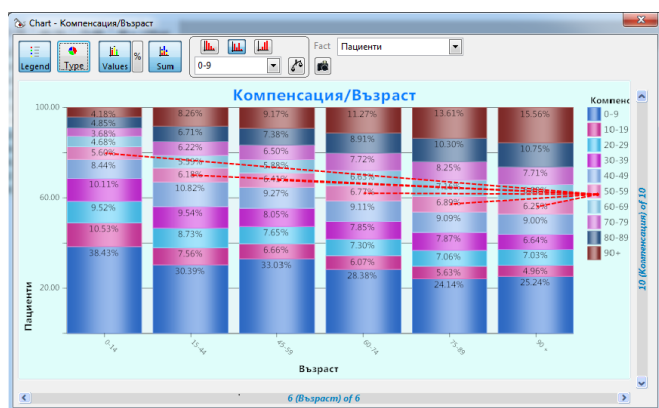


Fig. 8 Study of treatment quality – percentage of Diabetes Mellitus compensation per age groups

Prevention is focused on reducing the risk factors associated with chronic diseases. Thus prevention related applications include comprehensive studies of Diabetes Mellitus risk factors. Risk stratification for prediabetes patients was shown in [6, 7, 8], which discuss risk factors and comorbidities between several socially important diseases like Diabetes Mellitus, Mental Disorders, Cardiovascular diseases and the Chronic Obstructive Pulmonary Disease (CORD). Several artificial intelligence approaches were developed and applied in these studies – like natural language processing, data mining, and machine learning. In [6] we report about experiments with the dataset of patients who were in prediabetes condition in 2013-2014 and with Diabetes Mellitus onset in 2015. The data mining techniques identify some well-known risk factors but new interdependencies among the indicators were discovered as well. The latter will need further investigation from healthcare point of view.

One of the primary objectives of the Diabetes Registers is better treatment of diabetic patients [3]. In order to achieve this goal, research in several directions was performed:

- Comprehensive analysis of Diabetes Mellitus comorbidities [6, 7, 8],
- Study of Diabetes Mellitus complications and treatment side effect.

We investigated the side effect of Schizophrenia treatment with first and second generation antipsychotics for triggering some prediabetes conditions. There is a wide range of diseases that have comorbidities with Diabetes Mellitus. One of the most discussed relation is between Diabetes Mellitus and Cardiovascular Diseases. Fig. 9 shows the dependency between Hypertension and Diabetes Mellitus. Hypertension is considered not only as one of prediabetes conditions but also as an important complication related to patients with Diabetes Mellitus. Another interesting finding is the relation between Malignant neoplasm of breast and Diabetes Mellitus [6], or Gonarthrosis (arthrosis of knee) [7]. An analysis of comorbidities between Schizophrenia, Diabetes Mellitus and COPD is presented in [8]. Etiology examination of the comorbidity between disorders is very important for mortality prediction and other outcomes. Diabetes as a chronic disease is considered a primary factor for increase of mortality (Fig. 10). The onset of Diabetes Mellitus for males happens a little bit earlier than for females. Thus Diabetes complications for male patients are usually developed in a younger age, the mortality percentage is higher and male patients die earlier than females with the same age, especially male patients with less contacts to doctors.



Fig. 9 Number of patients with Hypertension and Diabetes in 2016

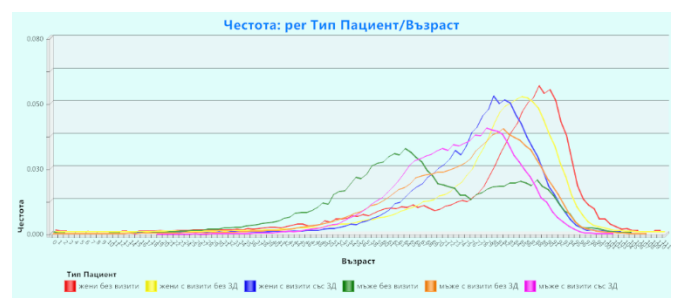


Fig. 10 Statistics about age of death – patients grouped by gender, with/without Diabetes, and frequency of visits to medical professionals. Diabetic male patients with less visits die earlier

4. Future Work: the eHealth Programme

The European Commission's eHealth Action Plan 2012-2020 [9] provides a roadmap to empower patients and healthcare workers, to link up devices and technologies, and to invest in research towards the personalized medicine of the future. The Action Plan admits the delay of introducing modern IT solutions in European healthcare and lists barriers that hamper the wider uptake of eHealth, among them:

- lack of awareness of, and confidence in eHealth solutions among patients, citizens and healthcare professionals;
- lack of interoperability between eHealth solutions;
- limited large-scale evidence of the cost-effectiveness of eHealth tools and services;
- lack of transparency regarding the utilisation of data collected by eHealth applications.

The Action Plan concludes that “the important issue concerning the lack of health data exchange can only be tackled by addressing in a coordinated way fragmented legal frameworks, lack of legal clarity and lack of interoperability”.

The Bulgarian National Research Programme eHealth² has been initiated by the Bulgarian Ministry of Education and Science with the aim to address most of the barriers listed above by development of specialized research prototypes and demonstrators. Briefly, collecting pseudonymized patient records from various sources we aim to show that the EHRs of Bulgarian patients can be generated almost automatically from the collections of electronic documents that are exchanged between the National Health Insurance Fund, General Practitioners, medical specialists in Primary Care, Hospitals, Clinical Labs that perform tests and send lab results via internet, and so on. Each of these documents is related to certain individual patient using his or her unique civil identifier called EGNumer. Therefore, it is relatively easy to build the patient record collection itself given that in Bulgaria many important patient-related documents are standardized because they are all submitted electronically to the National Health Insurance Fund for reimbursement. Further our aim is to demonstrate, using the big data base of anonymous patient records, how the quality of healthcare procedures and treatments can be assessed at national level together with its costs.

It is expected that the project will deliver a methodology and technological solutions for providing semantic operability among the heterogeneous data generated by the healthcare sector and will demonstrate how the patient-related data can be integrated in complex clinical systems. These large-scale evidences will increase the confidence in information technologies and big data processing by healthcare systems. Last but not least, the public demonstration how to achieve improvements of patient cure and quality of life, together with optimization of costs, will pave the way to real application and practical adoption of the EHR in Bulgaria. We plan to apply in the forthcoming research efforts all lessons learned during the construction of the national Diabetes Register which is now supported by USHATE in Medical University Sofia.

Acknowledgements

We acknowledge the support of the National Research Programme eHealth, funded by the Bulgarian Ministry of Education and Science in 2018-2021 with grant DOI-200/16.11.2018. Gratitude is also expressed to the NHIF and the Bulgarian Ministry of Healthcare.

References

1. Garroff, B., Björnberg, A., Phang, A.Y.: Euro Diabetes Index 2014. Health Consumer Powerhouse Ltd., ISBN 978-91-980687-4-0, 2014.
2. Hallgren Elfgren, I.M., Törnvall, E., Grodzinsky, E.: The process of implementation of the diabetes register in Primary Health Care. International Journal of Quality Health Care 24(4), 2012, 419-424.
3. Richardson, E. (ed.). National Diabetes Plans in Europe: what lessons are there for the prevention and control of chronic diseases in Europe? Policy Brief of the Joint Action on Chronic Diseases and Promoting Healthy Ageing across the Life Cycle, WHO Regional Office for Europe, ISSN 1997-8065, 2016.
4. Dalianis, H. Clinical Text Mining: Secondary Use of Electronic Patient Records. Springer Open, 2018, publicly accessible at <https://www.springer.com/gp/book/9783319785028>.
5. Tcharaktchiev, D., Zaharieva, S., Angelova, G., Boytcheva, S., et al. Building a national register of Diabetes. Social Medicine 1(2), Research Society of Social Medicine, Informatics and Health Management, 2015, 19-21. ISSN:1310-1757, <http://journals.mu-varna.bg/index.php/sm/article/view/1345>
6. Boytcheva, S., Angelova, G., Angelov, Z., Tcharaktchiev, D.: Integrating Data Analysis Tools for Better Treatment of Diabetic Patients. In: Kalinichenko, L., Manolopoulos, Y., Skvortsov, N., Sukhomlin, V. (eds.) Selected Papers of the XIX International Conference on Data Analytics and Management in Data Intensive Domains (DAMDID/RCDL 2017), CEUR Workshop Proceedings Vol. 2022, 2017, 230-237, <http://ceur-ws.org/Vol-2022/>
7. Boytcheva, S., G. Angelova, Z. Angelov and D. Tcharaktchiev. Mining comorbidity patterns using retrospective analysis of big collection of outpatient records. Health Information Science and Systems, 5(3), Springer Int. Publ. 2017, ISSN: 2047-2501, <https://link.springer.com/article/10.1007/s13755-017-0024-y>
8. Boytcheva, S., Nikolova, I., Angelova, G., Angelov, Z.: Identification of Risk Factors in Clinical Texts through Association Rules. Proceedings of the Biomedical NLP Workshop associated with RANLP 2017. (pp. 64-72). doi:10.26615/978-954-452-044-1_009, http://acl-bg.org/proceedings/2017/RANLP_W4%202017/pdf/BioNLP009.pdf
9. eHealth Action Plan 2012-2020 - Innovative healthcare for the 21st century. Communication from the Commission COM(2012) 736, <https://ec.europa.eu/digital-single-market/en/news/ehealth-action-plan-2012-2020-innovative-healthcare-21st-century>

² <https://ez.mu-sofia.bg/home> (in Bulgarian)

A MODEL OF BINDING OF DOXORUBICIN WITH HEPARIN AND ENOXAPARIN

Eng. Matuszak M. L.¹, Msc. Eng. Dalek P.¹, Prof. Langner M.¹, PhD Przybyło M.¹

Faculty of Fundamental Problems of Technology – Wrocław University of Science and Technology, Poland¹

matuszak.ma.le@gmail.com

Abstract: Chemotherapy is one of the most successful methods of fighting with cancer, but like almost any kind of therapy, it has disadvantages such as severe side effects due to the high dose and/or unrestricted distribution within all body compartments. There have been numerous attempts to overcome these difficulties. The first option is to create a new active compound, what has shown to be very costly and, in many cases, ineffective. The other solution is to develop a new way to transport and release of existing drug in the organism using targeted drug delivery systems. Doxorubicin has been selected as a cytostatic substance that are already approved for medical use. The strategy is based on two features; entrapment of the active ingredient within the carrier by associating it with polymer and release it using external trigger guided by an imaging technique. The doxorubicin can be associated with heparin or enoxaparin. In order to implement the heparin/doxorubicin complex into the carrier structure, the thermodynamics of the aggregate formation need to be quantitatively described. The isothermal titration calorimetry has been used to extract the quantitative measures of its formation and stability, necessary for the designing both; pharmacological strategy and production process. To this end, the theoretical model of the binding has been developed and tested on well-defined experimental systems using heparins with different polymer lengths.

Keywords: HEPARIN, DOXORUBICIN, ITC, BINDING MODEL

1. Introduction

Chemotherapy is the well-established pharmacological approach in the treatment of cancer. Despite unquestionable successes application of chemotherapy carries serious risks of potentially dangerous side effects, which imposes a limitation on the drug dose. One of the ongoing efforts is focused on the designing pharmacological strategy, which is based on supramolecular devices^{1,2}. The strategy utilizes a well-established compound as an element of the device design to deliver and release it at the selected locations within the body³. The main objective of our ongoing research is the construction of a new kind of carrier that will be injected to a patient body and a drug released by an external trigger such as ultrasounds. This approach will allow for a precise release of drugs at tumor location. The design of the effective release mechanism requires that the encapsulated drug is associated with a compound which will prevent its uncontrolled release.

For these purposes, the suitable polymer for the drug association needs to be selected and thoroughly described. At the first step, the binding stoichiometry will be determined. Next, the effect of different solvents on the aggregate stability will be evaluated. To this end, the calorimetric experiments have been performed and obtained thermograms analyzed.

For purpose of this research, the doxorubicin has been selected as an active compound and heparin and enoxaparin as polymer scaffolds for doxorubicin association. Doxorubicin is a substance that is widely used in oncology^{4,5,6}, hence its application as an active ingredient has already been approved by authorities.

2. Measurements

In order to collect the high-quality experimental data for model fitting, we test the variety of experimental arrangements. Base on these studies doxorubicin at concentration 1.84 mM as titrant was selected. As substance in the cell, we use 0.045 mg/ml of both heparin and enoxaparin dissolved in 10 mM HEPES. The doxorubicin and heparin solutions were prepared before each experiment. Before use, every solution was degassed for 30 min with mixing at temperature 22 °C. All measurements were performed using ITC calorimeter (TA Instruments NanoITC 2G). The volume of the sample cell and the titrating syringe were equal to 1019 μ l and 250 μ l respectively. Each experiment consisted of 25 injections of 10 μ l volumes, except the first one, which was equal 1.14 μ l and discarded in the subsequent analysis. Times between injections were set to be 300 s. All measurements were performed at 22 °C.

Results

Example of thermograms, obtained in the experiment when enoxaparin was titrated with doxorubicin, are shown in Figure 1, whereas the same experiment performed with heparin is shown in Figure 2. Left panel shows raw experimental data, whereas right panel the same data corrected for the baseline. When 0.045 mg/mL heparin was titrated with 1.84 mM doxorubicin similar but not identical thermograms were collected (Figure 2).

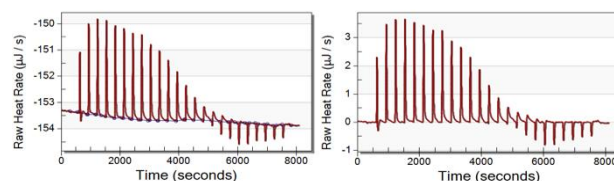


Figure 1. Example of thermograms obtained when 0.045 mg/mL of enoxaparin dissolved in 10 mM HEPES buffer (pH = 7.4) was titrated

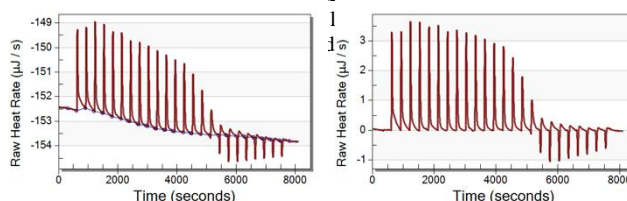


Figure 2. Example of thermograms obtained when 0.045 mg/mL of heparin dissolved in 10 mM HEPES buffer (pH = 7.4) was titrated with 1.84 mM doxorubicin. The left panel shows raw experimental data, whereas right panel the same data after baseline subtraction.

Quantities of heat flow in titration experiments were appropriately corrected for the heat of dilution. Example of such data is presented in Figure 3, where doxorubicin was titrated into

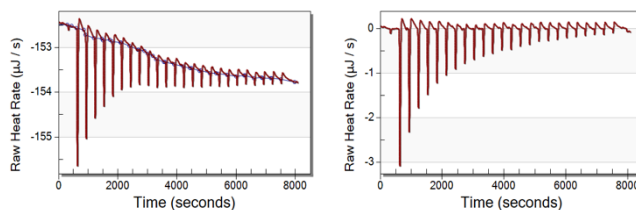


Figure 3 Example of thermograms obtained when 10 mM HEPES buffer (pH = 7.4) was titrated with 1.84 mM doxorubicin. Left panel shows raw experimental data, whereas the right panel the same data after baseline subtraction.

the 10 mM HEPES buffer alone.

3. The model

The doxorubicin-polymer binding process was approximating with the binding model, in which binding seats are independent and ligands are not interacting with each other. The binding is mainly driven by electrostatic interaction, which is described by the Stern model since doxorubicin and polymers are charged (Figure 5 and Figure 4).

Figure 1 Single heparin monomer⁷.

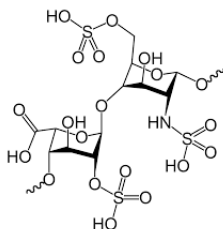
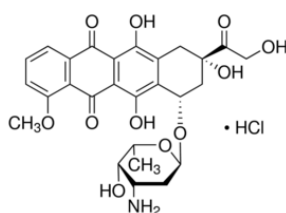


Figure 5 Chemical structure of doxorubicin⁸.



4. Model fitting to experimental data

All fitting procedures were done using NanoAnalyze v.3.8.0 software made by TA Instruments. Experimental data was fitted to the equation 3, that is a one of model contained in software that we use. Fitting quality was assessed on basis of Monte Carlo simulation checking the susceptibility of the model to random disturbances. The average deviation of ΔH was determined to be about 5 % of the determined value and the n deviation was between 2 and 5 %.

$$(1) \quad Q = \Delta H * 10^{-9} * (L_{Bound,i} - \frac{L_{Bound,i-1} * (V_t - V_i)}{V_t})$$

Where V_t – total volume, V_i – volume of i th injection.

$$(2) \quad L_{Bound,i} = \frac{a - \sqrt{(a - 1019 * 10^{-6})^2 - 4 \left(\frac{1}{K_d}\right)^2 L_i T_i n}}{2 \frac{1}{K_d}}$$

Where K_d – L_i – concentration of ligand after i th injection, T_i – concentration of cell after i -injection, n – stoichiometric number.

$$(3) \quad a = -\frac{1}{K_d} (L_i - T_i n)$$

Where K_d – L_i – concentration of ligand after i -injection, T_i – concentration of cell after i th injection, n – stoichiometric number.

The heat flow after each injection was calculated as an area under the peak calculated from thermograms.

Examples of experimental data along with fitted functions, for bot enoxaparin and heparin, are presented in Figure 5 and Figure 6. In both cases the difference between heats of binding and dilution are fitted.

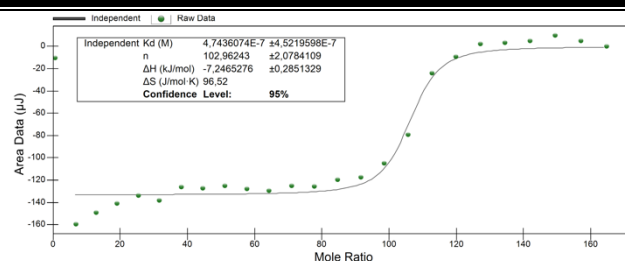


Figure 6 Example of fitting the heat flow generated by interaction between doxorubicin and heparin with the independent binding seat model.

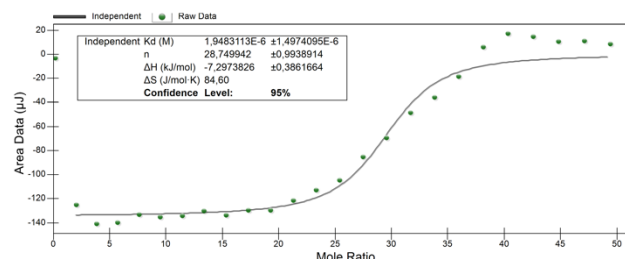


Figure 7 Example of fitting the heat flow generated by interaction between doxorubicin and enoxaparin with the independent binding seat model.

The average value for results of fitting experimental data determined for both polymers is presented in Table 1. Association of heparin with doxorubicin is accompanied by larger enthalpy change than that obtained for enoxaparin indicating stronger binding. This is accompanied by the large difference in a number of binding seats per heparin molecule and smaller dissociation constant.

Table 1 The average value of parameters retrieving from fitting of experimental data to the model.

Symbol	K_d	n	ΔH
Unit	M	-	kJ/mol
Heparin	4,50E-07	98,68	-7,84
Enoxaparin	1,74E-06	28,44	-6,55

5. Conclusion

Calorimetric data shows that the doxorubicin interacts with negatively charged polymers and that the interaction depends on the size (number of binding seats) on a polymer. Specifically, doxorubicin binds to heparin almost an order of magnitude stronger than with smaller enoxaparin. In addition, there are three times less binding seats on enoxaparin than heparin. The determined quantities are critical for the design of a carrier with tuneable parameters, which are important for an aggregate stability.

6. Acknowledgments

This work was supported by a Grant POIR.04.01.04-00-0050/15 by the National Centre for Research and Development (NCBiR).

7. References

- [1] J. E. Anderson, J. M. Hunt, I. E. Smith, Prevention of doxorubicin-induced alopecia by scalp cooling in patients with advanced breast cancer, Br Med J (Clin Res Ed). 1981 Feb 7; 282(6262): 423–42
- [2] C. M. Soref, W. E. Fahl, A new strategy to prevent chemotherapy and radiotherapy-induced alopecia using topically applied vasoconstrictor, Int J Cancer. 2015 Jan 1; 136(1): 195–203

- [3] N. A. Finn, H. W. Findley, M. L. Kemp, A Switching Mechanism in Doxorubicin Bioactivation Can Be Exploited to Control Doxorubicin Toxicity, *PLoS Comput Biol.* 2011 Sep; 7(9)
- [4] M. Cheng, A. Rizwan, L. Jiang, Z. M. Bhujwalla, K. Glunde, Molecular Effects of Doxorubicin on Choline Metabolism in Breast Cancer, *Neoplasia.* 2017 Aug; 19(8): 617–627
- [5] Q. C. Dias, Iseu da Silva Nunes, P. V. Garcia, W. J. Fávaro, Potential therapeutic strategies for non - muscle invasive bladder cancer based on association of intravesical immunotherapy with P-MAPA and systemic administration of cisplatin and doxorubicin, *Int Braz J Urol.* 2016 Sep-Oct; 42(5): 942–954
- [6] P. J. Gaillard, C. Appeldoorn, R. Dorland, J. van Kregten, F. Manca, D. J. Vugts, B. Windhorst, G. van Dongen, H. E. de Vries, D. Maussang, O. van Tellingen, Pharmacokinetics, Brain Delivery, and Efficacy in Brain Tumor-Bearing Mice of Glutathione Pegylated Liposomal Doxorubicin (2B3-101), *PLoS One.* 2014; 9(1)
- [7] R. Badkundri, A. Bhave, A. Athalye, R. Rege, V. Rangnekar, The GTF Group, Atlanta, GA, One hundred years of Heparin, Retrieved from <http://www.angiology.org/AngiologyOrg/media/system/Guidelines/NATF-GTF-Loyola-Poster-PDF.pdf>
- [8] Sigma-Aldrich, Doxorubicin hydrochloride Specification, <https://www.sigmaaldrich.com/catalog/product/sigma/d1515?lang=en®ion=US>

DETERMINATION OF SURFACTANT EFFECTIVE DIFFUSION COEFFICIENT USING INVERSE PROBLEM FOR WARD-TORDAI EQUATION

M.Sc. Eng. Stasiak M.¹, M.Sc. Eng. Andrzejewski A.², Prof. Prochaska K.²

Institute of Mathematics, Faculty of Electrical Engineering, Poznan University of Technology, Poland¹

Institute of Chemical Technology and Engineering, Faculty of Chemical Technology, Poznan University of Technology, Poland²

marcin.stasiak@put.poznan.pl

Abstract: The main purpose of the study was to assess the usability of a new calculation algorithm for determining the surfactants effective diffusion coefficient. The adsorption of a mixture of non-ionic surfactants onto flat water-air interface was considered. Presented algorithm is composed of a two parts: Ward-Tordai equation solver based on Nyström method for integral equations and golden ratio optimization method used in inverse problem. In the investigation the Langmuir model of an isotherm was assumed. Presented algorithm was successfully used to determine the non-ionic surfactant - Nafol 810D (BRENNTAG) effective diffusion coefficient in the diffusion controlled adsorption process.

Keywords: DIFFUSION COEFFICIENT, DIFFUSION, ADSORPTION, INTEGRAL EQUATION, INVERSE PROBLEM

1. Introduction

In modelling of mass transport processes an important role plays the diffusion process, which describes the movement of molecules from a domain of higher concentration to a region of lower concentration. The mass flux is caused by a gradient of concentration of a particle in a solution.

Adsorption is defined as the adhesion of atoms, ions or molecules from a gas, liquid or dissolved solid to a surface. This process, which is a consequence of surface energy, creates a film of the adsorbate on the surface of the adsorbent. In the systems with surfactants the monolayer is usually created, however the effects of electrostatic interactions are neglected [1]. Adsorption is usually described through the isotherms, that is, the amount of adsorbate on the adsorbent as a function of its pressure (if gas) or concentration (if liquid) at constant temperature. These functions describes the relationship between the bulk concentration $c \left[\frac{\text{mol}}{\text{m}^3} \right]$ and surface excess $\Gamma \left[\frac{\text{mol}}{\text{m}^2} \right]$ of an adsorbed compound. Many models of isotherms were proposed in the literature. Their level of complexity depends on the phenomena according to the considered model. The easiest way to describe the above mentioned relation is the linear correlation called Henry isotherm and is given by eq. 1 [2].

$$\Gamma = K_H c \quad (1)$$

where K_H is a Henry constant. It is a huge simplification of the real problem because it doesn't include the finiteness of the surface. It might be useful for modelling the adsorption process in the terms of the low concentration of surfactant. More compatible with the real processes is the non-linear Langmuir isotherm given by eq. 2 [2].

$$\Gamma = \Gamma_\infty \frac{K_L c}{1 + K_L c} \quad (2)$$

where K_L is Langmuir constant and $\Gamma_\infty \left[\frac{\text{mol}}{\text{m}^2} \right]$ is a maximum surface excess. Both of the presented isotherms are connected with a dynamics of adsorption process. However the Gibbs isotherm, given by eq. 3, is useful to determine the equilibrium value of surface excess $\Gamma_{eq} \left[\frac{\text{mol}}{\text{m}^2} \right]$ of the considered system

$$\Gamma = - \frac{1}{RT} \frac{d\gamma}{d \ln c} \quad (3)$$

where $R \left[\frac{\text{J}}{\text{mol K}} \right]$ is a gas constant, $T [K]$ is a temperature of the system and $\gamma \left[\frac{\text{mN}}{\text{m}} \right]$ is a surface tension of the system [2].

Adsorption of non-ionic surfactants is characterized by two mechanisms – diffusion of molecules to the interface and adsorption on the surface (see fig. 1).

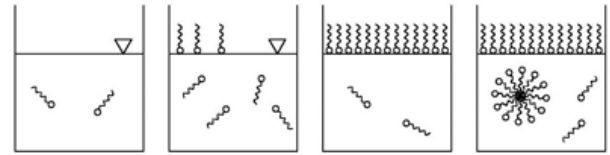


Fig.1. Diffusion and adsorption at the interface

When diffusion process is slower than adsorption process, what is a frequent situation in the real systems, one can say that the adsorption of surfactant is controlled by diffusion. This paper is focused on determination of surfactant effective diffusion coefficient which describes the rate of the whole process. The model of above presented process is given by one-dimensional

$$\frac{\partial c}{\partial t} = D \frac{\partial^2 c}{\partial x^2} \quad (4)$$

diffusion partial differential eq. 4 [3,4].

$$D \frac{\partial c}{\partial x} \Big|_{x=0} = \frac{\partial \Gamma}{\partial t} \quad (5)$$

$$\lim_{x \rightarrow \infty} c(x, t) = c_b \quad (6)$$

with boundary conditions (5) and (6):

$$c(x, t)|_{t=0} = c_b \quad (7)$$

for $t > 0$, where c_b is a bulk concentration, and initial condition (7):

The solution of diffusion model which describes dynamic of surfactant adsorption for a long time processes was given by Ward

$$\Gamma(t) = \sqrt{\frac{D}{\pi}} \left\{ 2c_b \sqrt{t} - \int_0^t \frac{c(\Gamma(\tau))}{\sqrt{t-\tau}} d\tau \right\} \quad (8)$$

and Tordai in 1946 by eq. 8 [5].

where $D \left[\frac{\text{m}^2}{\text{s}} \right]$ is a diffusion coefficient, $c(\Gamma(t))$ is the relations between concentration and surface excess and t is a time. Eq. 8 is a Volterra integral equation of the second kind. Linearity or non-linearity of this equation depends on chosen model of isotherm of adsorption. Linear case with Henry isotherm was solved

analytically by Sutherland [6]. In this paper the Langmuir isotherm will be used. The non-linear case doesn't have the analytical solution.

2. Results and discussion

The diffusion of the commercial surfactant was investigated (trade name Nafol 810D). The experimental data was given by the Du Nöuy ring method [7]. The fig. 2 shows the change of surface tension during the experiment of the samples of different bulk concentration.

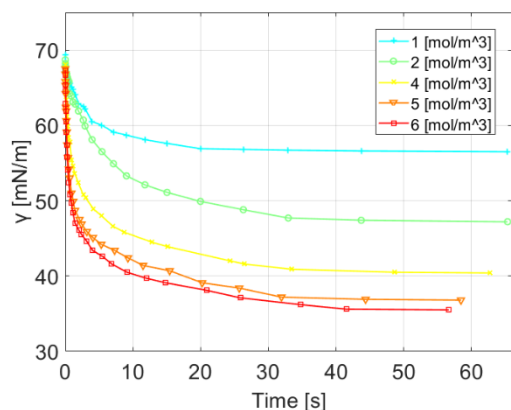


Fig.2. The change of surface tension during the experiment of the samples of different bulk concentration

The Szyszkowski isotherm, given by eq. 9 [8], was fitted to the experimental relation between the surface tension and the bulk concentration of the compound (fig. 3).

$$\gamma = \gamma_0 \left(1 - B_{sz} \ln \left(\frac{c}{A_{sz}} + 1 \right) \right) \quad (9)$$

where γ_0 is the water surface tension, γ is the surface tension associated with the surfactant concentration c , A_{sz} and B_{sz} are Szyszkowski constants, which have the physical meanings. A_{sz} describes the measure of tendency to interfacial adsorption and B_{sz} characterizes the orientation of the adsorbed molecule. Eq. 3 and 9 were used to determine the values of Γ_{eq} and Γ_{∞} of the considered system.

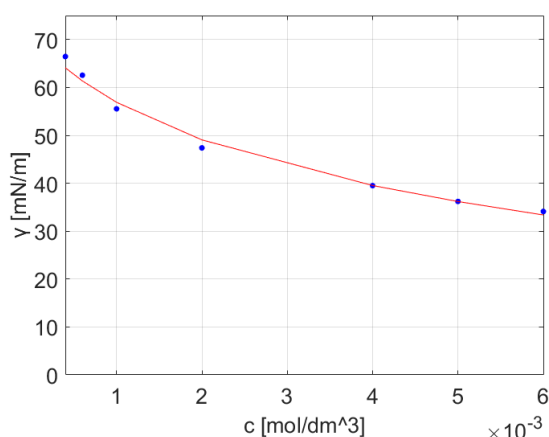


Fig.3. Experimental data of the equilibrium surface tension depending on the bulk concentration

The relation between surface excess and surface tension is given by eq. 10 [4,9]. It was used to determine the surface excess Γ as a function of time.

$$\Gamma(t) = \Gamma_{\infty} \left(1 - \exp \left(\frac{\gamma(t) - \gamma_0}{RT\Gamma_{\infty}} \right) \right) \quad (10)$$

The main purpose of the study was to assess the usability of a new calculation algorithm for determining the surfactants effective diffusion coefficient using the inverse problem for Ward-Tordai equation.

The diffusion coefficient was investigated in the interval $10^{-7} \div 10^{-16} \left[\frac{m^2}{s} \right]$. In order to solve the nonlinear Ward-Tordai integral equation associated with Langmuir isotherm the Nystrom method was used [10,11]. Nystrom method is a discrete method of solving integral equations. In short, the time interval is discretized into finite vector with constant time steps and the integral in eq. 8 is approximated by chosen quadrature. In a consider case the trapezium rule of integration was used. The final discretized form of eq. 8 is given by eq. 11 with initial step $\Gamma(0) = 0$, which means that any of surfactant molecule isn't adsorbed on the surface in the beginning of the diffusion process.

The golden ratio method was used in a optimization part of the inverse problem algorithm [12]. The aim function given by eq. 12 is the maximum norm of the subtraction of the experimental and numerical data vectors, respectively Γ_{num} and Γ_{exp} .

$$\Psi(D) = \|\Gamma_{num} - \Gamma_{exp}\|_{\infty} \quad (11)$$

The experimental data was compared with numerical data and error was minimized successfully in a numerical inverse problem algorithm for all considered samples. Fig. 4 shows the experimental and numerical data of the surface excess in the concentration bulk

$$\Gamma(t_i) = 2c_b \sqrt{\frac{Dt_i}{\pi}} - \frac{1}{K_L} \sqrt{\frac{D}{\pi}} \sum_{j=1}^i A_j \frac{\Gamma(\tau_j)}{\sqrt{t_i - \tau_j} (\Gamma_{\infty} - \Gamma(\tau_j))} \quad (12)$$

5 $\left[\frac{mol}{m^3} \right]$ case.

for $i = 2, 3, \dots$

In every time iteration the nonlinear eq. 12 has to be solved. Eq. 12 can be reformulated into quadratic eq. which discriminant is a positive number. Only one solution of this eq. has a physical meaning.

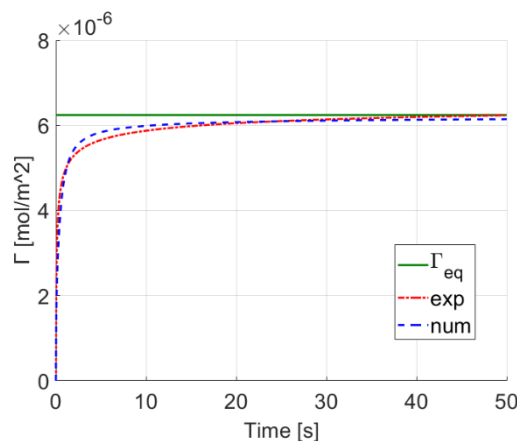


Fig.4. Experimental and numerical data of the surface excess in the bulk concentration 5 $\left[\frac{mol}{m^3} \right]$

Fig. 5 shows the minimization of the aim function during the optimization process. Fig. 6 shows reaching the optimal value of effective diffusion coefficient during the optimization process. Both figures are associated with the 5 $\left[\frac{mol}{m^3} \right]$ case as an example. The results of the first 15 iteration are showed. The optimal value for all investigated cases was reached after 30 ÷ 40 iterations.

The dependence between the effective diffusion coefficient and the concentration of the investigated compound is presented in the table 1.

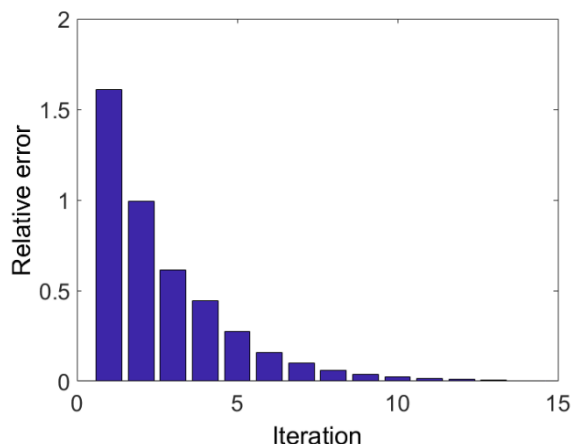


Fig.5. Experimental and numerical data of the surface excess in the bulk concentration $5 \left[\frac{\text{mol}}{\text{m}^3} \right]$

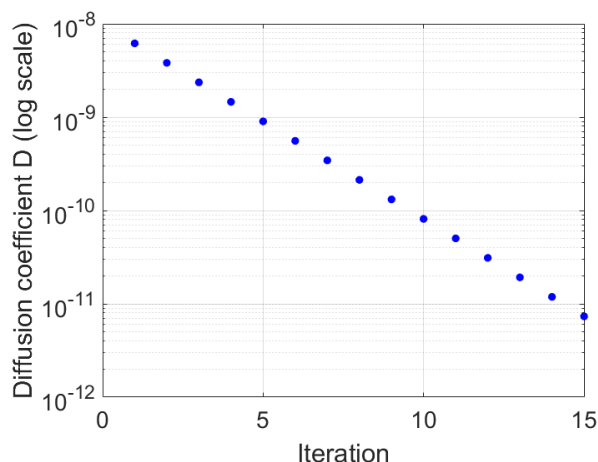


Fig.6. Experimental and numerical data of the surface excess in the bulk concentration $5 \left[\frac{\text{mol}}{\text{m}^3} \right]$

Table 1: Values of effective diffusion D coefficient for different bulk concentration c_b

Bulk concentration $c_b \left[\frac{\text{mol}}{\text{m}^3} \right]$	Effective diffusion coefficient $D \left[\frac{\text{m}^2}{\text{s}} \right]$
1	$2,87 \cdot 10^{-11}$
2	$3,34 \cdot 10^{-12}$
4	$1,62 \cdot 10^{-12}$
5	$1,68 \cdot 10^{-12}$
6	$1,14 \cdot 10^{-12}$

3. Conclusions

Above presented procedure was used to determine the effective diffusion coefficient of commercial surfactant Nafol 810D. In every case of the bulk concentration presented algorithm minimized the aim function and the inverse Ward-Tordai problem was solved. Result of the paper is the effective diffusion coefficient dependence on the bulk concentration of the surfactant.

Presented algorithm can be successfully use to determine the effective diffusion coefficient of amphiphilic surfactants based on the experimental data of dynamic of adsorption process.

4. Acknowledgments

This work was supported by the Faculty of Electrical Engineering, Poznan University of Technology, under grant no. 04/43/DSMK/010.

5. References

- [1] Chattoraj D. K., Birdi K. S., Adsorption and the Gibbs Surface Excess. New York and London, Plenum Press, 1984.
- [2] Rosen M. J., Kunjappu J. T., Surfactants and Interfacial Phenomena: Fourth Edition, New York, John Wiley & Sons Ltd., 2012.
- [3] Crank J., The Mathematics of Diffusion, Oxford, Clarendon Press, 1975.
- [4] Miller R., Joos P., Fainerman V. B., Dynamic surface and interfacial tensions of surfactant and polymer solutions, Adv. Colloid Interface Sci., vol. 49, no. C, 1994, p. 249–302.
- [5] Ward A. F. H. and Tordai L., Time-dependence of boundary tensions of solutions I. The role of diffusion in time-effects, J. Chem. Phys., vol. 14, no. 7, 1946, p. 453–461.
- [6] Sutherland K. L., Australian Journal of Scientific Research, Series A: Physical Sciences, vol. 5, 1952, p.683.
- [7] Gorevski N., Miller R., Ferri J. K., Non-equilibrium exchange kinetics in sequential non-ionic surfactant adsorption: Theory and experiment, Colloids Surfaces A Physicochem. Eng. Asp., vol. 323, no. 1–3, 2008, p. 12–18.
- [8] Radzio K., Prochaska K., Interfacial activity of trioctylamine in hydrocarbon/water systems with nonorganic electrolytes, J. Colloid Interface Sci., vol. 233, no. 2, 2001, p. 211–218.
- [9] Miller R., Aksenenko E. V., and Fainerman V. B., Dynamic interfacial tension of surfactant solutions, Adv. Colloid Interface Sci., vol. 247, 2017, p. 115–129.
- [10] Delves L.M, Mohamed J.L., Computational methods for integral equations, New York, Cambridge University Press, 1992.
- [11] Li X., Shaw R., Evans G. M., Stevenson P., A simple numerical solution to the Ward-Tordai equation for the adsorption of non-ionic surfactants, Comput. Chem. Eng., vol. 34, no. 2, 2010, p. 146–153.
- [12] Chapra S., Applied Numerical Methods with Matlab for Engineers and Scientist, Third Edition, New York, McGraw-Hill, 2008.

CLASSIFICATION OF PROTEIN STRUCTURES BY USING FUZZY KNN CLASSIFIER AND PROTEIN VOXEL-BASED DESCRIPTOR

Prof. Dr. Mirceva G., Prof. Dr. Naumoski A., Prof. Dr. Kulakov A.

Faculty of computer science and engineering, Ss. Cyril and Methodius University in Skopje, Skopje, R. Macedonia

georginamirceva@gmail.com

Abstract: Protein classification is among the main themes in bioinformatics, for the reason that it helps understand the protein molecules. By classifying the protein structures, the evolutionary relations between them can be discovered. The knowledge for protein structures and the functions that they might have could be used to regulate the processes in organisms, which is made by developing medications for different diseases. In the literature, plethora of methods for protein classification are offered, including manual, automatic or semiautomatic methods. The manual methods are considered as precise, but their main problem is that they are time consuming, hence by using them a large number of protein structures stay uncategorized. Therefore, the researchers intensively work on developing methods that would afford classification of protein structures in automatic way with acceptable precision. In this paper, we propose an approach for classifying protein structures. Our protein voxel-based descriptor is used to describe the features of protein structures. For classification of unclassified protein structures, we use a k nearest neighbors classifier based on fuzzy logic. For evaluation, we use knowledge for the classification of protein structures in the SCOP database. We provide some results from the evaluation of our approach. The results show that the proposed approach provide accurate classification of protein structures with reasonable speed.

Keywords: PROTEIN STRUCTURE, PROTEIN CLASSIFICATION, PROTEIN VOXEL-BASED DESCRIPTOR, K NEAREST NEIGHBORS, FUZZY LOGIC

1. Introduction

Bioinformatics community intensively analyze protein molecules for the reason that they are essential in the organisms. The processes in the organisms can be controlled by the interactions of proteins. The knowledge gathered from the examination of proteins may be used for drug design, where the functions of the proteins in these interactions is taken into consideration. Using various types of techniques, the structures of the protein molecules have been examined. The information about protein structures is stored in the Protein Data Bank (PDB) [1], [2]. Due to the fast improvements in these techniques, the structures of proteins are determined with fast speed. However, the methods that provide classification of proteins are not able to classify them with the same speed that leads to gap in the number of proteins with determined structures and the number of proteins that are classified. Thus, there is a great necessity for developing methods for classification of protein structures.

The current literature offers various methods for classification of proteins. In the SCOP (Structural Classification Of Proteins) method [3] the decision is done in manual way, where the experts visually examine the proteins. However, the manual methods are time consuming and are not able to follow the speed of determining novel protein structures. Therefore, there are also automatic methods and semiautomatic methods. For example, the CATH (Class, Architecture, Topology and Homologous superfamily) method [4] tries to classify proteins in automatic manner first, and if the decision could not be made, then manual decision is performed.

Some methods align the sequences of the protein structures, also known as primary structures, in order to perform classification of the proteins. The most known methods in this group are Needleman–Wunch [5], BLAST [6] and PSI-BLAST [7]. However, the protein sequence is a particular sequence of amino acid residues that folds in some specific way in the three-dimensional space. In that way, two amino acid residues could be close in the space, while far in the protein sequence. Therefore, the methods based on alignment of protein sequences are not able to recognize distant homology between proteins. For that purpose, also there is a group of methods that analyze the tertiary structures of proteins, like CE [8], MAMMOTH [9] and DALI [10]. Third group of methods, like SCOPmap [11] and FastSCOP [12], combines both sequence and structure alignment.

Besides alignment of the sequences or structures of proteins, feature vectors could be extracted, and then the proteins can be compared based on the distance between their feature vectors. In the

literature, there are methods that use features of the sequence [13] or structure [14] of proteins, as well as both of them. By extracting the vector of features, the protein is presented by a point in the feature space. Later, in the classification stage, the amount of information that is processed is significantly lower than by making direct alignment of proteins, so the time needed for classification is much lower. For that purpose, in our earlier study [15], we presented feature vectors that contain features that represent the protein structures. These feature vectors could be used as inputs and by using some classification method, a prediction model could be generated.

In this paper, we use the protein voxel-based descriptor presented in [15] and we apply a fuzzy k nearest neighbors classification method [16] to classify the unknown structures.

Here is an outline of the structure of the remaining of this paper. Section 2 provides description of the proposed approach, where the protein voxel-based descriptor [15] and fuzzy k nearest neighbors classification method [16] are presented. The results of the evaluation of the approach are presented and discussed in Section 3, whereas Section 4 presents the main conclusions and points out directions for further advancements of the approach.

2. The Proposed Approach

The approach used in this study has two steps. The first step performs extraction of the feature vectors of the training protein structures. In this study, we use the protein-voxel based descriptor [15]. After mapping the proteins in the feature space, next, in the second step we use the fuzzy k nearest neighbors classification method [16] to determine the class in which a given query protein would belong to.

Protein Voxel-Based Descriptor

The protein voxel-based descriptor contains features of the primary, secondary and tertiary structure of the protein. Regarding the tertiary structure, we use the voxel descriptor [17] that is originally proposed for comparing 3D objects. Concerning the primary and secondary structure, the features are extracted as in [18].

The extraction of the protein voxel-based descriptor is done in the following way. First, a mesh model of the protein structure is generated, by making triangulation of the atoms of the protein that are treated as spheres and with triangulation they are presented by a given number of triangles. In order to obtain feature vector that is invariant to translation, the protein is translated so that its center of

mass is in the center of the coordinate system. With the aim to obtain feature vector that is invariant to scaling, next we perform scaling of the mesh model thus the most distant vertex of the triangles in the mesh model is at a distance equal to 1 from the center of mass.

After obtaining the mesh model, next, a voxelization is made. With this step, we transform the continual into discrete space. For that purpose, first, discretization is made, where the continuous three-dimensional space is divided into equal cubes named voxels. Then, for each of the voxels, we calculate the ratio of the area of the mesh that is in the inspected voxel. For that purpose, the triangles are divided into p_j^2 triangles with a surface $\delta = S_j / p_j^2$, where S_j denotes the area of the triangle T_j that is currently divided. If a given triangle T_j has vertices in one voxel, then p_j is set to 1. Otherwise, it is calculated as

$$(1) \quad p_j = \left\lceil \sqrt{p_{\min} \frac{S_j}{S}} \right\rceil,$$

where S is the total surface of the triangles and p_{\min} defines the quality of the approximation. In this study, we use $p_{\min} = 32000$ as in [17]. For each voxel, the surface that is placed in the voxel is incremented for δ .

With the previous step, as output, we obtain three-dimensional matrix that could be used as feature vector. However, the number of features contained in this matrix could be significantly reduced. Moreover, this three-dimensional matrix as a feature vector is not invariant to rotation. Therefore, in the next step, we apply 3D Discrete Fourier Transform thus obtaining feature vector that is invariant to rotation. In this way, the new version of the feature vector is also a three-dimensional matrix.

Next, the indices are shifted so the voxel in the center has indices (0, 0, 0). Because there is a symmetry between the elements of the obtained feature vector, therefore only the non-symmetrical features are considered that corresponds to the values of the voxels with indices that satisfy $1 \leq |p| + |q| + |s| \leq N/2$, where (p, q, s) are the indices of the voxel and N is the number of slices for one coordinate used in the discretization of the space. Further, the features are divided by the feature that correspond to the voxel with indices (0, 0, 0). More details about the extraction of the geometrical features contained in the voxel descriptor can be found in [17] and [15].

Besides the features of the tertiary structure of the proteins, we also consider several features of their primary and secondary structure. In this study, we use the features used in [18]. Regarding primary structure, we consider the ratio of each amino acid and the ratio of the hydrophobic amino acids in the protein. From the features of the secondary structure, we consider the ratios of the types of helices, as well as the number of occurrences of each type of secondary structure element (helix, sheet and turn). More details about these features can be found in [18] and [15].

Fuzzy k Nearest Neighbors Classifier

For classifying a given query sample (protein chain in this case), first its protein voxel-based descriptor is extracted. Then, this query sample is compared with the training samples and its class is determined by using the fuzzy k nearest neighbors (Fuzzy KNN) classification method [16].

The Fuzzy KNN method is inspired from the well known k nearest neighbors (KNN) classification method [19], but adjusted for sets in fuzzy logic. KNN could be used to perform simple majority voting of the nearest neighbors, or the neighbors may have different weights in the voting in order to give higher significance to the votes of the closer neighbors. For the second approach, the distance between the examined sample and the nearest neighbor could be used in order to calculate the weight of the vote of that neighbor.

Let assume we are using k nearest neighbors for making decisions. The Fuzzy KNN method first identifies the k nearest neighbors for the inspected sample q , which are denoted as NN (nearest neighbors). For that purpose, the similarity between a given training sample x and the query sample q is calculated as $S(x, q) = 1/D(x, q)^2$, where $D(x, q)$ denotes the distance between x and q . Then, the examined sample q is classified by maximizing

$$(2) \quad \frac{\sum_{x \in NN} S(x, q) M_c(x)}{\sum_{x \in NN} S(x, q)},$$

where c is the examined class, while $M_c(x)$ denotes the membership function for that class. The membership function could be crisp, defined as

$$(3) \quad M_c(x) = \begin{cases} 1, & x \in C \\ 0, & x \notin C \end{cases},$$

where C is a set of the samples in class c . In this study, since we are using an approach based on fuzzy set theory, therefore instead of using a crisp function we are using the gradual function presented in [16]. The membership function that is used is defined as

$$(4) \quad M_c(x) = \begin{cases} 0.51 + 0.49 \frac{n_c}{k}, & x \in C \\ 0.49 \frac{n_c}{k}, & x \notin C \end{cases},$$

where $n_c = |C|$ is the size of the set C .

3. Results and Discussion

For evaluation, we used 6145 protein chains that are classified in 150 different SCOP domains. The protein chains correspond to the samples in the set, while the domains are the output classes (the possible values for the target attribute). The information about the classification of the protein chains in SCOP domains is obtained from the SCOP database [3]. The distribution of the protein chains used in this study is approximately uniform. This set is divided into training set (90% of the chains) and test set (10% of the chains). In this way, the training set that is obtained has 5531 chains, while the remaining 614 chains form the test set. As evaluation measure, the classification accuracy is used, which gives evidence about the percent of the test samples that are classified correctly. The experimental results are presented on Fig. 1. We made experiments by using different values for the number of nearest neighbors that are considered for making predictions ($k = 1, 2, 3, 4, 5, 10, 15, 20$). In order to give better picture of the benefit of using fuzzy sets instead of classical sets, we made experiments by applying the classical KNN classification method and the Fuzzy KNN classification method that is based on fuzzy logic.

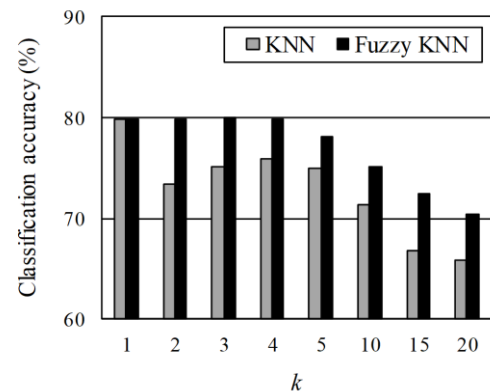


Fig. 1 Classification accuracy achieved by KNN and Fuzzy KNN classification methods by using different number of nearest neighbors k .

As it can be seen from the results, Fuzzy KNN provides better results than the classical KNN classification method. By using Fuzzy KNN, it is best to use between $k=1$ and $k=4$ nearest neighbors, and then by increasing the number of nearest neighbors that are considered for making decisions, the classification accuracy declines. Regarding KNN, the best result is obtained by using $k=1$ nearest neighbor. By using $k=2$ and $k=3$, lower accuracy is obtained than by using $k=4$. Then, by increasing the number of nearest neighbors (for $k>4$), the classification accuracy declines. The highest classification accuracy of 79.97% is achieved with Fuzzy KNN classifier by considering $k=3$ nearest neighbors.

The obtained results for the proposed approach are comparable to the results obtained with the existing approaches. Also, this approach provides classification of proteins with reasonable speed. Namely, the time needed for classification of all 614 test protein chains used in this study is in range of minutes, which is much better than the time needed with manual methods.

4. Conclusion

In this study, we proposed a novel approach that could be used to make decisions about the classification of protein chains into SCOP domains. For each training protein chain, its protein voxel-based descriptor is extracted, which is a feature vector that contains features about the primary, secondary and tertiary structure of the protein. The classification of an unknown test protein chain is done in two steps. First, its protein voxel-based descriptor is extracted, and then by applying the Fuzzy KNN classifier the class of the unknown protein chain is determined.

For evaluation, we used information about the classification of the protein chains in SCOP domains. The results show that it is best to use up to $k=4$ nearest neighbors, while by further growth of the number of nearest neighbors the results are getting worse. The Fuzzy KNN classifier was compared with the classical KNN method, and the results indicate that Fuzzy KNN is better.

As future work, we plan to extend this study in several directions. Regarding the feature vector, besides the protein voxel-based descriptor, we also plan to use some of the other feature vectors that we already used in our previous studies where these descriptors were used for retrieving similar protein structures. Concerning the classification method, we may also apply some other distance and similarity measures for estimating the similarity between two samples. Besides the Fuzzy KNN classification method, we plan to apply other classification methods, including methods based on classical set theory as well as fuzzy set theory.

Acknowledgment

This work was partially financed by the Faculty of Computer Science and Engineering at the "Ss. Cyril and Methodius University in Skopje", Skopje, R. Macedonia.

References

- [1] H. M. Berman, J. Westbrook, Z. Feng, G. Gilliland, T. N. Bhat, H. Weissig, I. N. Shindyalov, and P. E. Bourne, "The protein data bank," *Nucleic Acids Res.*, vol. 28, no. 1, pp. 235–242, 2000.
- [2] RCSB Protein Data Bank, <http://www.rcsb.org>, 2018.
- [3] A. G. Murzin, S. E. Brenner, T. Hubbard, and C. Chothia, "Scop: a structural classification of proteins database for the investigation of sequences and structures," *J. Mol. Biol.*, vol. 247, no. 4, pp. 536–540, 1995.
- [4] C. A. Orengo, A. D. Michie, D. T. Jones, M. B. Swindells, and J. M. Thornton, "CATH – a hierarchic classification of protein domain structures," *Structure*, vol. 5, no. 8, pp. 1093–1108, 1997.
- [5] S. B. Needleman and C. D. Wunsch, "A general method applicable to the search for similarities in the amino acid sequence of two proteins," *J. Mol. Biol.*, vol. 48, no. 3, pp. 443–453, 1970.
- [6] S. F. Altschul, W. Gish, W. Miller, E. W. Myers, and D. J. Lipman, "Basic local alignment search tool," *J. Mol. Biol.*, vol. 215, no. 3, pp. 403–410, 1990.

- [7] S. F. Altschul, T. L. Madden, A. A. Schäffer, J. Zhang, Z. Zhang, W. Miller, and D. J. Lipman, "Gapped BLAST and PSI-BLAST: a new generation of protein database search programs," *Nucleic Acids Res.*, vol. 25, no. 17, pp. 3389–3402, 1997.
- [8] I. N. Shindyalov and P. E. Bourne, "Protein structure alignment by incremental combinatorial extension (CE) of the optimal path," *Protein Eng.*, vol. 11, no. 9, pp. 739–747, 1998.
- [9] A. R. Ortiz, C. E. Strauss, and O. Olmea, "Mammoth: an automated method for model comparison," *Protein Sci.*, vol. 11, no. 11, pp. 2606–2621, 2002.
- [10] L. Holm and C. Sander, "Protein structure comparison by alignment of distance matrices," *J. Mol. Biol.*, vol. 233, no. 1, pp. 123–138, 1993.
- [11] S. Cheek, Y. Qi, S. S. Krishna, L. N. Kinch, and N. V. Grishin, "SCOPmap: automated assignment of protein structures to evolutionary superfamilies," *BMC Bioinformatics*, vol. 5, pp. 197–221, 2004.
- [12] C. H. Tung and J. M. Yang, "fastSCOP: a fast web server for recognizing protein structural domains and SCOP superfamilies," *Nucleic Acids Res.*, vol. 35, W438–W443, 2007.
- [13] K. Marsolo, S. Parthasarathy, and C. Ding, "A Multi-Level Approach to SCOP Fold Recognition," *IEEE Symposium on Bioinformatics and Bioeng.*, pp. 57–64, 2005.
- [14] P. H. Chi, Efficient protein tertiary structure retrievals and classifications using content based comparison algorithms, PhD thesis, University of Missouri-Columbia, 2007.
- [15] G. Mirceva, I. Cingovska, Z. Dimov, and D. Davcev, "Efficient approaches for retrieving protein tertiary structures," *IEEE/ACM Trans. Comput. Biol. Bioinform.*, vol. 9, no. 4, pp. 1166–1179, 2012.
- [16] J. M. Keller, M. R. Gray, and J. R. Givens, "A fuzzy k-nearest neighbor algorithm," *IEEE Transactions on Systems, Man, and Cybernetics*, vol. 15, no. 4, pp. 580–585, 1985.
- [17] D. V. Vranic, 3D Model Retrieval, Ph.D. Thesis, University of Leipzig, 2004.
- [18] P. Daras, D. Zarpalas, A. Axenopoulos, D. Tzovaras, and M. G. Strintzis, "Three-Dimensional Shape-Structure Comparison Method for Protein Classification," *IEEE/ACM Trans. Comput. Biol. Bioinform.*, vol. 3, no. 3, pp. 193–207, 2006.
- [19] D. Aha, D. Kibler, "Instance-based learning algorithms," *Machine Learning*, vol. 6, no. 1, pp. 37–66, 1991.

MODELLING THE RELATIONSHIP BETWEEN SATURATED OXYGEN AND DIATOMS' ABUNDANCE USING WEIGTHED PATTERN TREES WITH ALGEBRAIC OPERATORS

Prof. Dr. Naumoski A., Prof. Dr. Mirceva G., Prof. Dr. Mitreski K.

Faculty of computer science and engineering, Ss. Cyril and Methodius University in Skopje, Skopje, R. Macedonia

andrejanaumoski@mail.com

Abstract: Machine learning has been used in many disciplines to reveal important patterns in data. One of the research disciplines that benefits from using these methods is eco-informatics. This branch of applied computer science to solve environmental problems uses computer algorithms to discover the impact of the environmental stress factors on the organisms' abundance. Decision tree type of machine learning methods are particularly interesting for the computer scientists as well as ecologists, because they provide very easy interpretable structure without any practical knowledge in mathematics or the inner working of the algorithm. These methods do not rely only on classical sets, but many of them are using fuzzy set theory to overcome some problems like overfitting, robustness to data change and improved prediction accuracy. In this direction, this paper aims to discover the influence of one particular environmental stress factor (Saturated Oxygen) on real measured data containing information about the diatoms' abundance in Lake Prespa, Macedonia, using weighted pattern tree (WPT) algorithm. WPT is a decision tree method variant that combines fuzzy set theory concepts, like similarity metrics, fuzzy membership functions and aggregation operators, to achieve better prediction accuracy, improve interpretability and increase the resistance to overfitting compared to the classical decision trees. In this study, we use Algebraic operators for aggregation. One WPT model is presented in this paper to relate the saturated oxygen parameter with the diatoms' abundance and reveal which diatoms can be used to indicate certain water quality class (WQC). The obtained results are verified with the existing knowledge found in literature.

Keywords: ECOLOGICAL MODELING, ENVIRONMENTAL DATA, DIATOMS, FUZZY LOGIC, WEIGHTED PATTERN TREE (WPT), ALGEBRAIC OPERATORS

1. Introduction

The machine learning algorithms are more frequently used to discover underling drivers of the environmental stress factors that affects organisms' abundance. This is very important in ecological science that studies ecosystems that are threatened by pollution or they are under recovery program. In this case, monitoring is very important, as well as the data analysis. Data analytics usually is done by statistical algorithms, like canonical correspondence, detrended correspondence or principal component statistical analysis. These techniques provide useful understandings of the underling ecological processes. However, they are limited in terms of interpretability and in most cases, they suffer from subjective opinion of the domain expert. This is because the results are plotted on graph, from which the biological expert draws interpretations of the distances between groups and clusters of diatoms related with the environmental factors based on his previous knowledge. That gives the final model interpretation a degree of expert self-opinion, which should not be the case. That's why more and more experts use modelling techniques where the expert opinion is reduced to minimum, instead, an underling statistical procedure takes over to confirm the prediction model accuracy.

In this direction, the well-known ID3 [1], C4.5 [2] or CART [3] decision tree algorithms leave no room for expert influence, only in the stage when the model results needs to be verified with the existing knowledge found in literature [4]. Moreover, the decision tree algorithms produce easy interpretable model for which no mathematical knowledge is required, unlike the neural networks. There are various subgroups of decision tree algorithms, some of them differ on the type of heuristics used, some of them are different on how the model is learnt with different data partitioning strategies, and some of them on what type of sets is used to extract the knowledge (classical or fuzzy set theory). Fuzzy decision tree algorithm [5] is in a subgroup of decision tree algorithms that uses fuzzy set theory to improve descriptive and predictive performance of the models, as well as improve the interpretability of the models using fuzzy linguistic terms. Fuzzy linguistic terms play important role in interpretation, due to their similarity with the human language when transforming the model tree into rules. Beside this, the fact that in many research studies the fuzzy decision trees reported to have better performance than the crisp decision tree algorithms [6] at the expense of small increase of the time needed to build the model.

Further research is done in improving the fuzzy decision tree algorithms. In that direction, the authors in [7] give detailed description of the pattern tree algorithm, which further improves the accuracy of the fuzzy decision tree algorithm. This is done by combining different types of membership functions and aggregation operators with various similarity metrics to achieve not only multi criteria decision-making, but also improving predictive accuracy and producing a model that is more resistant to overfitting. The pattern tree algorithm produces fuzzy rules with linguistic terms that can be obtained from the traditional hierarchical tree like structure. Furthermore, for each branch, a similarity between the target attribute and the input attribute is obtained, which evaluate the level of confidence of predicting the output attribute with that input attribute. Since each dataset may contains multi-class target attributes, one pattern tree model is built for each class of the target attribute. In this way a forest of pattern tree models is obtained, without knowing which tree holds the highest confidence of predicting the target class from the descriptive attributes. In this direction, the authors in [8] have presented the weighted pattern tree algorithm (WPT), which weights each pattern tree model to a class of the target attribute. In this way, the decision-making expert can select which output model is confident of predicting a given class. The WPT algorithm uses the similarity value between the target class attribute placed at the root of the model tree and the fuzzy term of the input attribute on the root branch. The membership degree of each input attribute is obtained using the process of fuzzification, which transforms the crisp attributes into fuzzy attributes by using different mathematical functions (triangular, trapezoidal, Gaussian, Bell etc.). These membership functions are widely used for fuzzification, depending on the nature of the input dataset and the purpose of the fuzzy system. Consequently, many researchers found out [9] that the fuzzification process has high influence on the accuracy of the classifier. Beside the different membership functions that WPT algorithm uses to build the final model, the WPT also uses different similarity metrics to find the most informative attribute related to the target class. Additionally, the WPT algorithm uses aggregation operators that relate each input attribute to the output attribute as operation between two fuzzy sets to narrow the search space. In both cases (similarity metrics and aggregation operators) there are many metrics and operators that may fit the modeler's needs to obtain high predicting accuracy. We use the recommendations that we suggested in [10], which are based on the experimental evaluation with different membership functions.

In this paper, we obtain one WPT model that consist from four sub-models to predict the relationship between the diatoms' abundances as indicators of water quality classes based on saturated oxygen parameter. The mathematical modelling is performed on ecological dataset that is comprised with ten input attributes and one output attribute. The ten input attributes represent the ten most abundant diatoms found in Lake Prespa water ecosystem [11] and one output target attribute that describes the ecological water quality class based on saturated oxygen parameter [12]. In this way, the obtained WPT model relates the diatoms' indicator status with the certain water quality class based on saturated oxygen parameter.

The rest of the paper is organized as follows: Section 2 provides description of the WPT building blocks: membership functions, similarity metrics and aggregations operators, as well as dataset description. In Section 3, we present the WPT model, we discuss the results and verify the obtained knowledge with the existing knowledge found in literature. The main conclusions and our future work are outlined in the Section 4.

2. Algorithm Concepts and Data Description

The WPT algorithm relies on the fuzzy theory concepts like membership functions, similarity metrics and aggregation operators, same as the pattern tree algorithm. However, the WPT uses additional information from the tree root similarity value to assign a degree of confidence or weight each model. The performance of the model depends on the membership function that is used, as well as the type of the similarity metric and aggregation operator. Following the recommendation that we gave in [10], we use the Bell membership function for building model.

The Bell membership function is defined with three parameters a , b and c . In order to achieve complete evenness between the fuzzy terms, we replace the parameter a with 10, b is replaced by σ calculated using (1), while c is replaced with μ (mean value of the range of each fuzzy term).

$$(1) \quad \sigma = \sqrt{\frac{\ln[10]}{2 * \ln[0.5 * r]}}$$

In equation (1), r stands for the length of the fuzzy range. After all these changes take place, the calculation of the Bell membership function fuzzy terms is made by

$$(2) \quad f(x; \mu; \sigma) = \frac{1}{1 + \left| \frac{x - \mu}{10} \right|^{2\sigma}}$$

Additionally, very important factor that influence the model accuracy is the number of fuzzy terms used per attribute. This has effect on the interpretability of the models as well as on the type of analyses that is conducted on the obtained knowledge. That is why selecting the number of fuzzy terms can be done on basis of the needs of domain expert or based on experimental evaluation of the model. For this purpose, we use five fuzzy terms which corresponds with the number of classes used in the European Water Framework directive (Directive 2000/60/EC of the European Parliament) for water quality classification, where there are five categories (poor, bad, moderate, good and high).

The next component of the WPT model building process is selection of the appropriate similarity metric. The similarity metric can greatly affect the accuracy of the model as well as the selection process of the most confident model for prediction. For this purpose, we consider the same metric used in [10]. However, we want to note that maybe other similarity metrics, like Jacquard, Cosine or Squared Euclidean, could be more adequate for this purpose. The similarity metric Sim_{RMSE} used in [10] is based on the RMSE (Root mean squared error) distance metric and calculates the similarity between two fuzzy sets A and B as

$$(3) \quad Sim_{RMSE} = 1 - \sqrt{\frac{\sum_{i=1}^n (\mu_A(x_i) - \mu_B(x_i))^2}{n}}$$

The results of the calculations using (3) reside in range between 0 and 1. To calculate this, the Sim_{RMSE} similarity metric uses the membership degrees for a given crisp value x_i in two fuzzy sets A and B , which are denoted as $\mu_A(x_i)$ and $\mu_B(x_i)$. The value of the Sim_{RMSE} similarity is propagated in each branch all the way up to the root of the model tree. Using only the similarity metric for estimating the relationship between the input and output attributes leads to low performances of the models. Therefore, the WPT algorithm also uses fuzzy aggregation operators, which are operations over two fuzzy sets to learn better models. Typically, triangular norms and conorms are used in fuzzy induction algorithms, and also in fuzzy decision tree algorithms. In [10], we used two fuzzy aggregation operators: Algebraic AND (T-norm) and Algebraic OR (T-conorm), which are defined as

$$\text{Algebraic AND} = \mu_A(x_i) * \mu_B(x_i)$$

$$\text{Algebraic OR} = \mu_A(x_i) + \mu_B(x_i) - \mu_A(x_i) * \mu_B(x_i).$$

It is important to note that also some other Triangular T-norm or T-conorm aggregation operators can be used here, that may have influence on the performance of the model and its interpretation of the model.

The dataset used for modelling the relationship between saturated oxygen and diatoms' abundances is obtained from the EU funded TRABOREMA [11] project. The goal of this project was to assess the ecological status of the Lake Prespa. During the monitoring stage, valuable data about the physico-chemical parameters as well as organisms' relative abundance was collected. Overall, sixteen parameters were measured and 116 different diatom species are counted. For each sample, the relative abundance for all 116-diatom species is obtained. Using this type of monitoring, the relationship between the influencing factors and diatoms' relative abundance can be discovered. In the ecological literature [4], the relationship between environmental stress factors and diatoms as bio-indicators is well established, but for many diatoms, this relationship remains unknown. The environmental stress factors in the established ecological literature are represented with water quality classes (WQCs) based on a certain physico-chemical parameter. These classification systems can be found in the ecological literature, like the classification systems for Conductivity [13], pH [13], [12] and Saturated Oxygen [12]. The saturated oxygen classification system defines five classes for the target attribute, which are given in Table 1.

Table 1: Water quality classes for the saturated oxygen physico-chemical parameter.

Name of the water quality class	Parameter range
<i>Oligosaprobous</i>	> 85 %
<i>β-mesosaprobous</i>	70% - 85%
<i>α-mesosaprobous</i>	25% - 70%
<i>α-meso / polysaprobous</i>	10% - 25%
<i>Polysaprobous</i>	< 10%

Since WQC *Polysaprobous* doesn't contain any values in the measured dataset, this class was removed. Therefore, the final dataset contains 4 WQCs based on the saturated oxygen parameter. Considering this classification system, it is obvious that using machine learning algorithms we face with typical classification problems, where the saturated oxygen WQCs are the possible values for the target or predictive attribute, while the relative abundances of the top ten most abundant diatoms are the input or descriptive attributes. By using the parameters' settings described in the previously, in the next section we present the WPT model in order to describe the relationship between Saturated Oxygen and the diatoms as bio-indicators.

3. Results and Verification

Four models are obtained, one for each WQC, and for each model the highest similarity is given in Table 2.

Table 2: The highest similarity that is obtained from the WPT models for the WQCs..

Name of the water quality class	Highest similarity
<i>Oligosaprobous</i>	0.5249
<i>β-mesosaprobous</i>	0.5620
<i>α-mesosaprobous</i>	0.6897
<i>α-meso / polysaprobous</i>	0.8253

Based on the results in Table 2, the highest similarity is obtained for the WPT model for *α-meso / polysaprobous* WQC. The model for this class is presented on Fig. 1. The highest similarity obtained with this model shows that it has highest confidence to predict the corresponding WQC. The model depicts the diatoms that can be used to indicate this WQC.

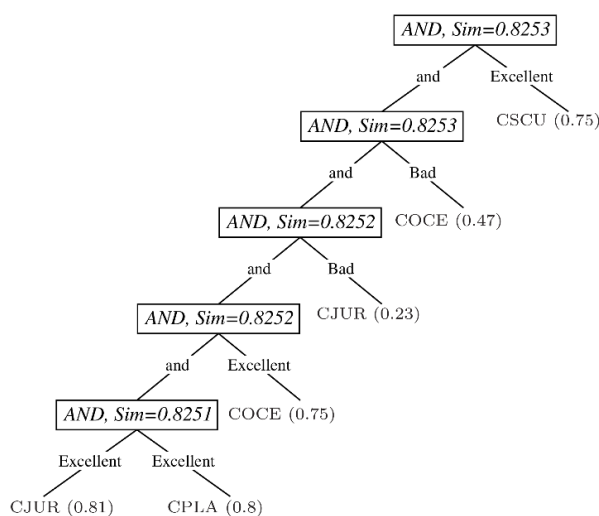


Fig. 1 WPT model for the *α-meso / polysaprobous* WQC for Saturated Oxygen. In brackets, the similarity between the membership degrees for a given fuzzy term for a diatom and the WQC is given.

According to the model, the *Cavinula scutelloides* (CSCU) and *Cocconeis placentula* (CPLA) diatoms can be used as excellent indicators for *α-meso / polysaprobous* WQC. The two other diatoms *Cyclotella juriljii* (CJUR) and *Cyclotella ocellata* (COCE) can be also used as excellent indicators since the similarity value between these two diatoms and the *α-meso / polysaprobous* WQC is higher compared to the similarity values for bad indicating properties.

For verification of the results, we compared them with the ecological preferences found in [4]. For the CJUR and NPRE diatoms no records exist for their ecological preferences because they are newly described taxa. The CPLA diatom is eutrophic with medium oxygen demand according [4], while the model shows that the CPLA diatom is an excellent indicator for waters with low values of saturated oxygen. On the other hand, the CSCU diatom is *alkalibiontic*, freshwater to brackish water specie, being *oligosaprobic* indicator with eutrophic preferences according [4]. The model gives directions that this diatom is an excellent indicator for *α-meso / polysaprobous* class opposite from which the known ecological literature directs. And finally, according to the model the COCE diatom is excellent indicator of *α-meso / polysaprobous* WQC, which if also obtained by other models that we generated with other experiments, thus this could add additional knowledge in the literature for this diatom. According [4], the trophic ecological preferences are the only one known for this diatom and since the trophic state index classification is out of the scope of this paper, adding new knowledge regarding the saturated oxygen demand for this diatom, could enrich its indicating properties.

4. Conclusion

In this paper, we presented a technique based on fuzzy set theory that could reveal the relationship between the saturated oxygen *α-meso / polysaprobous* WQC and the ten most abundant diatoms found in Lake Prespa. We built a model that presents which diatoms can be used for indicating the WQCs for saturated oxygen. The results from the WPT model are compared with the known ecological preferences found in the literature.

In future, we plan to investigate the influence of other similarity metrics and aggregation operators to further improve the accuracy of the models. Other type of membership functions could be more suitable for diatom modelling, thus revealing more valuable knowledge from the measured data. Also, modelling other water quality classes or trophic index classes could increase the applicability of the algorithm.

Acknowledgement

This work was partially financed by the Faculty of Computer Science and Engineering at the “Ss. Cyril and Methodius University in Skopje”, Skopje, R. Macedonia.

References

- [1] J.R. Quinlan, “Induction of decision trees”, Mach. Learn., vol. 1, pp. 81–106, 1986.
- [2] “C4.5: Programs for Machine Learning”, San Francisco, CA: Morgan Kaufmann, 1993.
- [3] L. Breiman, J. Friedman, R. Olshen, C. Stone, “Classification and Regression Trees”, Belmont, Wadsworth, 1984.
- [4] H. Van Dam, A. Martens, J. Sinkeldam, “A coded checklist and ecological indicator values of freshwater diatoms from the Netherlands”, Netherlands Journal of Aquatic Ecology, vol. 28, no. 1, pp. 117–133, 1994.
- [5] Y. Yuan, M.J. Shaw, “Induction of fuzzy decision trees”, Fuzzy Sets and Systems, vol. 69, no. 2, pp. 125–139, 1995.
- [6] Y.-l. Chen, T. Wang, B.-s. Wang, Z.-j. Li, “A survey of fuzzy decision tree classifier”, Fuzzy Information and Engineering, vol. 1, no. 2, pp. 149–159, 2009.
- [7] Z.H. Huang, T. D. Gedeon, “Pattern trees”, in: Proc. of IEEE International Conference on Fuzzy Systems, pp. 1784–1791, 2006.
- [8] Z. Huang, M. Nikraves, B. Azvine, T.D. Gedeon, “Weighted pattern trees: a case study with customer satisfaction dataset”, International Fuzzy Systems Association World Congress 2007, pp. 395–406, Springer, Berlin, Heidelberg, 2007.
- [9] M. Zeinalkhani, M. Eftekhari, “Fuzzy partitioning of continuous attributes through discretization methods to construct fuzzy decision tree classifiers”, Information Sciences, vol. 278, pp. 715–735, 2014.
- [10] A. Naumoski, G. Mirceva, K. Mitreski. “Experimental Evaluation of Different Membership Functions on Weighted Pattern Trees for Diatom Modelling”, 14th International Conference on Natural Computation; Fuzzy Systems and Knowledge Discovery, IEEE, 2018.
- [11] “TRABOREMA Project” WP3, EC FP6-INCO project no. INCO-CT-2004-509177, 2005–2007.
- [12] A. Van Der Werff, H. Huls, “Diatomeenflora van Nederland”, Abcoude - De Hoef, 1957, 1974.
- [13] K. Krammer, H. Lange-Bertalot, “Die Ssswasserflora von Mitteleuropa 2: Bacillariophyceae. 1 Teil”, pp. 876, Stuttgart: Gustav Fischer-Verlag, 1986.